Universidade do Minho
Escola de Engenharia

Jacinto João do Rosário da Silva

Continuous monitoring of deformability of stabilized soils based on modal identification

julho de 2017

Continuous monitoring of deformability of stabilized soils based on modal identificationse
Jacinto João do Rosário da Silva
UMinho | 2017

FCT Fundação para a Ciência e a Tecnologia
MINISTÉRIO DA CIÊNCIA, TECNOLOGIA E ENSINO SUPERIOR
POPH QUALIFICAR É CRESCER.
QREN QUADRO DE REFERÊNCIA ESTRATÉGICO NACIONAL
GOVERNO DA REPÚBLICA PORTUGUESA
UNIÃO EUROPEIA Fundo Social Europeu

Universidade do Minho
Escola de Engenharia

Jacinto João do Rosário da Silva

Continuous monitoring of deformability of stabilized soils based on modal identification

Tese de Doutoramento
Engenharia Civil

Trabalho efetuado sob a orientação de
Professor Doutor Miguel Ângelo Dias Azenha
Professor Doutor António Gomes Correia

julho de 2017

STATEMENT OF INTEGRITY

I hereby declare having conducted my thesis with integrity. I confirm that I have not used plagiarism or any form of falsification of results in the process of the thesis elaboration.

I further declare that I have fully acknowledged the Code of Ethical Conduct of the University of Minho.

University of Minho, July 27, 2017

Full name: Jacinto João do Rosário da Silva

Signature: Jacinto João do Rosário da Silva

To my Family…

…particularly to my Father

ACKNOWLEGDMENTS

The supervisors of this thesis are Professor Miguel Azenha and Professor António Gomes Correia who provided guidance of great importance and influence to the work conducted. I want to expose my gratitude to Professor Miguel Azenha for the availability provided as supervisor, for the enthusiasm and motivation as research colleague and as a friend. I would also like to thank to Professor António Gomes Correia for the availability and wise advices provided as supervisor and for his involvement provided during the thesis development. I want expose my satisfaction to be a part of this research team and acknowledge their contribution and concern to create the best conditions to the development of the work.

This research work has been developed in the scope of the Doctoral Programme in Civil Engineering, at the University of Minho, Portugal, and supported by the Portuguese Science and Technology Foundation (FCT), under grant No. SFRH/BD/74500/2010. This is gratefully acknowledged.

A special acknowledgment is given to ISISE – Institute for Sustainability and Innovation in Structural Engineering.

I would like to express my gratefulness to a group of Professors that contribute with their experience and knowledge during the development of some topics of thesis, namely: Professor Tiago Miranda, Professor Cristiana Ferreira and Professor Luís Ramos.

A special acknowledgment to my colleague José Granja, with which I continuously shared opinions, ideas, knowledge and strategies that resulted on the enrichment of my experience.

I would also like to recognize the contribution of the colleagues with which I had the pleasure of performing parts of the research work reported in this thesis: Luís Rios, Nelson Martins, Sónia Costa and Cláudio Pereira.

I would also like to thank the technical staff of the Civil Engineering Laboratory of Minho University, particularly to Mr. José Gonçalves, Marco Jorge and Carlos Jesus.

Finally, I would like to thank my family in general for their support, particularly my parents, parents in law, my wife Cristina and my twin daughters Daniela and Diana.

ABSTRACT

Soil stabilization with chemical binders is a technique that aims to improve the mechanical behaviour of soils in order to meet design requirements. In this context, the E-modulus is one of the most important properties for design of structures that involve stabilized soils. There has been a recent proposal of a technique termed as EMM-ARM (Elasticity Modulus Measurement through Ambient Response Method), which allows to continuously monitor the E-modulus evolution of cement-based materials. Such technique relies on placing the sample to be tested in a specific mould, under known support conditions, and apply modal identification techniques to infer the evolution of E-modulus of the tested material during cement hydration. It is remarked that before this PhD work, there had been a set of exploratory experiments using EMM-ARM applied to stabilized soils (made by the author of this thesis), which had pointed to the feasibility of this technique in the context of stabilized soils.

This thesis presents a set of subsequent developments of the EMM-ARM technique applied to soils stabilized with binders. The validation of EMM-ARM was made by comparing the results obtained with different testing techniques, such as unconfined cyclic compression testing and techniques based on the propagation of mechanical waves. A sampler was developed to allow the collection of samples from stabilized layers, immediately after compaction, in order to increase the representativeness of the tested samples. The use of alternative materials and geometries of the EMM-ARM test mould, involving polyvinyl chloride (PVC) tubes, aimed the increase of robustness and to simplify its application on sampling operations. A variant approach to EMM-ARM was further proposed, involving modal identification with explicit excitation of small amplitude of the testing beam. This adaptation aimed to increase the robustness of the technique under conditions with contamination of the ambient noise. Moreover, EMM-ARM was systematically applied to three types of soils stabilized with three different proportions of cement. EMM-ARM was also applied to a soil stabilized with lime for the first time, including curing at distinct temperatures, revealing an interesting E-modulus evolution with two phases and allowing to estimate apparent activation energies of the reactions involved. The final part of the thesis presents a methodology based on Bayesian inference to predict the E-modulus results at the reference age of 28 days, using the results obtained during the first 2 to 7 days of age.

RESUMO

A técnica de estabilização de solos com ligantes visa o melhoramento do comportamento mecânico dos solos de modo a cumprirem os requisitos de construção a que são destinados. Do ponto de vista do dimensionamento das estruturas que utilizam solos estabilizados, a deformabilidade é considerada uma das propriedades mais relevantes. Recentemente foi proposta uma técnica designada por EMM-ARM (Elasticity Modulus Measurement through Ambient Response Method) que permite a monitorização contínua do módulo de elasticidade através de técnicas de identificação modal de misturas contendo materiais cimentícios desde o estado fresco, após devida colocação de amostra em molde específico. Refira-se que anteriormente a este trabalho de doutoramento, apenas havia sido feito um conjunto de ensaios preliminares EMM-ARM (pelo autor desta tese) que demonstraram o potencial de aplicabilidade desta técnica ao estudo de solos estabilizados. Esta tese apresenta um conjunto de desenvolvimentos subsequentes da técnica EMM-ARM aplicada a solos estabilizados com ligantes. A validação de EMM-ARM efetuou-se através da comparação de resultados obtidos com diferentes técnicas de ensaio, tais como ensaios compressão uniaxial cíclica e metodologias baseadas em propagação de ondas mecânicas. Foi desenvolvido um amostrador que permite a obtenção de amostras de camadas estabilizadas, imediatamente após compactação, de modo a aumentar a representatividade das amostras ensaiadas. A utilização de materiais e geometrias alternativas para o molde de ensaio EMM-ARM, compreendendo tubos em cloreto de polivinilo (PVC), teve em vista um aumento da robustez do molde e facilitar a sua aplicação na recolha de amostras. É também proposta uma técnica de ensaio, que pode ser considerada uma variante a EMM-ARM, que envolve identificação modal com excitação explícita de pequena amplitude da viga de ensaio. Com esta metodologia, pretende-se aumentar a robustez da técnica perante contaminações do ruido ambiente. Adicionalmente, são apresentados os resultados de aplicação sistemática da técnica EMM-ARM a três tipos de solos estabilizados com três diferentes percentagens de cimento. Pela primeira vez são apresentados resultados da aplicação de EMM-ARM a um solo estabilizado com cal, incluindo a cura a distintas temperaturas, revelando uma interessante evolução do módulo de elasticidade em duas fases e permitindo estimar as energias de ativação aparente das reações envolvidas. No final da tese é apresentada uma metodologia baseada em inerência Bayesiana para previsão de resultados de módulo de elasticidade à idade de referência de 28 dias, com base em resultados obtidos com EMM-ARM nos primeiros 2 a 7 dias de idade.

CONTENTS

LIST OF FIGURES

LIST OF TABLES

LIST OF SYMBOLS AND ABBREVIATIONS

AR	Area ratio
BE	Bender-extender elements
CAH	Calcium aluminate hydrate
CPSD	Cross-power spectra density
CSH	Calcium silicate hydrate
D_e, d_e	External diameter
D_i, d_i	Internal diameter
D_s	Inside diameter of sampler
E	E-modulus / Young's modulus
$\bar{E}$	Homogenised E-modulus
E_a	apparent activation energy
E_{max}	Maximum secant E-modulus or dynamic modulus
E_{sec}	Secant modulus associated to a given strain level
E_{tan}	Tangent E-modulus associated to a given stress-strain point
$\mathrm{E_{eq}}$	Unload-load E-modulus associated to a given strain amplitude
E'_v	Young's modulus for loading in vertical direction
E'_h	Young's modulus for loading in horizontal direction
EMM-ARM	Elasticity modulus measurement through ambient response method
EMA	Experimental modal analysis
FFT	Fast Fourier Transform
FRF	Frequency response function
fs	Sampling frequency
G	Shear modulus
G'_{hv}	Shear modulus in the vertical plane
G'_{hh}	Shear modulus in the horizontal plane
I	Moment of inertia
$\bar{I}$	Homogenised moment of inertia

ICR	Inside clearance ratio
L	Span
k	Spring constant
K	Reaction rate constant
LHS	Latin Hypercube Sampling
LVDT	Linear Variable Differential Transformer
$L\left(E\middle\vert\theta^{(n)}\right)$	Likelihood function
m	Mass
$\bar{m}$	Uniformly distributed mass
m_p	Concentrated mass
M	Constrained modulus
N	Number of samples
NPSD	Normalized power spectrum density
OMA	Operational modal analysis
P	Compression wave
PP	Peak picking
PSD	Power spectra density
PVC	Polyvinyl chloride
$p(\theta)$, E_i'	Prior distribution
$p(\theta\|x)$, E_i''	Posterior distribution
qu	Unconfined compressive strength
R	Ideal gas constant
ρ	Density
s	Standard deviation
S	Shear wave
t_e	Equivalent age
t	Time / age
T	Total signal duration
T	Absolute temperature
T_{ref}	reference temperature

UC	Uniaxial compression test
UCC	Unconfined cyclic compression test
UPV	Ultrasonic pulse velocity
υ	Poisson's ratio
ν'_{vh}	Poisson's ratio for horizontal strain due to vertical strain
ν'_{hh}	Poisson's ratio for horizontal strain due to horizontal strain in the normal direction
Vp	Propagation velocity of compression wave
Vs	Propagation velocity of shear wave
x	abscise along beam length
a_r, β_r, τ_r	Fitting parameters
α_u	Ultimate degree of hydration
β	Hydration shape parameter,
τ	Hydration time parameter
δ	Deformation
$\phi(x)$	Vertical deflection mode
ξ	Damping
θ	Parameter
ω	Angular frequency

Nothing is permanent except the change

Heraclitus

Chapter 1

INTRODUCTION

1.1 Scope and motivation

The construction of civil engineering infrastructures, particularly highways and railways, frequently demands the improvement of the mechanical properties of underlying soils as an alternative to soil substitution. For this purpose, chemical additives for stabilisation have been used for several years (Ingles & Metcalf, 1972, Dupas & Pecker, 1979, Bell, 1996), with extensive applications in Europe, USA and throughout the world (Bartlett & Farnsworth, 2002, Dupas & Pecker, 1979, Bell, 1996, Kolias *et al.*, 2005, Jackson *et al.*, 2007, Hossain *et al.*, 2007). In fact, significant benefits to the strength and stiffness of soils can be achieved by incorporating small quantities of additives, such as lime (Bell, 1996, Al-Mukhtar *et al.*, 2010, Jauberthie *et al.*, 2010, Verbrugge *et al.*, 2011) or cement (Sariosseiri & Muhunthan, 2009, Viana da Fonseca *et al.*, 2009a, Ajorloo *et al.*, 2012). Soil stabilisation is usually preceded by a laboratory mixture formulation and the corresponding assessment of mechanical properties with adequate laboratorial techniques (Gomes Correia *et al.*, 2009b). In this context, the most commonly characterised mechanical properties are the compressive strength and stiffness modulus. In view of its relevance for the actual service life of structures using stabilised soil, stiffness or deformability is considered to be of utmost importance (Puppala, 2008, Atkinson, 2000). However, it is more difficult to characterise than compressive strength (Gomes Correia *et al.*, 2009b, Atkinson, 2000, Verbrugge *et al.*, 2011), mainly due to the non-linear behaviour of soils.

The assessment of stiffness properties can be performed by means of laboratory techniques such as unconfined compression tests with local strain measurement, triaxial tests (Ajorloo *et al.*, 2012, Gomes Correia *et al.*, 2006) and resonant column tests (Clayton *et al.*, 2010, Stokoe & Santamarina, 2000). However, the application of these techniques to stabilized soils at early ages usually presents some limitations, as they typically provide discrete results in time and a minimum curing period may be required before testing.

Wave propagation based techniques are frequently used as an alternative to traditional testing techniques, mainly due to their non-destructive nature and expeditious application (Ferreira, 2009, Dimter *et al.*, 2011). However, the interpretation of the results obtained with these techniques is frequently challenging and usually has some

associated uncertainty, due the influence of geometrical effects, experimental setups, and the algorithms used for data processing (Amaral *et al.*, 2011, Ferreira, 2009, Viana da Fonseca *et al.*, 2009c, Yuan & Nazarian, 1993, Beaty *et al.*, 2002).

Another important issue in soil improvement is quality control after treatment. *In situ* assessment of mechanical properties, namely stiffness, is therefore necessary to confirm that the performance requirements of the stabilised soil have actually been met. Among the most commonly used techniques for in-situ assessment of the stiffness of cement-stabilized layers, the following methods can be highlighted: the plate load test (Gomes Correia *et al.*, 2004), the light falling weight deflectometer (Benedetto *et al.*, 2012, Alshibli *et al.*, 2005) and the Humboldt stiffness gauge (Gomes Correia *et al.*, 2009a, Abu-Farsakh *et al.*, 2004). For the *in situ* measurement of wave propagation velocities, a number of geophysical methods are available, some of which are among the oldest techniques of soil surveying and profiling (Rayleigh, 1885, Love, 1892). These methods largely preceded the laboratory developments, and different setups and configurations have been devised over the years (Stokoe & Santamarina, 2000). The most frequently used methods are surface reflection, surface refraction and surface wave, which are non-intrusive methods, and cross-hole, down-hole and seismic cone penetrometer testing, which are intrusive methods (Stokoe & Santamarina, 2000).

A technique known as EMM-ARM (Elasticity Modulus Measurement through Ambient Response Method) was recently proposed for the continuous assessment of the concrete/cement paste E-moduli from the instant of its casting (Azenha *et al.*, 2010, Azenha *et al.*, 2012a). In its original conception, the material being tested was placed inside a mould of known geometry (e.g. a hollow tube), which was then placed in simple supported conditions and left under ambient excitation throughout the entire testing period. By monitoring the accelerations of the composite beam at mid-span, it was possible to perform the modal identification and to evaluate the first flexural resonance frequency of the beam. The resonant frequencies of the composite beam evolved as a result of the increasing stiffness of the cementitious material and were correlated with its E-modulus by applying the dynamic equation of motion. Therefore, it was possible to obtain a curve for the 'E versus time'. The performance of this methodology was demonstrated by Azenha (2009) and Azenha *et al.* (2010), and its results have been successfully compared to those obtained through unconfined cyclic compression (UCC) tests and loading cycles on the tested beam.

The first works with this technique applied to sand-cement mixtures have demonstrated the potential of monitoring the evolution of the E-modulus of these materials (Azenha *et al.*, 2011). In spite of the success of such preliminary application, it was limited to the first 7 days of age, and no methodology was proposed for sample collection from fresh stabilized layers.

1.2 OBJECTIVES, THESIS ORGANIZATION

The present thesis aims to extend the preliminary work of Azenha *et al* (2011), which emanated from the MSc work of the author of this PhD thesis, by introducing a set of improvements to EMM-ARM, as to increase its robustness and demonstrate its feasibility as a quality control tool for stabilized layers. The improvements include: modifications to the test mould (i.e., shape and length); extending the test period to reference age of 28 days of age; development of sampling methodology capable to obtain samples representative of stabilized layers suitable to be tested with EMM-ARM; reduce the effect of undesirable contaminations of the ambient noise increasing the robustness of the modal identification; development of methodology capable to predict with confidence the E-modulus at reference ages based on EMM-ARM results obtained during the firsts days of curing. The work performed also comprised a systematic application of EMM-ARM to different types of soils treated with chemical additives. The application of EMM-ARM to a mixture of a soil treated with quicklime cured at distinct temperatures (20ºC, 30ºC and 40ºC) allowed to observe the temperature effect on the E-modulus and to compute the apparent activation energies of the reactions involved in the curing. EMM-ARM developments were validated by comparison of results with unconfined cyclic compression (UCC) testing and wave propagation techniques (bender-extender elements (BE) and ultrasonic testing (US)), on specimens of same material.

The conducted research reported in this thesis is organized in a total of 7 Chapters, including the present introduction.

Chapter 2 briefly address the different stabilisation techniques with special emphasis on the chemical stabilisation with cement or lime, as these two binders were used as treatment agents during the experimental programs in the scope the present thesis.

Reference is also made to the deformational behaviour of soils and to the techniques used in this thesis to assess the stiffness of these materials. Finally, a discussion is made in regard to the disturbance phenomena associated to sampling, the main design parameters of samplers and the sampler methodologies most used to collect undisturbed samples for laboratory testing.

Chapter 3 addresses a critical review related to two main subjects of interest in the scope of this thesis, namely some basic principles of modal identification and the state of development of EMM-ARM. It starts by introducing the basic principles of modal identification of a single degree of freedom oscillator under ambient excitation (or operational modal analysis: OMA) and forced excitation (experimental modal analysis: EMA). These include the definition and the estimation of frequency response functions (FRFs) from experimental data, a reference to the actions that can be used to minimise the effects resulting of the conversion of analogue signals to discrete time series (minimising aliasing and leakage errors) and finally a brief description of the basic method in the frequency domain. The principles here presented include a more advanced modal analysis method than the one adopted in the original EMM-ARM technique, as this information is useful to better understand some of the improvements made in this research. The chapter also contains a review on the state of development of EMM-ARM prior to the present work, including its original application to cement based materials, as concrete, mortars and cement pastes, and the posterior adaptation to soil-cement mixtures. Regarding the EMM-ARM application to soil-cement, the main problematic issues are raised and, consequently, the opportunities of improvement are identified in the scope of testing stabilized soils.

Chapter 4 presents a set of modifications to EMM-ARM methodology with aim of overcoming the limitations raised in the previous chapter. The modifications comprise: the design of new prismatic and tubular moulds with higher slenderness than those used in previous works; the use of an alternative cheaper material (PVC - polyvinyl chloride) for tubular moulds; the development of sampling methodologies to collect the material to be tested directly from compacted layers; the implementation of experimental modal analysis (EMA) with forced vibration of low magnitude to reduce the effect of undesirable contaminations of the ambient noise increasing the robustness of the modal identification. The experimental programs included the preparation of pilot stabilized layers from which were collected intact samples used to monitor the E-modulus. The

validation of EMM-ARM developments was performed by comparison of results of unconfined cyclic compression (UCC) testing and wave propagation techniques, including bender-extender elements (BE) and ultrasonic testing (US), on specimens of same material.

Chapter 5 presents the results of systematic application EMM-ARM to different types of soils treated with chemical additives. A uniform sand, a sand and a granitic soil were treated with two different types of Portland cement (CEM II/B-L 32.5 N and CEM I 52.5 N) used in three different proportions (3%, 5% and 7%). This Chapter presents also the results of the first application of EMM-ARM to a soil treated with lime. In this study a mixture of a silt soil treated with quicklime was and tested with EMM-ARM at temperatures of 20ºC, 30ºC and 40ºC. With the obtained results, it was possible to compute the apparent activation energies of the reactions involved in the curing.

Chapter 6 is dedicated to the proposal of a methodology to estimate the E-modulus of soil-cement mixtures at 28 days using the results obtained from EMM-ARM since two days of curing. The proposed methodology uses Bayesian inference tools applied to the data obtained from EMM-ARM tests and a model based on the cement hydration is used to describe the E-modulus evolution.

The main conclusions of this thesis are summarized in Chapter 7, together with some suggestions for possible extensions to the performed research.

Chapter 2

SOIL STABILISATION AND QUALITY CONTROL

2.1 INTRODUCTION

Soil stabilisation consists on the application of one or several different treatment techniques with the aim to modify at least one of the intrinsic properties of the soil. This treatment can have a temporary or permanent effect on the soil and can be of chemical, physical or mechanical nature (Correia, 2011). The selection of the technique to use depends on several factors and a commitment must be found between economic, technical and environmental factors, design requirements and the type of soils available. Soil stabilization usually includes laboratorial studies to define the proportions of binders to be used *in-situ* and the treatment procedures. Nevertheless, a rigorous quality control is needed in order to assure the stabilized materials fulfils the design specifications.

This chapter briefly address the different stabilisation techniques with special emphasis on the chemical stabilisation with cement or lime, as these two binders were used as treatment agents during the experimental programs in the scope the present work. Is also made a short reference to the mechanical behaviour of soils and to some of the existing techniques used to access the mechanical properties of these materials, particularly in which concern the deformability. Finally, is discussed the disturbance phenomena associated to sampling, the main design parameters of samplers and the sampler methodologies most used to collect undisturbed samples for laboratory testing.

2.2 CHEMICAL STABILISATION

In general terms the stabilization of soils can be performed by mechanical and chemical processes. Mechanical stabilisation of soils involves the use of treatment operations that only results on the modification of the particle arrangement, as compaction, or changes in grain size distribution, as grain size correction. However, this thesis only addresses the chemical stabilization and consequently mechanical stabilisation is not developed in this research.

Chemical stabilisation consists in to adding and mixing chemical additives to the soil, leading to the development of chemical reactions which result in a binder effect on the soil. Cement and lime are the most used chemicals in soil stabilization, however, there

are some other additives whose application in soil tratment have been made or studied in the last years. These include high-furnace slag, fly ash (Kang *et al.*, 2013, Petry & Little, 2002), natural pozzolana, silica fume limestone filers polymers, ionic compounds, eznimes (Liu *et al.*, 2009) acid, petroleum emulsions, resins, lignosulfonates (Tingle & Santoni, 2003), gypsum (Ahmed & Issa, 2014) and microorganisms (bio-mediated treatment) (DeJong *et al.*, 2010).

2.2.1 Treatment with cement

The most used cement is the Portland cement that is mainly composed by tricalcium silicate ($3CaO.SiO_2$), dicalcium silicate ($2CaO.SiO_2$), tricalcium aluminate ($3CaO.Al_2SiO_3$) and tetracalcium aluminoferrite ($4CaO.Al_2SiO_3.Fe_2O_3$), which when in contact with water start some complex physical and chemical processes that are responsible for the improvement of the mechanical properties of the mixture. Some of the products yield during these reactions are the calcium silicate hydrate (CSH), calcium aluminate hydrate (CAH) and a small percentage of calcium hydroxide (Venkatarama-Reddy & Latha, 2014). Equations (2.1) and (2.2) present the hydration reactions of the calcium silicates, whose are the main component of the cement (about 75%). Due to the formation of cementitious products and calcium hydroxide (lime), Portland cement is a stabilizing agent suitable for both fine and granular soils and aggregates and other materials. In fact, these hydration products create water insoluble bonds and bind the gravel, sand and silt particles. Cementitious products such as CSH and CAH do not react with clay particles, whereas the small percentage of lime released during the cement hydration process can start pozzolanic reactions with alumina and silica of the clay minerals, forming additional cementitious products, as presented on Equations (2.3) and (2.4). These reactions have lower rates and are responsible for the long term improvement.

$$2(3CaO.SiO_2) + 6H_2O \rightarrow 3(CaO).2(SiO_2).3(H_2O) + 3Ca(OH)_2 \quad (2.1)$$

$$2(2CaO.SiO_2) + 4H_2O \rightarrow 3(CaO).2(SiO_2).3(H_2O) + Ca(OH)_2 \quad (2.2)$$

$$Ca(OH)_2 + SiO_2 + H_2O \rightarrow CaO.SiO_2.H_2O \quad (2.3)$$

$$Ca(OH)_2 + SiO_2 + Al_2O_3 + H_2O \rightarrow CaO.Al_2O_3.SiO_2.H_2O \quad (2.4)$$

Is relevant to state that small amounts of cement can form independent cores in the soil mass whilst high cement proportions can form interconnected cores in the soil mass.

As soil-cement mixtures usually has low content of binder the solidification of the soil mass depends on the bonds established in some contact points between grains and a low percentage of voids filled with hydration products. So, obtaining durable and resistant mixtures is directly related to the connection points between grains granted by the binder and by the partial involvement of soil particles by cement grains.

In the case of uniform sands, since these have a high void ratio and a reduced contact area between grains, cement dosage be typically higher than that in the well-graded granular soil. Silts and clays also cause difficulties for cement action, due to the colloidal particles of maximum size equal to the smaller size of the cement particles are absorbed by the cement grain surface forming a film that preclude the ions diffusion. This event disturbs the hydration process and inhibit the development of crystal reaction products. On well graded granular soils, because of its smaller number of voids, filling these becomes quite easier.

Stabilisation with cement is usually faster when compared to other binders, such as lime (Okyay & Dias, 2010). The permeability of cement stabilized materials is significantly reduced and as result of the treatment is obtained a highly durable and resistant material to the water action. Cement can be used to treat a variety of soils but is more effective in the treatment of silt and coarse particle size soils (Jauberthie *et al.*, 2010, Sariosseiri & Muhunthan, 2009).

For the Portland cement hydration process to take place correctly and efficiently, the soil must have low content of organic materials, otherwise there is a risk of the binder not hydrate, reducing performance and increasing waste. In soils with low organic material content and medium or low quantities of clay cement application, even in small dosage, leads to achieving high levels of strength and durability.

Soil stabilisation with cement consists of adding cement and water to a soil and then proceeding to the homogenization of the resultant mixture. The cement action is a

function of the added content of the stabilizer (Ajorloo *et al.*, 2012, Okyay & Dias, 2010, Sariosseiri & Muhunthan, 2009) and can occur according to two different mechanisms. Higher cement content promotes the formation of interconnected clusters of cement, distributed by the soil mass, increasing the mechanical strength and stiffness of the soil. Treatment with lower cement content causes a modification of the clay fraction of soil, by flocculation of clay particles, and the main improvement is decrease of plasticity and in some cases may lead to an increase of mechanical strength (Cruz & Jalali, 2006). Figure 2.1a shows the effect of cement content used in the mechanical strength of a fine granular soil. The treatment with cement is more effective for soils with lower plasticity (Miller & Azad, 2000). Another factor that interferes with the performance of cement stabilized soil is ratio between the void volume (Vv) and cement volume (Vc). In fact the mechanical strength and stiffness increase with decreased Vv / Vc ratio, as can be observed on Figure 2.1b (Viana da Fonseca *et al.*, 2009b).

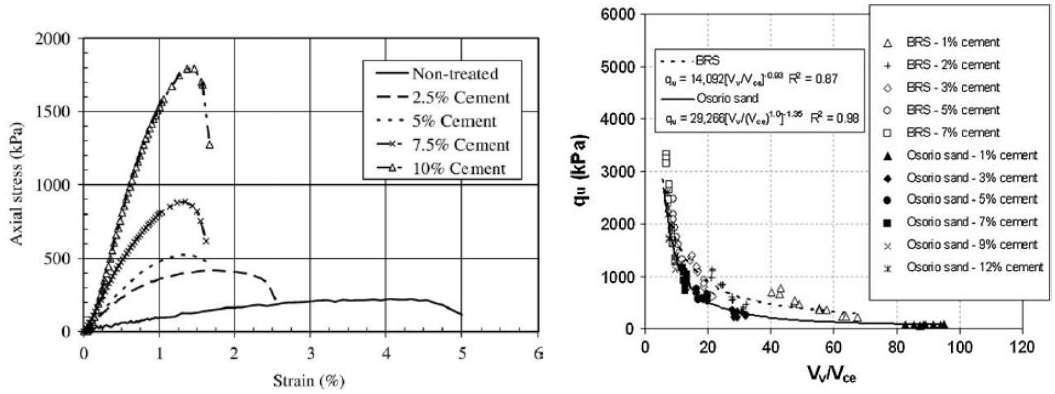

Figure 2.1. a) Effect of cement treatment on the strength of a granular soil (Sariosseiri & Muhunthan, 2009); b) Unconfined compressive strength versus voids/cement ratio (Viana da Fonseca *et al.*, 2009b)

There are some precautions to be taken during soil treatment process, such as the correct distribution of cement in the soil, as well as ensuring an effective homogenization and irrigation with water whenever necessary to correct the content water. Furthermore, the compaction should be made as soon as possible after mixing, otherwise significant loss in the treatment performance can occur, as depicted in Figure 2.2.

To minimize errors and distribution to other effects such as to overcome the wind drag is current practice apply binder quantity at least 1% higher than the dosage studied in laboratory (F.G.Bell, 2005). The behaviour of different types of cement depends on certain features such as the nature of the soil, grain size, chemical and mineralogical

composition and working conditions, particularly water content, as the means of spraying, homogenization and compression available (F.G.Bell, 2005).

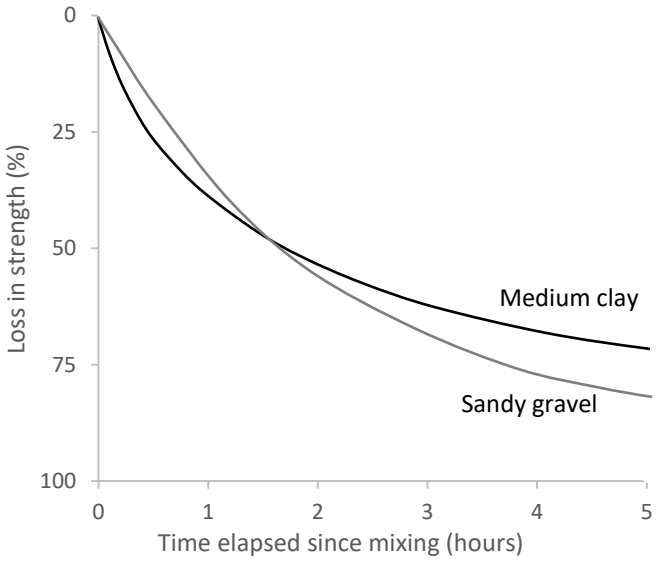

Figure 2.2. Loss in strength due to delay in compaction for two soils stabilized with 10% cement (adapted from Ingles & Metcalf, 1972, in:, F.G.Bell, 2005)

In practice there are technical recommendations that have been proposed by design manuals and technical recommendations in order to provide guidelines for application of this technique (SETRA-LCPC, 2004, Highways-England, 2015, Little & Nair, 2009, NLA, 2004). The parameters addressed by these documents usually include:

- Soil characterization (Atterberg limits, size distribution, maximum particle dimension, etc…);
- Performance intended for the final treated soil: (stiffness, strength, swelling);
- Characterization of treatment additives;
- Selection of treatment additives;
- Minimum quantities of a single additive or combination of multiple additives;
- Treated layer thickness;
- Compaction procedures;
- Density and water content of treated layers.

2.2.2 Treatment with lime

The soil treatment with lime consists in to mix lime with soil in presence of water resulting in some physicochemical modifications of the soil that occurs via two distinct processes: (i) the soil improvement or modification that occurs at early ages; (ii) the long term stabilisation. This two different processes usually are achieved by using different quantities of lime. The lesser amounts are used for drying and temporary modification of soil, providing a working platform for building or for temporary roads. An application in larger quantities, supported by appropriate design, testing and building techniques, leads to permanent structural stabilisation of soils (NLA, 2004, Bell, 1996, Al-Mukhtar *et al.*, 2012). The chemical reactions observed in soil-lime mixtures are usually classified as ion exchange, flocculation, cementation and carbonation. The main effects of lime on soil treatment are reduction in water content, improvements on plasticity, workability, strength, deformability, expansion and compressibility (Okyay & Dias, 2010).

Nevertheless, different types of soils can react differently to lime treatment, resulting in different rates of improvement of the mechanical properties. Used isolated or in combination with other materials, lime can be applied in the treatment of a wide variety of soils. However, mineralogical properties of the soil will determine the degree of reactivity with lime and the mechanical performance that will be achieved by the stabilized layer. In general, fine clay soil with a minimum of 25% passed the sieve #200 (0.074mm) (ASTM, 2009) and plasticity index greater than 10 are considered suitable for the lime stabilisation. Soils with relevant percentages or sulphates of organic matter (more than 1% and 0.3%, respectively) will require additional amounts of lime (NLA, 2004).

2.2.2.1 Reduction in water content

The simple fact that of adding a dried material (lime) to the soil results on a reduction of the water content. When quicklime is mixed with moist soil, it immediately hydrates through the reaction with water, releasing heat. This has a drying effect of the soil, because some of the water takes part in the reaction and additionally some may be evaporated due to heat loss. These two facts lead to a decrease of 0.6 to 0.8% in water content for each 1% water quicklime added (NLA, 2004). On the other hand, the

aeration caused during the mixing process, under favourable conditions, can cause a decrease in water content of about 2.5%. In the case of using hydrated lime, the drying effect occurs only due to the chemical changes that reduce soil water holding capacity (NLA, 2004).

2.2.2.2 Soil modification

The modification of the soil by lime occurs when the calcium ions of hydrated lime replace the exchangeable ions of the soil. As the clay particles are mostly electrically charged with negative charges they have the property to adsorb exchangeable cations on its surface. After initial mixing, the calcium ions (Ca^{2+}) from hydrated lime migrate to the surface of the clay particles and displace water and other ions (Na^{+} e K^{+}). This process leads to a reduction of the negative charges of the particles in suspension, decreasing the repulsive forces between the particles. Consequently, the attraction forces gain influence and the clay particles are attracted to each other in a process known as flocculation (Figure 2.3).

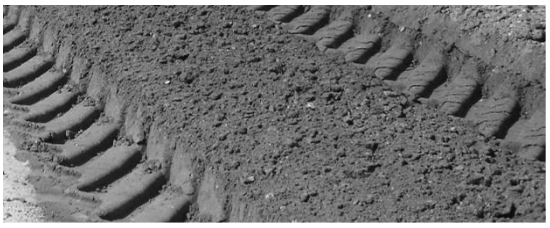

Figure 2.3. Flocculation on a lime treated soil

As result of this process some modifications on the geotechnical characteristics of the soil can be observed. The soil becomes friable and granular, making it easier to work and compact, the plasticity index of the soil decreases dramatically, as does its tendency to swell and shrink. It also can be observed a reduction of the maximum dry density, an increase on the optimum water content, better behaviour to freeze thaw cycles and improvements on shear strength (Okyay & Dias, 2010, Lemaire *et al.*, 2013). The lime amount required to achieve a maximum flocculation effect depends on the type of soil, more specifically the amount of clay materials present, but is typically less than 3% (Cristelo & Jalali, 2007). The soil modification process usually occurs in a matter of hours.

2.2.2.3 Soil stabilisation

After the development of ionic exchange and flocculation reactions, and if there is an excess of the lime in the soil, other reactions may occur yielding cementitious materials and leading to the stabilisation of the soil. The highly pH, above 12, provides conditions for releasing silica and alumina of the clay particles (Rajasekaran, 2005). These materials, also called pozzolans, are able to react with the calcium ions (Ca^{2+}) from the lime to form other compounds, such as calcium aluminates hydrates (CAH) and calcium silicates hydrates (CSH) (Millogo *et al.*, 2008), which are products similar to those formed with Portland cement. Typically, these are slow reactions since the lime needs to diffuse through the soil and break the clay particles, so as to come into contact with the silica and alumina. These reactions occur while there is calcium ions (Ca^{2+}), silicates and aluminates available. The released compounds form a matrix which contributes to an increasing in strength and stiffness of the soil (Al-Mukhtar *et al.*, 2012). In the process of forming this matrix soil undergoes a transformation, from a loose material into a relatively hard impermeable material, with a higher load capacity. This improvement process of the mechanical properties starts in a few hours but can take many years, as reported by De Bel *et al.* (2010).

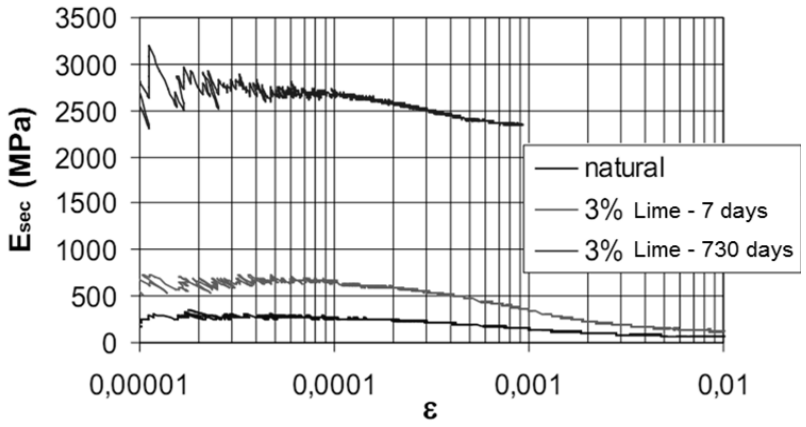

Figure 2.4. Secant modulus degradation curve of a soil and a lime treated soil (De Bel *et al.*, 2010)

Lime carbonation is a reaction that occurs in the presence of carbon dioxide and may occur when lime is exposed to air or carbon dioxide exists within the mixture, forming calcium carbonate. As a result of carbonation, lime reactivity decrease due to the reduction of lime quantity available. Furthermore carbonation may occur through

chemical modification of clay materials, mainly due to the reaction of carbonate or bicarbonate ions with calcium ions available in the minerals. Calcium carbonate is a material with weaker mechanical properties, with high plasticity, interferes with the development of the cementation reactions and its presence precludes the achievement of higher mechanical strengths (Cristelo & Jalali, 2007).

Is known, that the curing temperature can have a dramatic effect on soil-lime reactions, since higher temperatures accelerate the curing, although lower temperatures slow these (Bell, 1996). So, it can be recognised the importance of the knowledge of the temperature influence on the soil-lime reactions and the resulting development of the mechanical properties. This knowledge can have particular importance in the modification reactions predominant in the first days of curing, namely when these materials are subject to loads since early ages. As example of application can be mentioned the road foundations, which can be subject to loads after 3 to 7 days of curing due to the construction traffic (Rao & Shivananda, 2005).

2.3 GENERAL BEHAVIOUR OF STIFFNESS OF SOILS

In terms of elasticity theory, the general three-dimensional form of Hooke's law of elasticity relates strains and stresses by a compliance matrix [C] comprising 36 coefficients C_{ij} in the form presented on Equation (2.5).

$$\begin{bmatrix} \varepsilon_{xx} \\ \varepsilon_{yy} \\ \varepsilon_{zz} \\ \gamma_{yz} \\ \gamma_{zy} \\ \gamma_{xy} \end{bmatrix} = \begin{bmatrix} C_{11} & C_{12} & C_{13} & C_{14} & C_{15} & C_{16} \\ C_{21} & C_{22} & C_{23} & C_{24} & C_{25} & C_{26} \\ C_{31} & C_{32} & C_{33} & C_{34} & C_{35} & C_{36} \\ C_{41} & C_{42} & C_{43} & C_{44} & C_{45} & C_{46} \\ C_{51} & C_{52} & C_{53} & C_{54} & C_{55} & C_{56} \\ C_{61} & C_{62} & C_{63} & C_{64} & C_{65} & C_{66} \end{bmatrix} \begin{bmatrix} \sigma_{xx} \\ \sigma_{yy} \\ \sigma_{zz} \\ \tau_{yz} \\ \tau_{zy} \\ \tau_{xy} \end{bmatrix} \quad (2.5)$$

For an anisotropic material (which the elastic properties depends on the direction) the number of independent coefficients can be reduced from 36 to 21, since $C_{ij} = C_{ji}$ (Love, 1927). Given the complexity of subsurface geometry and the spatial variability of geo-materials, the determination of these coefficients is beyond the reach of practical soil mechanics (Clayton, 2011). So, in geotechnical engineering it is common to

consider identical soil properties in at least one direction, thus assuming transverse isotropy or cross-anisotropy. For a transversely isotropic material, where the plane of isotropy is horizontal, the relationship between strain and effective stress increments can be expressed as presented on Equation (2.6), where:

E'_v is the Young's modulus for loading in vertical direction;

E'_h is the Young's modulus for loading in horizontal direction;

ν'_{vh} is the Poisson's ratio for horizontal strain due to vertical strain;

ν'_{hh} is the Poisson's ratio for horizontal strain due to horizontal strain in the normal direction;

G'_{hv} is the Shear modulus in the vertical plane;

G'_{hh} is the Shear modulus in the horizontal plane.

$$\begin{bmatrix}\Delta\varepsilon_{xx}\\ \Delta\varepsilon_{yy}\\ \Delta\varepsilon_{zz}\\ \Delta\gamma_{yz}\\ \Delta\gamma_{zy}\\ \Delta\gamma_{xy}\end{bmatrix} = \begin{bmatrix} \frac{1}{E'_h} & -\frac{\nu'_{hh}}{E'_h} & -\frac{\nu'_{vh}}{E'_v} & & & \\ -\frac{\nu'_{hh}}{E'_h} & \frac{1}{E'_h} & -\frac{\nu'_{vh}}{E'_v} & & & \\ -\frac{\nu'_{hv}}{E'_h} & -\frac{\nu'_{hv}}{E'_h} & \frac{1}{E'_v} & & & \\ & & & \frac{1}{G'_{hv}} & & \\ & & & & \frac{1}{G'_{hv}} & \\ & & & & & \frac{1}{G'_{hh}} \end{bmatrix} \begin{bmatrix}\Delta\sigma'_{xx}\\ \Delta\sigma'_{yy}\\ \Delta\sigma'_{zz}\\ \Delta\tau'_{yz}\\ \Delta\tau'_{zy}\\ \Delta\tau'_{xy}\end{bmatrix} \tag{2.6}$$

As result of the relations presented on Equations (2.7) and (2.8), the seven parameters on Equation (2.6) correspond to only five independent elastic parameters.

$$G'_{hh} = \frac{E'_h}{2(1+\nu'_{hh})} \tag{2.7}$$

$$\frac{\nu'_{hv}}{E'_h} = \frac{\nu'_{vh}}{E'_v} \tag{2.8}$$

However, despite the anisotropic or the cross-anisotropic behaviour of soils, the most commonly assumed behaviour in practical geomechanics is probably the isotropic linear elasticity (Clayton, 2011). The assumption of isotropic elasticity has the merit of simplicity, as the characterisation of an isotropic elastic solid requires the determination of only two material parameters, from four possible measurements: Young's modulus E, Poisson's ratio υ, shear modulus G and constrained modulus M. The relation between these four properties is presented on Equations (2.9) and (2.10).

$$E = M \times \frac{(1+\upsilon)(1-2\upsilon)}{(1-\upsilon)} \tag{2.9}$$

$$E = G \times 2(1+\upsilon) \tag{2.10}$$

Before the 1970s, one of the major problems in ground engineering was the apparent difference between the stiffness of soils measured in laboratory tests and those back-calculated from observations of ground movements (Burland, 1979). In the past 40 years these differences have been largely reconciled through the understanding of the soil stiffness and the important influence of non-linearity. The maximum strain at which soils exhibit almost fully recoverable behaviour is found to be very small, around 10^{-6}, and is believed to be a fundamental property of all types of geotechnical materials including clays, silts, sands, gravels, and rocks (Benz, 2007), for drained and undrained loading conditions (Presti *et al.*, 1996) and under static and dynamic loading (Burland, 1989). However, some studies shown linear elastic behaviour within the range of 10^{-5} (Biarez *et al.*, 2005). With increasing strain, soil stiffness decays non-linearly and, on a logarithmic scale, stiffness-strain curves exhibit a characteristic S-shape. Figure 2.5 illustrates a typical stiffness-strain curve for soil and includes typical ranges of strain for laboratory testing and for structures.

By definition strains smaller than the limit of classical laboratory testing of 10^{-3}, as triaxial or oedometer tests without special instrumentation, are termed as small strains and strains above this limit are named as large strains. The limit of classical laboratory testing is of the same magnitude of characteristic shear strains that can be measured near geotechnical structures. However, the soil stiffness that should be used in the analysis of geotechnical structures is not the one that relates to these final strains. Instead, very

small-strain soil stiffness and its non-linear dependency on strain amplitude should be properly taken into account in all analysis that strive for reliable predictions of displacements (Benz, 2007).

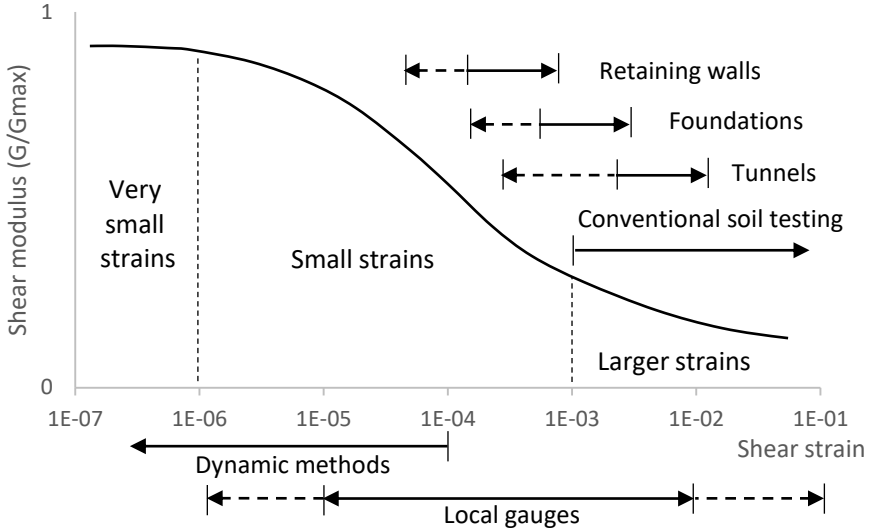

Figure 2.5 - Non-linear characteristic stiffness-strain behaviour of soil with typical strain ranges for laboratory tests and structures (after Atkinson & Sallfors, 1991, Mair, 1993)

The non-linear behaviour with strain leads to the definition of different deformability moduli. Thus, in contrast to other materials which only the elastic modulus is relevant to characterize the material, for the soils there is the need to define the intended modulus associated to the respective strain and stress levels (Gomes Correia, 2004). Figure 2.6 shows the typical moduli used in geomechanic engineering, where:

E_{max} is named as the maximum secant E-modulus or dynamic modulus and usually corresponds to strain levels lower than 10^{-5};

E_{sec} is the secant E-modulus associated to a given strain level;

E_{tan} is the tangent E-modulus associated to a given stress-strain point (A);

E_{eq} is the unload-load E-modulus and must be associated to a given strain amplitude.

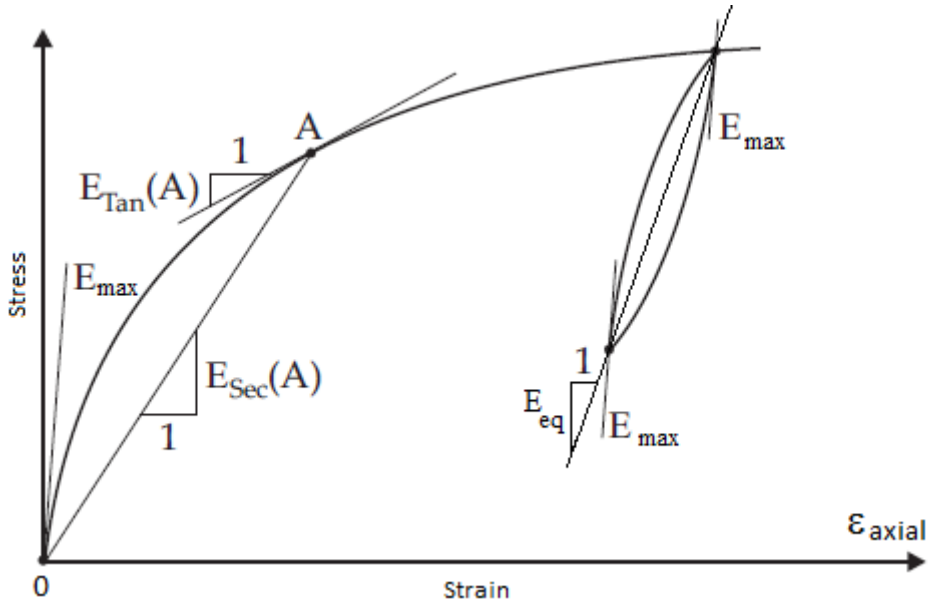

Figure 2.6. Definition of secant and tangent moduli (adapted from Benz, 2007)

2.4 STIFFNESS DETERMINATION OF STABILIZED SOILS

For many years, the main parameter used in the design of roads and railways was the strength properties of the support layers. This type of design was based primarily on empirical parameters based on the failure of soil specimens determined in laboratory conditions, such as the California Bearing Ratio (CBR), Soil Support Value (SSV) and Hveem R value (Puppala, 2008). Nevertheless, in view of its relevance for the actual service life of structures using stabilised soil, stiffness (or deformability) is considered to be of utmost importance (Puppala, 2008, Atkinson, 2000). Presently, it is generally recognised that the rupture of these structures usually is not due to the strength properties of the material and the design of these structures is now based on deformability parameters as the E-modulus (Puppala, 2008, LCPC-SETRA, 2000). However, it is more difficult to characterise the deformability the than compressive strength (Gomes Correia *et al.*, 2009b, Atkinson, 2000, Verbrugge *et al.*, 2011), mainly due to the non-linear behaviour of soils.

According to the technical guides *Réalisation des Remblais et des Couches de Forme* of SETRA-LCPC (2000), *Design Manual for Roads and Bridges* of Highways England (2015) and the *Guide for Design of Pavement Structures* of AASHTO (1993), the main

parameter used for structural design and performance evaluation of road and railway foundations is the reversible deformation modulus (E-modulus). In fact, according these guides the E-modulus is the main parameter to define the classes of subgrades. Given the importance of the E-modulus in the design of railway pavements and roads, this is one of the parameters to be determined in the quality control of stabilized soils processes (AASHTO, 1994). The knowledge of its evolution from the time of execution of the mixture and during the curing process, is of special interest for predicting the stress-strain behaviour since the early ages of the mixture.

There are several techniques that can be used to access the deformability properties of soils in laboratory or *in-situ*. The most advantage of laboratory methods is the possibility to conduce testing under controlled conditions, which is useful to perform parametric studies and to identify the effects that influence a given property. The main disadvantages of these methods usually include: the size of the specimen that may not be sufficiently representative of the in-situ soil; the difficulty to reproduce the site conditions by the laboratory equipment; the degree of disturbance of the soil sample during the sampling process. The main advantage of in-situ or field testing methods is that the tested material is under the real condition. However, it is impossible to control external conditions and the stress state, and the effect of each factor cannot be separated to study individually their influence. The heterogeneity of soils in field produces complex results that must be interpreted by experienced professionals that usually use complex and indirect approaches.

2.4.1 Unconfined compression testing

The uniaxial compression (UC) testing with local measurement of deformation consists of applying a compressive stress to a specimen of the tested material, which progressively increases with a well-defined increment rate, in a particular direction. The load value applied and displacements locally measured in the tested specimen (Figure 2.7) are recorded at each instant. The determination of E-modulus is then made from the observed stress-strain relationship. The local deformation measurement is important in order to allow to obtain the E-modulus in the range from very small to small deformations. In this type of technique it is possible to conduct destructive testing, if the stress values reach values that cause yielding or rupture of the tested material, or non-

destructive testing with load and unload cycles (usually named as unconfined cyclic compression, UCC, testing), by subjecting the specimens to stress that does not exceed the values on which the material has elastic behaviour (Silva, 2010).

The use of this technique for stiffness determination of soils, particularly in the range of small deformations, requires the measurement of displacement performed locally on the specimen using the instrumentation of high precision (Correia, 1985). Some of the most used transducers in laboratory for local deformations measurement are the Local Deformation Transducers (LDT), the Linear Variable Differential Transformer (LVDT) and Hall effect transducers (Correia, 1985).

As the LVDT was the transducer used to measure displacements during UCC tests in the scope of the present work its operating principle is here briefly described. The Linear Variable Differential Transformer (LVDT) is a linear displacement transducer that works through the principle of mutual inductance. The main elements are three coils, one primary and two secondary, and a mobile core of high magnetic permeability. By applying an electric current in the primary coil some electrical tension is induced in the secondary coils producing an electrical signal proportional to the position of the core relatively to the coils. The electrical tension in the secondary coils is related, via a linear relationship, with the deformation suffered by the specimen. Due to the operating principle of LDT, they are less sensitive to effects of temperature variation and electric noise, as compared with resistive type transducers. They also have great stability in the output signal and to measure accurately a wide range of deformation, allowing the measure of deformations in the order of 10^{-6}. The main disadvantage is related to the difficulty of fixing to the specimen due to its weight.

The first fixing system to be developed for the LVDTs, and still widely used, is a pair of rings that supports simultaneously all the LVDT's (Figure 2.7a). Some other fixing systems were developed in order to make easier the use of LVDT’s: one using an independent fixation on the specimen (Figure 2.7b), other using the individual rings for each transducer and a third one that uses springs (Reis Ferreira, 2003, Gomes Correia *et al.*, 2006). Nevertheless, as the ring system works as a set there is a possibility that it interferes with the material when the specimens are subject to deformations above very small to small range. This phenomena is not an issue for the other three fixing systems as each LDVT is individually attached to the specimen allowing its use in all range of working.

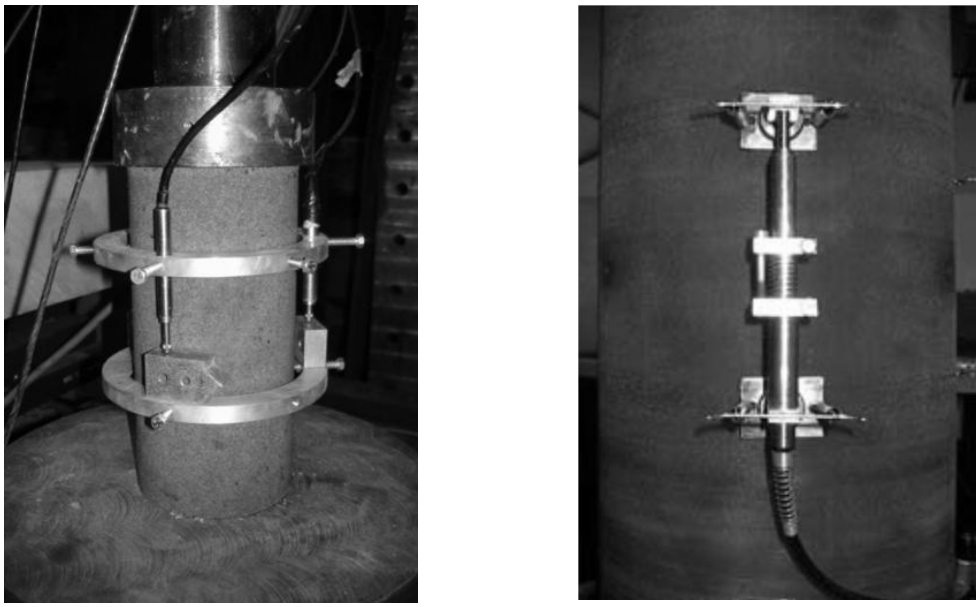

a) b)

Figure 2.7. LVDT's fixation systems: a) support rings (Silva, 2010); independent fixation on the specimen (Gomes Correia *et al.*, 2006)

2.4.2 Wave based techniques

The testing methods based on the transmission of ultrasonic waves are supported by the principle that the ultrasonic wave propagation velocity dependent on the density and elastic properties of the propagation medium (Meyers & Chawla, 2008). The physical principle of operation of these methods consists in to generate a wave in one face of a specimen and measuring propagation time over a known distance. Thus, these techniques can be used to determine the physical and mechanical properties of the soil (Christ & Park, 2009, Stephenson, 1978) as well as cementitious materials (Voigt *et al.*, 2006, Wang & Subramaniam, 2011, Khan *et al.*, 2006).

These methods can be used with recourse to the propagation of compression waves (P) and / or shear waves (S). If the propagation velocity of these two types of waves is known is possible to determine certain mechanical properties (Christ & Park, 2009), particularly the dynamic elastic modulus and Poisson's ratio, using the equations (2.11) and (2.12), where E is the dynamic elastic modulus, Vp and Vs are the propagation

velocities of compression and shear waves, respectively, ρ is the density and ν is the Poisson ratio.

$$E = \frac{\rho V_s^2\left(3V_p^2 - 4V_s^2\right)}{V_p^2 - V_s^2} \tag{2.11}$$

$$\upsilon = \frac{V_p^2 - 2V_s^2}{2\left(V_p^2 - V_s^2\right)} \tag{2.12}$$

Since the determination of E by this technique requires the information of the propagation velocities of P and S waves its application can become complex. One reason of this is that the sensors used only work with one type of wave, leading to the need to duplicate the test equipment. In the cases when the P-wave propagation velocity is determined, and if the Poisson's rate is not known, it is only possible to determine the constrained modulus (M) via of Equation (2.13). If it is possible the determination of the Poisson's ratio, E can be obtained from equation (2.9).

$$M = \rho \times {V_p}^2 \tag{2.13}$$

If only the S-wave propagation time is measured is possible to compute the propagation velocity of this wave which is directly related to the shear modulus (G). Equation (2.14) can be used to access the G-modulus of the material, where V_s is the propagation velocity of shear waves. If the information of Poisson's ratio υ is available, the elastic modulus Ecan be computed using Equation (2.10).

$$G = \rho \times {V_s}^2 \tag{2.14}$$

2.4.2.1 Ultrasonic pulse velocity (UPV)

The UPV transmission has been used in several works (Voigt *et al.*, 2006, Christ & Park, 2009, Khan *et al.*, 2006) and is schematic presented on Figure 2.8. In this type of application a wave transmitter transducer is placed on one side of a specimen of the tested material and a receiver is placed on the opposite side. A function generator emits a signal that is transmitted to the sample through the transmitting transducer. The wave passes through the sample to be detected by the receiver transducer. Usually these signals operate on a fixed frequency between 20 kHz to 1 MHz. The received signal is amplified for easier identification. The wave propagation time is then determined by the delay between the emitted wave and received wave (RILEM, 2011).

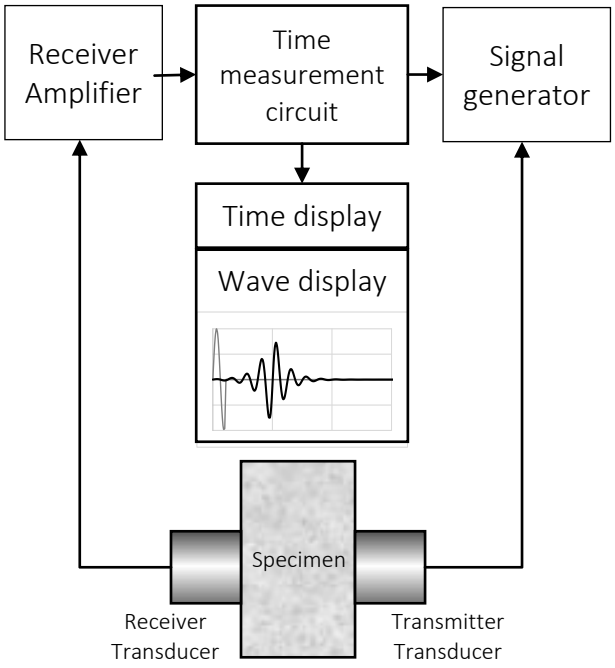

Figure 2.8. Ultrasonic pulse velocity application scheme (adaped from ASTM, 1991)

The correct determination of the wave propagation time is essential to the accuracy of this method. However, often this determination is a matter of difficult resolution, making the analysis time consuming and somewhat imprecise. The manual interpretation of the observed data is accompanied by some uncertainty in determining the time of arrival of the transmitted wave and depends of the operator sensitivity. The application of automatic interpretation algorithms can reduce the analysis time and increase the precision of the readings but the need for use of frequency control parameters can significantly affect the quality of the automatic estimation (Reinhardt &

Grosse, 2004). The need of using two different types of transducers, one for one for P waves and other for S waves, may increase the time and cost of the technique application. Aside these limitations, it is a non-destructive method with some simplicity in application and some previous works have shown the potential to use on the assessment of the properties of stabilized soils (Khan *et al.*, 2006).

2.4.2.2 Bender-extender elements

The "bender-extender elements" consists of a pair of piezoceramic plates rigidly connected to a central metallic plate and to electrodes in the outer faces (Ferreira, 2009). The "bender elements" are transducers that generate shear waves (S-waves) during its deformation. In case of "extender elements" deformation occurs along the extension of the transducers and compression waves (P-waves) are generated. When subjected to an electric signal variation the "bender-extender element" bends or deforms generating a wave that propagates in the mean in which it is inserted. On the other hand, a "bender-extender element" has the ability to detect movements and convert them into an electrical signal (Figure 2.9).

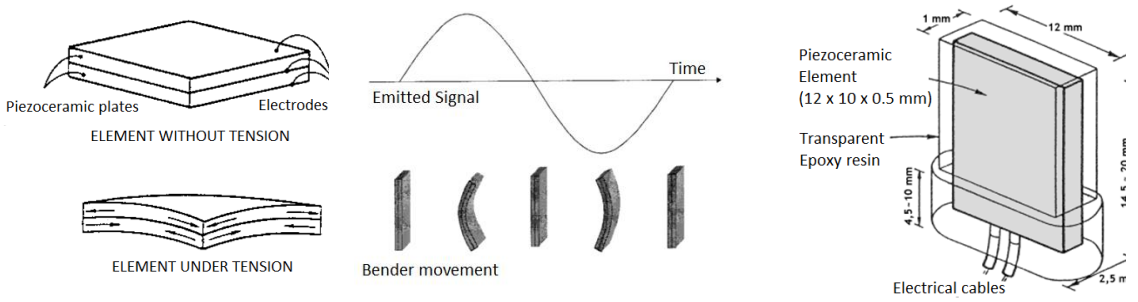

Figure 2.9 - B*ender-extender elements* (Ferreira, 2009): a) effect of an electric tension; b) scheme of the movement under a sinusoidal excitation; c) classical model proposed by Dyvik and Madshus (1985)

The main advantages of this methodology are the low cost, the low deformation imposed (from 10^{-7} to 10^{-5}) to the specimens and allow the stiffness measurement of materials by a non-destructive way. The disadvantages of these transducers are related to the uncertainty of measurement of distance and propagation time of the waves. There are some doubts about the distance to be considered for the propagation path of the waves, but some studies (Dyvik & Madshus, 1985, Viggiani & Atkinson, 1995) have

shown that the distance between the transducers must be considered. There are several factors that can cause some interference in the determination of the propagation time, as the ambient noise, the reflection of the waves at the specimen bounds and other phenomena associated with the generation and propagation of the wave. Another disadvantage is related to the need of the penetration of the transducers in specimens that may cause localized disturbances in the attaching zone (Gomes Correia *et al.*, 2006).

2.4.3 EMM-ARM: Elasticity modulus measurement through ambient response method

Recently, a technique called EMM-ARM (Elasticity Modulus Measurement through Ambient Response Method) has been developed for the continuous assessment of concrete/cement paste E-moduli since the instant of casting (Azenha *et al.*, 2010, Azenha *et al.*, 2012a), with the capability of being used for both laboratory and *in situ* measurements. This technique requires placing freshly mixed material to be tested inside a mould of known geometry, mechanical properties, and support conditions (e.g., a simply supported acrylic tube). Through continuous monitoring of the resonant frequency of the composite beam, which does not need to be externally excited, as ambient vibrations are sufficient for modal identification, it is possible to apply the dynamic equations of motion to the system and continuously infer the stiffness modulus of the tested material. The performance of this methodology has been demonstrated in a laboratory environment by Azenha *et al.* (2009, 2010) by comparing its results to those obtained through unconfined cyclic compression (UCC) tests. More recent applications have shown that the kinetics of stiffness evolution captured by EMM-ARM is in accordance with that obtained through ultrasound pulse velocity measurements and that mould geometry can be adapted to allow the re-use of moulds (Azenha *et al.*, 2012b). It has been further shown that the EMM-ARM methodology can be successfully used in *in situ* conditions by applying this technique within a pre-fabrication plant (Azenha *et al.*, 2012b). Based on the successful applications of EMM-ARM to concrete, preliminary laboratory experiments have been conducted in sand-cement mixtures, showing that the application of EMM-ARM in this material is feasible (Azenha et al., 2011). However, this preliminary application was limited to the first 7 days of age of the material and lacked the study of prospects for sample collection for *in situ* applications.

The main distinguishing features of EMM-ARM towards existing techniques based on resonant frequency for testing cement-based materials are: it relies on relatively slender specimens and does not require explicit excitation at each testing age, which permits the use of operational (output-only) modal identification techniques (Ren & Zong, 2004, Rodrigues, 2004); no handling of the specimen is necessary throughout the entire testing time, thus allowing continuous testing from the instant of placement in the mould, which is a significant advantage in the particular case of testing fresh cementitious mixes before its setting time. Additional information concerning the state of development of EMM-ARM is provided in subchapter 3.3.

2.4.4 Other techniques for stiffness assessment

There are other several testing techniques that can be used for the assessment of the stiffness properties of soils. Here is presented some of the main techniques used, in laboratory or *in-situ*:

- Triaxial testing is a laboratory equipment that allows the mechanical characterization (i.e. the determination of the mechanical parameters) of geotechnical materials for the linear and non-linear modelling of its behaviour. This category includes the standard triaxial, cyclic shear, torsional shear and hollow cylinder apparatuses. The development of laboratory techniques and equipment and the diffusion of automation in control and data acquisition has increased the capability of performing reliable laboratory tests under a generalised state of stress.
- The resonant column is a laboratory equipment used to determine the dynamic properties of soil specimens (Camacho-Tauta, 2011). Depending on the type of properties to be determined, the device can apply either axial force or torsion. The E-modulus and the associated damping ratio are obtained when the system vibrates under axial force, while shear modulus and shear damping ratio are obtained when the equipment induces torsion to the specimen. The types of resonant-column devices are usually classified by the boundary conditions at the end of the specimen. Those boundary conditions impose different shapes of vibration and, at the same time, are necessary to apply external loads, stresses and to measure pore pressure and volume changes.

2.5 DISCUSSION OF STIFFNESS EVALUATION

Typical laboratory techniques, such as unconfined compression tests with local strain measurement, triaxial tests (Gomes Correia *et al.*, 2006, Goto *et al.*, 1991, Ajorloo *et al.*, 2012, Dano *et al.*, 2004, Jardine *et al.*, 1984) and resonant column tests (Clayton *et al.*, 2010, Stokoe & Santamarina, 2000) are used for the determination of stiffness properties. For practical reasons, these techniques usually have limited applicability in stabilised soils at very early ages, as specimen testing requires handling, instrumentation and loading/excitation. Therefore, measurements are usually taken at discrete instants of time, e.g., after 7, 28 and 90 days of curing. Recently, the use of techniques based on wave propagation, such as ultrasonic contact-probes (Amaral, 2009, Dimter *et al.*, 2011, Yesiller *et al.*, 2001), bender-extender elements (Ferreira, 2009, Viana da Fonseca *et al.*, 2009c, Rios Silva *et al.*, 2009, Ferreira *et al.*, 2011, Arroyo *et al.*, 2006, Arroyo *et al.*, 2003) and impact response testing (Toohey & Mooney, 2012) has increased. Wave-based measurements are a practical, non-destructive, frequently non-invasive, and cost-effective means of determining the small-strain stiffness of soils. Given the particulate nature of soils, wave techniques present unique advantages for studying these materials without affecting their fabric or structural equilibrium and inherent mechanical properties (Ferreira, 2009, Fam & Santamarina, 1995). However, these techniques present limitations in the interpretation of results, not only due to the non-homogeneity and natural variability of the tested materials but also because of signal interpretation ambiguities of the received waves (Ferreira, 2009, Viana da Fonseca *et al.*, 2009c, Amaral *et al.*, 2011, Ferreira *et al.*, 2011).

Another important issue in soil improvement is quality control after treatment. *In situ* assessment of mechanical properties, namely stiffness, is therefore necessary to confirm that the performance requirements of the stabilised soil have actually been met. Among the most common used techniques for in-situ assessment of the stiffness of cement-stabilized layers, the following methods can be highlighted: the plate load test (Gomes Correia *et al.*, 2004), the light falling weight deflectometer (Benedetto *et al.*, 2012, Alshibli *et al.*, 2005) and the Humboldt stiffness gauge (Gomes Correia *et al.*, 2009a, Abu-Farsakh *et al.*, 2004).

For the *in situ* measurement of wave propagation velocities, a number of geophysical methods are available, some of which are among the oldest techniques of soil surveying

and profiling (Rayleigh, 1885, Love, 1892). These methods largely preceded the laboratory developments, and different setups and configurations have been devised over the years (Stokoe & Santamarina, 2000). The most frequently used methods are surface reflection, surface refraction and surface wave, which are non-intrusive methods, and cross-hole, down-hole and seismic cone penetrometer testing, which are intrusive methods (Stokoe & Santamarina, 2000).

EMM-ARM distinguish from the existing techniques mainly by allowing a continuous quantitative measurement of the E-modulus since very early ages without explicit excitation and handling of the specimen during the entire testing time. However, in previous applications of this methodology to stabilized soils, the material being tested needed to be placed and compacted directly in the mould (reconstituted specimens), which may raise issues in assuring the same compaction level as that of the actual *in situ* compacted layer. Additionally, this methodology is exposed to contaminations of the ambient random noise that can raise difficulties during the measurements. In fact, the overcoming of these limitations is one of the main objectives of the present thesis. Nevertheless, this methodology provides early knowledge of stiffness development of treated materials allowing early decision-making about compliance with the design speciation, which can result on technical and economical benefits.

2.6 SAMPLING

The microstructure have a major influence on the mechanical behaviour of stabilized soils. Therefore, the laboratory characterization of the mechanical properties must ensure the same conditions found in-situ on the stabilized materials. Although there are testing techniques that allow the in-situ determination of these mechanical properties an alternative approach is the sampling of undisturbed samples. For this, here is made a brief reference to sampling in soils and rocks to support the sampling technique proposed in this research for stabilized soils.

2.6.1 General considerations

The main objective of sampling operations is to obtain soil or rock samples representative of the ground from which they are taken either for description or

laboratory testing (Clayton *et al.*, 1995). The samples should be large enough to contain representative particle sizes, fabric, fissuring and fracturing and be obtained in such a way that they have not lost fractions of the sampled material (for example, coarse or fine particles of soil). It is usually considered adequate to take samples which have a minimum dimension of the order of 5 to 10 times the maximum particle size of the soil (Clayton *et al.*, 1995).

Samples are generally classified as disturbed and undisturbed. Disturbed samples contain all mineral constituents of the layer without contamination of other material but might not be representative of the state of water content or micro-structure (Nagaraj, 1993) and usually are obtained by drilling processes. Undisturbed samples are those which are obtained with the minimum disturbance to the in-situ conditions (Marcunson III & Franklin, 1979). Undisturbed samples are generally taken by cutting blocks of soil or rock, or by pushing or driving sampling tubes into the sampled soil. The type of the collected sample must be selected depending of the type of testing envisaged. Collecting undisturbed samples is particularly relevant when is intended to evaluate the mechanical properties of the soil such as the strength and the deformation modulus.

In general, soil samples can be obtained in shallow pits, shafts and exposures, and in boreholes, using either drive or rotary techniques. Drive samplers typically have tubular geometry and a sharp cutting edge at their base. These type of samplers are pushed into the soil without rotation and can cause displacement of the soil as they penetrate. Rotary samplers, also known as ‘corebarrels’, have a relatively thick and blunt cutting edge with inclusions of a very hard material. These types of samplers are rotated and pushed downwards cutting the soil.

2.6.2 Types of sample disturbance

The availability of engineering parameters for geotechnical design representative of the studied material depends not only on careful testing but also on the level of disturbance of the tested samples. As described by Baligh *et al.* (1987), the sampling process and specimen preparation for laboratory testing may result in a hypothetical stress path applied to the centre-line of the sample as shown in Figure 2.10. Sample disturbance can then occur at each of the stages shown in this figure due to: (a) changes in soil conditions ahead of the advancing borehole during drilling operations; (b) penetration of

the sampling tube and sample retrieval to ground surface; (c) water content redistribution in the tube; (d) extrusion of the sample from the tube; (e) drying and/or changes in water pressures; and (f) trimming and other activities required to prepare specimens for laboratory testing. Changes in stress condition occurs by reduction of the total horizontal and vertical stress, which can become from their in situ value to zero and can affect the structural bonding inside the soil specimen.

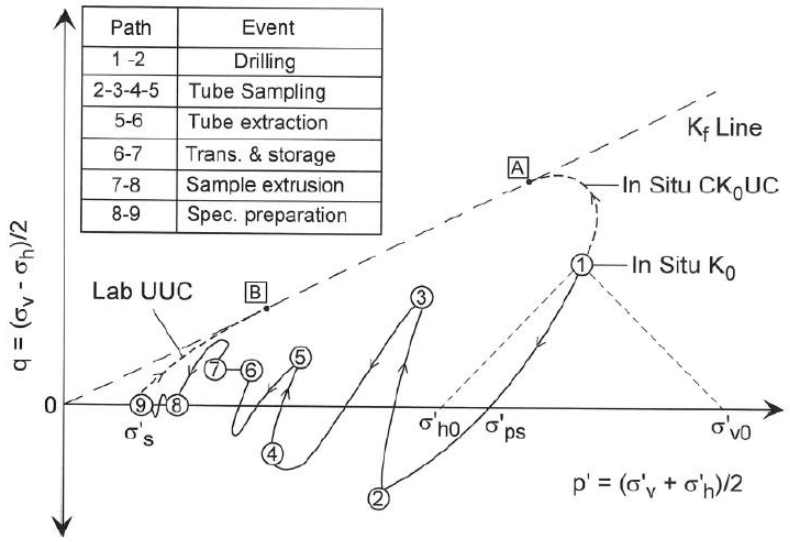

Figure 2.10. Hypothetical stress path during tube sampling and specimen preparation on the centre-line element of a clay (Ladd & DeGroot, 2003)

Mechanical deformations consists on shear distortions suffered by the soil sample during the sampling process with tube sampling. Changes in water content can occur due to swelling or consolidation of the soil sample, or a redistribution of moisture due to pore-pressure gradients. Chemical changes may occur in the pore water or the soil resulting from contact with drilling fluid or with sampling devices (Clayton *et al.*, 1995). Additional disturbances can be significant in special applications, as the expansion of dissolved gases when very deep offshore samples are brought to the surface; dynamic effects in hammered samples or during rough handling and transportation; temperature changes in chemically or biologically active deposits (Clayton *et al.*, 1995).

As mentioned before, these disturbance mechanisms can occur at different stages of sampling process with different velocities: some occur very quickly and others can take substantial time. Even some types of disturbance are unavoidable it can be minimized

when the mechanisms of disturbance are understood and the sampling process is optimized. The importance of a particular type of disturbance will depend not only upon the sampling processes being used, but also upon the type of soil being sampled. However, the stress condition of a soil sample is inherent to the sampling process. The main mechanisms of disturbance in soil sampling process are: changes in stress condition , namely stress relief, that is inevitable during the sampling process; the swelling that occurs as consequence of stress relief (Hopper, 1992); compaction, remoulding and displacement (depth affected can be up to three times the hole diameter) (Hvorslev, 1949); base heave, piping and caving as severe effects resulting of stress relief (Hight & Burland, 1990).

2.6.3 Sampling methods to obtain undisturbed samples

2.6.3.1 Block sampling

In block sampling the sample is cut from the ground, by trimming the soil with a sharp blade either from the base or side of a trial pit, or as part of a rotary drilling process. Traditionally block samples have been obtained from pits, but carefully controlled rotary drilling, or the use of the Sherbrooke samplers, aims to achieve a similar result. Despite the stress relief and swelling, the block sampling is the method that involves less disturbance, due to the fact that the soil is not subject to shear distortions. This method is also considered to be a reference in sampling (Siddique *et al.*, 2009). Excavation of a pit can be an economical way of acquiring a very detailed record of the complex soils conditions. Although, in some conditions, such as in normally and lightly over-consolidated clays, the excavation of a pit or shaft with more than a few meters is often impossible (Clayton *et al.*, 1995). The Sherbrooke sampler is a sampling device that can be used to overcome the problem to get block samples at greater depths. This equipment only requires a borehole of 40 cm diameter and has a trimming mechanism that cuts the soil. In this technique the sampler is lowered to the base of the hole using a mechanically-induced or electrically-induced rotation. A cylinder of about 250 mm in diameter is carved out by 3 circumferential blades at the base. Despite allowing high quality samples the process is complex and time-consuming.

2.6.3.2 Tube sampling (drive samplers)

Essentially, tube sampling consists in to pushing or hammering a tube into the ground without rotation. As result of the sampler movement soil can be displaced and distorted. This displacement introduces shear distortions into the ground that change the effective stress and the structure of the soil. In order to minimize these distortions is vital an appropriate design of the sampler. The characteristics of the tube samplers are related to the quality of the sample, therefore, it is important to consider its dimensions in the selection of the tube sampler to further obtain better sampling quality. The parameters used for design usually are the area ratio, diameter to thickness ratio, the cutting edge taper angle, the lid ratio, and inside clearance. The recommended values for these parameters results of empirical knowledge and field experience. In addition to the sampler geometry, the sample driving methods have a significant effect on the quality of the sample that is collected.

2..6.3.2.1 Area ratio

The area ratio, AR, (ASTM D1587 (2008)) is one of the most critical indexes when the disturbance potential of a sampler is evaluated. This parameter is defined by Equation (2.15), where D_e is the external diameter of the sampler cutting edge and D_i is the internal diameter of the sampler cutting edge, as presented on Figure 2.13. To minimize the soil disturbance low values are recommended for this parameter, preferably under 10% as prescribed by ASTM D1587-08 (ASTM, 2008). However, a very small AR implies a very thin sampler wall which will result in lower strength of the sampler. Some recommended values for AR are presented in Table 2.1.

$$AR = (D_e^2 - D_i^2)/D_e^2 \tag{2.15}$$

2..6.3.2.2 Diameter to thickness ratio

Another parameter used to evaluate the sample disturbance is the relation D_e/t: external diameter (B) to thickness (t) of the sampler. Through numerical analysis, (Clayton *et al.*, 1998) were able to estimate the strain caused by sampling along the sampler for

different B/t values, as presented in Figure 2.11. As can be seen, higher values of B/t correspond to less maximum strain and, therefore, better sample quality.

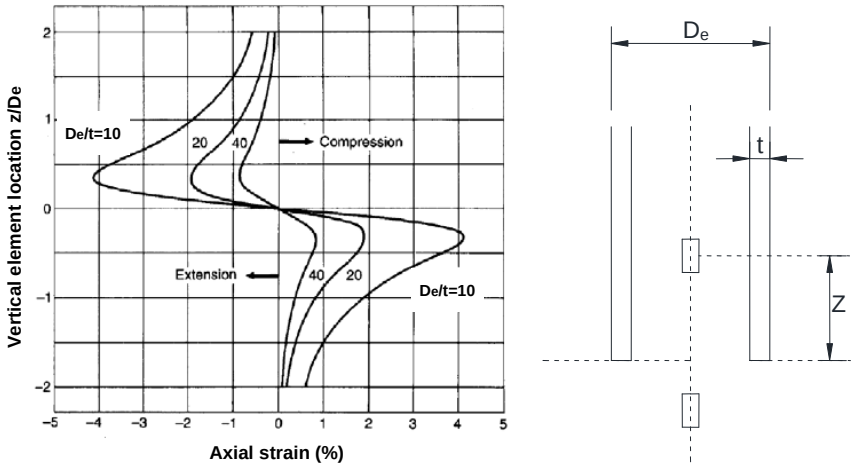

Figure 2.11 - Analytical solutions for axial strain history at the centre-line of a tube sampler for different D_e/t ratio (Clayton *et al.*, 1995)

The results of unconfined compression testing performed by Sidique *et al.* (2009) on samples of high plasticity silty clay collected by "block" and by "tube" samplers with different B/t ratio are presented on Figure 2.12. As can be observed, the "tube" sampling results in a slightly lower compression strength that increases as B/t decreases. The simplicity and precision of this ratio means that can be used in a practical and simple way to estimate disturbances of tube samplers. Values between 40 and 47 for B/t are used in United States practice (Baligh *et al.*, 1987).

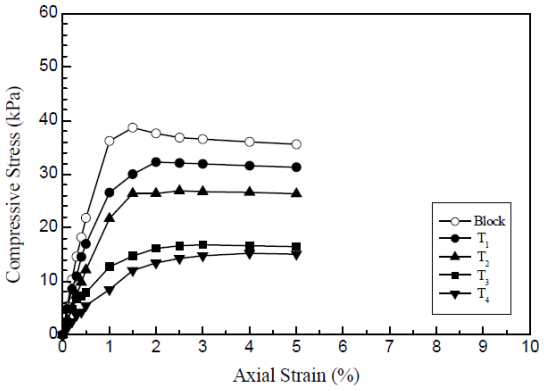

Sampler	t (mm)	D_e (mm)	D_i (mm)	D_e/t Ratio	Area Ratio (%)
T1	1.5	41	38	27,3	16.4
T2	3	44	38	14.7	34.1
T3	4.5	47	38	10.4	53.0
T4	6	50	38	8.3	73.1

Figure 2.12 - Comparison of compressive stress versus axial strain plots of "Block" and "Tube" samples of soft Dhaka clay in unconfined compression test (Siddique *et al.*, 2009)

2..6.3.2.3 Inside clearance ratio and length to diameter ratio

The inside clearance ratio (ICR) is defined by Equation (2.16), where D_s is the inside diameter of the sampler tube and D_i is the inside diameter of the cutting shoe. ICR is used to allow partial swelling and lateral stress reduction of the sample, however it should not allow excessive soil swelling or the loss of the sample when extracting the tube. Although these effects are undesirable, they are less undesirable than the consequences of high adhesion between the soil and the inside of the sample tube. Hvorslev (1949) recommendations suggest an ICR of 0.75% to 1.5% for samplers. Same author recommends that for samplers with internal diameter of 50 mm to 75 mm the maximum length to diameter ratios can be of 5 to 10, for loose to dense cohesionless soils, and 10 to 20, for soft to stiff cohesive soils.

$$ICR = (D_s - D_i)/D_i \tag{2.16}$$

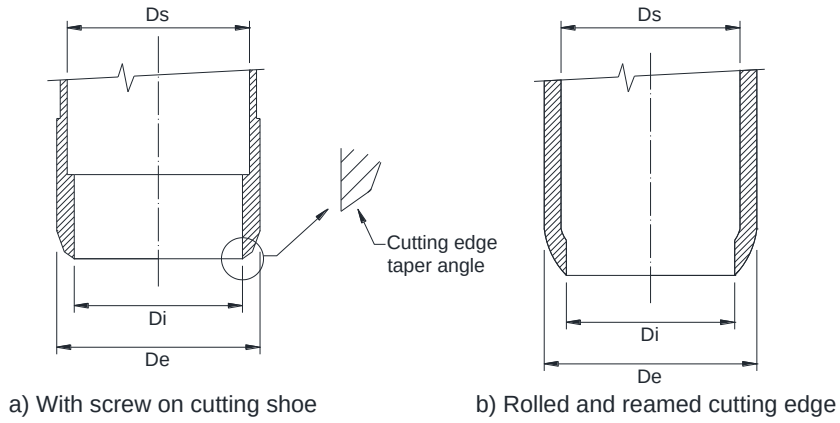

Figure 2.13 – Dimension definition for sampler design

2..6.3.2.4 Outside cutting edge angle

It's known that increasing area ratio will increase soil disturbance, remoulding and penetration resistance. But the use of very small area ratios leads to very fragile sampler tubes which may bend or buckle during driving the sampler into the soil. So, the need

for a large area ratio can be compensated by using a small cutting edge taper angle (OCA) as presented on Table 2.1 (Clayton *et al.*, 1995).

Table 2.1. Recommended area ratio and outside cutting angle (Clayton *et al.*, 1995)

Area ratio (%)	Outside cutting angle (degrees)
5	15
10	12
20	9
40	5
80	4

2..6.3.2.5 Examples of drive samplers

The thin-wall tube, also named Shelby sampler, is frequently used to collect relatively undisturbed samples of cohesive soils for strength and consolidation testing. Typically, these samplers are available in outside diameter between 51 mm and 76 mm and lengths from 700 mm to 900 mm and the test procedure is described in some standards, as the ASTM D 1587 (ASTM, 2008). These samplers can be made of carbon steel, galvanized-coated carbon steel, stainless steel, and brass. It is recommended that the thin-walled tube sampler should be pushed slowly with a single and continuous motion by hydraulic system. After the insertion of the sampler is completed a waiting period of at least ten minutes before collection is required to allow the sample to swell slightly within the tube. Then, the sampler must be rotated through two complete revolutions to shear off the sample and slowly removed from the borehole.

A thick-walled sampler is a sampler whose AR is greater than 20%. Although is a more expensive sampler than a thin-walled, has more strength and is more suitable for harshest soils. The sample retrieved is usually more disturbed than in thinner samplers. The British U100 is one of the most common thick-walled samplers. It has a nominal radius of 100 mm and a length of 450mm, an AR of 27%, that is increased when a liner is used (40%), and an OCA above 20 (Clayton et al. 1995). As these values of AR and OCA are very high a poor quality is expectable for the sample. The sampler is driven into the ground through a slide-hammer (Bell, 2004).

Split barrel samplers are thick-walled samplers which are divided into two halves lengthwise. During the introduction into the soil these are held together by the shoe and head which are screwed on to each end (Clayton et al. 1995). This allows to easily examine and extract samples from the sampler itself as the soil can be retrieved when the sampler is opened. The sampler used during the standard penetration test and the modified California sampler are examples of split barrel samplers. This type of sampler has a very high area ratio, it is used primarily with sand and gravels, and it has be acknowledged to collect disturbed samples well suited for soil identification and classification purposes (Briaud, 2013).

The piston sampler is essentially a thin-wall tube sampler with a piston, a rod and a modified sampler head. This type of sampler, that includes the Osterberg or Hvorslev sampler, can be used in stiff soils but is particularly useful for sampling soft soils where sample recovery is often difficult. The probability of obtaining a satisfactory samples is high when using this type of samplers. The fixed piston helps prevent the entrance of excess soil at the beginning of sampling limiting the swelling and helps the soil enter the sampler at a constant rate during the sampling push. The head on this sampler creates a better vacuum which helps retain the sample better than the ball valve used in thin-wall tube samplers. (Mayne *et al.*, 2002, Clayton *et al.*, 1995)

The Laval sampler is considered to be one of the most effective tube samplers available for sampling soft and sensitive clays. In fact, the quality of the samples of soft and sensitive soil obtained with this sampler is almost the same that can be achieved using block sampling techniques. The device consists of a thin-walled sampling tube mounted on a sampler head, and housed within an external corebarrel. Despite the low disturbance of the samples obtained its use is considered to be expensive, time-consuming and delicate for routine sampling (Clayton *et al.*, 1995).

2..6.3.2.6 Driving methods

Driving a sampler into the soil comprises a load application on the sampler. However, the way the load is transmitted to the sampler will affect the sample quality. In fact, the velocity and continuity of the motion with which the sampler is forced into the soil have a manifest influence on the disturbance of the retrieved sample (Nagaraj, 1993). The sampler can be driven through blows or continuous pushing. Hvorslev (1949) pointed out some driving methods as presented in Table 2.2. The method that induces highest

disturbance to the soil is the one based on blows of a hammer, whereas the method that is less disturbing for the soil is pushing the sampler into the ground at a high and constant speed (Clayton *et al.*, 1995).

Table 2.2. Hvorslev's driving methods (in, Nagaraj, 1993)

Mode	Method	Nature of movement	Remarks
Hammering	Repeated blows of a drop hammer	Intermittent fast motion	Simple but causes disturbance
Jacking	Levers or short commercial jacks	Intermittent slow motion	Reaction frame is required Some disturbance possible
Pushing	Steady force without any interruption	Continuous uniform motion	Simple, disturbance mainly due to inside friction
Single blow	Blow of a heavy drop hammer		Simple, relatively less disturbance
Shooting	Force generated by explosives	Continuous very fast movement	Desirable, least disturbance

In spite of being an easy and cheap method, hammering results in poor quality samples. When the sampler is hammered into the soil, under each blow the sampling tube advances downward, then rebounds slightly. This upward rebound action stresses the soil at the bottom of the sampler in tension and often causes separations. This tension creates a series of tensile fractures/discontinuities between zones of compression (Rogers, 2006). In Figure 2.14 is possible to observe the contrast between hammering and pushing the sampler into the soil. Pushing is considered the best practical method and with the support of instrumentation, as a load cell and a controlled actuator, it is possible to supply a steady downwards force. Indeed, most experienced geotechnical engineers favour this method (Rogers, 2006). In any case the rotation of the sampler for downward movement needs to be avoided to prevent disturbance to the soil (Nagaraj, 1993).

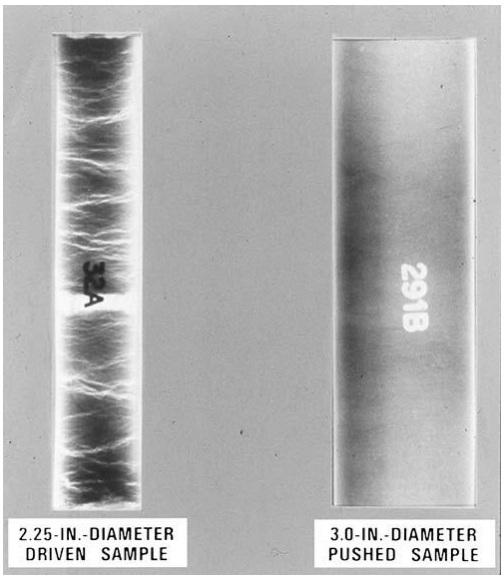

Figure 2.14. X-ray photographs of sampling by hammering (left) and pushed (right) (Briaud, 2013)

2.6.3.3 Rotary samplers

The rotary drilling uses the rotation combined with a downward force on the material and allows retrieving undisturbed samples of rocks. The rotary samplers can be applied to rocks and soils, but are more easily used in intact rocks than in fractured rocks and soils (Clayton *et al.*, 1995). The quality of the samples retrieved by the rotary samplers depends on the sampled material. Usually, is possible to get good samples, however is not suitable for loose cohesionless soils and soft cohesive soils (Marcuson III & Franklin, 1979).

The simplest form of a rotary corebarrel consists, of a single tube with a coring bit at its lower edge which is loaded and rotated while a pressurized fluid passes around the bit (Clayton *et al.*, 1995). In drive sampling, the soil displaced by the walls of the sampler is moved to it vicinities but with the rotary samplers the material is ground up and removed by air, circulating water, or by a drill fluid (Nagaraj, 1993). Samples collected with a single tube corebarrel may experience some disturbances due to torsion, swelling or contamination by the drilling fluid (Murthy, 2002). The modern corebarrels have multiple tubes. A double tube rotary samplers have an outer tube that rotates and an inner tube that remains stationary. Typically, inner tubes are provided with a swivel head that prevents the core from rotating and eroding (Nagaraj, 1993). This type of samplers include the pitcher tube sampler and the Denison corebarrel.

Chapter 3

PRINCIPLES OF MODAL IDENTIFICATION AND STATE OF DEVELOPMENT OF EMM-ARM

3.1 INTRODUCTION

This chapter addresses the state of the art concerning two subjects that are central to this thesis, namely some basic principles of modal identification and the state of development of EMM-ARM. The first part of the chapter addresses the basic principles of modal identification of a single degree of freedom oscillator under ambient excitation (or operational modal analysis: OMA) and forced excitation (experimental modal analysis: EMA). These include the definition and the estimation of frequency response functions (FRFs) from experimental data, as well as several other relevant issues concerning modal identification in the frequency domain. The main reasons for this introductory review on modal identification are two: (i) they facilitate the adequate understanding of the initial state of development of EMM-ARM before the work of this thesis as shown in the second part of the chapter; (ii) they assist in understanding the improvements to EMM-ARM in the scope of modal identification that will be presented in Chapter 4.

The second part of this chapter reviews the state of development of EMM-ARM prior to the present work, including its original application to cement based materials, as concrete, mortars and cement pastes, and the posterior pilot experiments with soil-cement mixtures. Regarding the EMM-ARM application to soil-cement, this Chapter includes a description of the main features, as well as its limitations. Consequently, the opportunities of improvement can be identified and discussed.

3.2 PRINCIPLES OF MODAL IDENTIFICATION

The topics presented in this subchapter are addressed in detail by Clough & Penzien (2003), Maia & Silva (1997), Chopra (1995), Caetano (1992) and are also discussed in the works of Rodrigues (2004), Ramos (2007) and Magalhães (2004).

Firstly, the definition of Frequency Response Functions (FRFs) of single and multiple degrees of freedom systems are presented, followed by the estimation of FRF and power spectra density (PSD) functions from experimental data. Then, the data discretization and the main related errors, including leakage and aliasing errors are

addressed. Finally, a brief reference is made to the Peak Picking method for modal identification.

3.2.1 Frequency Response Function of single degree of freedom oscillator

The movement of a single degree of freedom oscillator, with mass m, stiffness k and viscous damping c is ruled by the differential equation of motion presented on Equation (3.1) (Chopra, 1995), were $u(t)$ is the oscillator response to an excitation $p(t)$, whereas $\dot{u}(t)$ and $\ddot{u}(t)$ are the first and second order derivatives of $u(t)$ in order to the time t, respectively.

$$m\,\ddot{u}(t) + c\,\dot{u}(t) + k\,u(t) = p(t) \tag{3.1}$$

Equation (3.1) can be solved in the time domain or, alternatively, in the frequency domain by applying the Fourier transform to each of its members. With the resolution of this problem in frequency domain is possible to obtain the explicit system response from the actuating excitation. As the derivative in the time domain is transformed into the product by $i\omega$ in the frequency domain (Clough & Penzien, 2003), the differential equation of motion results in the algebraic equation presented on Equation (3.2), were $U_1(\omega)$ and $P_1(\omega)$ are the Fourier transform of $u(t)$ and $p(t)$ respectively and ω is the angular frequency. Equation (3.2) can then be rewritten assuming the form presented in Equation (3.3).

$$-m\,\omega^2\,U_1(\omega) + c\,i\,\omega\,U_1(\omega) + k\,U_1(\omega) = P_1(\omega) \tag{3.2}$$

$$U_1(\omega) = \frac{1}{-m\,\omega^2 + c\,i\,\omega + k}\,P(\omega) = H_1(\omega)P_1(\omega) \tag{3.3}$$

The function $H_1(\omega)$ presented in Equation (3.3) is known as Frequency Response Function (FRF) of a single degree of freedom system. Using Equations (3.4) and (3.5), where ω_1 is the first natural frequency and ξ is the damping of the system, is possible to define the FRF as presented on Equation (3.6). The FRF is a function in the frequency domain that characterizes the system and allows to obtain its response from the excitation.

$$\omega_1 = \sqrt{k/m} \tag{3.4}$$

$$c = 2\,.\,\xi\,.\,m\,.\,\omega_1 \tag{3.5}$$

$$H_1(\omega) = \frac{1/m}{\omega_1^2 - \omega^2 + 2\,i\,\xi\,\omega\,\omega_1} \tag{3.6}$$

Figure 3.1 presents the plot of this complex function, composed by real (R) and imaginary (I) parts, through its amplitude (Equation (3.7)) and phase angle (Equation (3.8)), for an oscillator with natural frequency ω_1 and for different damping coefficients. From Equation (3.6), it is possible to conclude that the FRF amplitude has a maximum for $\omega = \omega_1.\sqrt{1-\xi^2}$, which for small damping coefficients is a good estimate of the natural frequency of the oscillator (for small damping coefficients $\omega \cong \omega_1$).

$$FRF\ amplitude = \sqrt{R^2 + I^2} \tag{3.7}$$

$$FRF\ phase\ angle = arctg(I/R) \tag{3.8}$$

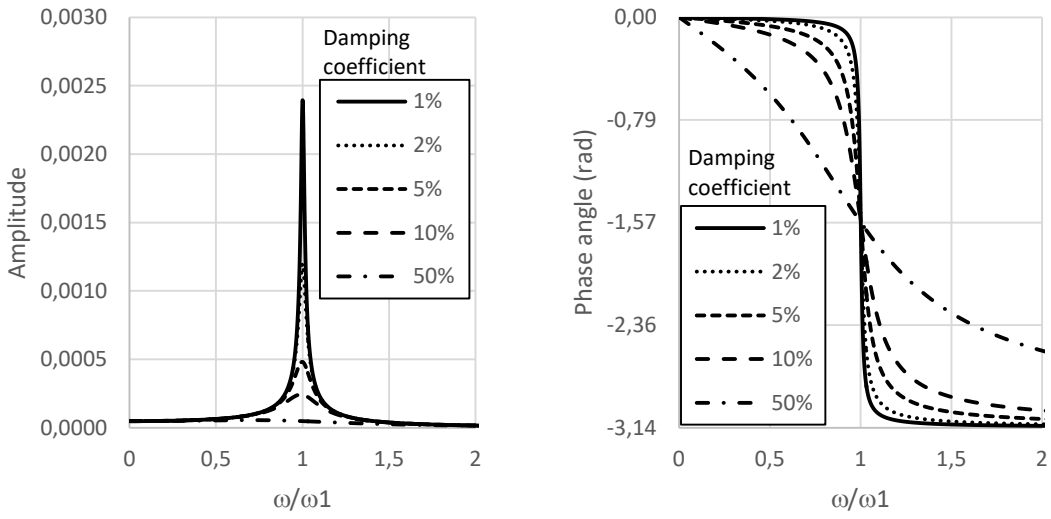

a) b)

Figure 3.1. Frequency Response function: a) amplitude; b) phase angle

The plot of the FRF allows to estimate the natural frequency of the oscillator, through the frequency corresponding to the maximum amplitude, which in turn coincides with a shift of π radians on the phase angle diagram. The shape of the peak of the FRF amplitude is also an indicator of the system's damping. In fact, a sharper peak corresponds to a lower damping coefficient.

The FRF presented on Equation (3.6) relates forces with displacements. However is possible to define FRFs to relate forces with velocities or forces with accelerations, as presented on Table 3.1. These FRFs can be obtained by successively multiplying the first FRF by $i\omega$.

Table 3.1. Frequency response functions

Designation	Expression	Relation
Receptance	$H_1(\omega) = \dfrac{1/m}{\omega_1^2 - \omega^2 + 2\,i\,\xi\,\omega\,\omega_1}$	Force and Displacement
Mobility	$H_1(\omega) = \dfrac{i.\omega/m}{\omega_1^2 - \omega^2 + 2\,i\,\xi\,\omega\,\omega_1}$	Force and Velocity
Inertance	$H_1(\omega) = \dfrac{-\omega^2/m}{\omega_1^2 - \omega^2 + 2\,i\,\xi\,\omega\,\omega_1}$	Force and Acceleration

3.2.2 FRF measurement

The identification of the dynamic characteristics of a system can be performed by correlating the measured response of the structure with a corresponding known artificial stimulation; or merely by analysing the response of the system when solely subject to ambient excitation, assumed as a white noise.

3.2.2.1 FRF measurement with known forced excitation

For single degree of freedom systems, and for the cases where the excitation is known, the FRF ($H_1(\omega)$) can be determined in the frequency domain by relating the Fourier transform of the time history of the system's response $U_1(\omega)$ and the Fourier transform of the time history of the excitation $P_1(\omega)$ through Equation (3.3) (Caetano, 2000), or through other different relations presented on Equations (3.9), (3.10) and (3.11). These

relations include the use of cross-power spectra density (CPSD) functions between the excitation and the response, $S_{u,p}(\omega)$ and $S_{p,u}(\omega)$, and auto-spectra or power spectra density (PSD) functions of the response and of the excitation: $S_{u,u}(\omega)$ and $S_{p,p}(\omega)$, respectively. Upon knowledge of excitation and response of the system, Equation (3.9) only allows to determine the FRF amplitude, while Equations (3.10) and (3.11) further allow to determine the FRF amplitude and phase angle.

$$S_{u_1u_1}(\omega) = H_1(\omega).H_1(\omega)^*.S_{p_1p_1}(\omega) = |H_1(\omega)|^2.S_{p_1p_1}(\omega) \tag{3.9}$$

$$S_{p_1u_1}(\omega) = H_1(\omega).S_{p_1p_1}(\omega) \tag{3.10}$$

$$S_{u_1u_1}(\omega) = H_1(\omega).S_{u_1p_1}(\omega) \tag{3.11}$$

The cross-power spectral density functions, denoted by $S_{x1,x2}(\omega)$, can be obtained by using Equation (3.12), where $x_1(t)$ and $x_2(t)$ are the time history of two processes, $F_{T,r}[x_i(t)]$ is the Fourier transform of the r realisation of the $x_i(t)$ process, limited to the time range $[-T/2\,;T/2]$. Equation (3.12) can also be used for auto-spectrum calculation by considering $x_1(t) = x_2(t)$.

$$S_{x1,x2}(\omega) = \lim_{\substack{T\to\infty \\ n\to\infty}} \frac{1}{n}\sum_{r=1}^{n} \frac{F_{T,r}[x_1(t)]^*.F_{T,r}[x_2(t)]}{T} \tag{3.12}$$

However in practice as the measurements are discrete in time and spaced of Δt, Equations (3.9) to (3.12) can only be estimated at discrete frequency values ω on a frequency spacing $\Delta\omega$ (Equation (3.13)) defined by the sampling frequency fs and the number of samples N in the time history.

$$\Delta\omega = 2\pi.fs/N \tag{3.13}$$

Therefore, the FRFs and the spectra are calculated as estimation of the real values by Equations (3.14), (3.15) and (3.16), where superscript $\hat{}$ means estimate. Consequently, the Fourier transforms are replaced by discrete Fourier transforms $X_i(\omega)$ (Clough & Penzien, 2003), the sum extended to all realisations disappears and the analysed temporal segment have now a finite duration and equal to $N.\Delta t$.

$$\widehat{H}_{i,j}(\omega) = \widehat{U}_i(\omega)/\widehat{P}_j(\omega) \tag{3.14}$$

$$\left|\widehat{H}(\omega)\right|^2 = \hat{S}_u(\omega)/\hat{S}_p(\omega) \tag{3.15}$$

$$\hat{S}_{x_1x_2}(\omega) = \frac{X_1(\omega)^*.X_2(\omega)}{N.\Delta t} \tag{3.16}$$

In practice, the discrete Fourier transforms can be efficiently determined using a mathematical algorithm known as Fast Fourier Transform (FFT) proposed by Cooley & Tukey (1965), reducing significantly the number of mathematical operations during the computation process. Its implementation requires that the discretized time series has a number of points N equal to any power of 2 ($N = 2^k, k$ is a positive integer). However, discrete Fourier transforms of discretized and finite length signals results in some unacceptable errors, including leakage and aliasing, which must be minimized. Some practices to minimize these type of errors are addressed in 3.2.2.3.

3.2.2.2 FRF measurement with ambient excitation

The operational (output-only) modal identifications techniques or ambient vibration techniques are based on the dynamic response measurements of a system under natural or ambient conditions. The main assumption for the excitation of the system is the consideration of the ambient excitations $p(t)$ as a stationary Gaussian white noise stochastic process in the frequency range of interest. This assumption means that the power spectra density (PSD) function, $\hat{P}_j(\omega)$, of the excitation can be considered as constant, $\hat{P}_j(\omega) = R$ (Cunha, 1990). So, Equation (3.15) assumes the form presented on Equation (3.17), where is possible to observe that the FRF depends only on the PSD function of the excitation and on a constant (R). Because of the fact that the PSD of the response is proportional to the FRF, it becomes possible to obtain the dynamic properties of the structure from the PSD functions estimated by solely evaluating the measured response.

$$\left|\hat{H}(\omega)\right|^2 = \hat{S}_u(\omega)/R \tag{3.17}$$

3.2.2.3 Data acquisition and data processing

Prior to the any spectra or FRF estimation, the analogue signals are measured/recorded by digital acquisition systems as discrete time series. So, it is important to define a correct sampling frequency or sampling rate, fs, in order to ensure that the measured signal represents effectively the continuous behaviour under measurement. In fact, a same signal measured at different sampling frequencies can produce different measured signals. This error is known as the aliasing phenomenon and itis illustrated in Figure 3.2, where an insufficient sampling frequency results in a rather incorrect assessment of the real behaviour. To avoid this error, the sampling frequency must be at least twice as large as the frequency of interest of the studied phenomena (or even slightly higher). Brinker *et al.* (2001) recommend a minimum value for fs of 2.5 times the frequency of interest.

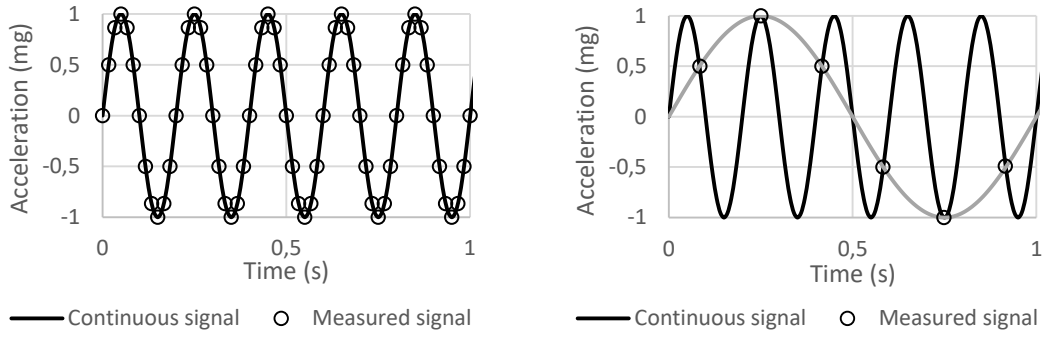

a) b)

Figure 3.2. Aliasing phenomena: a) signal measured at correct sampling frequency; b) signal measured at low sampling frequency

The leakage error is due to the finite nature of time series and appears when the measuring time is not an integer multiple of the signal period, which always happens in experimental testing. This error manifests itself through the energy distribution associated with a specific frequency by frequency in its neighbourhood. Figure 3.3 presents an example of the leakage error when the measuring time is not a multiple of the signal period. In Figure 3.3a the signal measuring time is an integer multiple of the

signal period and, consequently, the respective spectrum (Figure 3.3c) displays only one occurrence at expected frequency. However, for the case presented on Figure 3.3b, were the measuring time is not a multiple of the signal period, the respective spectrum (Figure 3.3d) displays contamination of artefact influences in the in the neighbourhood of the expected frequency.

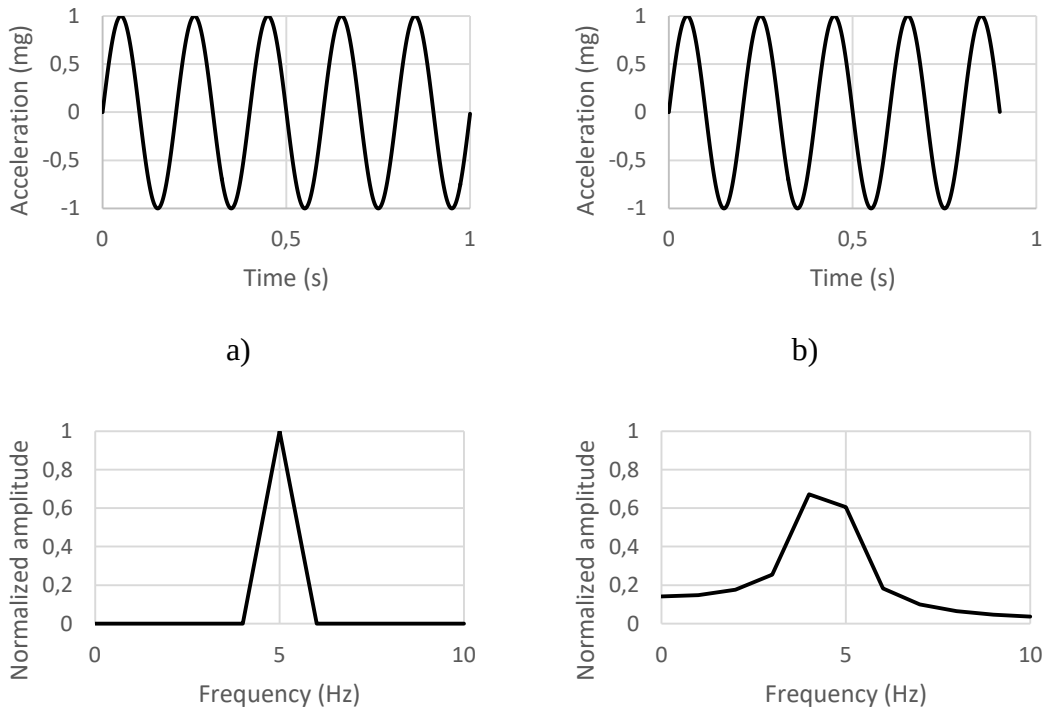

Figure 3.3. Leakage error: a, c) signal and spectrum, respectively, when measuring time is an integer multiple of the signal period; b, d) signal and spectrum, respectively, when measuring time is not a multiple integer of the signal period

The leakage error can be minimized by multiplying the signal by a window function $\omega(t)$, in a process known as windowing, in order to rescale the initial and final parts of the time series. Different windows types can be used (Maia & Silva, 1997) but for stationary random signals the most used is the Hanning window, that can be described by Equation (3.18), where t is time and T is the total signal duration in seconds. Figure 3.4 presents an example of application of a Hanning window to the same signal presented on Figure 3.3b. Figure 3.4a is the signal which measuring time is not an integer multiple of the signal period. Figure 3.4b is the representation of the

Hanning window function. Figure 3.4c is the signal after windowing and Figure 3.4d is the improved spectrum that can be compared with Figure 3.3d.

$$\omega(t) = \frac{1}{2}.\left[1 + \cos\left(\frac{2\pi t}{T}\right)\right], |t| \leq \frac{T}{2}\ ;\ \omega(t) = 0, |t| \geq \frac{T}{2} \qquad (3.18)$$

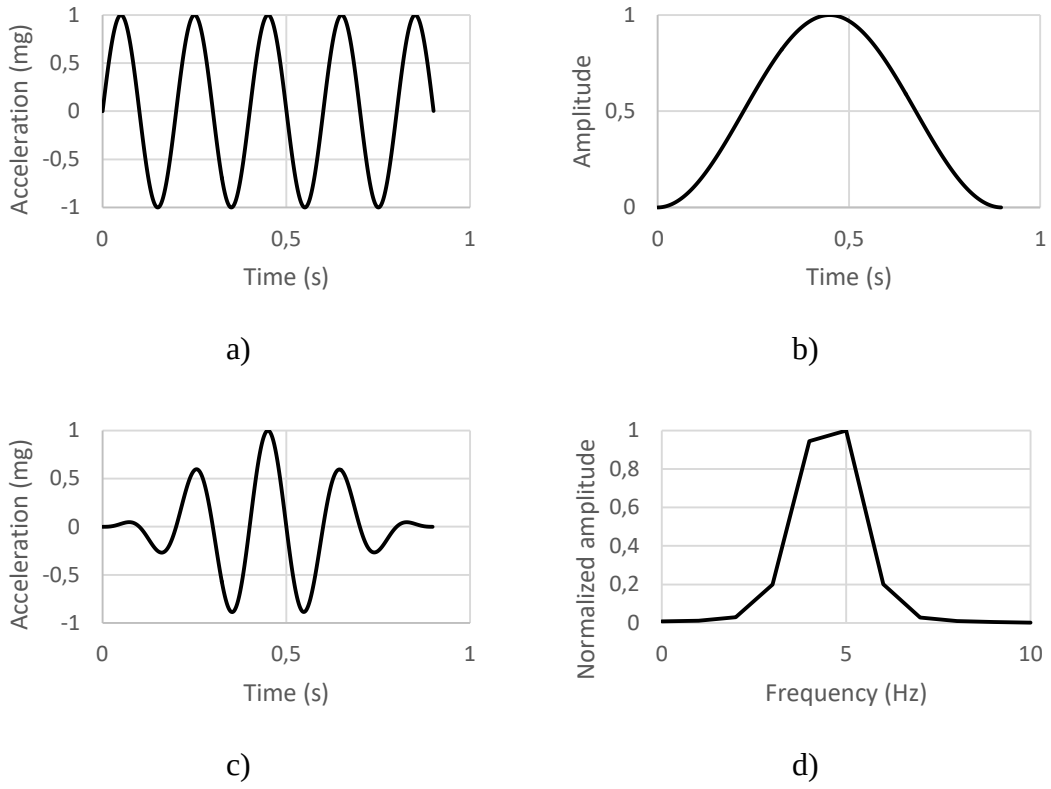

Figure 3.4. Application of Hanning window error: a) signal when measuring time is not a multiple integer of the signal period; b) Hanning window function; c) signal after window application; d) improved spectrum

In addition to the actions used to minimize the leakage and aliasing errors, an averaging process is applied to the signals in order to reduce spurious random noise and increase statistical reliability of the data. This process consists in: (i) dividing the time series in several samples (segments) with shortest duration; (ii) application of FFT algorithm to each of the samples; (iii) averaging the signal transform, resulting in the normalized power spectrum density (NPSD) (Welch, 1967). For a large number of segments, the variance of the mean estimate will decrease, resulting in a smoothed spectrum. However, the adoption of a larger number of segments implies using samples with shorter duration and, consequently, the transform to frequency domain will result in an

increase of leakage error and a diminution of frequency resolution. This problem can be minimised by partially overlapping the segments resulting in an increase of all segments. Even though different overlapping ratios can be used, the overlap of 50% is the most common for random signals (Rodrigues, 2004). The application of Hanning windows with an overlapping of 50% means that all the elements of the time series will have the same contribution, as the sum of multiple Hanning windows with 50% overlapping result in a horizontal line in the overlapping areas, as can be observed on Figure 3.5. This procedure of spectra estimation based on the segmentation of time series, applying a window to each segment, FFT calculation of each segment and finally the averaging, resulting in the NPSD, is known as Welch procedure (Welch, 1967).

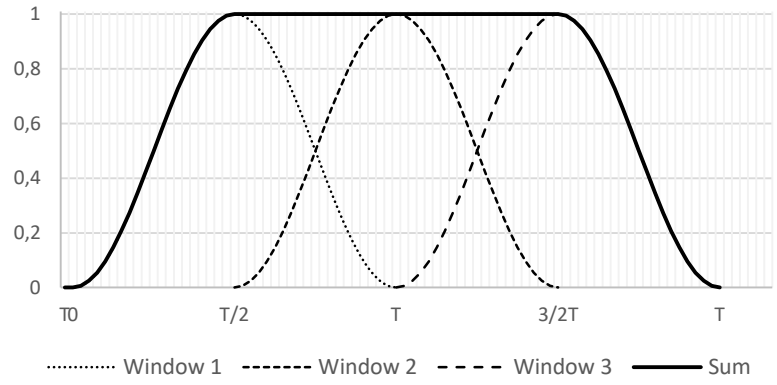

Figure 3.5. Hanning windows with 50% overlapping

3.2.3 Peak picking modal identification method

The peak picking (PP) method, also known as the basic method in the frequency domain, is one of the most known methods in modal analysis. The theoretical foundations of the current format of the method were developed by Bendat and Piersol (1980). This is a frequency domain method based on the assumption that, in the vicinity of a resonant frequency, the dynamic response is dominated by the resonant mode shape. Thus, assuming this hypothesis as valid, in the vicinity of the resonance frequency the FRF can be simulated by a FRF of a one degree of freedom oscillator with same frequency ω_k and same damping coefficient ξ_k of the resonant mode. This

approximation is only valid when the frequencies associated with the different modes of vibration are sufficiently spaced out. When this is not observed, the method is not able to distinguish the contributions from distinct modes with frequencies close to the measured response of the system, which is the main limitation of the method. The PP method can be used both in forced vibration (input-output) and ambient vibration (output-only) testing.

The resonant frequencies ω_k are associated to the peaks of the FRF (or NPSD) amplitude and damping, ξ_k, can be estimated by using the Half-Power Bandwidth method (Clough & Penzien, 2003). For that, consider ω_1 and ω_2 are frequencies in the vicinity of the resonant frequency ω_k, respectively at left and right, which is associated an amplitude that is half of the amplitude associated with the resonant frequency (in FRF or NPSD). The damping, ξ_k, can then be obtained according to Equation (3.19), or alternatively, damping can also be estimated by fitting the respective Frequency Response Function expression, presented on Table 3.1 (inertance expression for acceleration), to the respective peak on the measured FRF. A graphical representation of Peak Picking method is presented on Figure 3.6.

$$\xi_k = \frac{\omega_2 - \omega_1}{2.\,\omega_k} \tag{3.19}$$

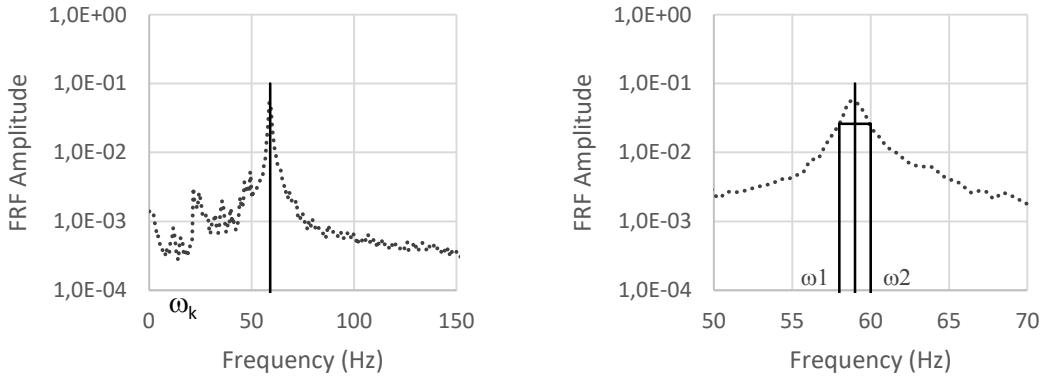

a) b)

Figure 3.6. Graphical representation of Peak Picking method: a) estimation of the resonant frequency; b) estimation of the damping coefficient using the Half Power Bandwidth Method

3.3 STATE OF DEVELOPMENT OF EMM-ARM

3.3.1 EMM-ARM original application to cement based materials

EMM-ARM is a resonance based method initially proposed by Azenha *et. al.* (2010) to assess the E-modulus evolution of concrete since early ages. In the original conception of EMM-ARM for the study of concrete (Azenha *et al.*, 2010), fresh concrete was poured into an acrylic tube (92 mm inner diameter; 100 mm outer diameter; 2000 long), forming a composite beam. The beam was then placed horizontally on four concrete cubes through two horizontal rods that laterally trespassed the beam through its cross-sectional centre in locations neighbouring its extremities. With this configuration the system behaves as simple supported beam with a free span of 1800mm, as presented on Figure 3.7.

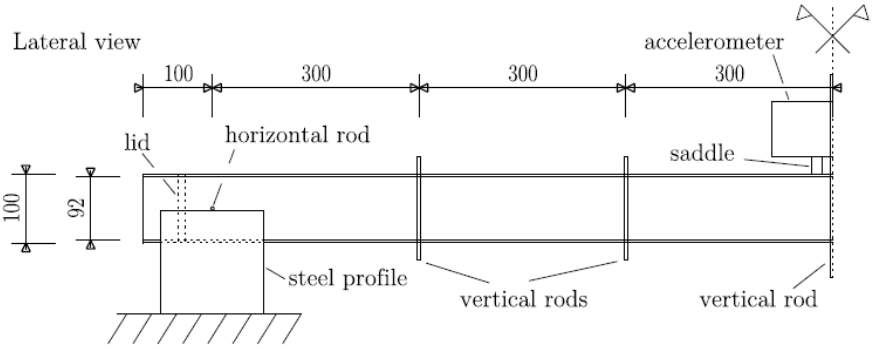

a)

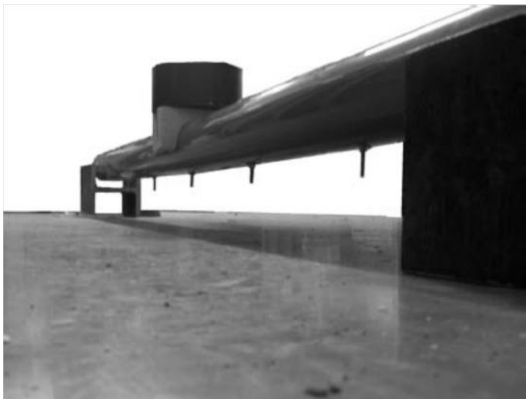

b)

Figure 3.7. Original EMM-ARM beam (Azenha, 2009): a) dimensions; b) global view

The testing beam was left undisturbed throughout the entire testing period, thus being only excited by vibrations that naturally occur in the surrounding environment, i.e.,

ambient vibrations, which can be assumed to have same characteristics of white noise (or a stochastic process with constant spectral intensity in all frequencies of interest). The beam response was measured in the vertical direction by means of an accelerometer placed at mid span. Due to the high slenderness of the testing beam, it is very excitable and the ambient noise is sufficient to induce vibrations susceptible to be measured by the accelerometer. Even so, a fan was placed in the vicinity, and pointing towards the testing beam in order to amplify the level of ambient vibrations. Despite the fixed frequency of the rotation of the fan, the complex turbulence associated with the airflow caused the corresponding excitation to the beam to have a reasonably wide spectrum, thus resembling white noise in the frequency range of interest, and improving the quality of the modal identification.

Through a continuous non-parametric modal identification of the composite beam, it was then possible determine the evolution of the flexural resonance frequency of the first mode of vibration. As geometry, support conditions, mass and mould E-modulus are known, it is possible to quantitatively estimate the E-modulus of the concrete inside de acrylic mould.

The encouraging results obtained for the pilot experiment in concrete Azenha *et. al.* (2010) led to additional developments in the study of cement pastes (Azenha *et al.*, 2012a) with small cantilevered composite beams (Figure 3.8) that allowed very clear identification of the resonant frequency of the tested specimens.

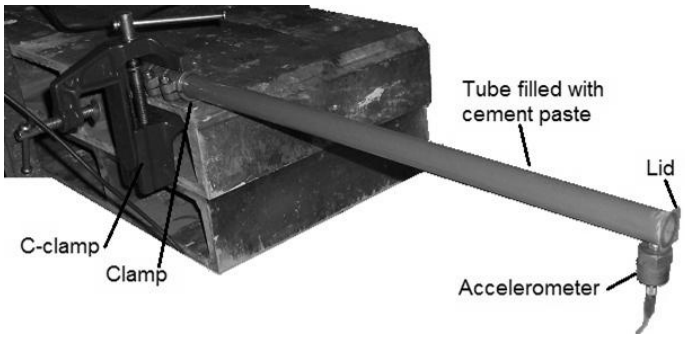

Figure 3.8. EMM-ARM experimental setup for cement pastes

The original version of EMM-ARM uses operational modal analysis (OMA), also known as ambient response modal analysis, to identify the resonant frequency of the first flexural mode of vibration of the testing beams. It relies on the Peak-Picking method in the frequency domain. The setup, overall workflow of the modal

identification and E-modulus computation process is schematically presented in Figure 3.9.

Figure 3.9a presents the testing beam with accelerometer vertically attached at mid span and connected to a data acquisition system (Figure 3.9b). Figure 3.9c-f corresponds to the modal identification and Figure 3.9g is the resultant E-modulus curve.

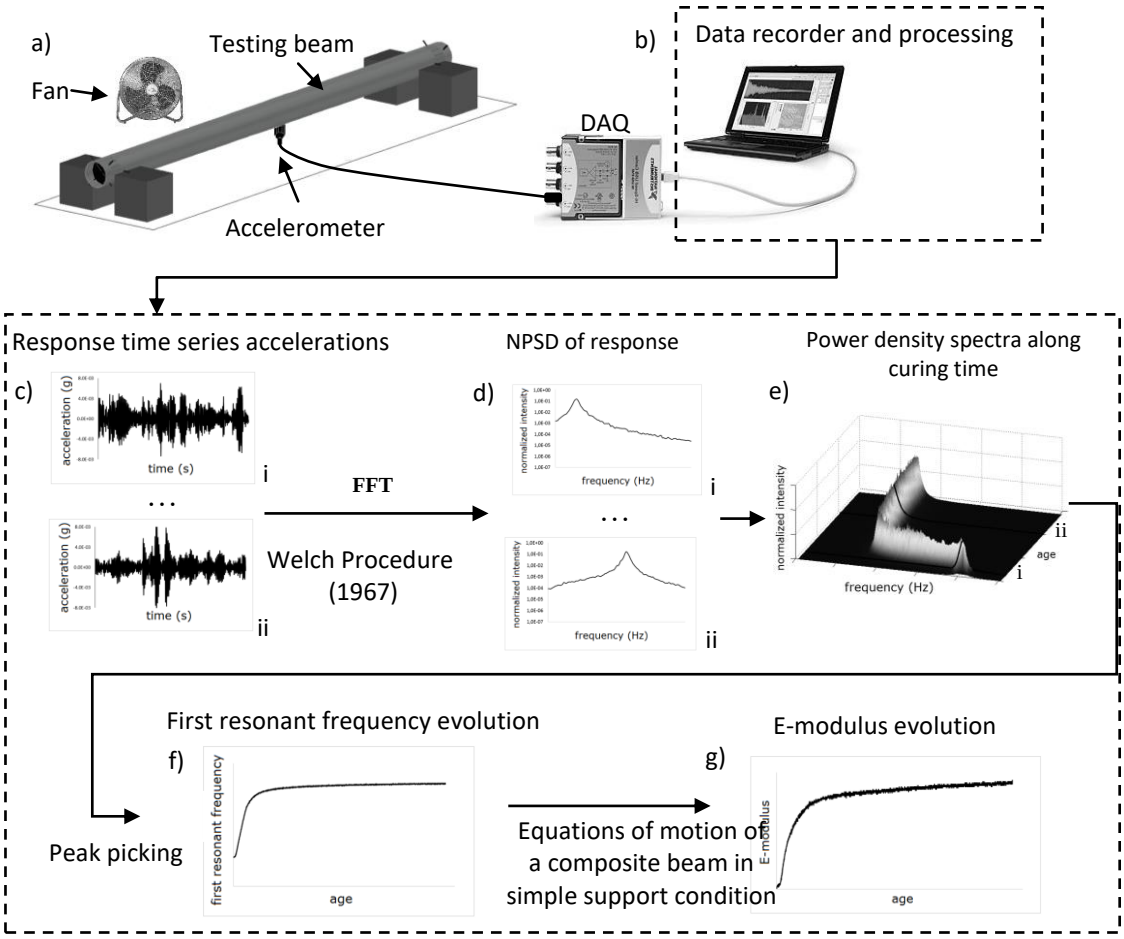

Figure 3.9. EMM-ARM data processing

3.3.1.1 Modal identification

In a typical EMM-ARM test, accelerations were measured in sets of time with 900 seconds of duration and recorded at a specified frequency rate, fs (200 Hz) (Figure 3.9c). For each set, the recorded acceleration time series were converted to frequency domain (Figure 3.9d) following the Welch procedure (Welch, 1967) that included: 4096 points (N) for each segment; using a Hanning window with overlap of 50% for

signal processing; applying the Fast Fourier Transform (FFT) to the windowed segments; averaging the spectra associated to obtain the NPSD. By positioning each NPSD obtained along curing time side-by-side, it was possible to obtain a time *versus* frequency colour map (or surface chart) with colouring that is proportional to the intensity of the NPSDs (Figure 3.9e). The resonance frequencies of the first mode of vibration are obtained from the highest peak in each NPSD (peak-picking method). From the identification of the resonant frequencies of the calculated spectra at different instants, it was possible to obtain their evolution along time (Figure 3.9f).

Figure 3.10a presents an example of a colour map of several side-by-side NPSD and Figure 3.10b the respective resonant frequency evolution obtained (Azenha, 2009).

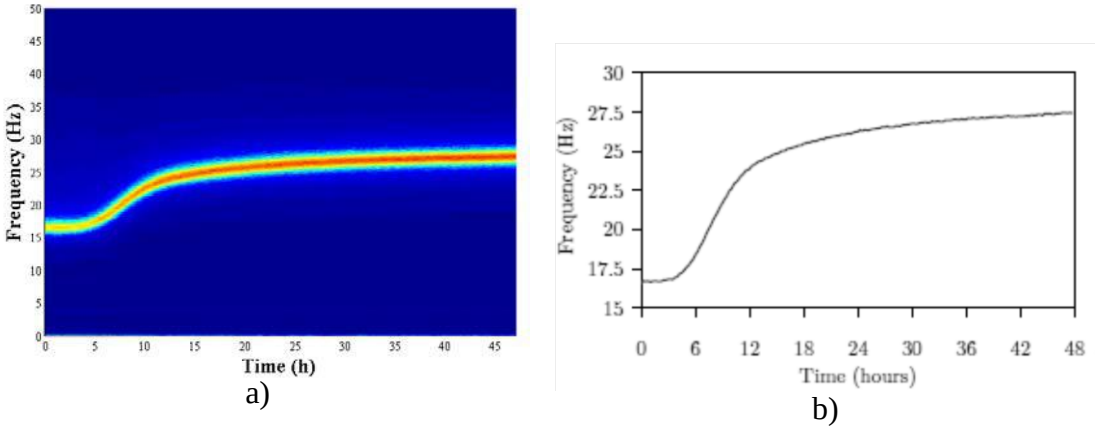

Figure 3.10. a) Colour map of several side-by-side NPSD; b) Resonant frequency evolution (Azenha, 2009)

3.3.1.2 E-modulus computation

The resonant frequency of the composite beams is related to the E-modulus of the tested material by applying the dynamic equations of motion (Figure 3.9e). This process is relatively straightforward and uses the analytical solution for the eigenvalues of the equations of motion. As testing beam is symmetric, its geometry can be considered as presented on Figure 3.11, where $\phi(x)$ is the vertical deflection mode, x is the abscise along the beam length, $\bar{E}$ and $\bar{I}$ are, respectively, the homogenised E-modulus and moment of inertia of the cross-section. $\bar{m}$ is the uniformly distributed mass along the beam, m_p is a concentrated mass applied at mid span, k is a spring constant relative to the beam supports and L is half of the total span of the beam.

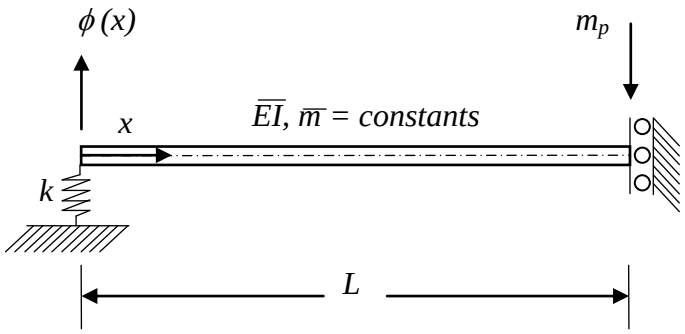

Figure 3.11. EMM-ARM schematic representation of half testing beam

The evolution of the first resonant frequency can then be related with the E-modulus of the tested material by means of the equation of motion of a simply supported beam with a mass at mid span (Clough & Penzien, 2003), as depicted by Equation (3.20), where $Y(t)$ is the amplitude of transversal displacement along time t expressed in relation the deflection mode $\phi(x)$.

$$\frac{\partial^4[\phi(x)\,Y(t)]}{\partial x^4} + \overline{m}\frac{\partial^2[\phi(x)\,Y(t)]}{\partial t^2} = 0 \qquad (3.20)$$

From Equation (3.20) is possible to express $\phi(x)$ as a function of the real constants A_1, A_2, A_3 and A_4, as can be observed on Equations (3.21) and (3.22), were ω is the angular frequency and f is the linear frequency.

$$\phi(x) = A_1\cos(a\,x) + A_2\cos(a\,x) + A_3\cosh(a\,x) + A_4\sinh(a\,x) \qquad (3.21)$$

$$a = \sqrt[4]{\frac{\omega^2\,\overline{m}}{\overline{EI}}}\,,\omega = 2\pi f \qquad (3.22)$$

For the present EMM-ARM beam, with a vertical spring on the left (at $x = 0$) and a vertical sliding support on the right (at $x = L$), the boundary conditions presented on Equation (3.23) must be applied to Equation (3.21).

$$\begin{aligned} At \quad x = 0: \qquad & \overline{EI}\ \phi''(0) = 0\ ; \quad \overline{EI}\ \phi'''(0) = -k\ \phi(0) \\ At \quad x = L: \qquad & \phi'(L) = 0\ ; \quad \overline{EI}\ \phi'''(L) = -\omega^2 \phi(L) m_p \end{aligned} \tag{3.23}$$

By applying these boundary conditions to Equation (3.23) a set of equations is then obtained, whose eigenvalues ω may be computed according to Equation (3.24).

$$\frac{1}{2\,k}\begin{bmatrix} \overline{EI}\ a^3\omega^2\ m_p[1+\cosh(aL)^2-\sinh(aL)^2+2\cos(aL)\cosh(aL)] \\ +2\ k\ \ \omega^2\ \ m_p\ [\cos(aL)\sinh(aL)+\cosh(aL)\sin(aL)] \\ +2\ \overline{EI}\ a^6\ [\sin(aL)\ \cosh(aL)+\cos(aL)\ \sinh(aL)] \\ +4\ \overline{EI}\ a^3 k\ \cos(aL)\ \cosh(aL) \end{bmatrix} = 0 \tag{3.24}$$

After identification of the resonant frequency of the beam, all variables in Equation (3.24) are known except for $\overline{EI}$. For the present beam with composite tubular section with known external and internal diameters d_e and d_i, respectively, and known E-modulus of the mould E_m is possible to determine the E-modulus of the tested material E_c through Equation (3.25) (where I_c.and I_m are the moments of inertia of the cross-section of the tested material and of the mould, respectively).

$$\overline{EI} = E_c\ I_c + E_m\ I_m = E_c \frac{\pi\ d_i^4}{64} + E_m \frac{\pi(d_e^4 - d_i^4)}{64} \tag{3.25}$$

By applying this procedure to the sets of data collect during the test is possible to obtain the curve E-modulus of tested material versus time of curing (Figure 3.9g).

The performance of this methodology has been demonstrated in a laboratory environment by Azenha *et al.* (2009, 2010) by comparing its results to those obtained through unconfined cyclic compression (UCC) tests. More recent applications have shown that the kinetics of stiffness evolution captured by EMM-ARM is in accordance with that obtained through ultrasonic pulse velocity measurements, and that mould geometry can be adapted to allow the re-use of moulds (Azenha *et al.*, 2012b). It has been further shown that the EMM-ARM methodology can be successfully used in *in*

situ conditions by applying this technique within a pre-fabrication plant (Azenha *et al.*, 2012b).

3.3.2 EMM-ARM application to soil-cement

Based on the successful applications of EMM-ARM to concrete, it was successfully applied to cement pastes and mortars (Azenha *et al.*, 2012a) and preliminary laboratory experiments have been conducted in stabilized soils (sand-cement mixtures), showing that the application of EMM-ARM in this material is feasible (Azenha et al., 2011). In fact, the first works of adaptation to stabilised soils were performed by the same author of the present thesis as part of his Master of Science dissertation (Silva, 2010).

To adapt EMM-ARM for the study of sand-cement, modifications were necessary with regard to the original methodology devised for concrete. In fact, as the stiffness of hardened concrete is much higher than the stiffness of sand-cement, the mould was redesigned to assure that the range of resonant frequencies during the test was large enough to allow the proper identification of stiffness evolution. Moreover, an open 'U'-shaped cross-section was adopted for the mould, making it reusable. The redesigned mould applied in the pilot application for stabilized soil (Azenha *et al.*, 2011) was made of polycarbonate and had an inner cross-section of the sample of 40 mm × 40 mm and a span of 495 mm (Figure 3.12) and steel profiles were used to materialize the beam supports.

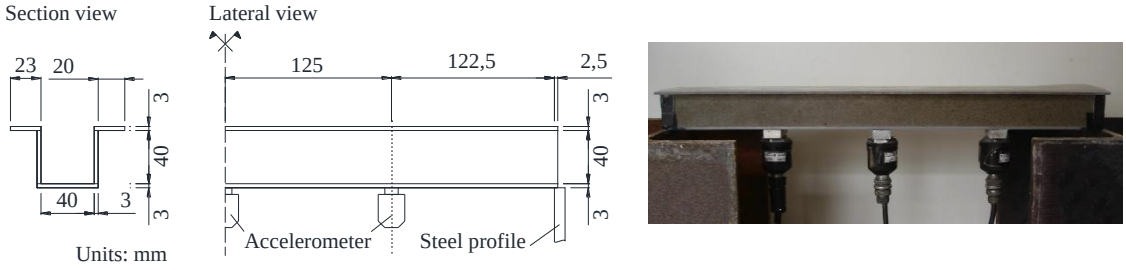

Figure 3.12. EMM-ARM pilot application (Azenha *et al.*, 2011)

One of the main issues that can be raised in this adaptation to sand-cement is related to the representativeness of sample tested. In fact, for these experiments the samples were reconstituted inside the mould and the density was controlled by weighing the sample. This practice may raise doubts regarding the uniform distribution of the material inside the mould that can affect the representativeness of the tested material. Due to the low

slenderness of the composite beam, when comparing to the original application to concrete, the range of resonant frequencies during the experiment (50 Hz – 110 Hz) pertained to higher frequencies than previous applications to mortar/concrete (8 Hz – 40 Hz), thus evidencing the need for using more equipment and more sophisticated modal identification. In addition to the accelerometer placed a mid-span two additional accelerometers (placed at 1/4 and 3/4 of the span) were used to monitor the accelerations and the modal identification was made using a parametric identification algorithm based on the Stochastic Subspace Identification SSI-Data (Van Overschee & De Moor, 1991). This is a drawback as more equipment has to be attached to the beam, increasing the complexity of the test, and the more advanced modal analysis technique used did not eliminate the susceptibility to interferences resulting from contaminations of ambient noise, as desirable. The robustness of the new reusable mould was found inappropriate, as some deboning was observed between parts of the mould after repeated use. The pilot application provided limited results as it was restricted to the first 7 days of age. Despite these limitations, the results were very promising. It was found that the results obtained with the EMM-ARM technique revealed the same trend of the relative stiffness evolution obtained with other methods, including "bender-extender elements" (M-modulus). Moreover, the E-modulus values obtained from EMM-ARM technique exhibited a very good agreement with the results obtained from unconfined cyclic compression testing as shown in Figure 3.13.

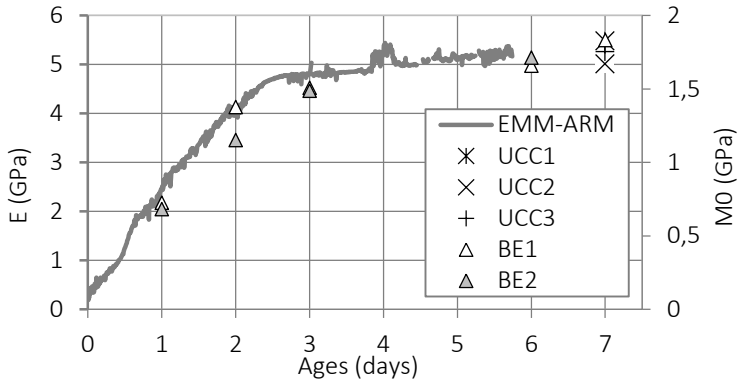

Figure 3.13. EMM-ARM pilot application results (Azenha *et al.*, 2011)

Chapter 4

IMPROVEMENTS TO EMM-ARM APPLIED TO SOIL STABILISATION

4.1 INTRODUCTION

Despite the success of the first application of EMM-ARM to soil-cement mixtures, there are some points where improvements are desirable. In fact, the pilot application of EMM-ARM to sand-cement reported by Silva (Silva, 2010) and Azenha *et. al.* (2011) allowed the identification of some fundamental drawbacks, as reported on subsection 3.3.2. Thus, this chapter presents a set of modifications to EMM-ARM methodology whose aim to overcome these limitations. The modifications comprise: the design of new prismatic and tubular moulds with higher slenderness than those used in previous works; the use of an alternative and cheaper material (PVC) for tubular moulds; the development of sampling methodologies to a collect the material to be tested directly from compacted layers; the use of tubular moulds with similar slenderness to the moulds used previously by Azenha *et. al.* (2011); the implementation of experimental modal analysis (EMA) with forced vibration of low magnitude to reduce the effect of undesirable contaminations of the ambient noise increasing the robustness of the modal identification. The validation of EMM-ARM developments was performed by comparison of results different complementary techniques.

4.2 METHODOLOGIES USED FOR EMM-ARM VALIDATION

The validation of EMM-ARM results was made by comparison with results obtained from complementary techniques. These included qualitative comparisons with results of shear and restrained moduli obtained with bender-extender elements (BE) and ultrasonic (US) testing, respectively, and quantitative comparison with E-modulus obtained in unconfined cyclic compression (UCC) testing on specimens of same mixtures.

4.2.1 Unconfined cyclic compression testing

UCC testing with on-sample strain measurements was performed to quantify the E-modulus of cylinder-shaped specimens (Gomes Correia *et al.*, 2006). The specimens were prepared by two different methodologies: one involved the collection of intact specimens directly from compacted layers; the other methodology involved the preparation of reconstituted specimens and is described in detail in the present section.

To prepare the UCC reconstituted specimens, samples of fresh stabilized soil (from same mixture tested with EMM-ARM) were compacted inside metallic moulds with internal dimension intended for the specimen, as described in the following points:

P1. The UCC mould consisted of a metallic cylinder with internal dimensions of 200 mm height and a diameter of 100 mm, as depicted on Figure 4.1a). To make the unmoulding operations easier, a polytetrafluoroethylene membrane, commonly known as Teflon, was used in the interior of the mould on Figure 4.1b).

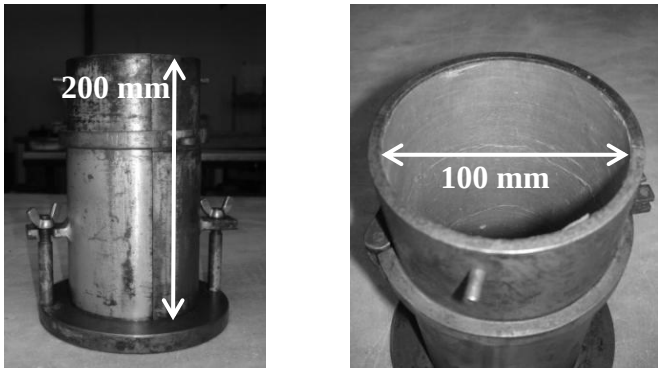

a) b)

Figure 4.1. UCC Mould for specimen preparation: a, b) dimensions; b) mould with polytetrafluoroethylene liner

P2. The required mixture (soil-cement) mass to achieve the intended density inside the mould was weighted, and divided in 3 equal portions;

P3. A portion of the mixture was placed inside the specimen mould (Figure 4.2a), followed by a manual light compaction of the part using a small wooden rammer (Figure 4.2b); the part was then compacted using a mechanical hammer (model Kango hammer type 638), until 1/3 of the total mould height was achieved (Figure 4.2c). Each part had a height of about 66 mm, as presented on Figure 4.3.

a) b) c)

Figure 4.2. UCC Mould for specimen preparation: a), b) dimensions; c) Teflon liner

P4. The surface of the recently finished part was slightly scarified in order to create a good connection with the subsequent part. This was done by scraping with a metallic rod the top surface of the part, as presented on Figure 4.4a;

P5. Another mixture portion was added and the procedure was repeated from point P3. For the execution of the third part a mould extension was used in order to facilitate the introduction and compaction of the mixture, as presented on Figure 4.4a and Figure 4.4b;

P6. After the compaction of all parts, the specimen was removed from the mould, stored at room temperature (about 20ºC), and covered with plastic film to minimize the water exchange with air.

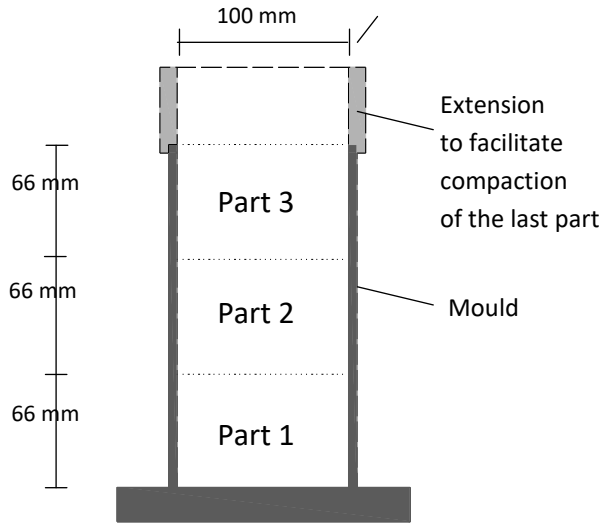

Figure 4.3. Mould geometry for UCC testing specimen preparation

a) b)

Figure 4.4. UCC specimen preparation: a) scarifying the surface of the layer; b) UCC specimen inside the mould with extension after final compaction

The specimens were subjected to unconfined cyclic compression testing with on-sample strain measurements at different ages of curing. In the absence of specific regulations for conducting this experiment, the selection of the strain range for these tests was made with basis on the previous works of Gomes Correia (2004) and Gomes Correia *et al*. (2006, 2009b), according to which the amplitude of the loading/unloading cycles should be very small to ensure that the strain response cycles are closed and nearly linear. In view of this, the strain level should be kept within 10^{-4}. As UCC testing was conducted at several distinct ages, the corresponding stress range at each age of testing was adjusted to ensure that the maximum strain during testing remained around 5×10^{-5}. A load rate of 50 N/s has been applied in coherence with the recommendations for compressive strength testing (LNEC, 1972b). Three continuous loading/unloading cycles were applied from an axial pre-load of about 38 kPa (corresponding to the minimum required pre-load of 300 N of the testing system) to the maximum strain at each age of testing, using a 50 kN hydraulic actuator, which included a load cell. Strain measurement was performed with 3 transducers (LVDTs) that were supported by 2 rings attached to the specimens to measure the on-sample displacement, as shown in Figure 4.5.

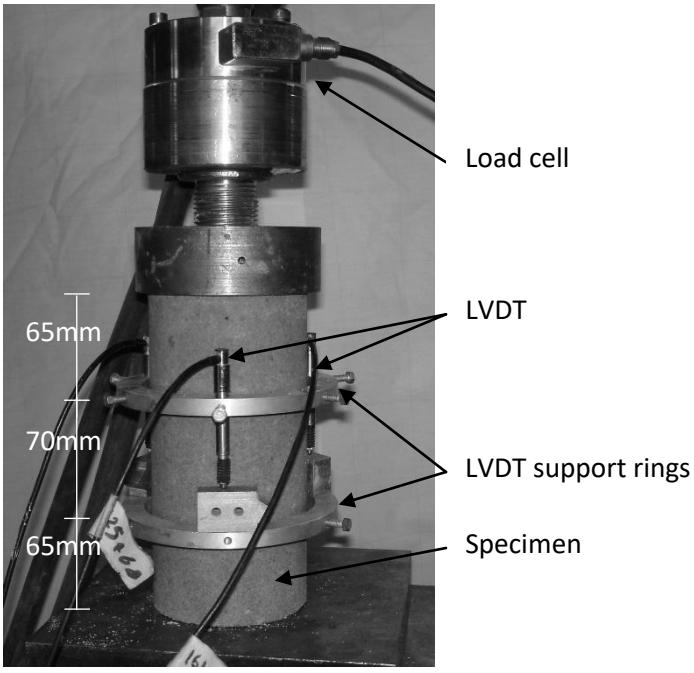

Figure 4.5. Unconfined cyclic compression testing setup

The E-modulus is then obtained by calculating the slope of the best-fit line to the stress-strain curve obtained on the second and third cycles of loading. With this methodology, the measured stress–strain response of all UCC tests was linear, with r^2 coefficients higher than 0.995, and the maximum strain levels remained below 5×10^{-5}. This strain level is considered to be in the very small-strain domain, in accordance with existing studies on cement-stabilised soils (Biarez *et al.*, 2005). For illustrative purposes, a typical stress–strain curve and the respective E-modulus obtained with this methodology on a sand-cement specimen tested at 7 and 28 days of age is presented in Figure 4.6.

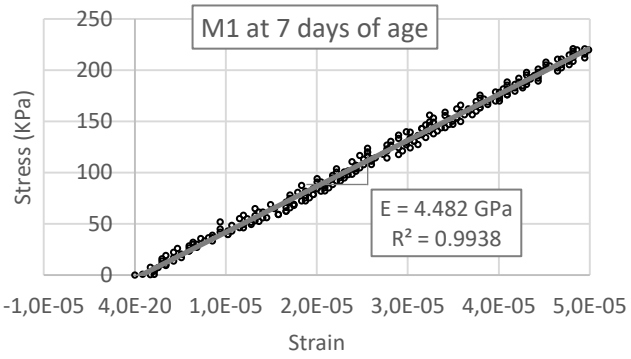

a)

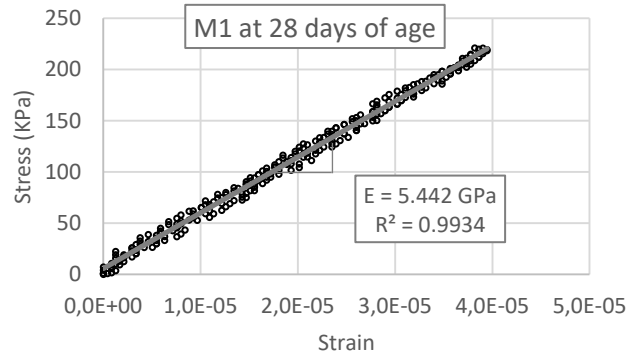

b)

Figure 4.6. Stress-strain curves and E-modulus determination for a sand-cement specimen at: a) 7 days of age; b) 28 days of age

4.2.2 Wave propagation based techniques

Wave propagation velocities were measured in cylindrical specimens by two distinct techniques: ultrasonic transducers (US) and bender element transducers BE. The P-wave wave velocity was measured by an US integrated system that comprised a central unit for signal generation and reception (Proceq Pundit Lab (Poceq, 2013)) together with two 54 kHz circular transducers (transmitter/receiver) (Figure 4.7). All US tests were carried out using an input frequency of 54 kHz and signal amplitude of 500 V. During the test, the transducers were kept in contact with the specimen and conductive gel was used to ensure maximum coupling. The constrained modulus M was determined through Equation (2.13) using the specimen density and the P-wave propagation velocity.

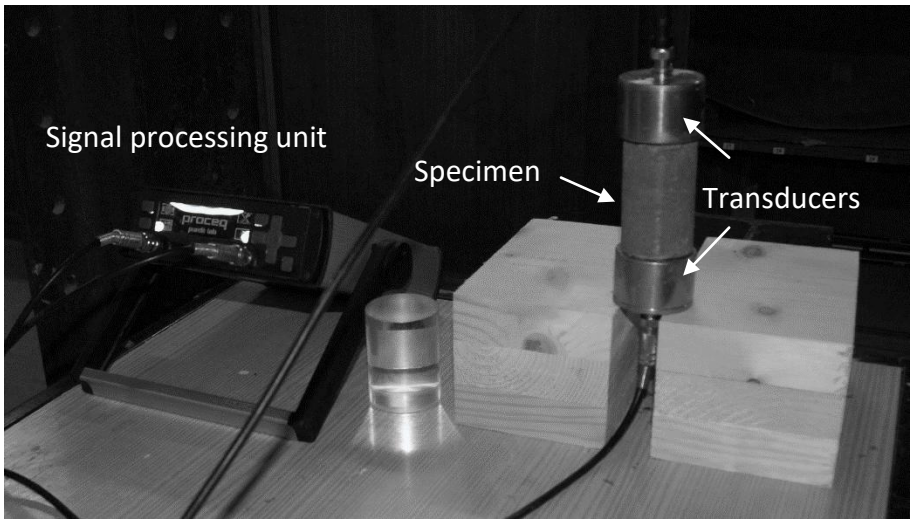

Figure 4.7. Ultrasonic wave propagation testing equipment

For BE testing, GDS transducers (GDSInstruments, 2009) (Figure 4.8) were used together with a function generator (TTI - TG1010A 10 MHz DDS Function Generator) and a 4-channel oscilloscope (PicoScope - 4424). A sinusoidal pulse signal was configured in the function generator for an input voltage of ±10 V. The input signal frequency was adjusted from the range of about 10 kHz to 30 kHz (at 1 day age) to the range of about 30 kHz to 65 kHz (at 28 days age), to account for the increasing stiffness of the specimens. Three measurements were made for each sample at atmospheric pressure at each testing age. The shear modulus, S, was determined via Equation (2.13) using the specimen density and the S-wave propagation velocity.

a) b) c)

Figure 4.8. a) top and b) bottom pieces with transducers embedded c) detail of bender-extender element

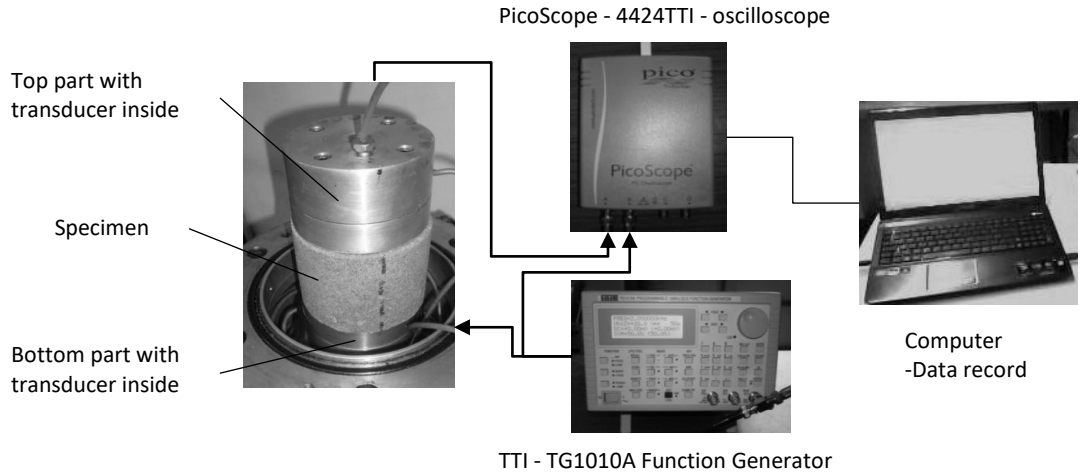

Figure 4.9. Setup of testing with bender-extender elements

4.3 EMM-ARM BASIC EXPERIMENTAL SETUP AND PROCEDURES

Despite the modifications made to EMM-ARM methodology presented in this chapter, particularly in regard to mould geometry and sample preparation, there were some common characteristics shared by all standard EMM-ARM experiments. Testing beams were placed under simply supported conditions and operational modal analysis was performed at room temperature (about 20ºC). The accelerations of the beams were measured in sets of time with 300 seconds of duration every 900 seconds of testing and recorded at sampling rate of 200 Hz by piezoelectric accelerometers placed at mid-span (PCB 393B12 accelerometers: frequency range of 0.15-1000 Hz; measurement range of ±0.5 g; sensitivity 10 V/g; resolution 8 μg; 210 g of mass). The accelerometers were connected to a dynamic signal acquisition system (National Instruments NI-USB-9234

DAQ: 24-bit; measurement range ±5V; 4 analogue input channels), which in turn was connected to a computer that recorded the data (Figure 4.10). A custom-made LabView code was used to operate the data acquisition system. The level of the ambient vibrations was increased by placing a fan nearby (pointed towards the testing beams). The identification of the resonant frequency of first mode of vibration followed the same procedure presented on sub-section 3.3.1.1 and included the following configuration for application of the Welch (1967) procedure: 4096 points for each segment; Hanning window with overlap of 50% for signal processing. The resonant frequency of determined for each set of time was related with E-modulus of the tested material through the process presented on sub-section 3.3.1.2.

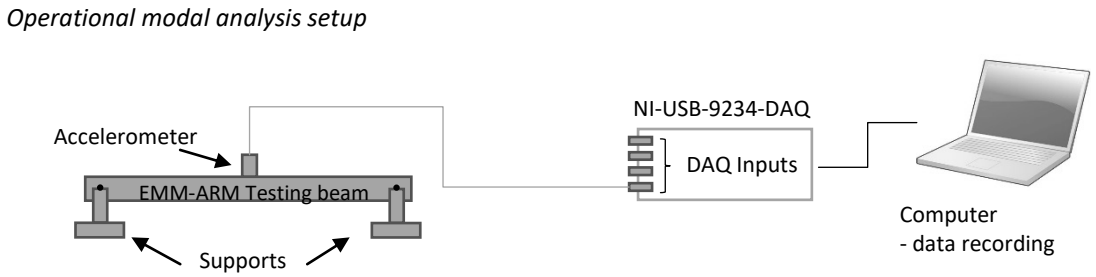

Figure 4.10. Scheme of the EMM-ARM basic experimental setup

4.4 MATERIALS AND MIXTURES TESTED

The experimental work presented in this chapter included the preparation and testing of two sand-cement mixtures, named as M1 and M2. These types of mixtures are similar to those used in the first application of EMM-ARM to stabilized soils (Silva, 2010, Azenha *et al.*, 2011). This section presents the materials characterization and proportions of each material used to prepare the mixtures.

4.4.1 Mixture M1

The first mixture, M1, comprised a uniform sand (S1) and an ordinary Portland cement CEM I 42.5R (CEN, 2005), provided by the cement producer SECIL. The sand was mainly composed of quartz, with traces of feldspar and basalt and its grading curve is presented on Figure 4.11. The sand can be considered as relatively regular as about 81.9% of the grains were retained by sieve 0.25mm.

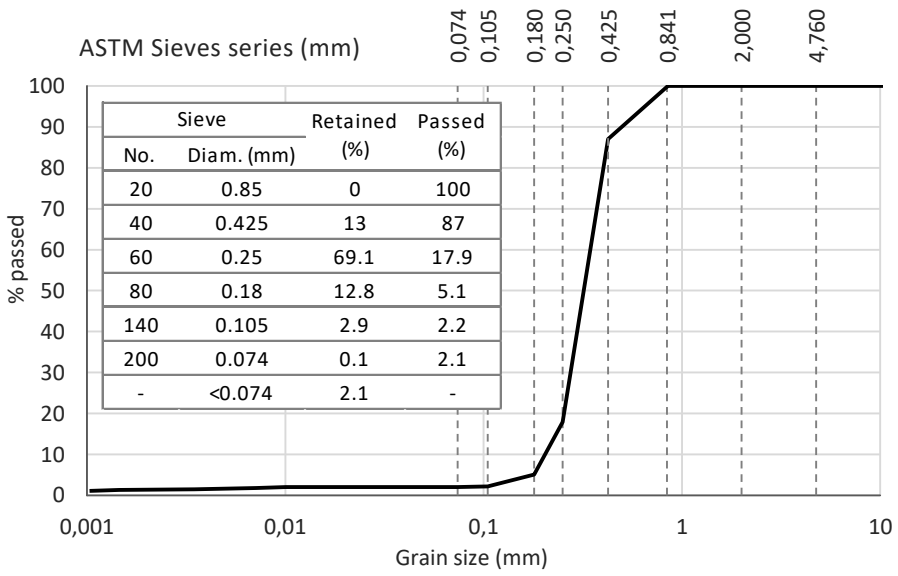

Sieve		Retained	Passed
No.	Diam. (mm)	(%)	(%)
20	0.85	0	100
40	0.425	13	87
60	0.25	69.1	17.9
80	0.18	12.8	5.1
140	0.105	2.9	2.2
200	0.074	0.1	2.1
-	<0.074	2.1	-

Figure 4.11. S1 sand grading curve (LNEC, 1966a)

The proportions of the mixture, by mass, comprised 7% of cement and 9% of water, measured in terms of the dry mass of sand. The compaction curves of the sand (S1) and of the sand-cement mixture (M1), were determined according to the Standard Proctor testing defined in the Portuguese standards E 197-1966 (LNEC, 1966b) and E 262-1972 (LNEC, 1972a). The corresponding results are presented in Figure 4.12.

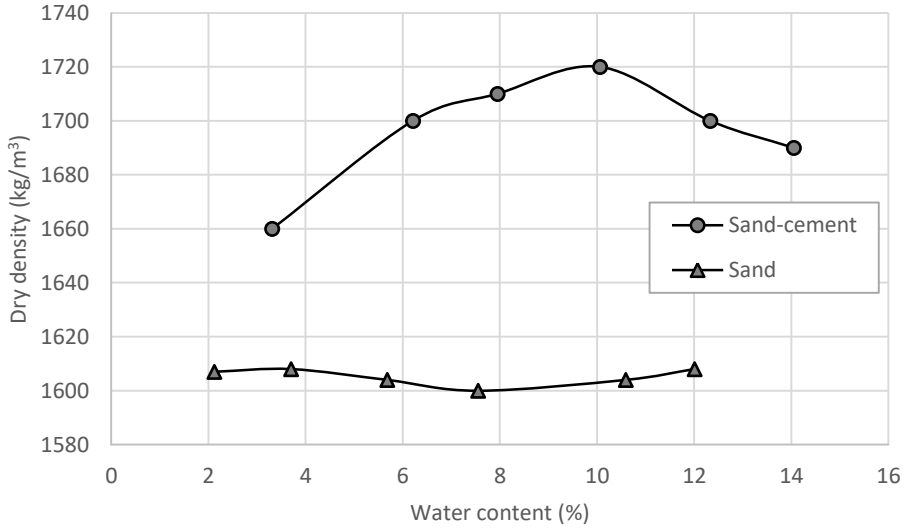

Figure 4.12. S1 sand and M1 sand-cement compaction curves (LNEC, 1966b, LNEC, 1972a)

It can be observed that the sand compaction curve has an irregular and unusual shape, not presenting a sharp peak for the maximum dry density, and therefore not having a single value for the optimum water content. This phenomenon is characteristic of granular soils without fine fractions because they are less sensitive to the water content moisture due to its permeability. The increase in the dry density observed for lower water contents is due to the action of capillary tension between particles (Santos, 2008). The sand-cement mixture, which exhibits a compaction curve that is coherent with the expectable shape, has an optimum water content of about 10% and a maximum dry density of 1724 Kg/m^3.

4.4.2 Mixture M2

The second tested mixture, referred as M2, was a mixture of a uniform sand (S2) and a Portland cement CEM II/ B-L 32.5N (CEN, 2005), provided by the cement producer CIMPOR. Sand S2 was also mainly composed of quartz, with traces of feldspar and basalt however its grading curve was slightly different than S1, as presented on Figure 4.13. The sand S2 can also be considered as relatively regular as about 85.8% of the grains were retained by sieve 0.25mm.

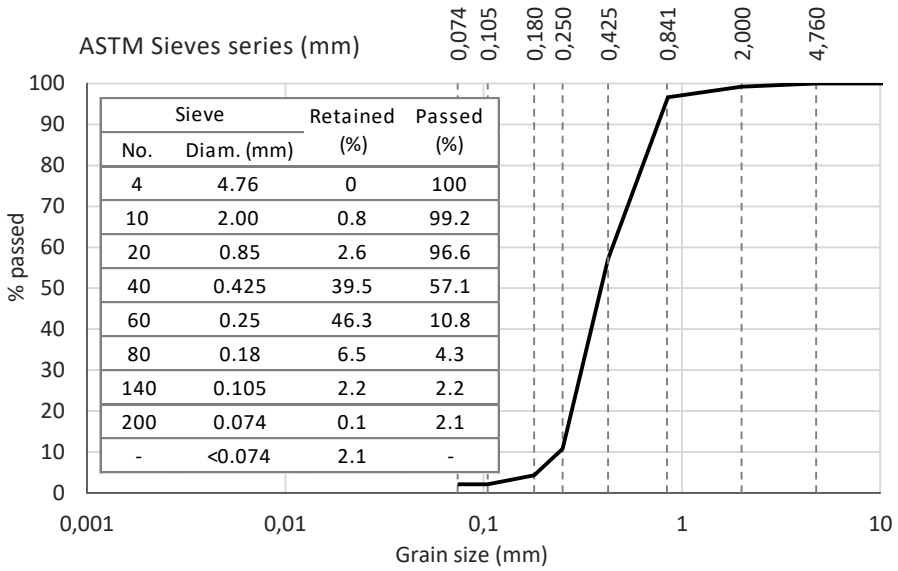

Sieve		Retained	Passed
No.	Diam. (mm)	(%)	(%)
4	4.76	0	100
10	2.00	0.8	99.2
20	0.85	2.6	96.6
40	0.425	39.5	57.1
60	0.25	46.3	10.8
80	0.18	6.5	4.3
140	0.105	2.2	2.2
200	0.074	0.1	2.1
-	<0.074	2.1	-

Figure 4.13. S2 sand grading curve (LNEC, 1966a)

The sand-cement mixture comprised 7% of cement and 9% of water, measured in terms of the dry mass of sand. The compaction curves of the sand (S2) and sand-cement mixture (M2), were determined through Standard Proctor testing as devised in Portuguese standards E 197 -1966 (LNEC, 1966b) and E 262-1972 (LNEC, 1972a). The corresponding results are presented in Figure 4.14. The optimum water content for the S2 sand is of about 10% and the dry density of 1670 Kg/m^3. The sand-cement mixture M2 has optimum water content of 9.6% and a maximum dry density of 1803 Kg/m^3.

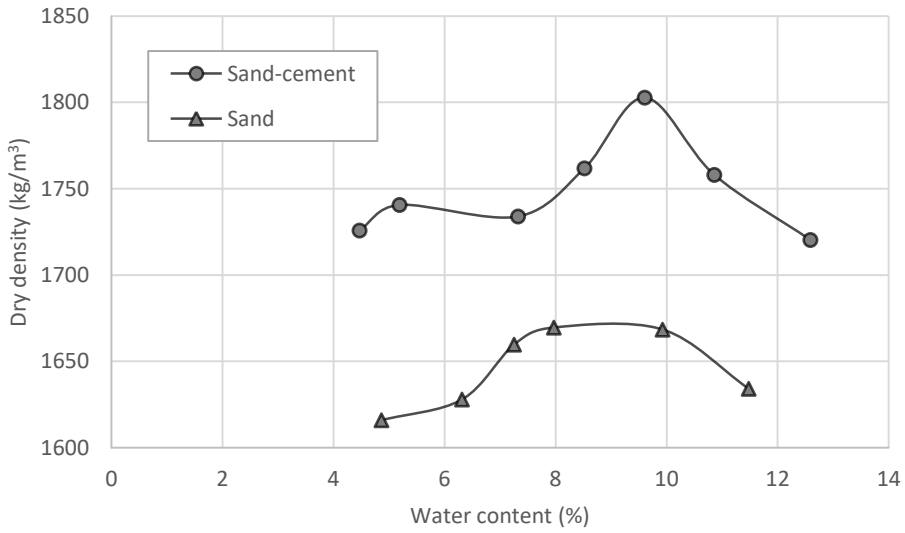

Figure 4.14. S2 sand and M2 sand-cement compaction curves (LNEC, 1966b, LNEC, 1972a)

4.5 MODIFICATIONS TO EMM-ARM MOULDS AND SAMPLING

The current subchapter describes a set of developments and experiments whose objective was to extend the preliminary work of Azenha *et al.* (2011) by introducing improvements to the test mould (i.e., shape and length) and extending the test period to 28 days of age. The mould alterations aim to simplify the experimental procedure and allow the collection of specimens directly from compacted cement-stabilised layers. These new developments started by proposing and assessing two different types of testing moulds and two different sampling approaches. For that purpose, EMM-ARM samples were directly collected from a pilot layer, prepared specifically for this process. The results obtained using EMM-ARM were compared with the stiffness moduli evaluated through direct measurements of shear and compression wave velocities by bender elements (BE) and ultrasonic (US) contact probes, respectively, as well as

through unconfined cyclic compression (UCC) tests on sand-cement specimens collected from the same layer and on specimens reconstituted with same sand-cement mixture. Based on the experience and results obtained, new improvements were proposed. These included the development of a steel tubular sampler that was used to collect samples from the top surface of a sand-cement compacted layer, to be tested though EMM-ARM. The results obtained using EMM-ARM were validated by comparison with E-modulus assessed by UCC testing on specimens reconstituted with same tested material.

4.5.1 Design considerations

Taking into account the results and conclusions from previous implementations and in order to make the method more suitable for systematic use, the following basic principles were considered for the preliminary design of EMM-ARM moulds: (i) the testing beams should be easily excited by the ambient vibrations in order to allow the easy application of ambient modal identification; (ii) a significant resonant frequency shift of the composite beam during the experiment is desirable, so that a good resolution in the E-modulus estimation can be achieved; (iii) the mould should endure negligible deflections, thus assuring the absence of second-order geometric effects; (iv) in situ sampling should be feasible with the adopted mould; (v) mould type and experiment strategy should assure adequate repeatability.

Particularly in regard to principles i), ii) and iii), sensitivity analyses were conducted, taking into account typical values of the E-modulus of the sand-cement mixtures after hardening (e.g., 7 GPa at an age of 28 days) as well as the typical density of the sand-cement mixtures. Furthermore, a desired resonant frequency shift between 10 and 50 Hz during testing was imposed for the testing beams. The lower bound of 10 Hz corresponds to the resonance frequency at the initial time of testing. It was selected to avoid any potential interference due to human activities nearby which may interfere with modal identification at low frequencies (e.g., walking usually occurs around 2 Hz). It should also be noted that limiting the minimum resonant frequency of the beam also has a positive impact on the limitation of its deflections, as stated in principle iii). The upper bound of 50 Hz corresponds to the resonance frequency at the end of testing, which was limited based on experience gathered in previous works (Azenha *et al.*,

2011). In fact, as the resonant frequency increases, the excitability of the beam decreases, making the ambient modal identification process more difficult and less accurate. Figure 4.15 presents the relation between the mixture E-modulus and the corresponding computed resonant frequency of tubular beams with different spans (800 mm, 900 mm and 1000 mm). The following additional characteristics were considered in these simulations: mixture density =1850 kg/m^3; mould density=1200 Kg/m^3; mould E-modulus =3.4 GPa; external diameter (d_e) = 50 mm; internal diameter (d_i) = 47 mm. Is possible to observe that the beam with a span of 800 mm does not satisfy the ranges proposed in the first approach for the mixture E-modulus and resonant frequency of the beam. In fact, with this geometry, for a mixture with a final E-modulus of 7 GPa, it is expected to reach a flexural resonant frequency of about 57.40 Hz this beam, thus exceeding the intended limit of 50 Hz. For the beams with span of 900 mm and 1000 mm, is possible to see that they satisfy the intended E-modulus and frequency limits. However, the beam with a span of 900 mm is a more desirable solution as it has higher resolution in terms of frequency: for an E-modulus variation from 0 to 7 GPa the expected frequency variation is about 30 Hz for the 900 mm beam, as compared to a 24 Hz shift for the 1000 mm beam.

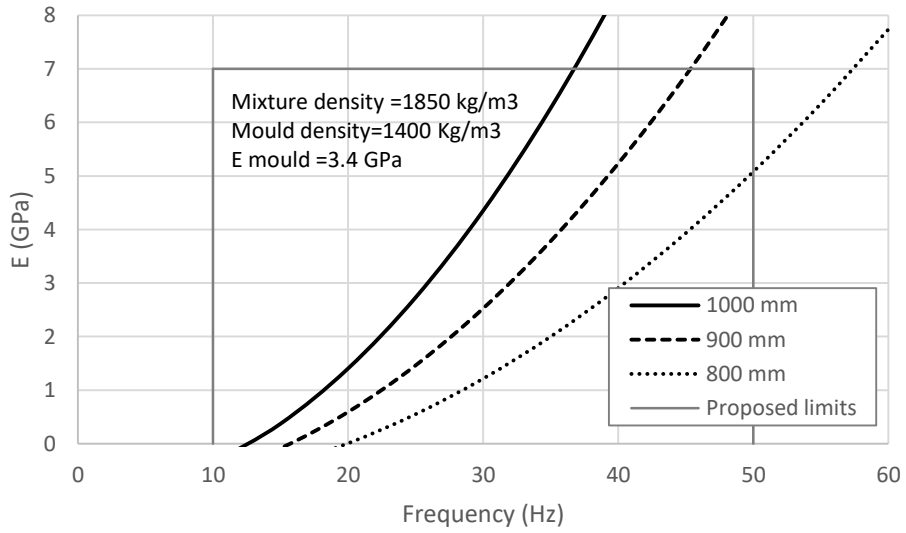

Figure 4.15. Relation between the mixture E-modulus and the resonant frequency of tubular beams with different spans

In regard to principle iii), the deformation δ at mid-span of the beams was estimated with equation (4.1), where q is the total distributed load per unit length (includes mould

and tested material), L is the beam span, E_m and I_m are respectively the E-modulus and moment of inertia of the cross section of the mould.

$$\delta = 5.q.L^4/(384.E_m I_m) \quad (4.1)$$

As the upper limit of the deformation at mid-span, the L/500 value has been selected in accordance with the recommendations of Eurocode 2 (CEN, 2010b) for concrete structures. Table 4.1 presents the results obtained for the same beams presented on Figure 4.15. The stiffness of the sand-cement mixture was not considered in the estimation of the deformation of the beam, which is a conservative simplification.

(Azenha *et al.*, 2011)

Table 4.1. Deformation at mid-span

L (mm)	L/500 (mm)	δ (mm)
800	1.6	0.80
900	1.8	1.28
1000	2.0	1.95

Concerning the cross-sectional size, it was imposed that the minimum dimension of the beams (diameter or edge) should be at least 3 to 5 times larger than the maximum nominal size of the particles of the tested mixture (ASTM, 2002). Symmetric cross-sections where adopted as to assure the coincidence of the gravity/rigidity centres of the mould and of the tested mixture inside the mould. Without this symmetry, the gravity/rigidity centre of the composite mixture might vary during the test and Equation (3.25) would not be applicable, leading to a more complex processing of the results.

In previous works with the EMM-ARM technique (Azenha *et al.*, 2011, Silva, 2010), in which a "U"-shaped mould was used, some problems with wear were found. In fact, after some utilizations of the mould, a certain amount of detachment was observed in the glued connections between the plaques. This poor performance jeopardizes the reutilization of the mould and compromises the repeatability of the technique using that kind of mould. In order to overcome this problem and to satisfy item v), the "U"-shaped mould was abandoned and new moulds were designed.

4.5.2 Moulds design

Taking in account the principles described, two types of moulds were designed. The first type of mould consisted on a 900 mm long polyvinyl chloride tube (PVC – density=1200 kg m^{-3}; E_{PVC}=3.4 GPa) with an inner diameter of 47 mm and a wall thickness of 1.5 mm, as shown in Figure 4.16. With this configuration, the expected range of resonant frequencies for the sand-cement mentioned in the previous section is about 15 to 45 Hz, satisfying principles i) and ii). The ratio deformation/span estimated for this beam was of about L/700, satisfying iii), and the computed area ratio was of 13.2% which practically meets principle iv). Even though this type of mould cannot be reused, it is quite cheap when compared to those used in previous works (Azenha et al., 2011) and has no joints susceptible to debonding, thus contributing to the satisfaction of principle v).

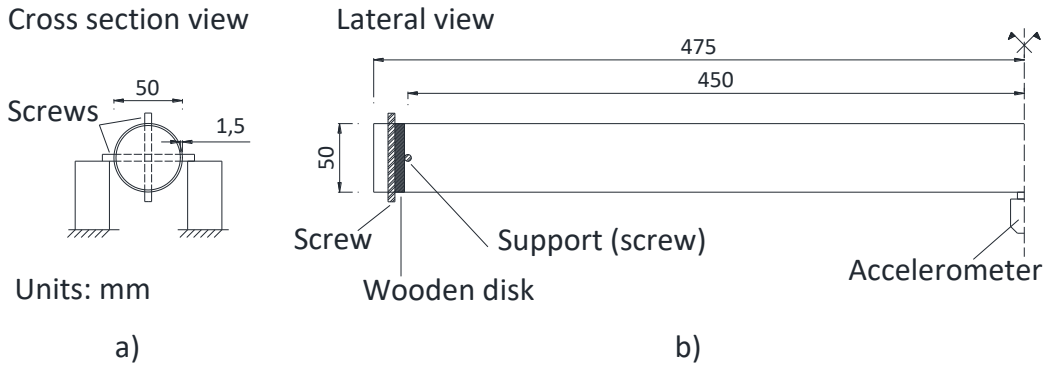

Figure 4.16. Tubular PVC mould: (a) cross-section; (b) lateral view (units: mm)

The placement of samples into the tube can be made in situ by inserting the tube laterally into the recently compacted layer (see a detailed description of the sampling procedure in subsection 4.5.3.2). At the extremities of the beam, screws are used to materialize the simple supports of the beam on stiff bases in an analogous way to the original implementation of EMM-ARM (Azenha *et al.*, 2010).

The second redesigned mould, shown in Figure 4.17, consisted of 4 polycarbonate plates (density=1180 kg m^{-3}; E-modulus=2.2 GPa) forming a hollow beam with an inner cross-section of 40 mm×40 mm to hold the cemented-sand sample. Screws were used to connect the plates, allowing the full disassembly of the mould after testing. In order to accommodate the screwed connections, the side plates had a larger thickness (8 mm) than the other plates of the mould (3 mm). With this configuration, the expected range

of resonant frequencies is 22 to 45 Hz and the estimated ratio deformation/span is L/1500, satisfying principles i), ii) and iii). The sampling process required a specially designed sampler shown in Figure 4.18. Detailed information regarding the sampling procedure is given in subsection 4.5.3.2.

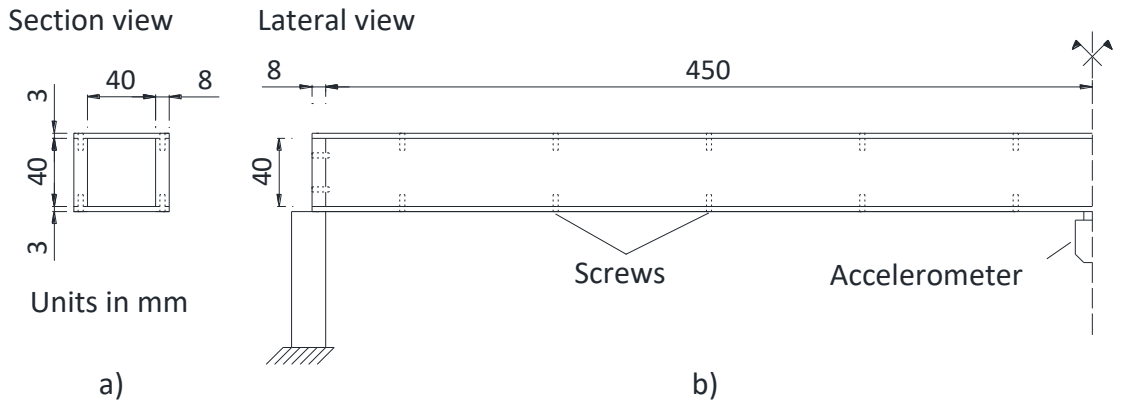

Figure 4.17. Prismatic mould: a) cross-section; b) Lateral view

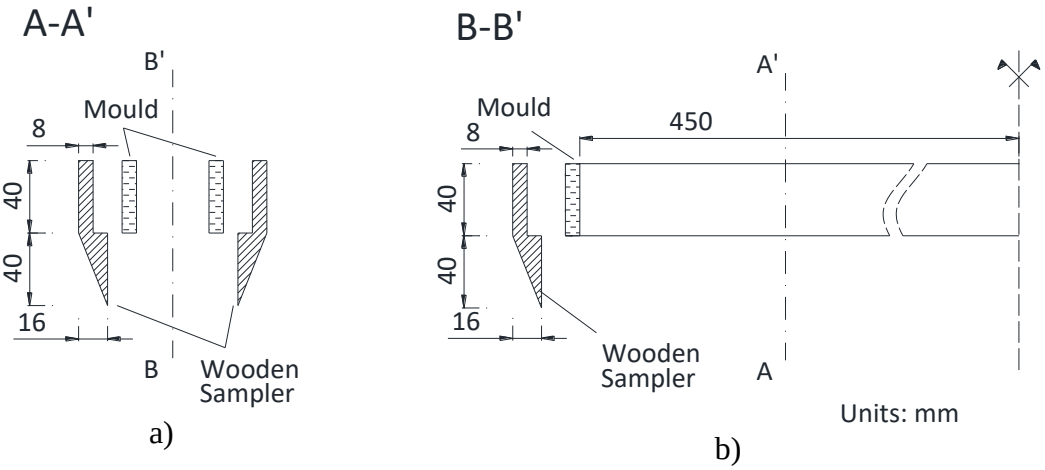

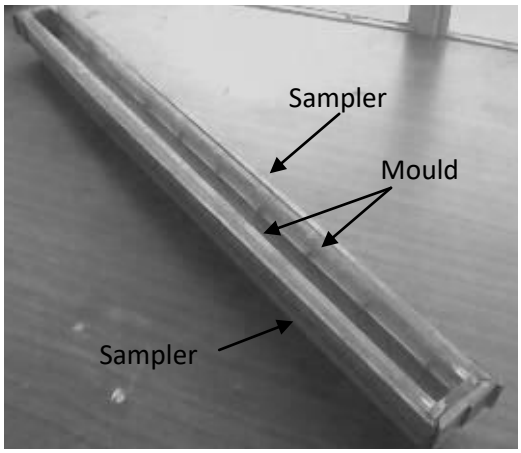

c)

Figure 4.18. Prismatic mould/sampler set: a) cross-section detail; b) longitudinal detail; c) mould inside the sampler

4.5.3 Validation

To test the performance of the designed moulds and the possibility of using them for *in-situ* sampling, a test program was performed following the strategy presented on Figure 4.19. This included the execution of a pilot layer of a compacted sand-cement mixture from which several specimens were collected to be tested by EMM-ARM, UCC, bender-extender elements (BE) and ultrasonic (US) contact probes. Additionally, some specimens were prepared by reconstitution using the same mixture used in the preparation of the pilot layer and tested by UCC, BE and US. The validation of the sampling and EMM-ARM modifications was made by comparison of results obtained by the different methodologies.

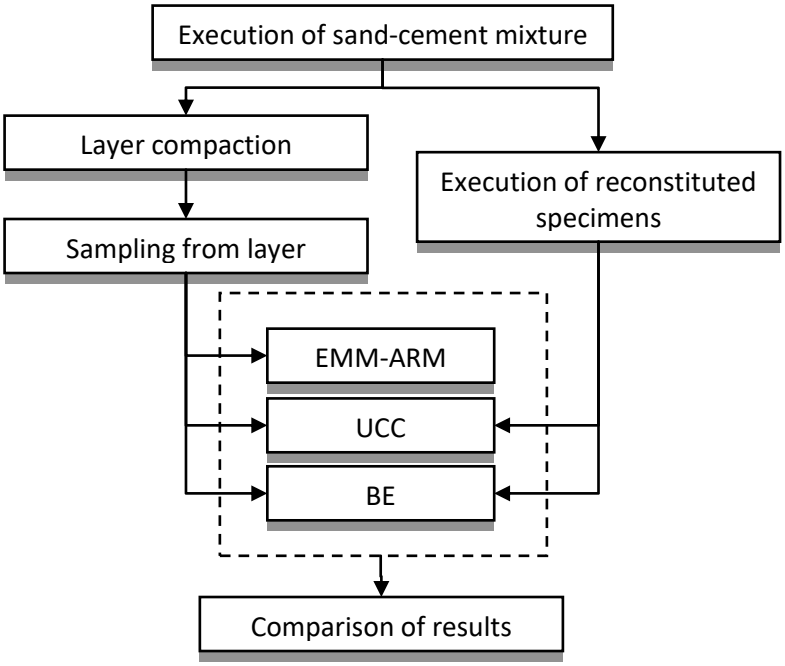

Figure 4.19. Overall strategy for sampling validation and E-modulus testing

4.5.3.1 Layer compaction

A stabilised sand-cement layer, of mixture M1 (described in 4.4.1), was compacted inside a wooden box with inner dimensions of 1.0 m × 1.5 m × 0.3 m (450 litres), as shown in Figure 4.20. The mixing procedure was performed in a 150-litre concrete mixer with a 45º inclined axis and a rotation speed of 17 rpm with the following steps:

with the mixer stopped, sand was placed inside the mixer bucket; the mixer was then turned on, and the cement was immediately added; 2 minutes after turning the mixer on, water was added, and the mixer operated continuously for five minutes. Due to the volume limitation of the available mixer, the mixture was executed in 3 consecutive batches. The layer was compacted inside the wooden box in three parts, corresponding to individual batches of 150 litres each. For reference, the instant t=0 for the experiments refers to the time at which the water was mixed with cement in the first batch. The instant of contact with cement for water for batches 2 and 3 occurred at t=30 minutes and t=55 minutes, respectively.

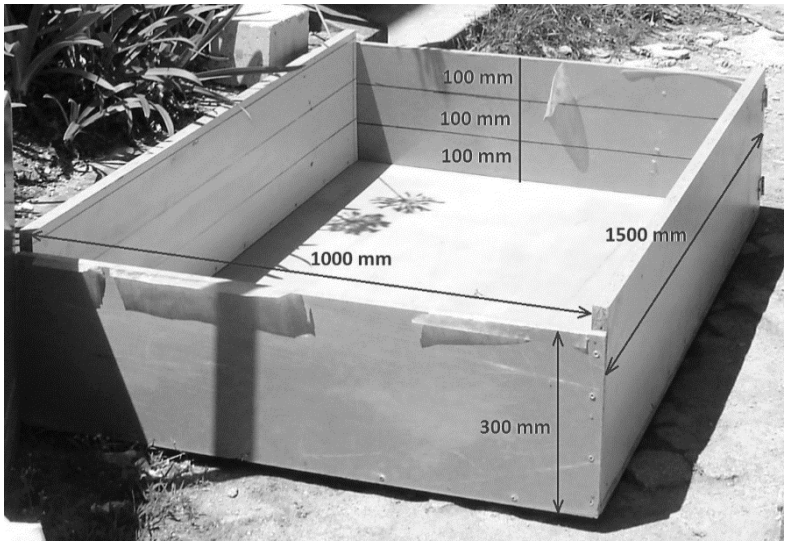

Figure 4.20. Wooden box with layer dimensions before mixture placed

The intended dry density of the sand-cement layer was 100% of the maximum density obtained in the Standard Proctor test (LNEC, 1972a). Based on the intended density, the volume of each batch and the dimensions of the wooden box, horizontal lines were marked inside the wooden box, spaced by 0.1 m, which were used as reference lines to determine the thickness of each of the three stages of placement to be achieved during the compaction process. The height of each layer was slightly smaller than standard practice for cement-stabilised soils, which usually range between 25 cm and 70 cm (LCPC-SETRA, 2000). However, this fact was not considered problematic for the representativeness of the experiments.

After execution of each mixing batch, the stabilised mixture was placed inside the wooden box, and each part was compacted with a manually-operated cylinder compactor that was 500 mm wide and weighted 60 kg, as shown in Figure 4.21a-c. The prescribed layer thickness was attained after an average of 9 passes (±1), thus ensuring an expectable similar density for all layers. The compaction of each stage of the layer was finished at approximately t=15 min, t=45 min and t=70 min, for the first, second and third stages, respectively.

a) b) c)

Figure 4.21. Execution of sand cement layer: a) first stage compaction; b) final compaction; c) layer after final compaction

4.5.3.2 Sampling procedure

After the final compaction of the layer, several specimens for EMM-ARM, UCC, and BE/US testing were prepared by tree distinct methodologies: *i*) cylindrical shaped specimens directly sampled from the layer; *ii*) prismatic specimen directly sampled from the layer; *iii*) reconstituted specimens with material collected from the layer and manually compacted into the mould. Methodology *i*) includes the use of PVC tubular moulds, with internal dimensions equivalent to the diameter of the intended specimen (see Table 4.2), statically pushed into the layer. With this procedure, it was expected that undisturbed representative specimens would be obtained with the same density and mechanical properties as the layer. The area ratio of the tubes is 10.7% for the UCC and BE/US samplers and 13.2% for the EMM-ARM tubular samplers, which is fairly similar to the upper limit of 10% prescribed by ASTM D1587-08 (ASTM, 2008) for the collection of intact samples. In methodology *ii*) a prismatic polycarbonate mould, as presented in Figure 4.17a,b, was used to receive the sample. The sample was obtained from the top surface of the compacted layer and the process involved the necessity of

using the sampling device shown in Figure 4.17 and Figure 4.18. With methodology *iii*), specimens were reconstituted. This means that they were prepared by collecting the material from the layer, and manually compacting it inside the corresponding mould with a steel rammer and mechanical hammer. The final density of these reconstituted specimens was controlled by regular weighting along the compacting procedure.

To collect the EMM-ARM samples, referenced as T1 and T2, two PVC tubes were introduced horizontally in the compacted layer (as described in sub-section 4.5.2) by applying pressure to the free extremity (Figure 4.22a). Specimens for UCC testing (UCC-V1 and UCC-V2) and for BE/US testing (BE-V1 / US-V1, BE-V2 / US-V2 and BE-V3 / US-V3) were also collected directly from the compacted layer by vertically pressing the corresponding PVC moulds on the top of the layer until the mould was completely filled (Figure 4.22b). The specimens used for BE and US testing were the same, but for the sake of the presentation of results, different names were assigned. Thus, the results of BE-Vx and US-Vx pertain to the same specimen.

a) b)

Figure 4.22. PVC tube introduction on the layer: a) laterally for EMM-ARM sample collection; b) from top for UCC testing

The sampling procedure for the square cross-section mould EMM-ARM PV (shown in Figure 4.17) is less straightforward. The sampler held the lateral plates of the mould, and it was pressed vertically into the compacted layer according to the progressive process shown in Figure 4.23a-f and Figure 4.24a-c. This process needed to be done sequentially by applying downward pressure and removing small quantities of the sand-cement around the sampler until the sample exceeded the top side of the mould (Figure 4.23f and Figure 4.24). The excess material was removed and the top side of the mould

was attached with screws (Figure 4.23g). Then, the set was rotated upside down, the sampler was opened, the excess material was removed and the mould was closed and screwed (Figure 4.23h), forming the final composite beam. It should be noted that, being an initial prototype, this sampling device was made of wood to reduce costs. In fact, due to the low stiffness of the sampling device, difficulties were observed during the insertion into the compacted layer due to the wood deformation.

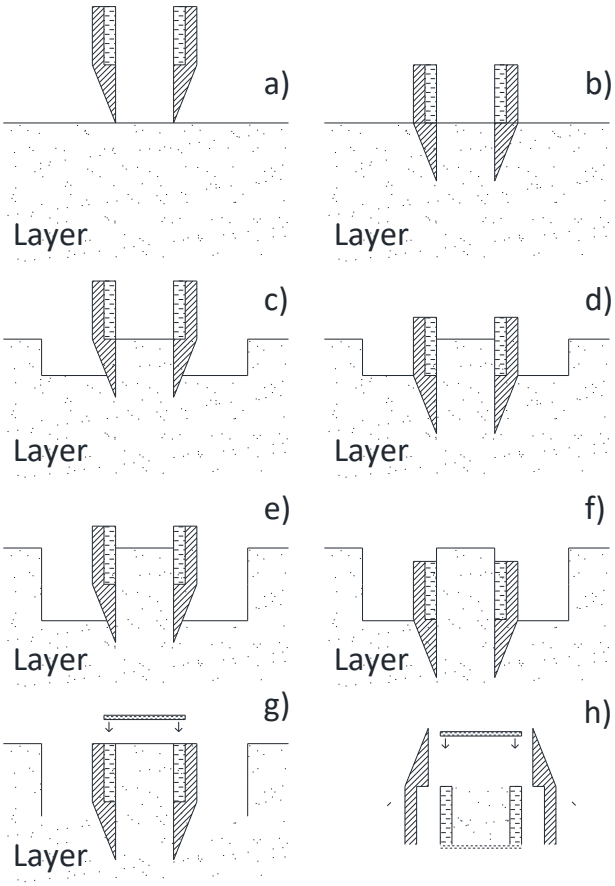

Figure 4.23. Phases of the sampling process with the prismatic mould

Additionally, reconstituted specimens for EMM-ARM (i.e., EMM-ARM PR) and specimens for BE/US testing (i.e., BE-R1 / US-R1, BE-R2 / US-R2 and BE-R3 / US-R3) were prepared using material extracted from the layer according to methodology *iii*) described earlier in this section. The UCC reconstituted specimens (i.e., UCC-R1, UCC-R2 and UCC-R3) were prepared using same procedure described in sub-section 4.2.1.

a) b) c)

Figure 4.24. Prismatic sample collection: a) sampler introduction in the layer surface; b) removing sand-cement around the sampler; c) sample exceeding the top side of the mould

Reconstituted specimens (EMM-ARM prismatic, BE/US and UCC) had same dimension of those that were sampled from the layer. The size, instant of collection, ages of testing, quantity and references of the specimens performed for the E-modulus determination by the different techniques are presented in Table 4.2, and the layout of the specimens collected through methodology *i*) is presented in the plan view of the layer shown in Figure 4.25a. Figure 4.25b illustrates a section view that identifies the vertical relative position of collection of each specimen. After the collection process, all UCC/BE/US specimens were sealed with a PVC film to hinder water loss and stored in a room with an air temperature of 19.2±0.5ºC. EMM-ARM testing was also performed under the same environmental conditions.

Table 4.2. Specimens performed for stiffness determination

Tests	Diameter × Length (mm)	Collection instant (t) (min)	Ages of testing (days)	Quantity		Reference
				i) Intact specimens	*ii*) Reconstituted specimens	
UCC	100 × 200	100 to 120	7, 14, 21, 28	2	-	UCC-V1 UCC-V2
				-	3	UCC-R1 UCC-R2 UCC-R3
BE / US	100 × 70	120 to 140	1, 2, 3, 7,14, 21, 28	3	-	BE-V1 / US-V1 BE-V2 / US-V2 BE-V3 / US-V3
				-	3	BE-R1 / US-R1 BE-R2 / US-R2 BE-R3 / US-R3
EMM-ARM	47 × 900	80 to 90	Continuous until 28 days	2	-	EMM-ARM T1 EMM-ARM T2
	40 × 40 × 900	140 to 170		1		EMM-ARM PV
					1	EMM-ARM PR

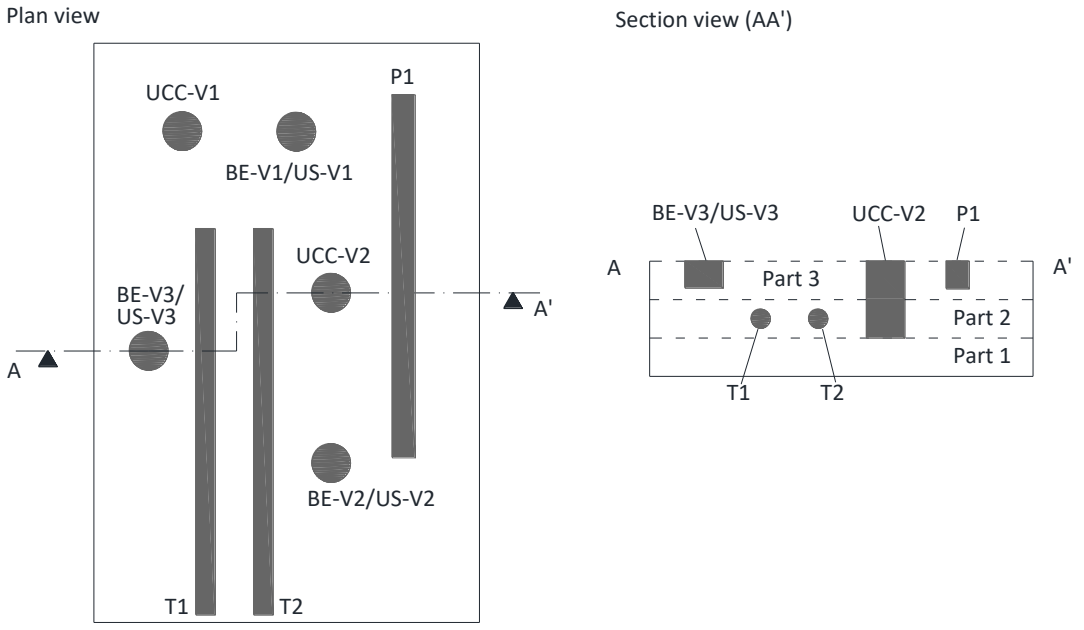

a) b)

Figure 4.25. Layout of specimen collection: a) plan view; b) section A-A' view

The EMM-ARM beams were then placed in simply supported conditions, the accelerometers were attached at mid span (Figure 4.26) and monitoring of accelerations started at the age of approximately 4 hours after mixing. The measurements were carried out for a total period of 28 days. The initial 4 hours of delay between mixing and testing were related to logistics issues, such as the compaction of the layers and sampling operations.

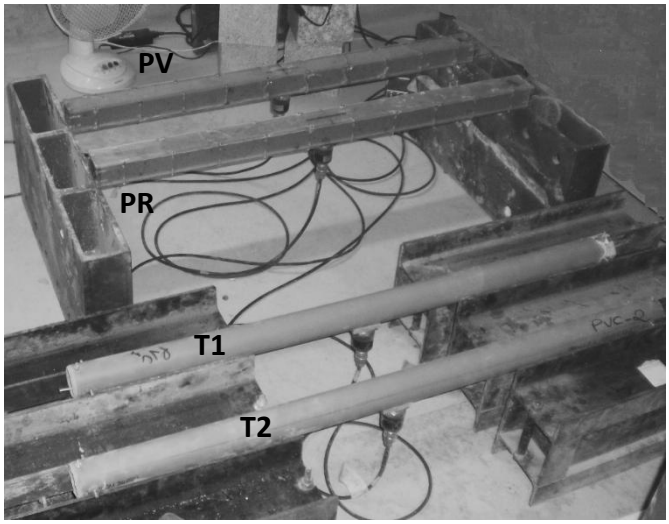

Figure 4.26. EMM-ARM testing beams during acceleration monitoring

4.5.3.3 Specimen density

The bulk densities of the tested samples are presented in Table 4.3. It is possible to observe that the values obtained are relatively similar in all specimens except for the EMM-ARM PV beam. In fact, its higher value of density was possibly caused by an over compaction during trimming of the soil-cement to the level of the mould. For the other specimens, the maximum variation of the bulk density was less than ±3.5%, which indicates a good uniformity of the sample compacted in the wooden box and accuracy in sampling procedures.

Table 4.3. Specimen bulk densities

Test	Reference	ρ (kg/m^3)
EMM-ARM	EMM-ARM T1	1823
	EMM-ARM T2	1860
	EMM-ARM PV	1982
	EMM-ARM PR	1884
UCC	UCC-V1	1816
	UCC-V2	1814
	UCC-R1	1796
	UCC-R2	1780
	UCC-R3	1758
BE / US	BE-V1/US-V1	1773
	BE-V2/US-V2	1777
	BE-V3/US-V3	1760
	BE-R1/US-R1	1815
	BE-R2/US-R2	1781
	BE-R3/US-R3	1799

4.5.3.4 Resonant frequency identification

The time *versus* frequency surface charts for specimens PR, PV, T1 and T2 are presented on Figure 4.27a, b, c and d, respectively. The discontinuities observed in Figure 4.27a,b were due to electrical problems occurred with the experimental setup, which made it impossible to monitor the accelerations of the beams PR and PV at those ages. The surface charts of prismatic beams (PR and PV) present two different evolution paths for each specimen during curing time. In fact, the evolution paths marked as (i) represents the evolution of the first mode of vibration in the vertical plane, whereas evolution paths at higher frequencies, marked as (ii), might be related to a mode of vibration in the horizontal plane of the beam. Regarding specimens T1 and T2, the surface charts are very clear and each one presents a single evolution corresponding to the resonant frequency evolution of first mode of vibration.

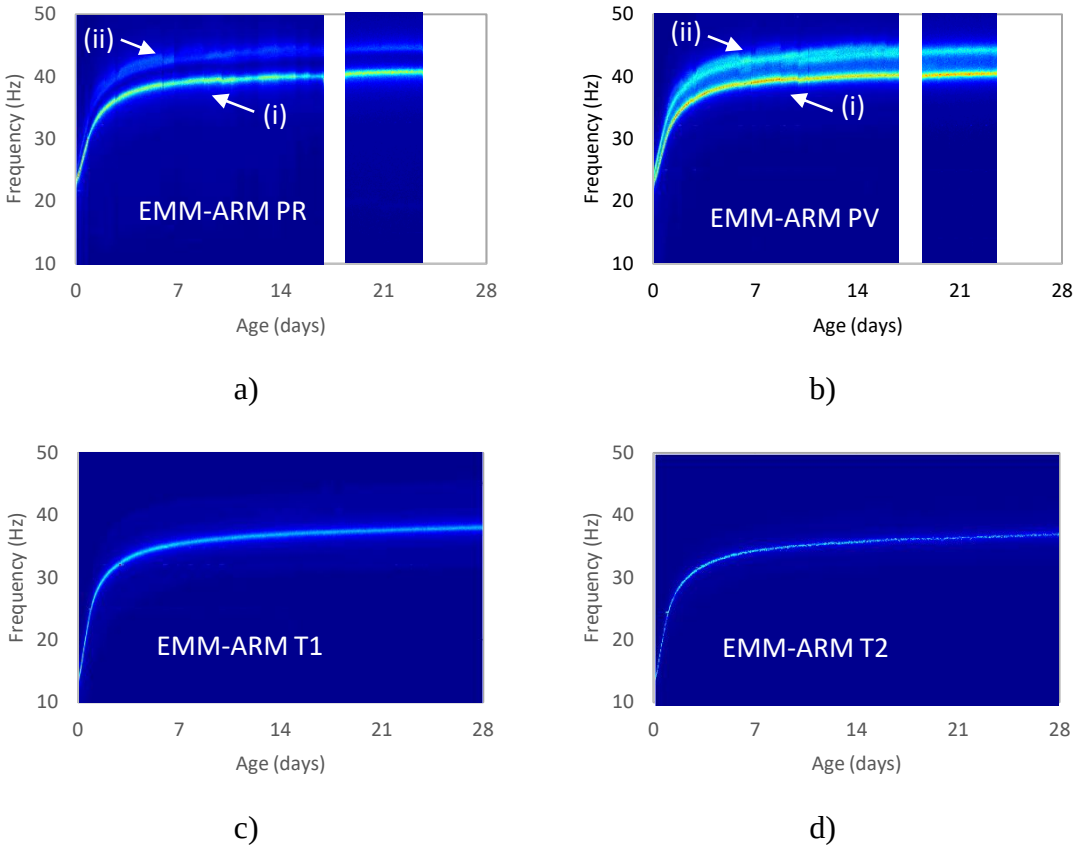

Figure 4.27. Time *versus* frequency surface chart obtained from EMM-ARM testing: a) PR, b) PV, c) T1 and d) T2

The Normalized Power Spectra Density (NPSD) estimation obtained for EMM-ARM testing beams, T1 and T2 at the ages of 0.2, 1, 7 and 28 days and PR and PV at the ages of 0.2, 1 and 21 days, are shown in Figure 4.28a-d. In these figures, it is possible to clearly identify the peaks corresponding to the first resonant frequency of the EMM-ARM beams at the presented ages. In the spectra obtained with prismatic beams (PR, PV), Figure 4.28a,b, it is further possible to observe a second peak at frequencies higher than the resonant frequency of first mode of vibration in the vertical plane, concerning other mode of vibration in the horizontal plane of the beam, as observed before in the surface charts. It is also possible to identify a set of small and thin peaks around the frequency of 25 Hz, which are more evident in some spectra of Figure 4.28a,c. These peaks are considered to be disturbances, probably resulting from power line harmonics contamination that can occur during the data acquisition. Theses types of disturbances can appear at power line frequency and respective harmonics (in Portugal the nominal power line frequency is 50 Hz, and 25 Hz is one of it sub-harmonics) and usually it is

difficult to totally eliminate its effect. However, it can be minimized by properly connecting all equipment to the ground (Butler & Russell, 2003). Even so, for this experiment, these peaks have no relevant significance when compared to the peaks corresponding to the resonant frequencies. The low significance of noise in the NPSDs and the ease for identification of the resonant frequencies indicates a good performance of the methodology adopted for modal identification with the use of a single accelerometer. Is also possible to observe that there is a reduction on the peak amplitude as the resonant frequency increases. This amplitude reduction can be explained by the reduction of the beam's excitatibility as the mixture stiffness increases.

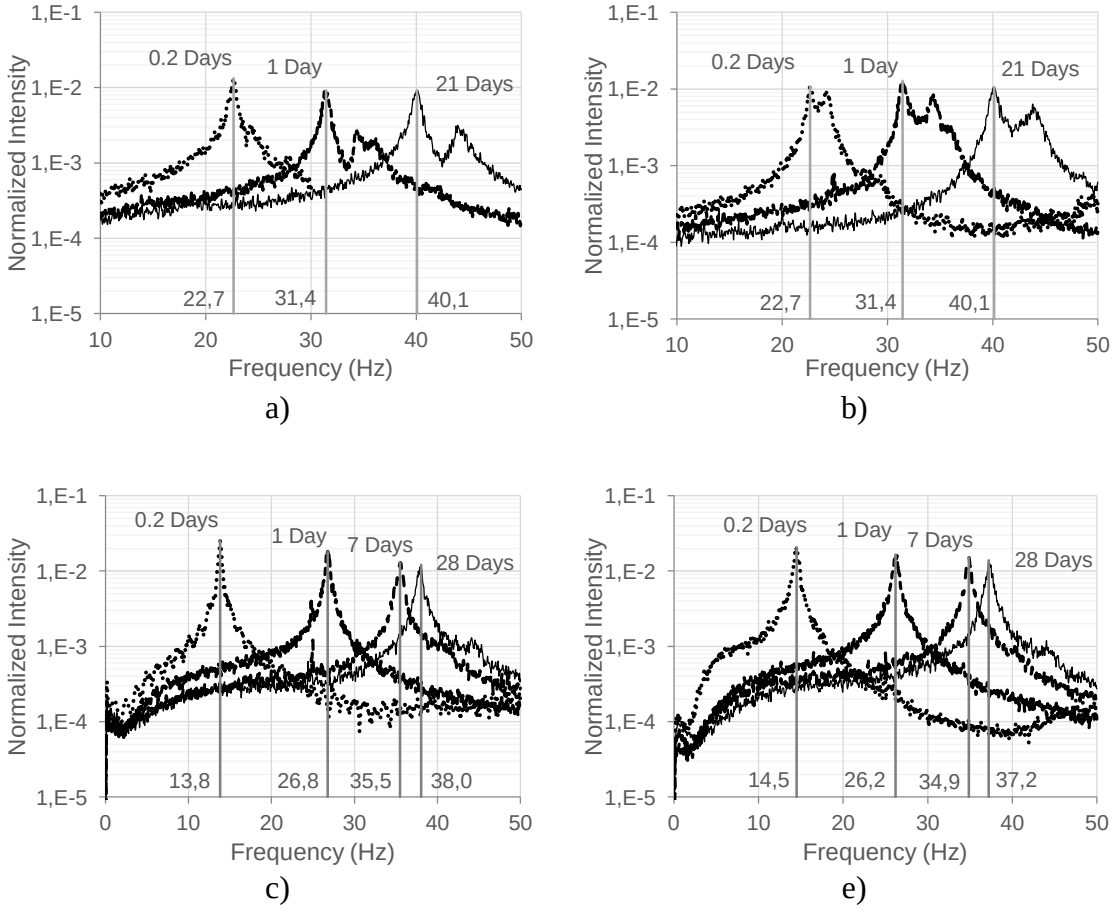

Figure 4.28. NPSD of EMM-ARM testing beams: a) PV and b) PR at ages of 0.2, 1 and 21 days; c) T1 and d) T2 at ages 0.2, 1, 7 and 28 days

The first resonant frequencies of the EMM-ARM beams PV, PR, T1 and T2, obtained from the surface charts, are compiled in Figure 4.29. Both tubular beams (T1, T2) showed similar evolutions during the test period. Considering the similar densities of

sand-cement in both tubular beams, this coherence in resonant frequency evolution indicates the good repeatability of the experimental technique. In the case of the prismatic beams the comparison in terms of frequency evolution is not straightforward as a considerable differences were observed for the densities of these specimens.

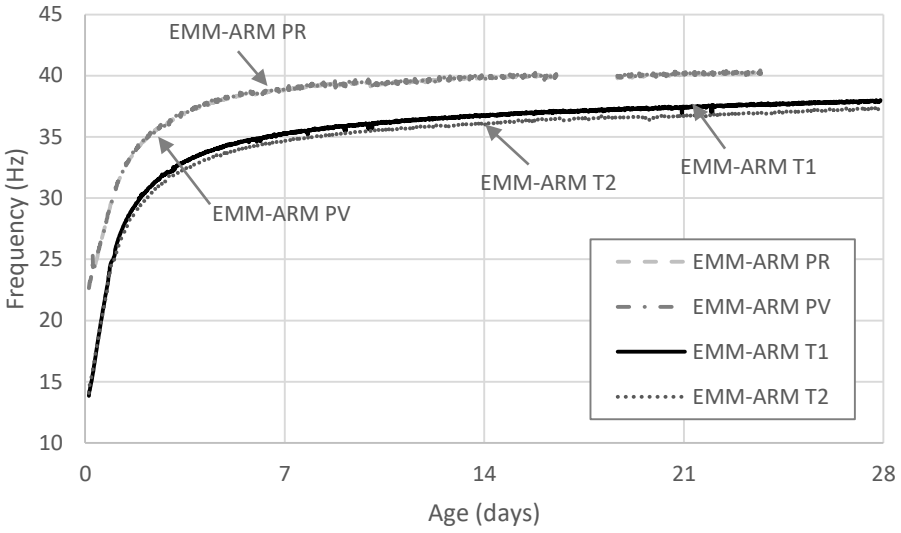

Figure 4.29. Evolution of first resonant frequency of EMM-ARM beams during 28 days of testing

4.5.3.5 E-modulus evolution

The estimated evolution of the E-modulus of the sand-cement during the first 28 days of age, computed with basis on the resonant frequencies for the four beams is shown in Figure 4.30. The agreement between the two tubular specimens and the prismatic specimen EMM-ARM PR is very good, with absolute stiffness differences under 3%. In fact, the small differences obtained can be related to the slight differences observed in these specimens densities. The results of the EMM-ARM allow a clear identification of the early hydration kinetics and the instant at which the stiffness development rate endures an intense deceleration (at t≈4days). Remarks should be also given regarding the EMM-ARM results obtained with EMM-ARM PV. The E-moduli estimated with this specimen is larger than those obtained by EMM-ARM T1, T2 and PR. This difference is of about approximately 10% at most instants and can be related with the fact of the tested material on this beam (PV) has a higher density (see Table 4.3) resulting on the higher stiffness observed.

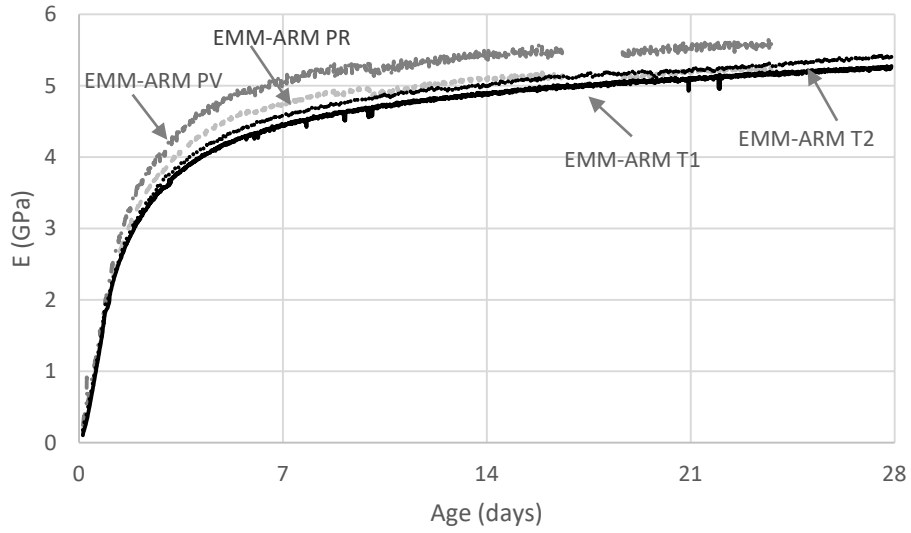

Figure 4.30. E-modulus estimation using EMM-ARM technique

Table 4.4 presents the discrete E-modulus obtained through unconfined cyclic compression testing (UCC) and Figure 4.31 presents these same results together with the evolution of the E-modulus obtained using EMM-ARM. In regard to EMM-ARM T1 and T2, the agreement with UCC tests is remarkable at all tested ages, with absolute stiffness differences always remaining below 5%. This is a very good indication regarding the feasibility of using this kind of geometry and sampling technique, which end up being simple and cheap.

Table 4.4. E-modulus determined from UCC testing

Age (Days)		7	14	21	28
E (GPa)	UCC-V1	4.38	4.89	5.03	5.32
	UCC-V2	4.24	4.77	5.06	5.18
	UCC-M1	4.48	4.80	5.21	5.44
	UCC-M2	4.14	4.46	4.90	4.99
	UCC-M3	3.95	4.54	4.85	4.99

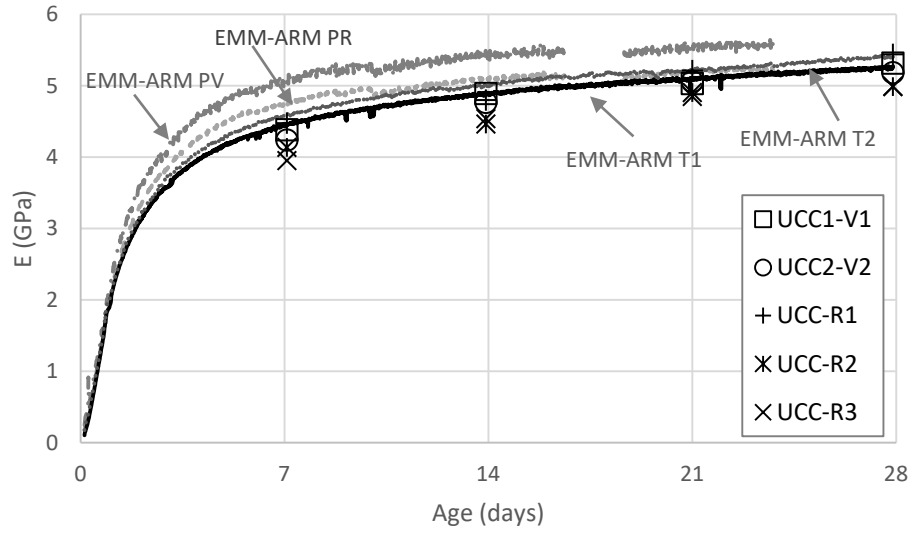

Figure 4.31. E-modulus obtained with EMM-ARM and UCC

4.5.3.6 Stiffness estimation with wave propagation based techniques

The process of determining the propagation time of the shear waves using BE involved some uncertainty. In fact, doubts often existed in determining the exact instant of the first arrival of the propagated wave at the output sensor. In order to reduce this uncertainty, each BE measurement was initiated with the search for the most adequate range of input frequencies, that is, those which generated clearer output signals. In general, at least three different frequencies were recorded at each BE measurement, for comparative analysis in the determination of the travel time. Moreover, to overcome this difficulty, different possible values for the propagation time were found and registered: the best estimate and the upper and lower bounds. An example is presented in Figure 4.32 from the results obtained with BE measurements on the BE-R2 specimen at 2 days of age for an input frequency of 26.4 kHz. By observing this figure, it is possible to see that the maximum amplitude of the output signal was very small compared to the input signal applied to the transmitter BE. It is also possible to see that, in this result, the amplitude of the electrical noise is about half that of the output signal. Under these experimental conditions, the measured signal is significantly affected by electrical noise, making signal interpretation more difficult. For the output signal in Figure 4.32, it is difficult to clearly identify the exact instant of the first arrival of the received wave. However, based on accumulated knowledge, it is possible to state that this instant most likely occurs between 100.6 μs and 108.3 μs, which correspond to the first local

minimum at the arrival of the received signal and its zero-crossing, respectively. The best estimate of the travel time is usually defined from the observation and comparison of the received waves of different input frequency signals (variable according to the specimen stiffness and to the quality of the signals), as proposed by Viana da Fonseca *et al.* (2009c) and Ferreira (2009). This procedure enables the reduction of subjectivity and uncertainty. In view of these results, the interpretation process involved registering the best estimate of the wave travel time in addition to an interval of possible values, leading to the definition of the lower and upper bounds for travel time. The results of this interpretation are summarised in Table 4.5.

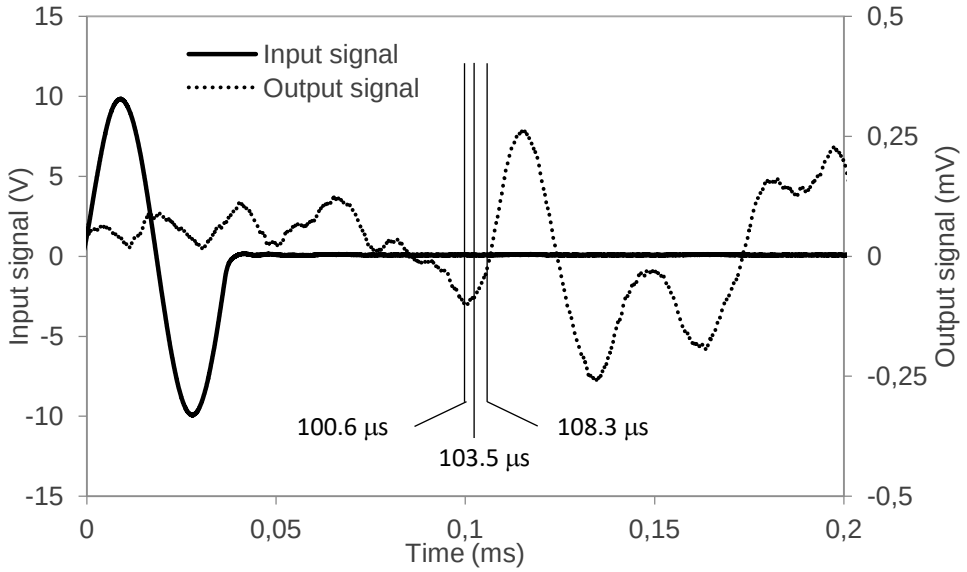

Figure 4.32. Determination of shear wave propagation time using BE for specimen BE-M2 at age of 2 days

From the analysis of the variability of the shear wave velocities obtained from the three possible values of travel time, it can be noted that the best estimate frequently corresponds to the average of the extreme values. The maximum variation between extreme values and the best estimate, in terms of shear wave velocities, was found to be ±12%. The shear modulus determination may thus be affected by a maximum error of ±24% (according Equation (2.14) on subsection 2.4.2), which is considerable. Despite the application of a consistent BE testing framework to improve signal interpretation, the observed margins of errors are far from ideal. A combination of factors apparently led to this situation, namely the need to use high input frequencies at which BE tend to

overshoot (Viana da Fonseca *et al.*, 2009c, Amaral *et al.*, 2011, Pallara *et al.*, 2008), potential issues associated with incomplete coupling between the BE transducers and the surrounding soil, the high noise-to-signal ratio and the relatively low Poisson's ratio of this material which is reflected in the proximity between P- and S-wave travel times (with consequences to the clarity of signal interpretation).

Table 4.5. S-wave velocity measured by BE sensors (from the best estimate and upper and lower bounds of travel time)

		Shear wave velocity - V_S (m/s)					
Age (days)	Estimate	BE-V1	BE-V2	BE-V3	BE-M1	BE-M2	BE-M3
1	Best	630	554	584	683	509	578
	L	620	539	564	667	509	552
	U	653	597	594	761	515	620
2	Best	900	778	807	780	686	683
	L	875	733	708	762	670	662
	U	928	789	831	865	706	711
3	Best	940	827	873	890	810	845
	L	908	800	793	866	787	787
	U	962	839	883	997	841	888
7	Best	986	993	1025	1009	967	1056
	L	943	971	1006	943	926	1004
	U	1066	1046	1055	1075	1055	1126
14	Best	1081	1106	1122	1092	1092	1103
	L	1046	1058	1066	982	997	1042
	U	1115	1136	1146	1158	1183	1140
21	Best	1138	1136	1142	1136	1127	1170
	L	1096	1099	1068	1015	1076	1129
	U	1181	1154	1178	1162	1199	1191
28	Best	1138	1149	1178	1153	1164	1173
	L	1113	1113	1094	1061	1092	1127
	U	1169	1205	1198	1175	1275	1221

L - Lower bound; U - Upper bound

To further analyse the variability of BE results and their impact on the accurate determination of stiffness, these results have been compiled with the EMM-ARM T1 stiffness measurements, as shown in Figure 4.33. For comparison purposes, the stiffness measurements were normalised to the 28-day measurement. The graphs include the best estimate and upper and lower bounds of the shear modulus obtained from the bender elements. The trends of relative stiffness evolution with age are similar; however, bender element results tend to provide lower relative stiffness values at early ages than the EMM-ARM method. The reconstituted specimens (R1 to R3) exhibited higher stiffness variability, which was likely related to the sample preparation method.

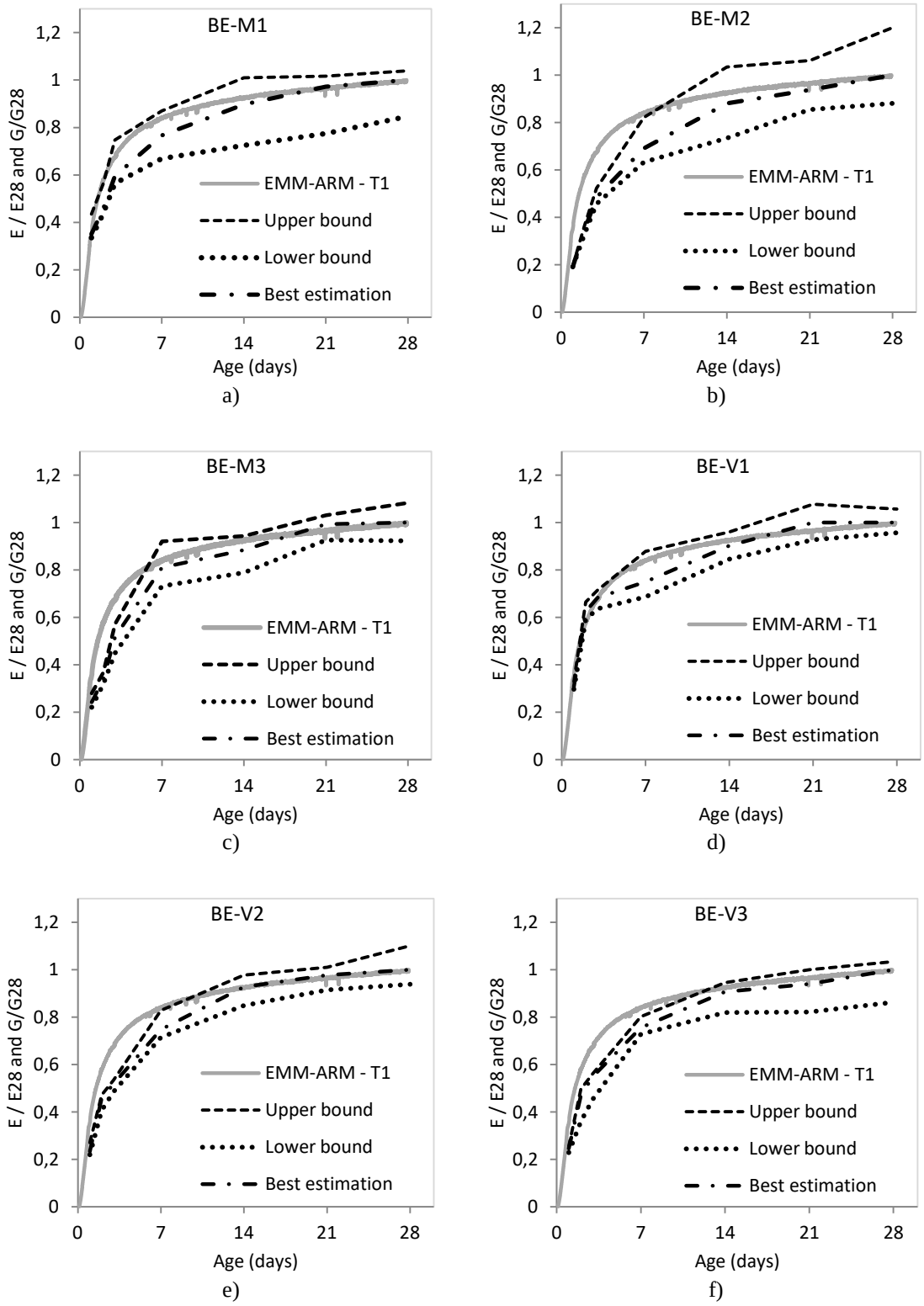

Figure 4.33. Stiffness measured using EMM-ARM T1 and BE, normalised at 28 days: a) BE-R1; b) BE-R2; c) BE-R3; d) BE-V1; e) BE-V2; f) BE-V3

The compression wave velocities of the sand-cement specimens, determined by the ultrasonic sensors, are presented in Table 4.6. Figure 4.34 illustrates the measurement of the wave propagation time for the US-V3 specimen at 1 day of age. In general, the

output signal of the receiver sensor had low noise contamination, allowing for a relatively easy determination of the compression wave propagation time.

Table 4.6. Compression wave velocity measured by US sensors

	Compression wave velocity - V_P (m/s)					
Age (days)	US-V1	US-V2	US-V3	US-M1	US-M2	US-M3
1	1215	997	1074	1378	1340	1400
2	1602	1378	1403	1775	1715	1793
3	1722	1513	1571	1829	1859	1892
7	1841	1653	1695	2059	1989	2140
14	2059	1747	1776	2177	2171	2227
21	2071	1805	1851	2238	2254	2320
28	2120	1852	1911	2317	2283	2320

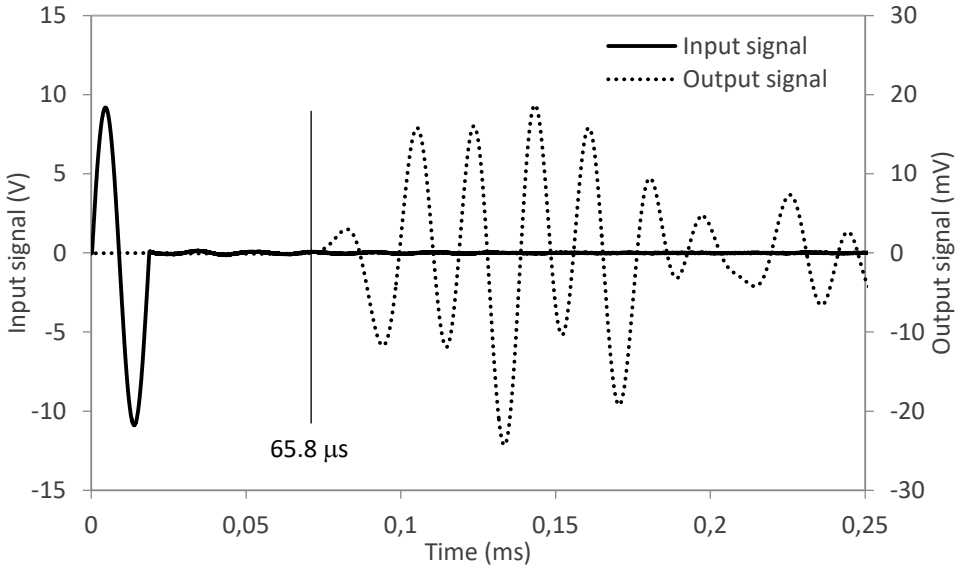

Figure 4.34. Determination of compression wave propagation time with ultrasonic sensors for specimen US-V3 at age of 1 day

The continuous stiffness results obtained from EMM-ARM, together with the discrete constrained modulus (M) results estimated from the US wave velocities, normalised to t=28 days, are presented in Figure 4.35. When comparing the relative evolution of M results obtained from US testing with E-modulus obtained with EMM-ARM, a similar trend in stiffness evolution is observed. This moduli evolution is consistent along time with time, though some US specimens were collected directly from the compacted layer

(US-V1, US-V2 and US-V3 – Figure 4.35a) and other US specimens were reconstituted inside the moulds (US-M1, US-M2 and US-M3 – Fig. Figure 4.35b).

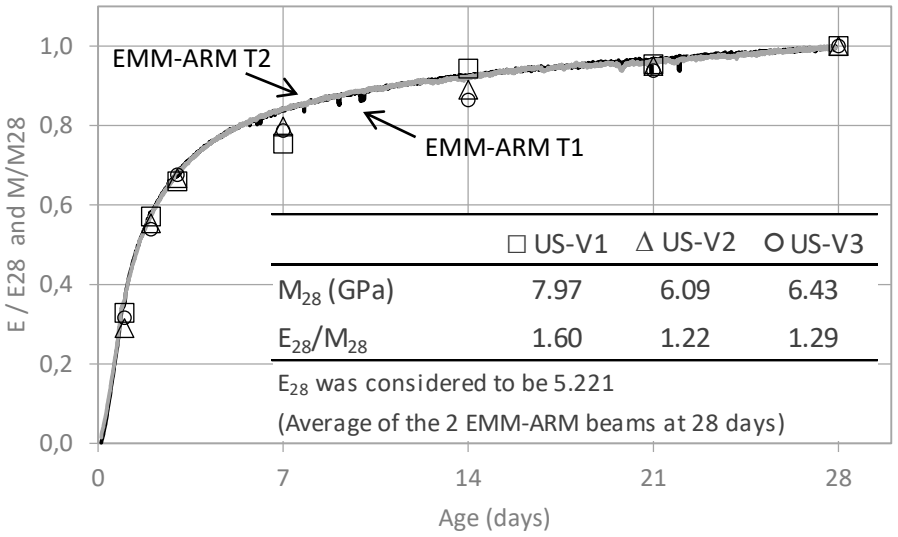

a)

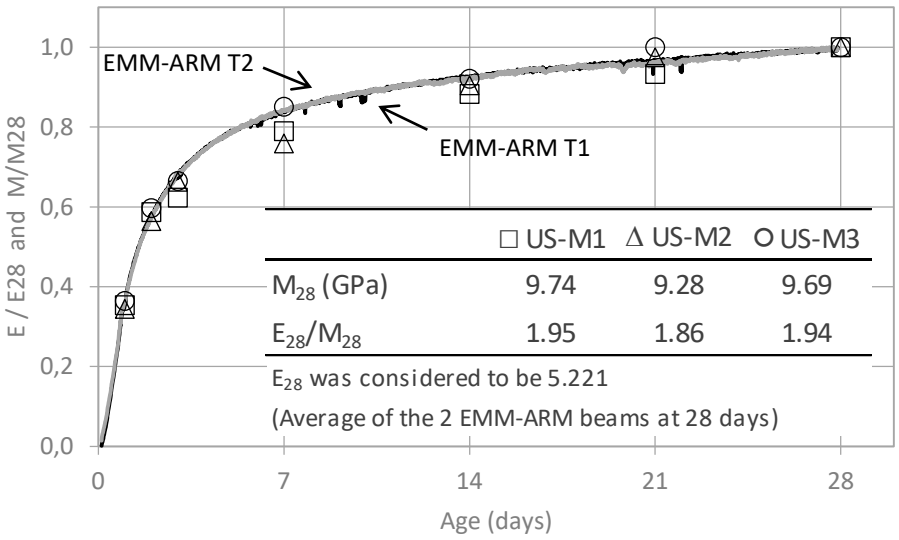

b)

Figure 4.35. Stiffness measured using EMM-ARM T1 and US, normalised at 28 days: a) intact specimens; b) reconstituted specimens with same layer material

The normalisation at 28 days implies that the end points will naturally coincide, therefore, for informative purposes, the ratio between *M* and *E* at 28 days is embedded table within the graphic. Since *M* is a function of *E* and Poisson's ratio, coincident overlay of results could only be obtained if Poisson's ratio was effectively constant over

the testing period. The computation of the Poisson's ratio from both seismic wave velocities indicates that the curing process causes a slight reduction in Poisson's ratio with time, as would be expected due to the stiffening of the specimens. This enables to justify subtle differences between E/E_{28} and M/M_{28} at the very early ages, which tend to disappear rapidly during curing. However, given the uncertainties in S-wave measurements, the assessment of the evolution of Poisson's ratio along curing is a topic that should be addressed in future research.

From the results obtained in this experimental program is possible to summarise the main conclusions forwarded in the next paragraphs.

PVC tubes and the selected geometry proved to be good options for use as EMM-ARM moulds, as it was possible to clearly identify the resonant frequency of the EMM-ARM beams through Peak Picking output-only modal identification technique. The E-modulus results obtained using EMM-ARM tubular PVC moulds demonstrated good repeatability. A strong coherence was found when quantitatively comparing EMM-ARM results obtained with tubular beams to the static E-modulus obtained with classical UCC testing at several ages. The application of the bender element technique in these experiments was not straightforward, mainly due to the high noise-to-signal ratio, which required using a bandwidth of possible results for comparison with EMM-ARM. Similar stiffness evolution trends were observed between EMM-ARM and bender elements, although the bender elements provided lower stiffness values at the very early ages. The comparison between the relative stiffness evolution of sand-cement estimated using EMM-ARM and that obtained from ultrasound wave propagation velocities has shown good results, which indicates the applicability of these two techniques to the sand-cement mixtures.

The results obtained in this experimental study indicate the suitability of the moulds used for EMM-ARM testing and the potential for using the sampling methodology for in situ applications. However, lowering the slenderness of the testing beams would definitely be desirable, particularly for the collection of samples from the top surface of in-situ compacted layers. The use of a metallic sampler may be also required in order to allow the sample collection from partially hardened materials and with larger grains.

4.5.4 Improvements on sampling and supports

The first sections of the current subchapter (4.5) have demonstrated the potential of using tubular PVC moulds to collect samples from compacted layers to be tested test with EMM-ARM. However, the access to the layer was made laterally, which may not be a feasible strategy under *in-situ* conditions. Furthermore, the use of PVC tubes as samplers may result in some damage to them, particularly if the test material has larger grains or higher initial stiffness than the material studied herein. Therefore, the current section presents a set developments in EMM-ARM targeted to avoid these potential limitations. These include the development of a metallic sampler to protect the mould during the sampling operations, suitable for collection of samples from the top surface of a compacted layer. The EMM-ARM moulds associated to this sampler are PVC tubes similar to the tubular moulds presented in 4.5.2. However, the length was reduced in order reduce the size of the collected sample and therefore facilitate the sampling operations. A new type of metallic supports for the EMM-ARM beams was also used in order to simplify the beam positioning for testing. Figure 4.36 presents the strategy followed to validate the improved sampler.

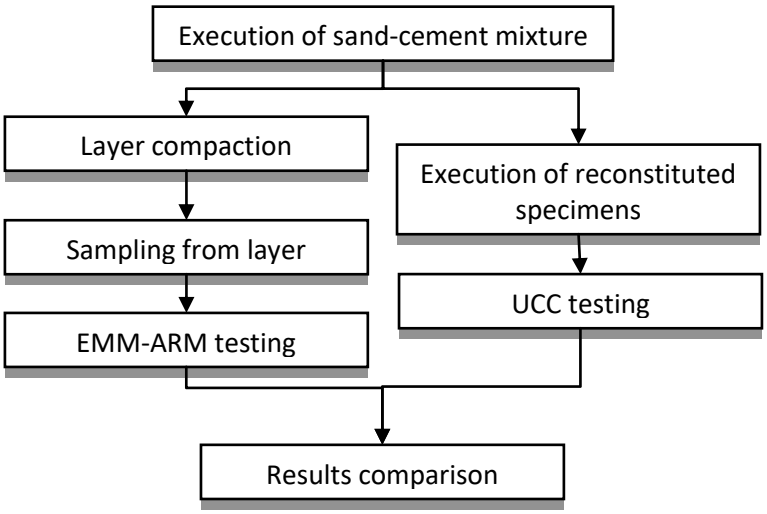

Figure 4.36. Overall strategy for sampling and E-modulus testing

For that, two small dimension sand-cement pilot layers were performed inside tubular containers with diameter of 350 mm and 700 mm height. Two samples were then collected (one from each layer) using the developed sampler, forming the beams for

EMM-ARM testing. The sampler procedure was validated by comparing the E-modulus obtained by EMM-ARM testing with the results obtained with UCC testing on reconstituted specimens of same mixture.

4.5.4.1 Sampler design

Based on the results and conclusions of previous sampling processes for EMM-ARM testing, the following recommendations were proposed for the development of a new sampler:

(i) the sampler has to accommodate a PVC liner that should be easily removed and used in the EMM-ARM testing;
(ii) the sampler needs be slightly longer than the PVC liner and have a cutting head (cutting angle) to facilitate the penetration into the compacted mixture;
(iii) recommendations of section 2.6.3.2 of this document, namely lower values of area ratios (preferably under 10% (ASTM, 2008)), must be taken in to account in order to keep the disturbance limited to reasonable limits;
(iv) the PVC liner should maintain some slenderness to keep the resonance frequencies of the testing beam within an acceptable range that allows the use of a simple modal identification technique;
(v) to reduce costs, the sampler and PVC tube dimensions were restricted to commercially available sizes.

The proposed sampler was a steel thick-walled tube, with internal diameter of 51 mm, 2 mm thickness and 600 mm long. This tube was able to internally accommodate a PVC tube (as a liner) with an external diameter of 50 mm, 1.5 mm thickness and 550 mm long. In order to simplify the extraction of the liner after driving the sampler, it comprised two parts: one with length of 550 mm, including a 50 mm cutting edge, and a further extension ring on the top, as presented on Figure 4.37, were the actuator applied the driving force. The resultant AR for the sampler was 36.9%, which is fairly superior to those proposed by literature (see subsection 2.6.3.2). A more recommendable AR value (i.e. nearing the desired 10% (ASTM, 2008)) could be achieved by increasing the diameter of the sample. However, an increase in diameter would compromise the manoeuvrability of specimens and the inherent decrease in the slenderness of the specimen would induce difficulties in the processes of resonant frequency identification.

To compensate for the high AR a 5º cutting edge was selected, according Table 2.1. The proposed sampler has no ICR, in order to limit the lateral swelling and maximize the sample quality.

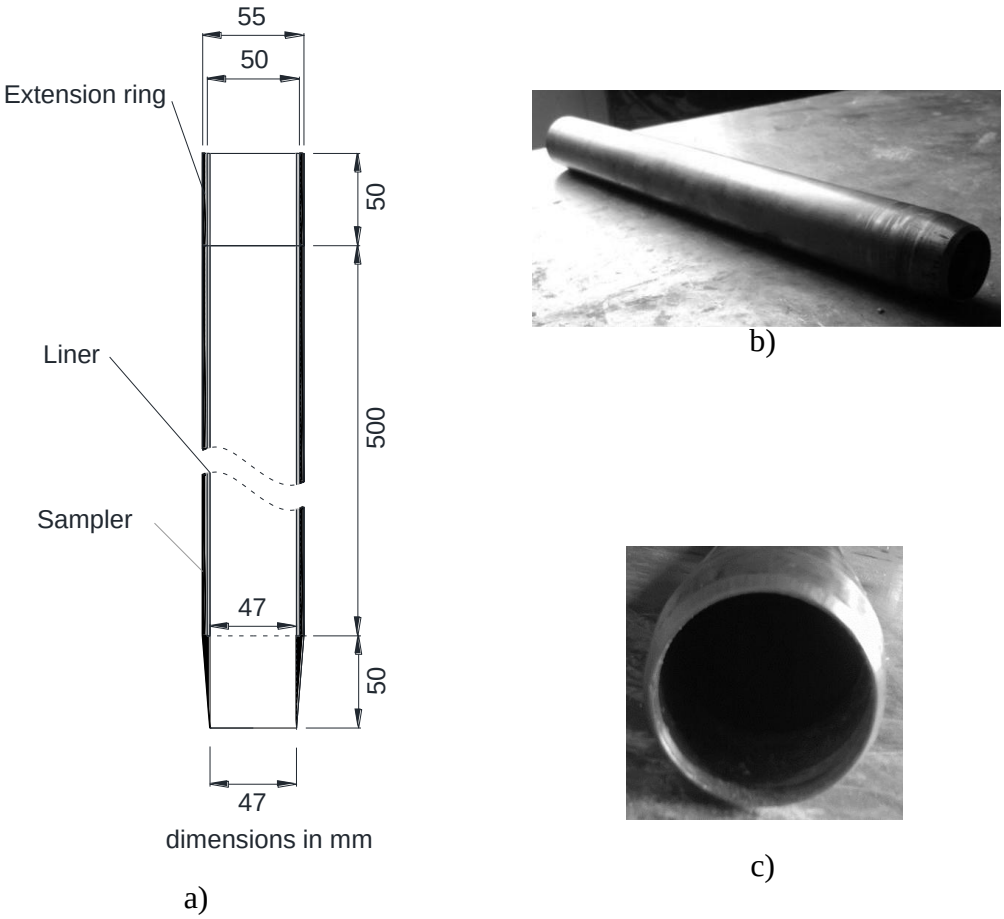

Figure 4.37. Sampler: a) lateral view and dimensions; b) global view; c) cutting head

The tubular mould to be preplaced inside the sampler consisted on a PVC tube with an inner diameter of 47 mm and a wall thickness of 1.5 mm similarly to the one used in previous sampling experiments. However, its length was reduced from the original value of 950 mm to 550 mm, as to fit inside the sampler. Upon testing, the beam had a free span of 500 mm, as presented on Figure 4.38. After sampling, steel rods with 6 mm of diameter were used to materialize the supports and polystyrene caps were introduced at extremities to prevent the outflow of the sample.

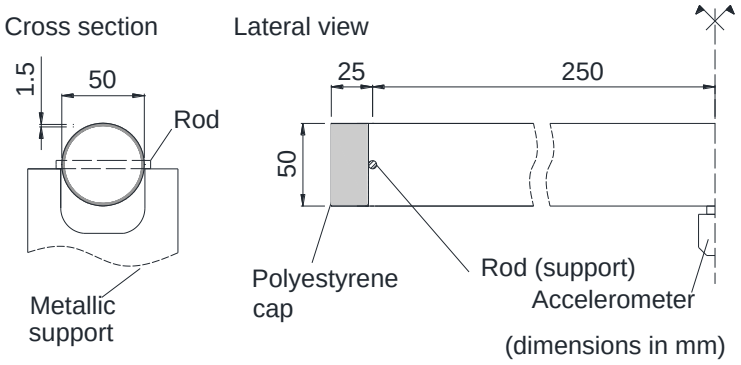

Figure 4.38. Testing beam geometry

The relation between the mixture E-modulus and the resonant frequency of an EMM-ARM tubular beam using this shorter mould is presented on Figure 4.39, with consideration of the following assumptions: span of 500 mm, mixture density =1850 kg/m^3, mould density=1200 Kg/m^3, mould E-modulus =3.4 GPa, external diameter (d_e) = 50 mm and internal diameter (d_i) = 47 mm.

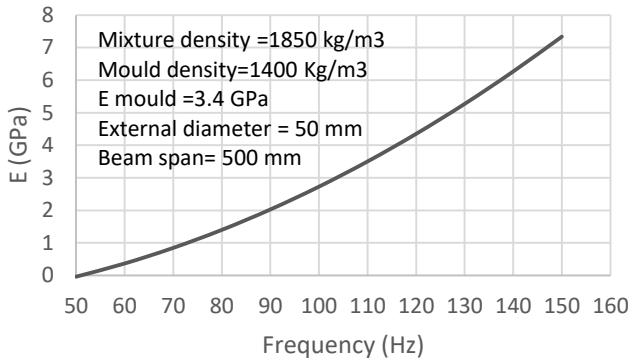

Figure 4.39. Relation between the mixture E-modulus and the resonant frequency of tubular beam 500 mm long

For this geometry, and for a mixture with a final E-modulus of 7 GPa, it is expected that the resonance frequency varies from about 51 Hz to up to almost 147 Hz. This range of frequencies is similar to the ranges obtained with the U-shaped mould used by Azenha *et. al.* (2011). Thus, there is a possibility to face same type of problems found by this author when applying the ambient (output-only) modal analysis. However, based on the results obtained with tubular moulds (presented on subsection 4.5.3.4) a better performance is expected for this mould when comparing to U-shaped and prismatic

moulds used previously. Despite these potential problems this wide frequency range induced an improved resolution to EMM-ARM testing, which is definitely quite positive for the experimental method.

4.5.4.2 Supports

In order to increase the support stiffness and to simplify the beam positioning for testing a new type of beams supports were developed, based on the work of Granja *et. al.* (2014), targeted for use with tubular beams with a maximum diameter of 50 mm. The new supports are made of steel and each pair is composed by a fixed support (Figure 4.40a, Figure 4.41a) and a support that allows some rotation around an axis parallel to the longitudinal axis of the beam (Figure 4.40b, Figure 4.41b). The purpose of using a support capable of rotating around the longitudinal axis of the beam is to allow some adjustment to the four contact points of the beam (Figure 4.41c) and ensure a correct positioning of the beam (ensure the beam is supported by the four contact points and ensure simply supported conditions). The adjustable support includes two screws that can be fastened after the positioning of the beam to prevent its inadvertent rotation (Figure 4.41d).

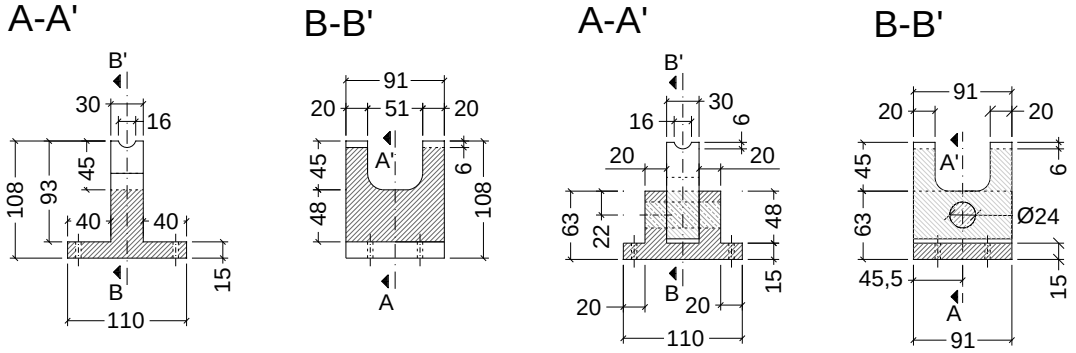

a) b)

Figure 4.40. Testing beams supports: a) fixed support; b) adjustable support (dimension in mm)

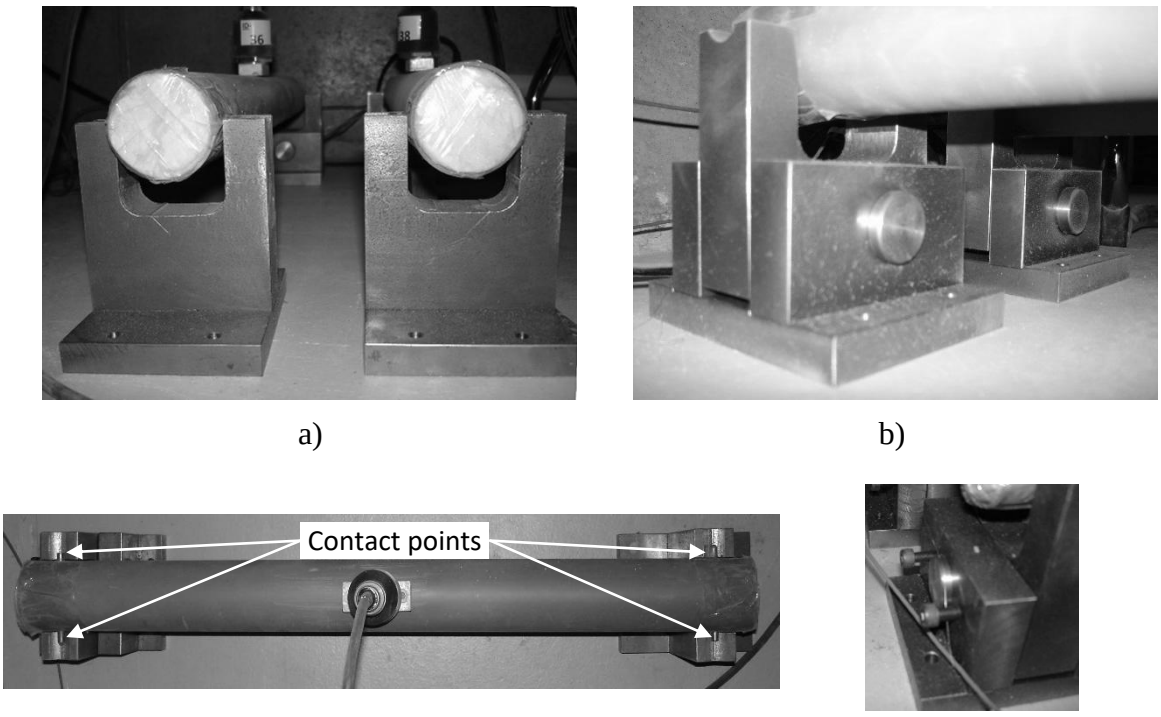

a) b)

c) d)

Figure 4.41. Steel supports for testing beam: a) fixed support; b) rotation capable support; c) beam contact points; d) detail of rotating support screws

4.5.4.3 Layer compaction and sampling

To test the proposed sampler, two specimens were collected from two sand-cement pilot layers specifically prepared for this purpose. One of the specimens, named as EMM-ARM S2, was tested by EMM-ARM methodology (see subchapter 4.3), whereas the other specimen, named as EMM-ARM S1 was used to teste a new testing methodology proposed on subchapter 4.6. The sand-cement layers were prepared by compacting the mixture M2 inside cylindrical containers with a diameter of 350 mm and 750 mm height, having about 72 Litres of capacity (Figure 4.42). These containers were directly purchased with these dimensions and were composed of multi-laminated paper layers (normally used as formwork for concrete columns). The mixing procedure was performed in a 50-litre concrete mixer with a 45º inclined axis and a rotation speed of 17 rpm with the following steps: (i) with the mixer stopped, sand was placed inside the mixer bucket; (ii) the mixer was then turned on, and the cement was immediately added; (iii) two minutes after turning the mixer on, water was added, and the mixer operated continuously for five minutes. Due to the volume limitation of the available mixer, the mixture was executed in 2 consecutive batches for each layer (4 batches in total). For

reference, the instant t=0 for the experiments refers to the time at which the water was mixed with cement in the first batch (each layer have distinct initial times). The instant of contact with cement for water for the second batches occurred at about t=15 minutes. After the conclusion of each first batch the mixture was compacted while another batch was prepared. The compaction was performed inside the container in five parts of 15 cm of height each (Figure 4.42), by a jack hammer (model Kango type 638). The mixture prepared on first batches was used for the first three parts of each the layer and the second batches were used for parts four and five. The target bulk density of the layer was 1970 Kg/m3 and it was controlled by the successive weighing of the layer during production.

a) b)

Figure 4.42. Layer inside cylindrical container: a) after compaction of first part; b) after final compaction

During sampling operations for EMM-ARM testing, the sampler (with the PVC liner inside) was vertically pushed into the layer by means of a hydraulic actuator duly instrumented with a load cell (Figure 4.43). This load actuator has a maximum amplitude of 300 mm for each movement, so the sampler had to be driven in two stages, as presented on Figure 4.44, in order to achieve the full 600 mm needed for complete penetration of the sampler. After the total introduction of the sampler into the layer the load actuator was raised, the tube with the sample was rotated by 360º and the testing beam - PVC with the undisturbed sample inside - was easily recovered from the interior of the sampler. Two samples were collected by this methodology. One of the samples, named as EMM-ARM S2 beam, was prepared and continuously tested through EMM-

ARM from about 0.2 days up to 29 days of age. The other sample, named as EMM-FRM S1 (EMM-FRM: Elastic Module Measurement - Force Response Method), was tested through another proposed methodology, which is presented in the following subchapter 4.6.

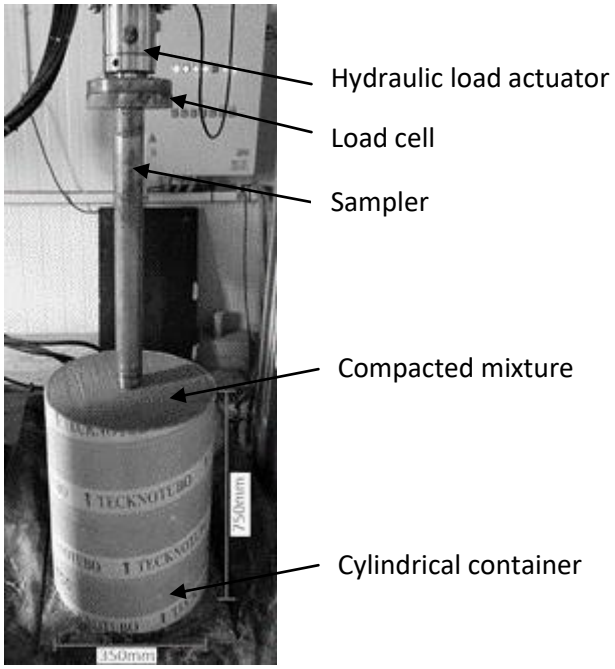

Figure 4.43. Sampling apparatus and compacted layer

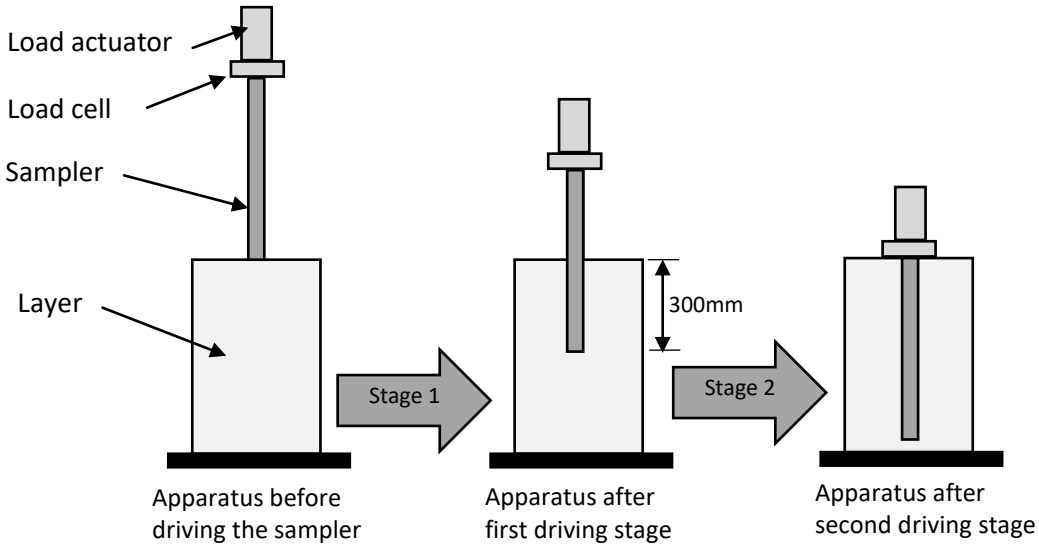

Figure 4.44. Stages for sampler driving into the layer

Three specimens for UCC testing were reconstituted in a metallic mould with 200 mm height and an inside diameter of 100 mm according the same procedure described in subsection 4.2.1.

4.5.4.4 Results

The load applied by the actuator and the respective displacement of the sampler recorded during both sampling trials are presented on Figure 4.45. There is a discontinuity in the diagrams at ~300mm displacement, associated to the necessity of performing the penetration in two stages, as mentioned before. After the first driving stage the load equipment had to be repositioned and then the second driving stage was executed.. In the figure, it is also possible to observe that a significant load was necessary to drive the sampler, having been reached a maximum final value of about 32 kN. As a comparison term of the magnitude of the load, the force required for driving a similar sampler (U100) into red clays (Hallam & Northmore, 1993) is of about 14 kN, which is about half of the value observed in this case. A smaller load would have probably been necessary to drive the sample into the layer if an ICR index higher than 0 had been adopted for the sampler. Such ICR would allowed some swelling of the sample upon entry into into the liner, thus reducing the friction between the sample and the sampler. However, an adoption of an ICR index greater than 0 could have reduced or even compromised the sample quality due to a reduction of the bulk density of the specimen (Marcuson III & Franklin, 1979).

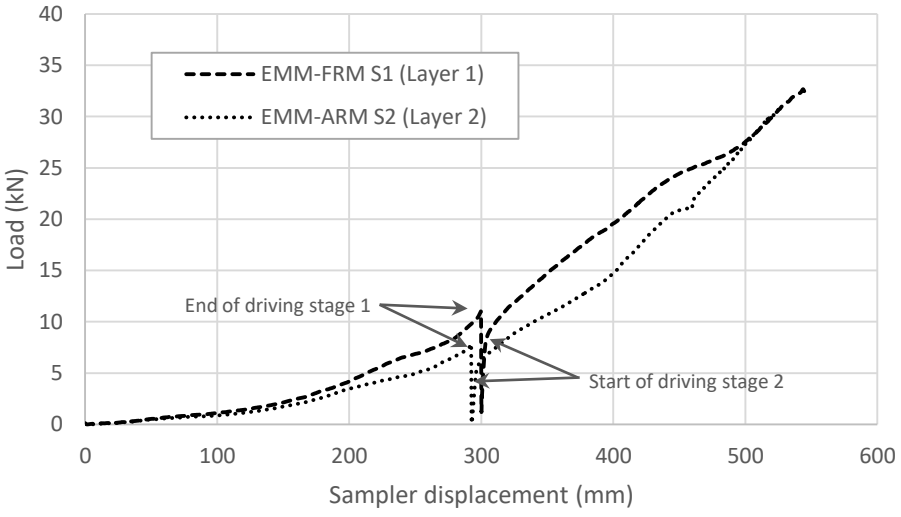

Figure 4.45. Load versus displacement for EMM-FRM S1 and EMM-ARM S2 sampling

The EMM-FRM S1, EMM-ARM S2 and UCC specimen bulk densities are presented on Table 4.7. The slight difference between EMM-FRM S1 and EMM-ARM S2 samples may be partially explained by an eventual deviation of sampler upon entry into the layer. In fact, such situation is corroborated by the overall higher load that was necessary to drive the sampler into layer 1, when compared to layer 2. However, this difference can be considered irrelevant and it is possible to affirm that all samples were representative of the density of the layer, as it was compacted for a target bulk density of 1970 kg/m^3. The maximum difference observed to this target value was less than to 1.25%.

Table 4.7. Specimen bulk densities

Test	Reference	ρ(kg/m^3)
EMM-ARM	EMM-FRM S1	1994
	EMM-ARM S2	1969
UCC	UCC1	1981
	UCC2	1960
	UCC3	1972

For the reasons stated above, the EMM-FRM S1 sample will be discussed in subchapter 4.6. Therefore, the following results concern only to the EMM-ARM S2 specimen.

The surface chart obtained for EMM-ARM S2 specimen is depicted on Figure 4.46. Despite some contaminations of the ambient noise observed, mainly since about 14 days to about 23 days of age (marked with white arrows), the evolution of resonant frequency of first mode of vibration is easily identified during the entire testing period. To have a view of the magnitude of the contaminations of ambient noise observed within the ages of 14 days to 23 days, a typical NPSD (14 days of age) is presented on Figure 4.47. In this NPSD, it is possible to observe multiple peaks, probably resulting for sources (other equipment) in the vicinity of the testing equipment. For the current test, the peak with highest amplitude matches the resonant frequency of the beam and the contaminations of ambient noise did not compromise the modal identification. However, this test was performed in laboratory conditions with relatively controlled ambient vibrations, which possibly cannot be ensured under *in-situ* conditions.

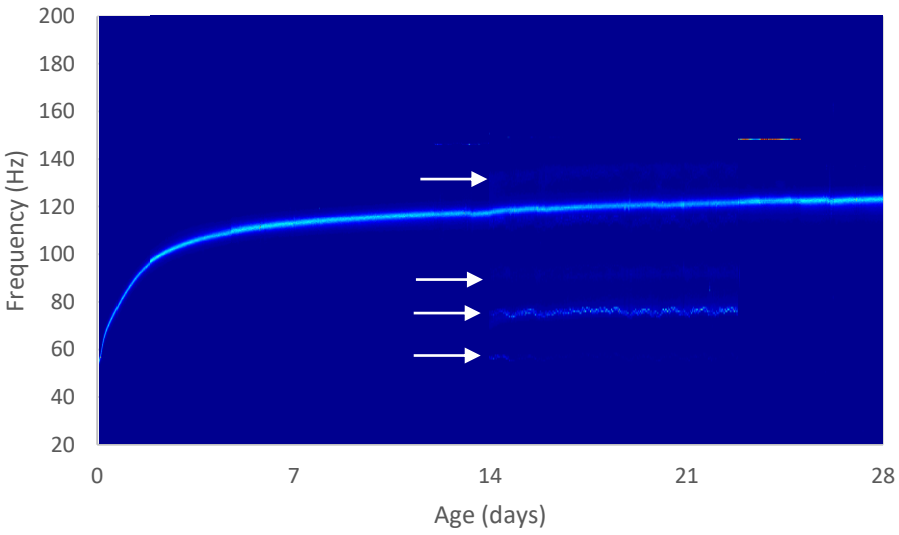

Figure 4.46. Time *versus* frequency surface chart of EMM-ARM S2 beam

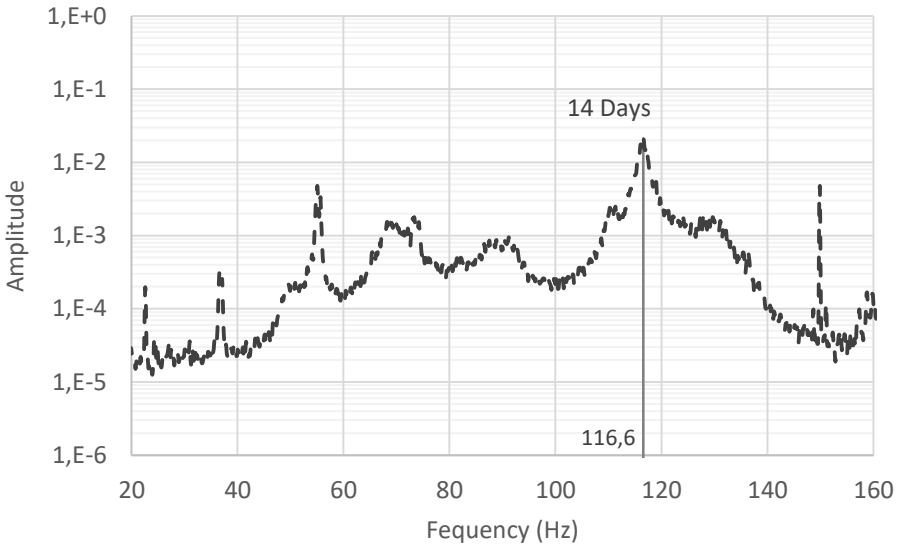

Figure 4.47. Power Spectra Density estimation for EMM-ARM S2 beam at 14 days of age

The Normalized Power Spectra Density (NPSD) obtained for EMM-ARM S2 specimen at the ages of 0.22, 1, 7 and 28 days (obtained at instants when lower level of contaminations of ambient noise was observed) are shown in Figure 4.48. From these NPSDs is possible to easily identify the resonant frequencies at presented ages (51.3, 78.1, 114.5 and 122.9 Hz, respectively) as the corresponding peaks are well defined and the perturbations to ambient noise have no relevance in these testing conditions.

Nevertheless, is possible to observe a sharp peak around 100 Hz in the NPSD obtained at 7 days that probably results from power line harmonics contamination (Butler & Russell, 2003. Is also possible to observe a reduction on the peak amplitude as the resonant frequency increases, which can be justified by a reduction of the excitability of the beam as the stiffness of the stabilized soil increases.

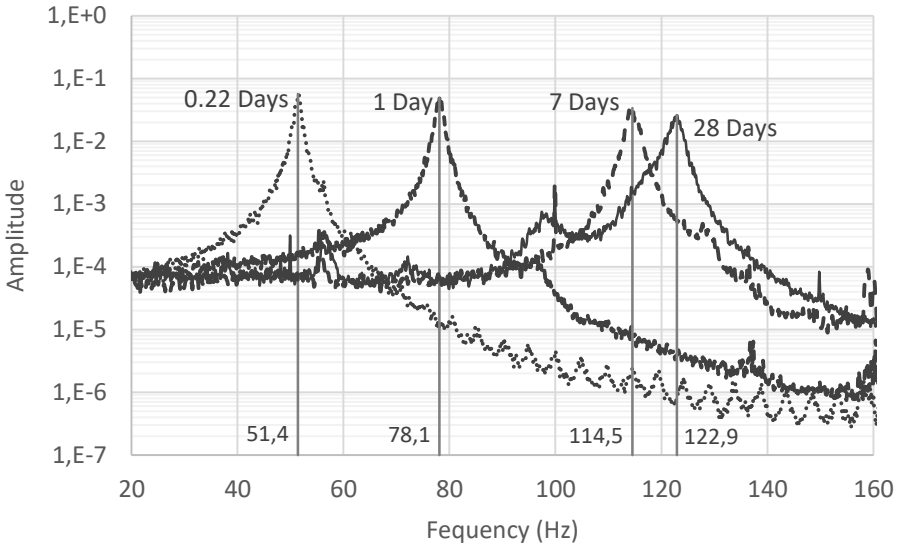

Figure 4.48. Power Spectra Density estimation for EMM-ARM S2 beam at 0.22, 1, 7 and 28 days of age

Given the distinctness of the peaks obtained in the NPSD the identification of the resonant frequencies was very straightforward during all EMM-ARM testing. Thus, the resonant frequency evolution of EMM-ARM S2 specimen from 4 hours up to 29 days of age is presented on Figure 4.49.

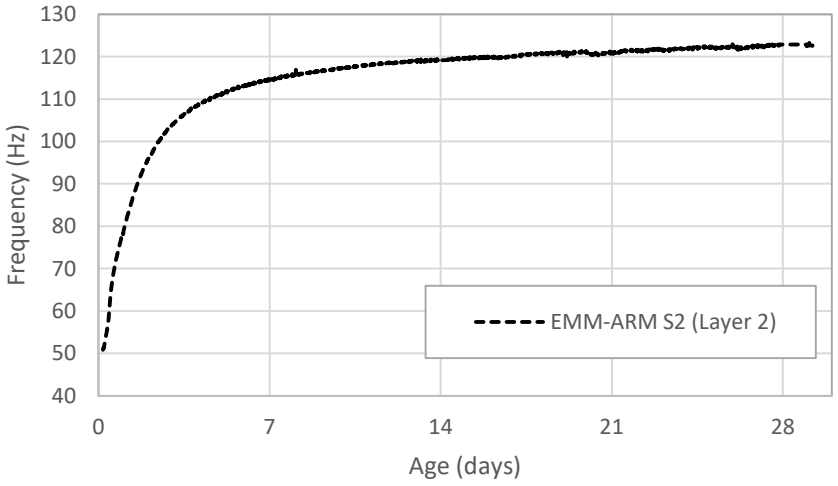

Figure 4.49. Evolution of first resonant frequency of EMM-ARM S2 beam during 29 days of testing

Table 4.8 presents the E-modulus results obtained from UCC testing at 10 and 29 days of age, which are in turn presented on Figure 4.50, together with the E-modulus results obtained with and EMM-ARM S2 from 4 hours up to 29 days of age. The EMM-ARM results were validated by remarkable consistency with the available UCC results. At 10 days of age the results of EMM-ARM (about 5.6 GPa) were within the results obtained from UCC tests (between 5.3 and 5.9 GPa). At 29 days of age the results obtained with UCC1 specimen revealed about 1 GPa difference to EMM-ARM, however, the results obtained with the other two UCC tests nearly matched the EMM-ARM results (differences less than 0.1 GPa). These results indicate that despite the lower slenderness of the testing beam (as compared to the initial implementation shown in section 4.5.2, with 90 mm span), the adopted methodology for modal identification (ambient vibration with the use of a single accelerometer) is applicable for these conditions of testing within the observed frequency range.

Table 4.8. E-modulus obtained from UCC testing at ages of 10 and 29 days

Age (Days)		10	29
E (GPa)	UCC1	5.68	7.23
	UCC2	5.32	6.29
	UCC3	5.91	6.31

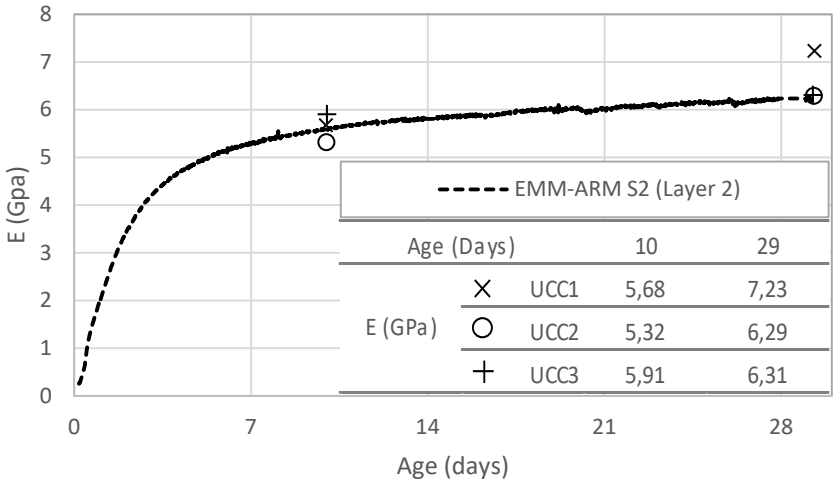

Figure 4.50. E-modulus evolution obtained with EMM-ARM and UCC

4.5.5 Discussion

The coherence of the results of the tubular sample retrieved with the metallic sampler from the layer with the UCC results, aligned with results presented on the previous subsection (4.5.3), indicate the feasibility of the sampling technique developed. Therefore, it can be concluded that the EMM-ARM methodology now has a sampling process that allows retrieving adequately undisturbed samples that are representative of the in-situ conditions. However, more experiments with different mixtures and conditions are recommended in order to further validate its application. The obtained results also indicate the possibility of using tubular testing beams with lower slenderness, as compared to previous works, resulting in an increase on the testing resolution, easier sampling (as the sample length is smaller) and easier handling. Moreover, this experiment revealed a better performance with the used PVC tubular mould when comparing to the results obtained with U-shaped moulds (Azenha *et al.*, 2011) and prismatic moulds presented previously in this thesis (in subsection 4.5.2). However, despite the good results observed with tubular moulds the ambient vibration modal identification is exposed to eventual contaminations of the ambient random noise that can occur in the testing site making difficult the identification of the resonant frequency.

4.6 EXPERIMENTAL MODAL ANALYSIS

The original version of EMM-ARM is based on the modal identification of a composite testing beam through operational modal analysis (or ambient vibration techniques). However, the performance of these identification techniques can be seriously affected by contaminations of the ambient noise in the vicinity of the testing place. In fact, this type of contaminations may occur in construction sites were heavy equipment is often used, which may produce significant vibrations in certain frequency or range of frequencies, capable to interfere with range of frequencies identified by EMM-ARM testing. Additionally, with the reduction of span, testing beams became less slender and, consequently, less excitable, which may result on an increase on sensitivity of EMM-ARM to contaminations of ambient noise and difficulties on the identification of resonant frequency. Therefore, this subchapter addresses the possibility to implement experimental modal analysis (forced vibration techniques) on EMM-ARM in order to overcome these potential problems and increase the robustness of the methodology. However, despite the benefits on modal identification that can be obtained by using forced vibration techniques, it should be noted that the application of external vibrations during the curing ages of cementitious materials may affect the development of the mechanical properties, particularly during the early ages (Hong & Park, 2015, Fernandes *et al.*, 2011). In fact, even vibrations with maximum accelerations of about 14 mg may have measurable impacts on the mechanical properties of cementitious materials (Hong & Park, 2015). Thus, these concerns were considered during the development of the device to impose the forced vibrations to the testing beam in order to minimize the impact on the mechanical properties of the sand-cement mixture under testing.

4.6.1 Development of the excitation device

The implementation of experimental modal analysis requires an explicit excitation of the testing beam, which can be done by means of an actuator vertically placed at mid span. However, it is also necessary to take into account that the application of Equation (3.24) assumes a structural system comprised of a simply supported beam with a concentrated mass at mid-span, but does not include the existence of any interaction with the actuator device. Consequently, to keep the applicability of such equation, it is

necessary that the actuator does not represent added stiffness to the testing system, otherwise a spring should be considered and quantified in the boundary conditions used to derive the equation. With this in mind, an electromagnetic actuator was developed in order to allow the induction of forces of very small magnitude without any physical contact with the testing beam. This actuator comprises the use a cylindrical permanent magnet (diameter of 6 mm diameter and 20 mm long; made of an aluminium, nickel, cobalt and iron - Alnico5 - alloy; magnetic field of 1200 Gauss) and a coil (made with copper wire of 0.22 mm and 3140 turns; internal diameter of 10 mm; external diameter of 25 mm; 30 mm long) as depicted in Figure 4.51. One of the magnet extremities is vertically attached to the bottom of the testing beam at mid span and the coil is positioned under the testing beam in a such way that the magnet goes into its hole with no contact, as presented in Figure 4.51 and Figure 4.52. When an electric current is applied to the coil terminals, a magnetic field is generated inducing a vertical force on the magnet, whose magnitude and direction depends on the current intensity and polarity. The coil frame was made of a non-ferromagnetic material to avoid any possible magnetic interaction between the permanent magnet and the body of the actuator and so to prevent the introduction of spring effect at that position.

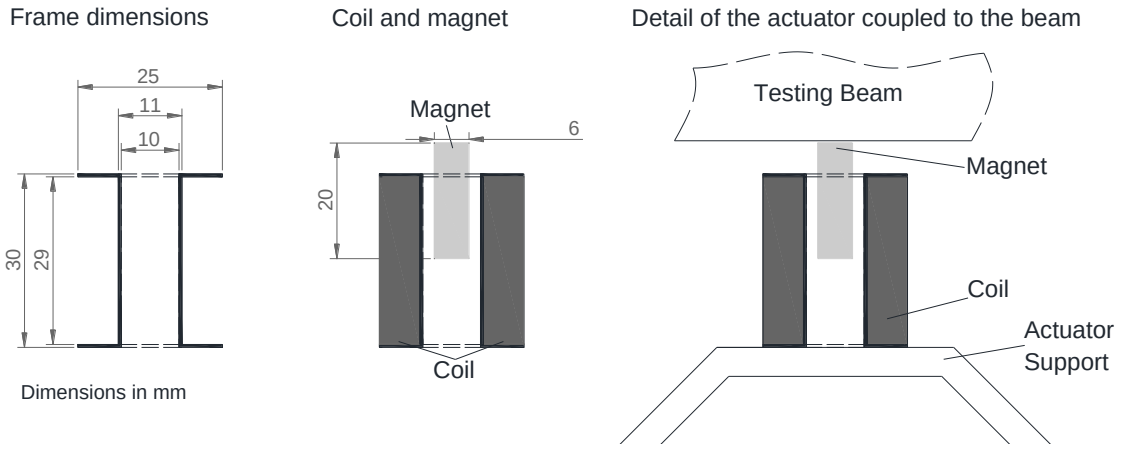

Figure 4.51. Actuator: a) frame (lateral view); b) coil and magnet (lateral view); c) actuator coupled to the testing beam

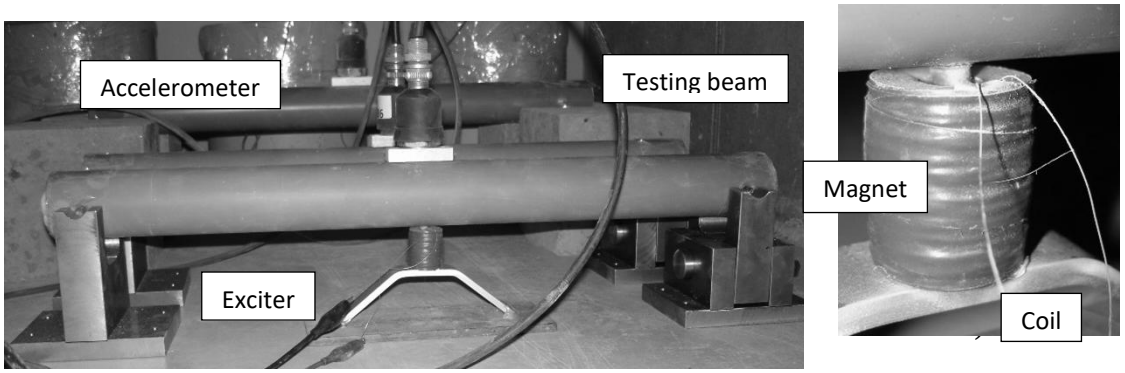

a)

Figure 4.52. Testing beam for forced experimental modal analysis: a) lateral view; b) actuator

4.6.2 Experimental setup

The excitation of the beam was performed by sending a continuous sine sweep function with a duration of 40 seconds, linear variation of frequencies between 20 Hz and 180 Hz, amplitude of ± 2.5 V, and sampling rate of 5000 Hz. The output channel of the dynamic signal acquisition module was used for this purpose (National Instruments NI-USB-4431 DAQ: 24-bit; 4 analogue input channels ±10 V; 1 analogue output channel ±3.5 V). The response of the beam (acceleration) was measured by a piezoelectric accelerometer (PCB 393B12: frequency range of 0.15-1000 Hz; measurement range of ±0.5 g; sensitivity 10 V/g; resolution 8 μg; 210 g of mass) attached at mid-span. Both excitation signal and the beam accelerations were acquired simultaneously by the same signal acquisition module used to generate the excitation signal. The excitation signal and data record was performed simultaneously in sets of 320 seconds at time intervals of 900 seconds. The signal acquisition module was operated by a computer with a custom-made LabView code that recorded the collected data at sampling rate (fs) of 500 Hz. The testing beam used for forced vibration testing consisted on the EMM-FRM S1 obtained by sampling as presented on section 4.5.4 and was tested simultaneously with the ambient testing of EMM-ARM S2 beam presented on same section. The scheme of the experimental setup is depicted in Figure 4.53. In order to compere the effects of ambient testing and forced vibration testing on same beam, forced vibration testing was performed during the periods of time of 0.22 days to 2 days, 5 days to 14 days and 23 days to 28 days and ambient testing (of same beam) from 2 days to 5 days, from 14 days to 23 days and at 28 days of curing.

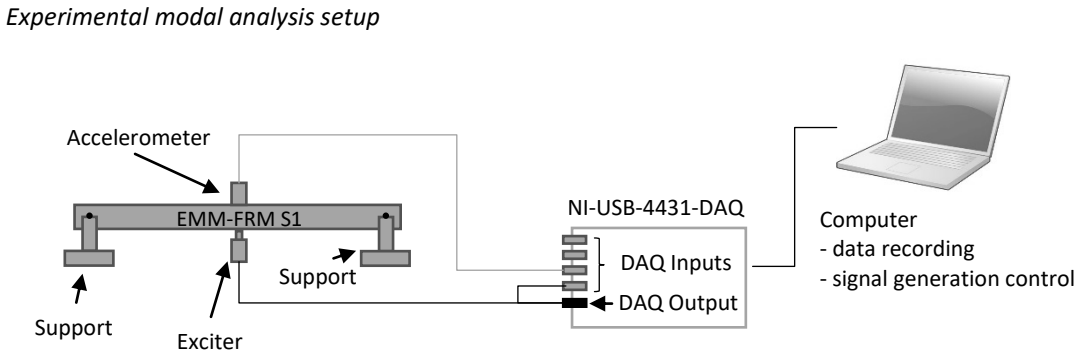

Figure 4.53. Scheme of the testing setup for forced vibration testing

4.6.3 Modal analysis results

Figure 4.54 presents the imposed voltage and acceleration response of EMM-FRM S1 beam for a 40 s excitation cycle at 0.22 days of testing. It is possible to observe that in the vicinity of the resonant frequency of the testing beam (121.8 Hz) the amplitude of the beam response is notoriously higher than the amplitude response observed for other frequencies. The maximum acceleration suffered by the beam, on the resonant frequency, ranges about ±5 mg, value that according Hong & Park (2015) does not interfere with the development of mechanical properties. Therefore, is possible to infer that this exciter and excitation procedure are appropriate for application to EMM-ARM testing beams without disturbing the development of the sand-cement microstructure.

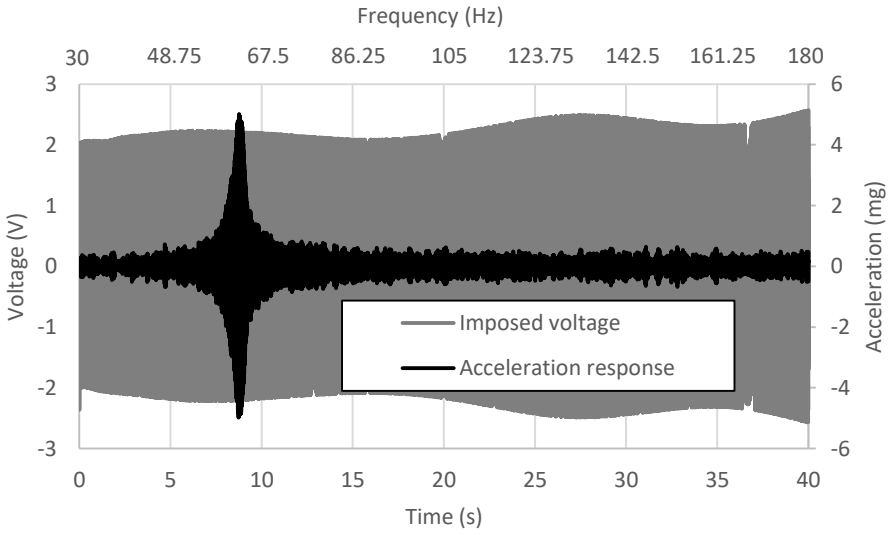

Figure 4.54. Imposed voltage and acceleration response of EMM-FRM S1 at 0.22 days of testing

Figure 4.55 shows the time *versus* frequency surface chart obtained for EMM-ARM S1 specimen obtained by placing side-by-side the FRFs (0.22 to 2 days, 5 to 14 days and 23 to 28 days) and NPSDs (2 to 5 days and 14 to 23 days). Here, is possible to easily identify the continuous evolution of the resonant frequency both in the FRFs and in the NPSDs.

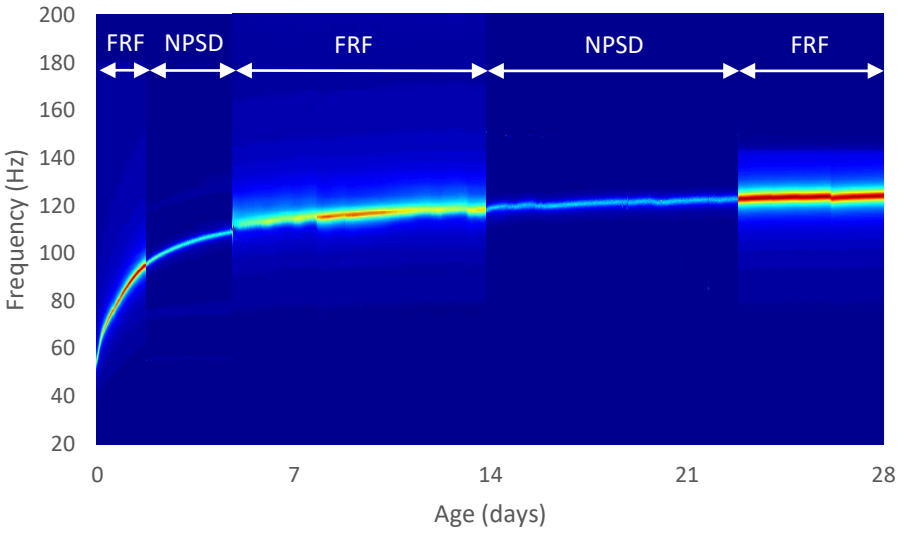

Figure 4.55. Time *versus* frequency surface chart of EMM-ARM S1

Figure 4.56 a, c, e, g) present the Normalised Power Spectra Density (NPSD) functions of the input signal and output response together with the Cross Power Spectra Density (CPSD) amplitude of input-output data recorded for EMM-FRM S1 at 0.22, 1, 7 and 28 days of age. The respective FRF functions are presented in Figure 4.56 b, d, f, h). From this figures is possible to note that the NPSD of input signal is almost constant in the frequency range of the input sine sweep, which means that the testing beam was excited in a relatively uniform way within this frequency range. Each FRF amplitude has a single and clear defined peak that matches the shift in the FRF phase angle. From these peaks, the resonant frequency and the damping of the testing beam could be easily obtained.

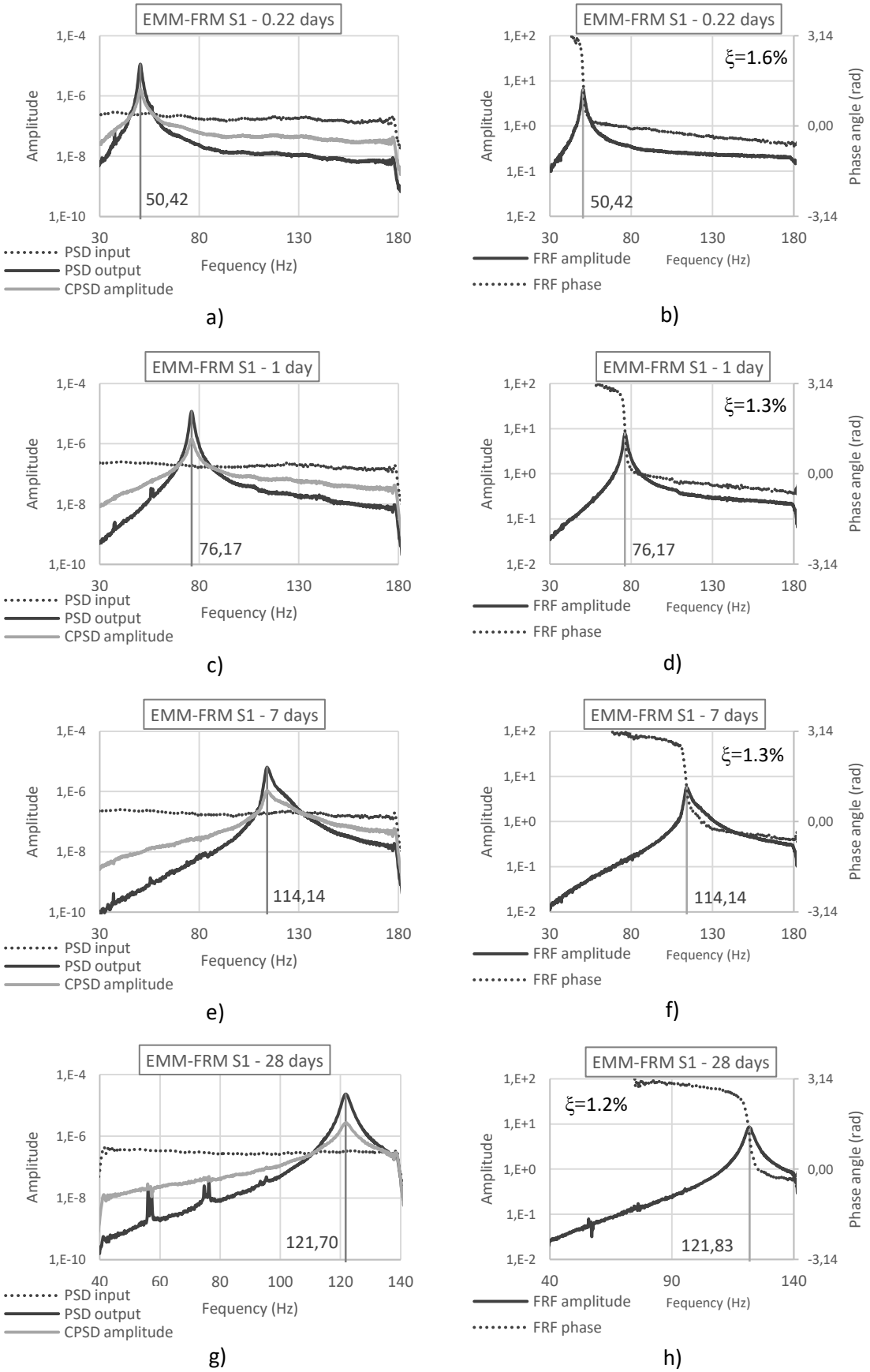

Figure 4.56. Input-output PSD and CPSD (a, c, e, g), and FRF (b, d, f, h) for EMM-ARM S1 at 0.22, 1, 7 and 28 days of age

To better compare the results obtained from forced vibration with results obtained from ambient vibration, NPSDs obtained at 2, 5, 28 days of age are presented in Figure 4.57 together with the FRFs determined from data recorded at acquisition sets immediately before (i.e. there is a time gap of 900 s between the FRF and NPSD presented on each figure). From these figures is possible to note that NPSDs obtained from ambient testing are substantially more irregular than the FRFs determined from forced vibration testing. In fact, the presented NPSDs have multiple peaks on distinct frequencies that cannot be associated to flexural vibration modes and probably result of contaminations of ambient noise from unidentified sources. Furthermore, the NPSD obtained at 28 days of age the peak with highest amplitude does not match the resonant frequency of the testing beam. However, the FRFs curves obtained from forced vibration testing identification are fairly regular presenting a very distinct peak corresponding to the first flexural resonant frequency of the beam. This indicates that a forced vibration approach, even with a very low amplitude excitation, can easily overcome this type of concerns, as contaminations of ambient noise, that are passible to occur during EMM-ARM testing.

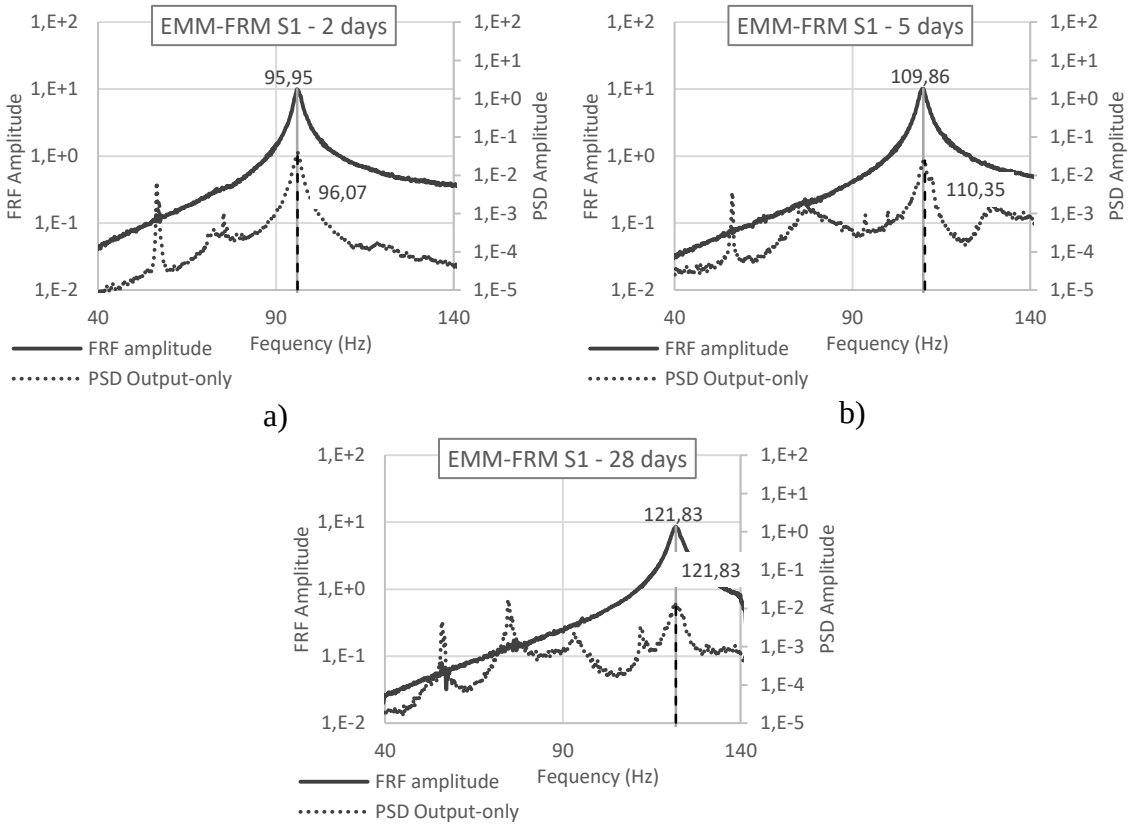

Figure 4.57. FRF of input-output and PSD of output-only signals at: a) 2 days; b) 5 days; c) 28 days

The resonant frequency evolution of EMM-FRM S1 (tested with forced and ambient vibration) and EMM-ARM S2 (tested with ambient vibration) specimens from 4 hours after start of first mixture execution up to 29 days of age are presented on Figure 4.58. Both beams present similar and almost coincident behaviour in terms of the first resonant frequency evolution. Assuming that the soil-cement mixtures in both specimens have similar density, it is possible to infer that these results are pointing towards a good coherence between the specimens in terms of E-modulus evolution.

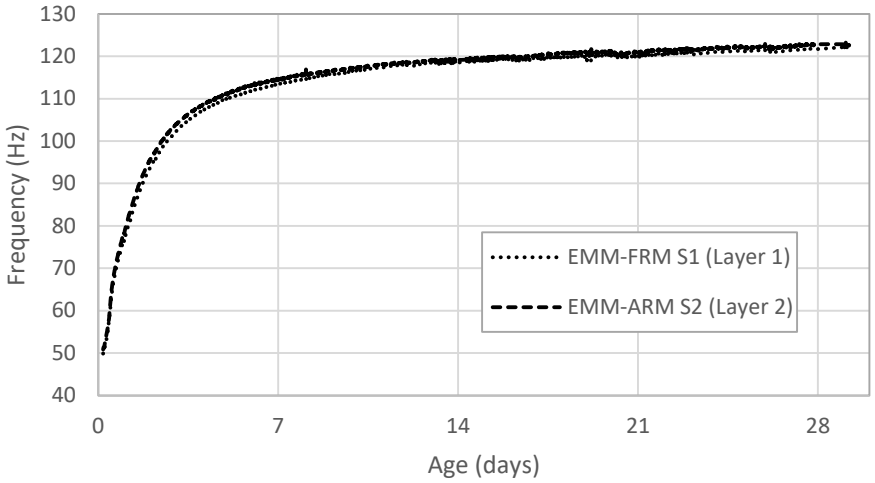

Figure 4.58. Evolution of first resonant frequency of EMM-FRM S1 and EMM-ARM S2 beams during 29 days of testing

4.6.4 E-modulus estimation

The continuous E-modulus evolution computed from the resonant frequencies of EMM-ARM S2 and EMM-FRM S1 testing beams from 4 hours up to 29 days of age and the respective ratio between both results is presented on Figure 4.59. From this figure is possible to observe a very good coherence between the results obtained with these two distinct approaches (ambient vibration and forced vibration). In fact, the ratio between the E-modulus values obtained with the two methodology variants is quite close to one at all instants. Note that E-modulus results of EMM-ARM S2 were previously validated against results of UCC testing (see subsection 4.5.4). From these results is possible to confirm that the accelerations applied to testing beam EMM-FRM are so low that any

possible interference in the microstructure and curing reactions of the tested sand-cement mixture is not visibly reflected in the E-modulus evolution.

The results obtained with EMM-FRM S1 are very promising since the experimental modal analysis approach gives more robustness to the methodology and will give confidence to results obtained in environments which could be considered less favourable for EMM-ARM testing (with contaminations of ambient noise).

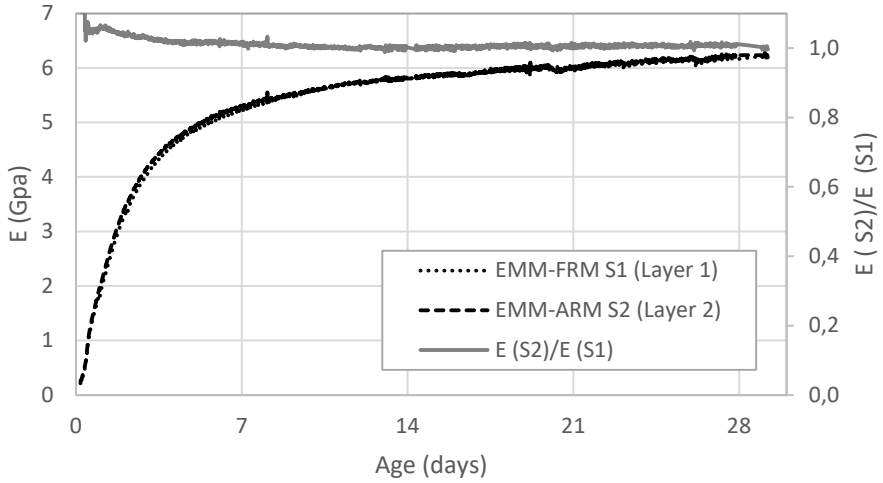

Figure 4.59. E-modulus evolution computed from EMM-FRM S1 and EMM-ARM S2

Chapter 5

EMM-ARM SYSTEMATIC APPLICATION TO STABILIZED SOILS AND EXTENSION TO THE STUDY OF TEMPERATURE EFFECTS

5.1 INTRODUCTION

In this chapter the EMM-ARM is used to assess the E-modulus evolution of different types of soils treated with chemical additives. The soils treated with cement include a uniform sand (S3), a sand (S4) and a granitic soil (GS). Two types of Portland cement were used (CEM II/B-L 32.5 N and CEM I 52.5 N) in three different proportions (3%, 5% and 7%) to prepare the studied mixtures. A silt soil was stabilized with quicklime and tested with EMM-ARM at temperatures of 20ºC, 30ºC and 40ºC.

Due to the number of specimens tested and the limited testing equipment available some of the developments presented in the previous chapter were not feasible for these experiments. These limitations include the impossibility of using of an exciter for each testing beam, the limited number of metallic supports available and the impossibility to prepare pilot layers for sampling purposes due to the high variety of mixtures prepared. Thus, EMM-ARM testing were performed using operational modal analysis (ambient vibration testing), concrete cubes were used as supports for the testing beams (due to their availability) and testing beams were prepared by reconstitution (the mixtures were compacted directly inside the moulds).

For the soil-cement mixtures, E-modulus evolution kinetics was monitored since the first half of hour of age up to 7 days and at 28 days of age. Regarding the soil-lime mixture, it was possible to observe an interesting multistage kinetics along the curing process. From the EMM-ARM results obtained for soil-lime mixture cured at different temperatures, it was possible to compute the apparent activation energies of the reactions involved in the different phases of curing.

5.2 EMM-ARM SETUP

The EMM-ARM tests presented in the present chapter shared same type of mould and followed the procedure for data analysis. The moulds used consisted of a 580 mm long polyvinyl chloride tube (PVC; density= 1,200 kg m^{-3}; E-modulus=3.4 GPa) with an inner diameter of 47 mm and a wall thickness of 1.5 mm (Figure 5.1). After compaction of the mixture inside the mould, the extremities were closed with polystyrene caps. The mixture density was controlled by weighing the mould/mixture set. At 40 mm from the

extremities horizontal screws were used for support during testing, thus constituting a 500 mm span beam in simply supported conditions. Specimens were tested by EMM-ARM (with ambient vibration testing and the equipment used for data acquisition, the procedure for first resonant frequency estimation and E-modulus computation in these experiments was the same presented in subchapter 4.3.

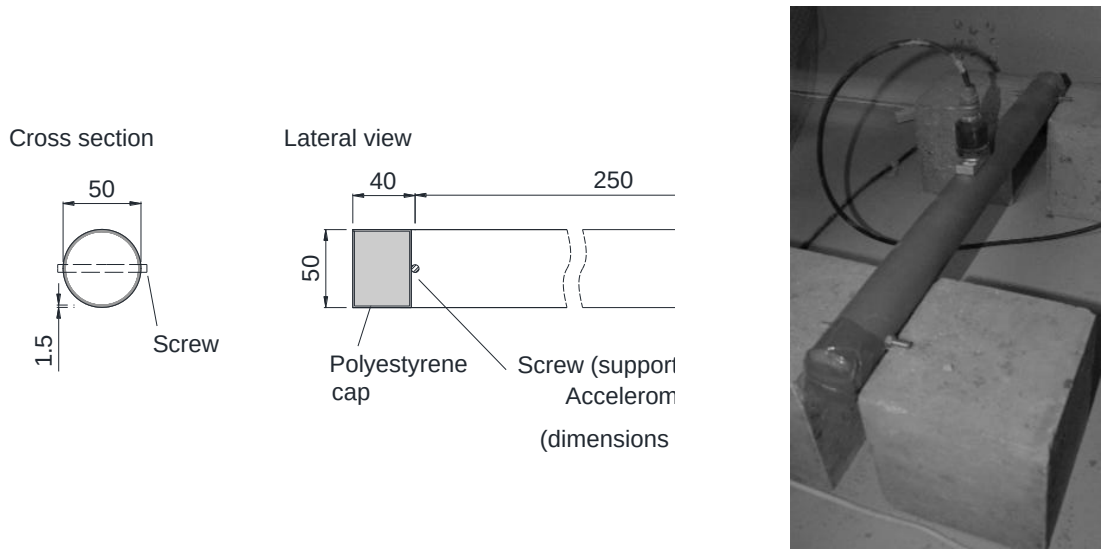

a) b)

Figure 5.1. a) Scheme with dimensions of EMM-ARM testing beam; b) beam during testing

5.3 APPLICATION TO SOIL-CEMENT

5.3.1 Materials

The aim of the experiments presented on this subchapter was to evaluate the EMM-ARM performance to monitor the E-modulus evolution of different types of soil-cement mixtures. The prepared mixtures include three different soils and two types of cement used in three proportions. The soils consisted on a uniform sand (S3) from the region of Coimbra, a sand (S4) from same supplier of S1 and S2 sands and a granitic residual soil (GS) from the region of Guimarães. The grading curves of S3, S4 and GS soils are presented in Figure 5.2 and Table 5.1. The stabilizing agents used were a Portland cement CEM II/B-L 32.5 N from SECIL and a Portland CEM I 52.5 N from Lafarge (CEN, 2005), at proportions of 3%, 5% and 7%. Whereas the last two proportions are

typical values used for soil stabilisation, the proportion of 3% was used in order to evaluate the effect resulting of the application of small percentages of cement. All mixtures comprised a proportion of 12% of water. All proportions were determined in terms of the weight of dry soil.

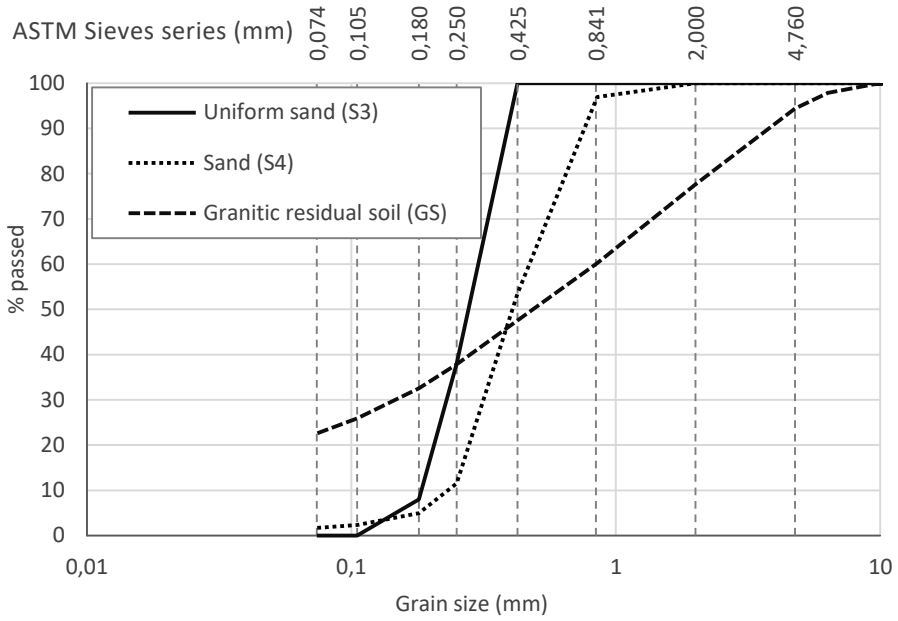

Figure 5.2. S3, S4 and GS grading curves

Table 5.1. S3, S4 and GS soils grading curves

	Uniform sand (S3)		Sand (S4)		Granitic Residual Soil (GS)	
Diam. (mm)	Retained (%)	Passed (%)	Retained (%)	Passed (%)	Retained (%)	Passed (%)
12.7	0.0	100.0	0.0	100.0	0.00	100.00
9.52	0.0	100.0	0.0	100.0	0.20	99.80
6.35	0.0	100.0	0.0	100.0	1.97	97.83
4.76	0.0	100.0	0.0	100.0	3.45	94.38
2	0.0	100.0	0.0	100.0	16.76	77.62
0.85	0.0	100.0	3.0	97.0	17.39	60.23
0.425	0.0	100.0	43.4	53.5	12.68	47.55
0.25	62.0	38.0	42.0	11.5	9.72	37.83
0.18	30.0	8.0	6.5	5.0	5.31	32.52
0.105	8.0	0.0	2.6	2.4	6.64	25.88
0.074	0.0	0.0	0.7	1.7	3.28	22.60
<0.074	0.0	-	1.7	-	22.6	-

5.3.2 Experimental procedure

5.3.2.1 Mixture preparation

The mixtures were prepared on a vertical axis mixer, with a 20 litre capacity bowl, that operated with a planetary speed of 40 rpm and beater speed of 100 rpm. The mixing procedure started by placing the dried soil and the cement (3%, 5% or 7%) inside the mixer bowl. The mixer was turned on and the materials were mixed until a homogeneous mixture was achieved (for these mixtures, it took approximately 2 minutes of mixing time). Then, 2 minutes after turning on the mixer, 12% of water was added and the mixer operated 2 more minutes. Typically, adding the water took about 5 seconds, and the conventional time "0" for each mixture was considered at this instant. After completing the mixture, the bowl was covered with plastic film in order to minimize water exchange with air.

5.3.2.2 Specimen preparation and curing

In order to monitor the E-modulus evolution of the soil-cement mixtures, specimens for EMM-ARM and UCC testing were prepared. For that purpose, the soil-cement mixtures were compacted inside moulds that ensured the necessary dimensions for testing, and density was controlled by regular weighing. The target bulk density of the mixture for all specimens is presented on Table 5.2.

Table 5.2. Target bulk densities for soil-cement mixtures

Soil (used on cement mixtures)	Target bulk density (kg/m^3)
Uniform sand (S3)	1800
Sand (S4)	2060
Granitic residual soil (GS)	1935

water proportion was 12% for all mixtures

After compaction, UCC specimens were covered with plastic film to minimize water exchange with air. One EMM-ARM specimen was prepared and tested for each soil-cement mixture (18 in total). Four UCC specimens per mix were prepared for some of

the soil-cement mixtures (for reference and comparison purposes). Table 5.3 presents the references and ages of testing for each specimen. During the curing period (28 days) all specimens were kept in a room with a temperature of about 20±1ºC.

Table 5.3. Soil-cement mixtures for EMM-ARM and UCC testing

Soil	Cement	Cement proportion	EMM-ARM Specimen reference	EMM-ARM ages (days)	UCC Specimen reference	UCC ages (days)
Uniform sand (S3)	CEM II/B-L 32.5 N	3%	S3 32.5 N 3%	0 to 7 and 28	-	-
		5%	S3 32.5 N 5%		UCC S3 32.5 N 5%	7 and 28
		7%	S3 32.5 N 7%		-	-
	CEM I 52.5 N	3%	S3 52.5 N 3%		-	-
		5%	S3 52.5 N 5%		UCC S3 52.5 N 5%	7 and 28
		7%	S3 52.5 N 7%		-	-
Sand (S4)	CEM II/B-L 32.5 N	3%	S4 32.5 N 3%		-	-
		5%	S4 32.5 N 5%		-	-
		7%	S4 32.5 N 7%		-	-
	CEM I 52.5 N	3%	S4 52.5 N 3%		-	-
		5%	S4 52.5 N 5%		-	-
		7%	S4 52.5 N 7%		-	-
Granitic residual soil (GS)	CEM II/B-L 32.5 N	3%	GS 32.5 N 3%		-	-
		5%	GS 32.5 N 5%		UCC GS 32.5 N 5%	7 and 28
		7%	GS 32.5 N 7%		-	-
	CEM I 52.5 N	3%	GS 52.5 N 3%		-	-
		5%	GS 52.5 N 5%		UCC GS 52.5 N 5%	7 and 28
		7%	GS 52.5 N 7%		-	-

5.3.2.3 Testing strategy

Due to equipment availability, EMM-ARM testing was performed continuously since instants after compaction up to 7 days of age. At 7 days of age the data acquisition was stopped and the accelerometers were removed from the testing beams and used in subsequent specimens. When the tested specimens reached 28 days of age, the accelerometers were re-attached as to resume the testing of the beams and acquisition was continued at such instant. With this strategy it was possible to test 16 distinct beams simultaneously with a single set of 4 accelerometers, as can be observed on Figure 5.3.

Figure 5.3. EMM-ARM beams during testing

5.3.3 Results and discussion

The bulk densities of each EMM-ARM specimen are presented in Table 5.4. These values are very close to the intended target density for the mixtures (within less than 0.2%) due to the rigorous weighing made during sample preparation.

Table 5.4. EMM-ARM specimens bulk density

EMM-ARM Specimen reference	Bulk density (Kg/m^3)	Target bulk density (kg/m3)
S3 32.5 N 3%	1799	1800
S3 32.5 N 5%	1797	
S3 32.5 N 7%	1799	
S3 52.5 N 3%	1799	
S3 52.5 N 5%	1799	
S3 52.5 N 7%	1797	
S4 32.5 N 3%	2063	2060
S4 32.5 N 5%	2057	
S4 32.5 N 7%	2057	
S4 52.5 N 3%	2057	
S4 52.5 N 5%	2057	
S4 52.5 N 7%	2057	
GS 32.5 N 3%	1934	1935
GS 32.5 N 5%	1934	
GS 32.5 N 7%	1934	
GS 52.5 N 3%	1934	
GS 52.5 N 5%	1934	
GS 52.5 N 7%	1934	

The E-modulus evolution of the soil-cement mixtures obtained from EMM-ARM and UCC testing is presented on Figure 5.4. The intentionally programed discontinuities observed on EMM-ARM results from 7 to 28 days can be recognized. Even so, from these results, it is easily possible to infer the actual E-modulus evolution occurred within this period. The coherence between EMM-ARM and UCC results obtained for specimens S3 32.5 N 5%, S3 52.5 N 5%, GS 32.5 N 5% and GS 52.5 N 5% confirms not only the validity of EMM-ARM testing *per se*, but also the possibility to interrupt the acceleration monitoring and accelerometer removal without compromise the results of EMM-ARM testing after reinstall accelerometers and continue the monitoring.

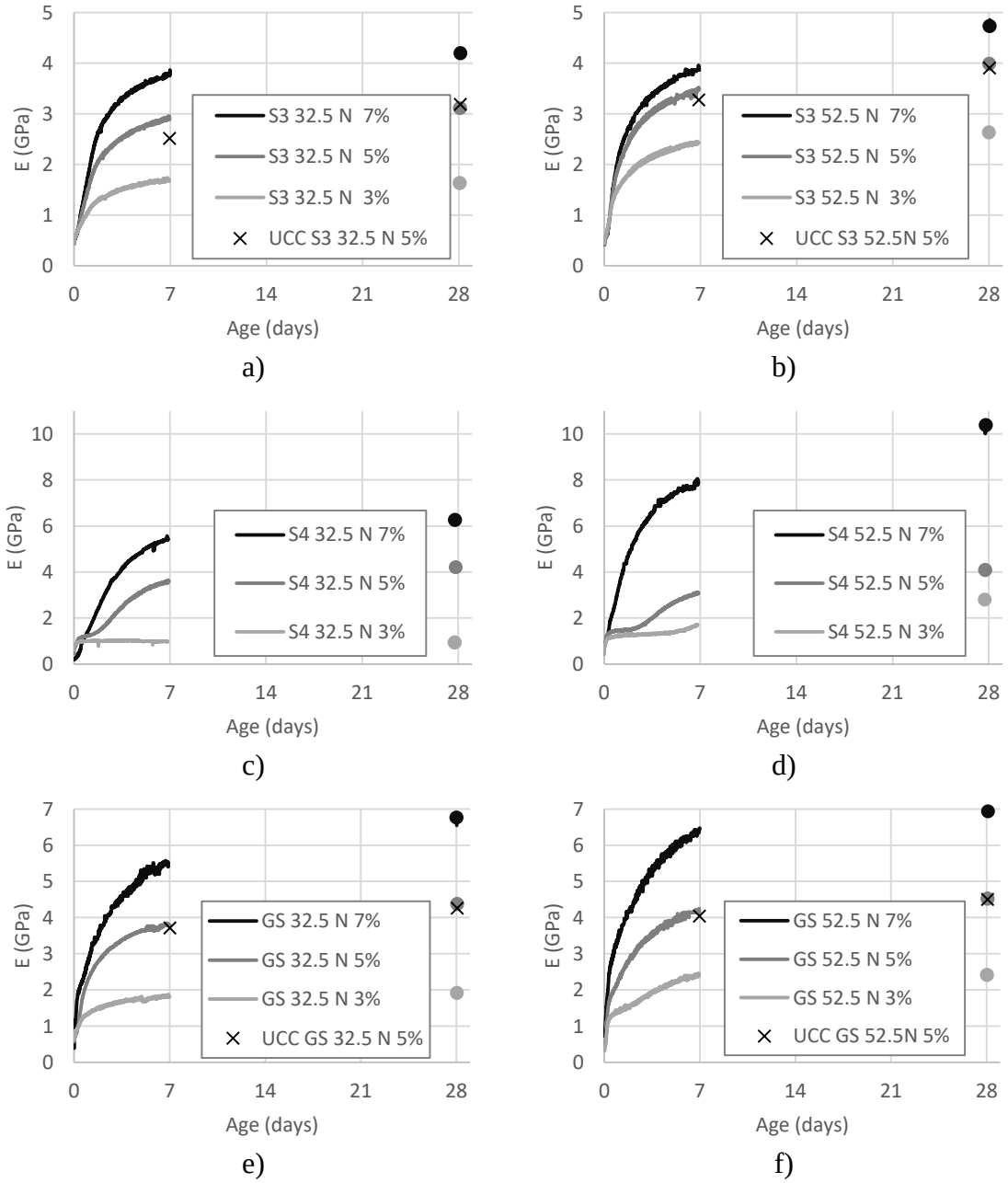

Figure 5.4. E-modulus evolution obtained from EMM-ARM testing

Table 5.5 and Figure 5.5 present the E-modulus results obtained at 7 and 28 days of age. As expected, higher quantities of cement resulted on higher E-modulus values at 7 and 28 days. When observing the relative E-modulus evolution from 7 to 28 days of mixtures containing CEM II/B-L 32.5 N it is possible to note an increase in E-modulus variation with the raise of cement percentage. This means that for lower percentages of cement the curing reactions are almost completed in the first days and higher percentages of cement lead to binder availability for longer periods of time. However, for CEM I 52.5 N mixtures was not possible to establish a trend for all soils. In fact, each soil-cement mixture presented a distinct behaviour with the variation of percentage of cement.

The negative variation observed for specimen S3 32.5 N 3% from 7 to 28 days should not be interpreted as an actual decrease on the E-modulus. It can result of the precision of the method associated to a very small variation of the E-modulus occurred from 7 to 28 days of age, or some type of disturbance eventually occurred in the testing beam, as an accidental repositioning of supports or different positioning of the accelerometer cable.

Table 5.5. E-modulus at 7 and 28 days of age

Specimen	E(GPa)					
	EMM-ARM			UCC		
	7days	28days	7 to 28 days	7days	28days	7 to 28 days
S3 32.5 N 3%	1,67	1,64	(-1,3%)*	-	-	-
S3 32.5 N 5%	2,88	3,17	8,9%	2,66	3,19	16,5%
S3 32.5 N 7%	3,79	4,23	10,4%	-	-	-
S3 52.5 N 3%	2,42	2,66	8,8%	-	-	-
S3 52.5 N 5%	3,47	4,04	14,2%	3,28	3,91	16,2%
S3 52.5 N 7%	3,86	4,85	20,4%	-	-	-
S4 32.5 N 3%	0,97	0,95	-2,3%	-	-	-
S4 32.5 N 5%	3,55	4,20	15,3%	-	-	-
S4 32.5 N 7%	5,45	6,35	14,1%	-	-	-
S4 52.5 N 3%	1,70	2,81	39,4%	-	-	-
S4 52.5 N 5%	3,07	4,13	25,7%	-	-	-
S4 52.5 N 7%	7,89	10,22	22,8%	-	-	-
GS 32.5 N 3%	1,81	1,92	5,6%			-
GS 32.5 N 5%	3,79	4,35	12,8%	3,716	4,263	12,8%
GS 32.5 N 7%	5,40	6,82	20,8%			-
GS 52.5 N 3%	2,42	2,43	0,3%			-
GS 52.5 N 5%	4,15	4,60	9,9%	4,044	4,504	10,2%
GS 52.5 N 7%	6,47	6,88	5,8%			-

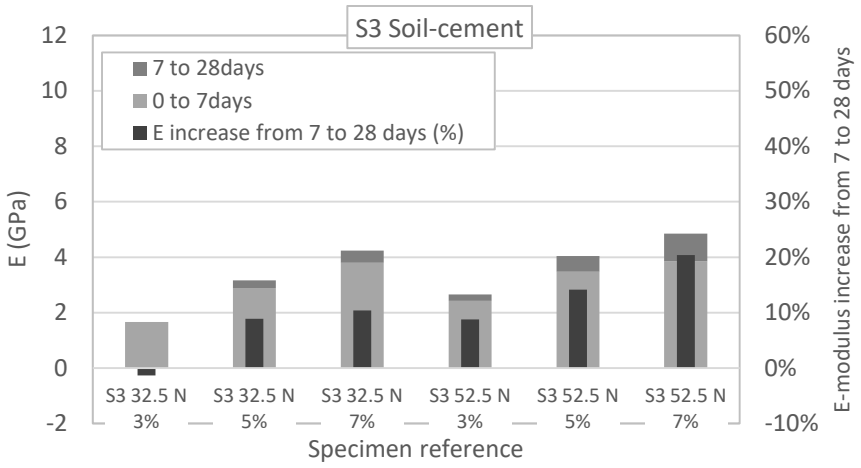

a)

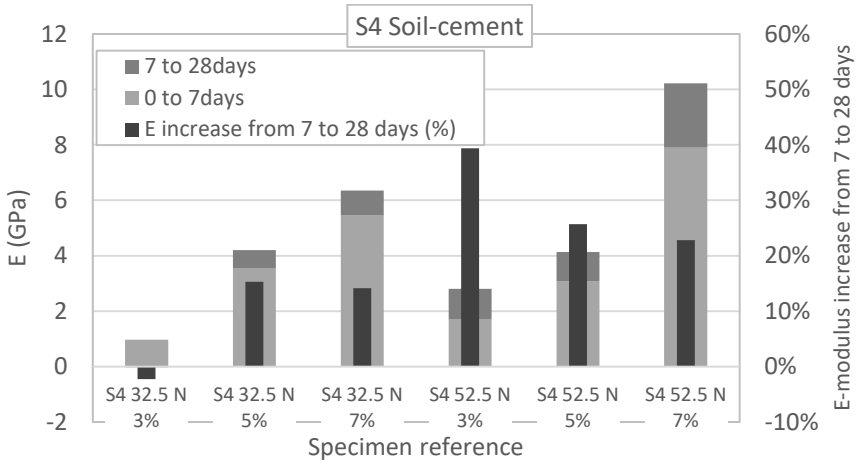

b)

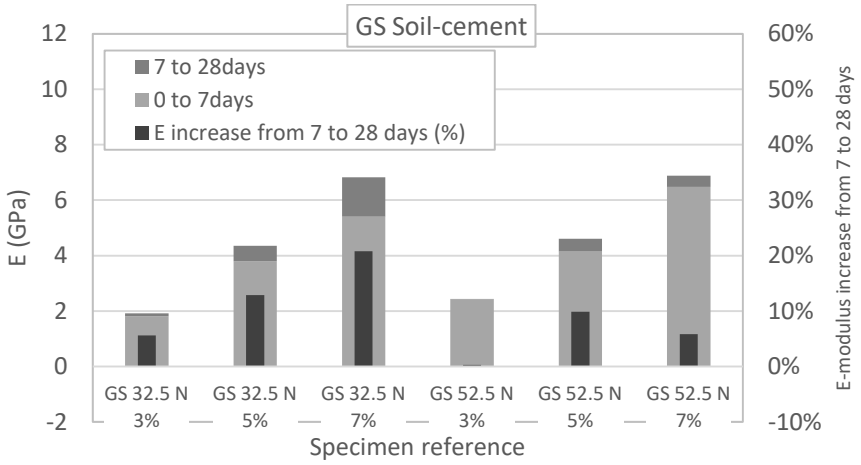

c)

Figure 5.5. E-modulus at 7 and 28 days of age and respective percentage of increase from 7 to 28 days

When comparing the effect of using different types of cement, for same cement proportion, is possible to note that globally mixtures with CEM I 52.5 N cement developed higher E-modulus at 28 days than mixtures with CEM II/B-L 32.5 N. However, this difference is more significant (in terms of percentage) for lower proportions of cement, as can be noted on Figure 5.6.

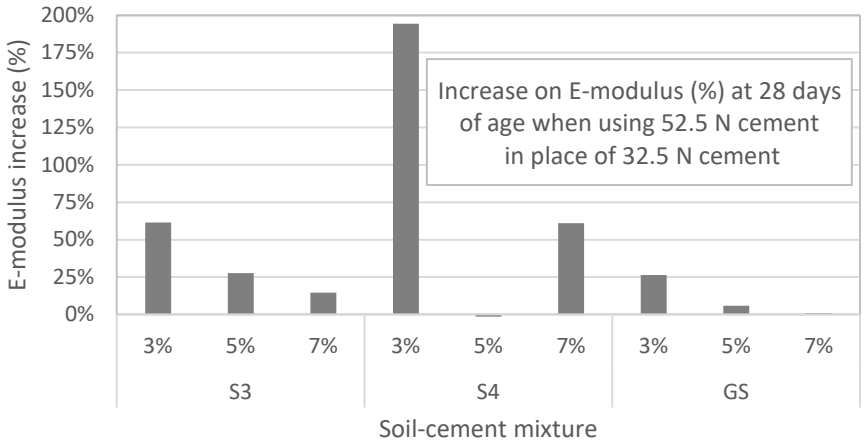

Figure 5.6. E-modulus difference (percentage) at 28 days when using cement 52.5 N in place of cement 32.5 N

When observing the results for S4 soil-cement mixture (Figure 5.4c,d), a distinctive kinetics of evolution can be found in comparison to the other soil-cement mixtures (S3 and GS), as well as to those already presented in previous works of EMM-ARM applications to soil-cement (Silva, 2010, Azenha *et al.*, 2011, Silva *et al.*, 2013, Silva *et al.*, 2014). On mixtures of S4 soil with 3% and 5% percent of cement, it is possible to see an E-modulus increase at early ages (less than 1 day) followed by a period with no apparent change on the stiffness. After this stabilisation period (that extends up to 2 or more days, depending on the mixture) a new increase on E-modulus could be observed (except mixture S4 32.5 N 3% which no additional E-modulus increase was observed after day 1). This phenomenon can be related to the different stabilisation processes that can occur in soil-cement mixtures, as referred in subsection 2.2.1. The E-modulus increase at first ages may result from bonds established by the hydration products in some contact points between grains. After this initial increase the cement particles hydrate filling the voids between the soil particles without providing a solid skeleton with the surrounding soil or cement particles. Once the new connexion between particles is assured a new increase on E-modulus can be observed. The fact of this

phenomenon was not observed in S3 and GS soils can be related to the grading curves of the tested soils. GS soil has higher diversity of grain sizes which can result in a better arrangement of the particles. Regarding S3 and S4 soils, S4 particles are bigger than S3 particles, resulting in larger voids between particles, whose will need more quantity of cement hydration products to be totally filled. In order to better understand this phenomena, specific additional research works are necessary, particularly in the study of different soil-cement mixtures of uniform soils with different particle sizes.

Besides the interest of the results obtained regarding the curing kinetics of the studied materials, it is also pertinent to mention the usefulness of the strategy adopted for these EMM-ARM tests. In fact, even with insufficient number of accelerometers available for all the specimens is was possible to obtain very interesting information of the E-modulus evolution of a large number of specimens (comparing to the number of accelerometers available). The operation of removing the accelerometers from the testing beams, with subsequent use in distinct specimens and then re-attaching to the originally tested specimens at 28 days of age, was performed with success. Therefore, with this strategy is possible to obtain important information of the E-modulus evolution during the first days of age, making available the monitoring equipment to be used with different specimens when the rate of the stiffness evolution is lower and then make discrete EMM-ARM tests to confirm the obtained values at reference ages (as 28 or 90 days).

5.4 APPLICATION TO SOIL-LIME AND EVALUATION OF TEMPERATURE EFFECTS

5.4.1 Introduction

This subchapter presents a study of the E-modulus evolution, performed through EMM-ARM, of a silt soil treated with quicklime cured at temperatures of 20ºC, 30ºC and 40ºC. This was the first application of EMM-ARM methodology to soils treated with lime, allowing to observe with detail the corresponding kinetics of stiffness evolution. Ultrasonic pulse velocity (US) and unconfined cyclic compression (UCC) testing with local measurement of deformations were used for the discrete measurement of the stiffness evolution of the soil-lime mixture cured at 30º in order to compare and validate

EMM-ARM testing results. The apparent activation energy of the reactions involved in the soil-lime curing was estimated by using EMM-ARM results obtained at studied temperatures and by applying principles of equivalent age.

5.4.2 Materials

The soil used consisted on a silt from Marche-Les-Dames (MLD) region on Belgium. It is composed of 52% of silt, 18% of clay and 30% of thin-grained sand with a D50 (grain diameter at 50% passing in the grain size distribution) of about 30μm, and its size distribution curve is presented on Figure 5.7 and Table 5.6 (NF P 94-056, 1996, NF P 94-056, 1992). The Atterberg limits (NF P 94-051) were 20.1% for the plastic limit and 31.0% for the liquid limit. The maximum dry density was of 1844 kg/m^3 with an optimum water content of 15,1% determined by normal proctor testing (NF P 94-093), as presented on Figure 5.8.

The soil was treated with 3% of quicklime CL 90-Q (EN 459-1) from Lhoist group, wtih the particle size distribution being 98.9% < 0.5 mm and 84.1% < 90 μm. The resulting soil-lime mixture presented a maximum dry density of 1739 kg/m^3 with an optimum water content of 17.1% determined by normal proctor testing (Figure 5.8). These tests were part of a collaborative work performed with the Université Libre de Bruxelles and the materials used (soil and lime) have been studied in other contexts (De Bel *et al.*, 2013).

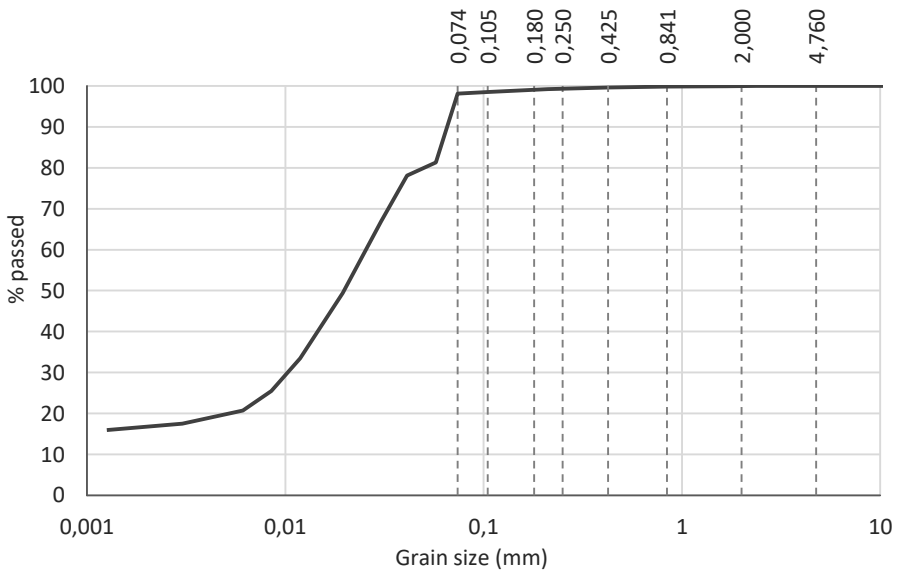

Figure 5.7. MLD soil grading curve (NF P 94-056, NF P 94-057)

Table 5.6. MLD soil sand grading curve

Diam. (mm)	Retained (%)	Passed (%)	Diam. (mm)	Retained (%)	Passed (%)
2.38	0.0	100	0.04118	21.7	78.1
1.68	0.0	99.9	0.03039	29.7	66.9
0.84	0.9	99.8	0.01948	47.2	49.4
0.42	2.3	99.6	0.01188	60.0	33.5
0.21	3.5	99.2	0.00849	66.4	25.5
0.105	4.6	98.5	0.00611	69.6	20.7
0.074	5.1	98.1	0.00302	77.6	17.5
0.05737	16.9	81.3	0.00126	82.4	15.9

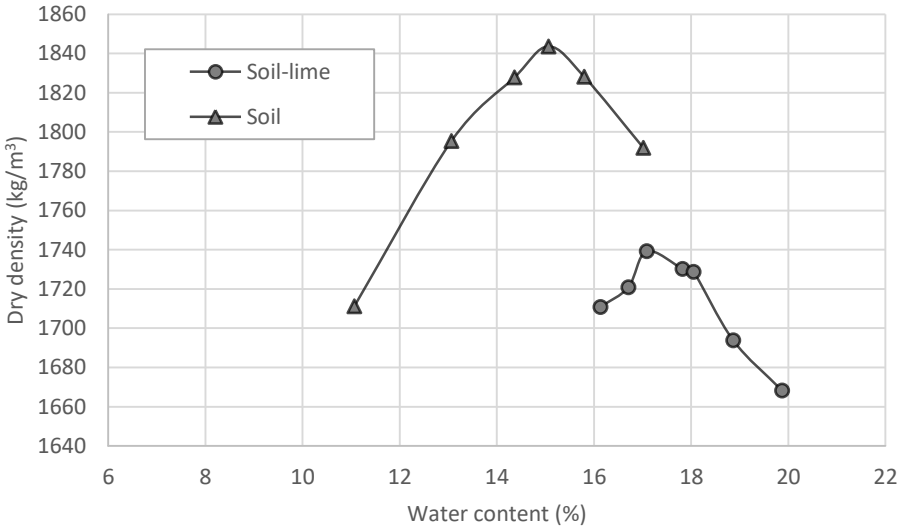

Figure 5.8. MDL soil and MLD soil-lime compaction curves

5.4.3 Experimental procedure

5.4.3.1 Mixture preparation

The mixture was prepared on a vertical axis mixer, with a 20 litres capacity bowl, that operated with a planetary speed of 40 rpm and beater speed of 100 rpm. The mixture procedure starts by mixing the dried soil together with 3% of lime. Then, 5 minutes after turning on the mixer 19% of water is added and the mixer operates 5 more minutes. All the quantities were measured in terms of mass of dried soil. The mixture age starts at instant when the water is added to the soil-lime mixture. After completing

the mixture the bowl was covered with plastic film in order to minimize water exchange with air.

5.4.3.2 Specimen preparation and curing

In order to monitor the stiffness evolution of the soil-lime mixture at different temperatures, several specimens were prepared. The soil-lime mixture was compacted inside moulds with internal dimensions intended for the specimens. The target bulk density of the mixture for all specimens was 1950 kg/m^3. After compaction, UCC and US specimens were covered with plastic film to minimize water exchange with air. In total three specimens were prepared for EMM-ARM testing, two specimens for UCC testing and four specimens for US testing. The specimens were cured under controlled room temperatures. One EMM-ARM specimen (EMM-ARM 20) was cured inside a room where the temperature was controlled and kept around 20ºC. One EMM-ARM specimen (EMM-ARM 30), two UCC specimens and four US specimens were cured at environmental temperature of 30ºC, and the other EMM-ARM specimen (EMM-ARM 40) was cured at room temperature of 40. Table 5.7 presents the geometry, number and designation of specimens prepared to be used in each type of testing and the respective curing temperatures.

Table 5.7. MLD soil-lime specimens prepared

Type of testing	Diameter (mm)	Length (mm)	Number of specimens	Curing temperatures (ºC)	Specimen reference
EMM-ARM	47	500	1	20	EMM-ARM 20
			1	30	EMM-ARM 30
			1	40	EMM-ARM 40
UCC	100	200	2	30	UCC1, UCC2
US	44	70	4	30	US1, US2, US3, US4

Tests at temperatures of 30ºC and 40ºC were made inside a box with temperature control (Figure 5.9). This box was made of polystyrene plates of 40 mm of thickness, had external dimensions of approximately 1.2 ×1.2 × 0.6 m^3 and was provided with a fan and a 2000 watt fan heater connected to a thermostat module (STC 1000) in order to

keep the air temperature inside the box close to the intended values for the testing. Temperatures were recorded by means of temperature sensors (Sensirion).

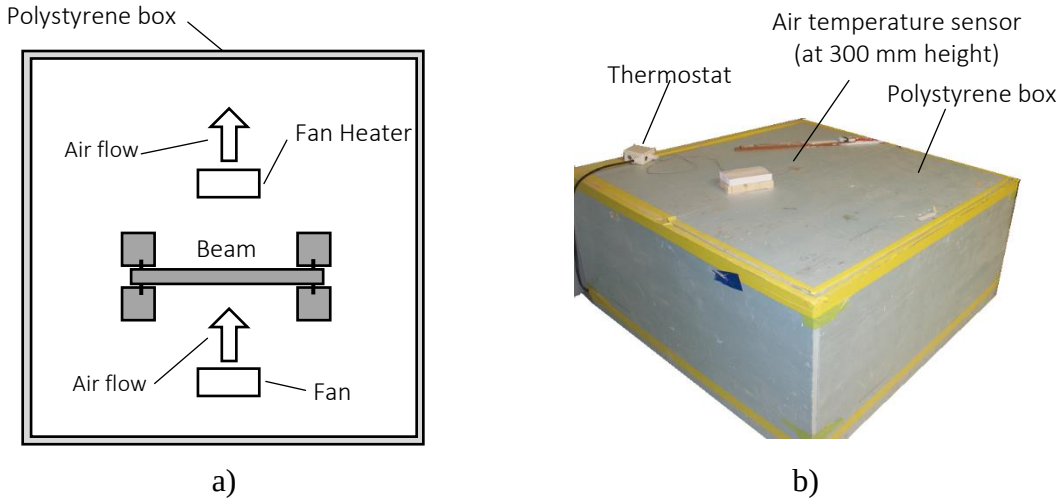

Figure 5.9. Polystyrene box for 30ºC and 40ºC tests: a) top view scheme; outside view

5.4.4 Results and discussions

5.4.4.1 Density of test specimens

The bulk densities obtained for each specimen are presented on Table 5.8. The maximum variation observed was less than ±1.5%, when comparing to the target bulk density, which indicates a good performance during specimen preparation.

Table 5.8. Specimen bulk densities

Type of testing	Specimen	Bulk density (kg/m^3)
EMM-ARM	EMM-ARM 20	1953
	EMM-ARM 30	1957
	EMM-ARM 40	1952
UCC	UCC1	1950
	UCC2	1940
US	US1	1977
	US2	1976
	US3	1944
	US4	1935

5.4.4.2 Ultrasonic testing results

Figure 5.10 presents a typical response signal measured with the US sensors obtained in this campaign, where the measured travel time corresponding to the first deflection of the compression wave is represented. In general, the output signals measured with US had low noise contamination allowing an easy identification of the travel time of the compression wave.

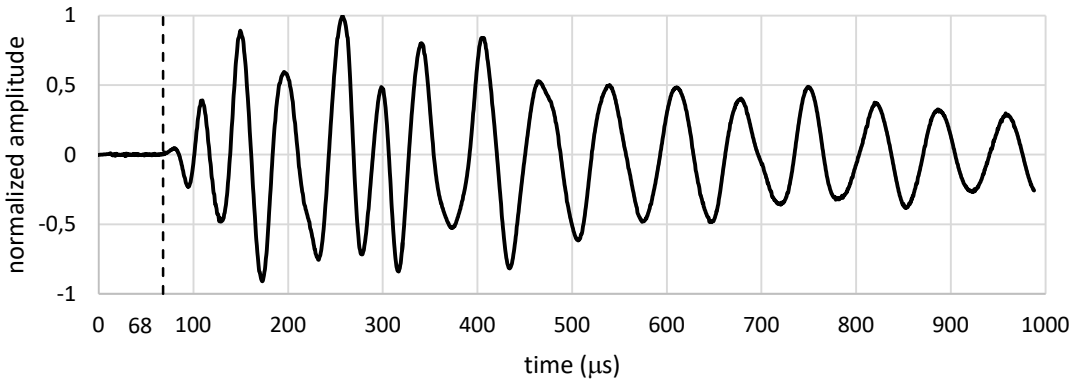

Figure 5.10. US response for UM-US3 (30ºC) at 7 days of age

The constrained modulus (M) values computed from the wave velocities measured with US sensors, on specimens cured at 30ºC, up to 52 days are presented on Figure 5.11. Despite some dispersion observed, namely after 21 days of age, it was possible to distinguish two different phases on the evolution of the M-modulus: the first occurs in the initial 12 days of curing and the second after 12 days. This behaviour of stiffness evolution results of the different reactions that occur along the curing process and will be further addressed on the discussion of the E-modulus evolution (section 5.4.5).

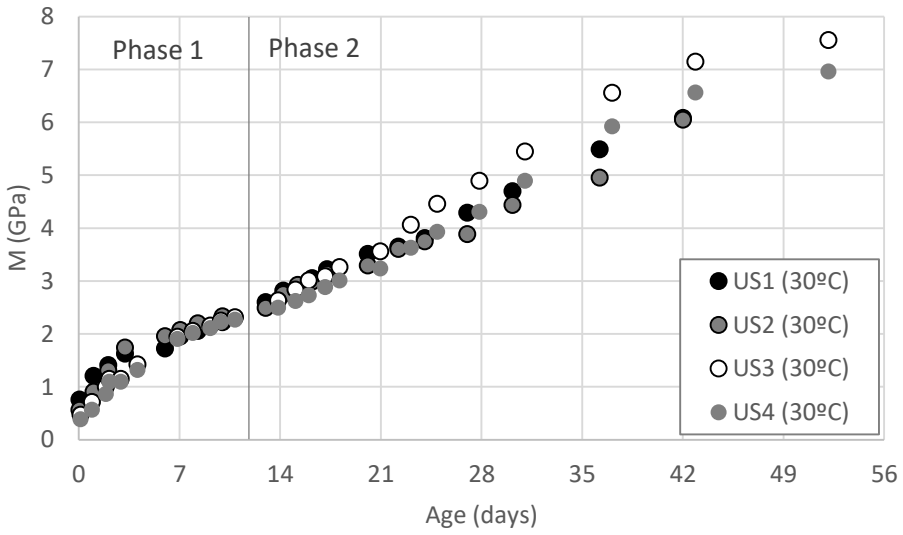

Figure 5.11. M-modulus (M) values computed from the wave velocities measured with US sensors on specimens cured at 30ºC

5.4.4.3 E-modulus and stiffness evolution

The E-modulus results obtained from UCC testing at 8, 28 and 84 days of age, for specimens cured at 30ºC, are presented in Table 5.9. Results from UCC testing exhibit results a quasi linear elastic behaviour of the soil-lime mixture for the strain level (around 4×10^{-5}) of the loading.

Table 5.9. E-modulus obtained from UCC testing at ages of 8, 28 and 84

Age (Days)		8	28	84
E (GPa)	UCC1	1.031	2.520	3.817
	UCC2	0.904	2.194	3.486
	UCC3	1.031	2.520	3.817

Figure 5.12 presents the E-modulus evolution of the soil-lime mixture in the first 90 days at curing temperature of 30ºC, obtained from EMM-ARM and UCC testing. Figure 5.13 presents the E-modulus (EMM-ARM) and M-modulus (US) normalized at 43 days of age. The good coherence observed with EMM-ARM and UCC results confirms the reliability of EMM-ARM.

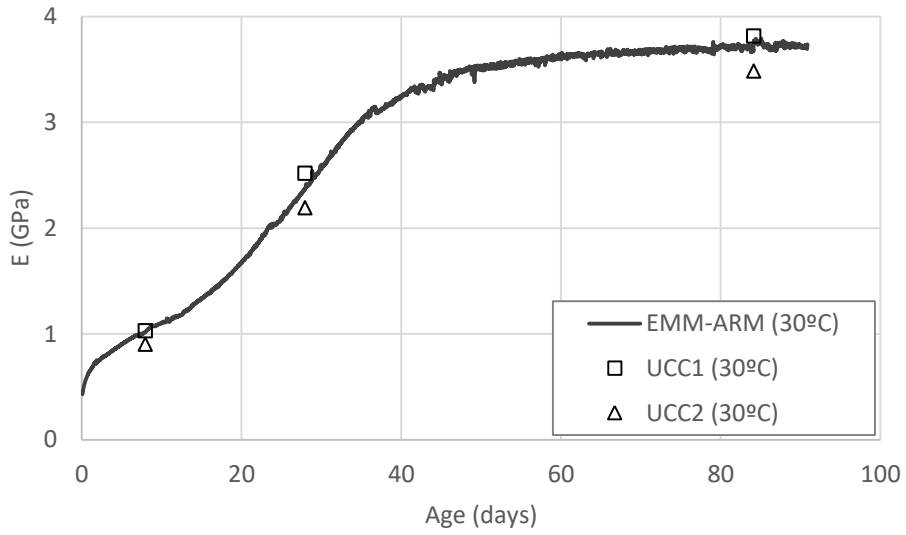

Figure 5.12. E-modulus evolution obtained by EMM-ARM and UCC

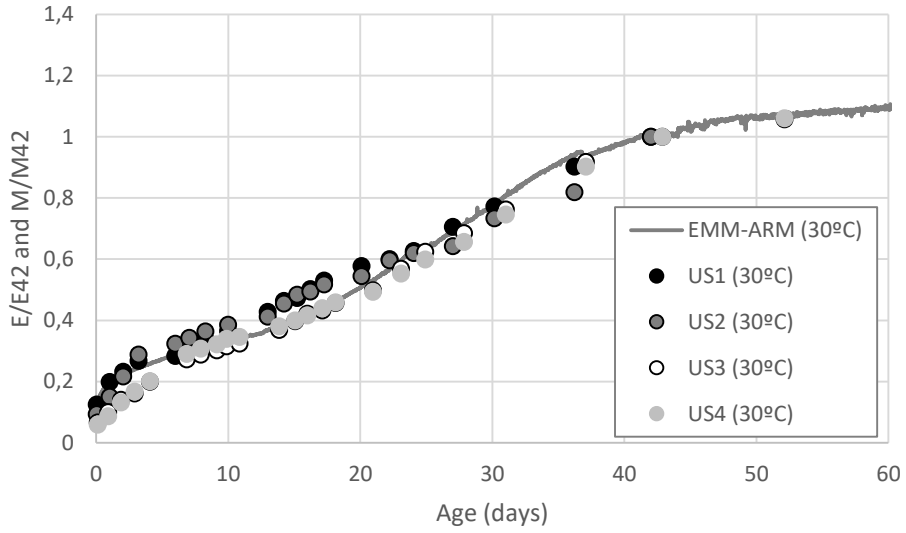

Figure 5.13. E-modulus (EMM-ARM 30) and M-modulus (US) normalized at 43 days

When comparing the relative evolution of M-modulus results obtained from US testing with E-modulus obtained with EMM-ARM (Figure 5.13), a similar trend in stiffness evolution is observed. Is also evident that two distinct phases of the stiffness evolution can be identified: the first phase starts immediately after compaction of the mixture, with a high rate of stiffness increase in the first hours followed by a continuous decrease on the rate until about 12 days; the second phase starts about 12 days of age, with a new

augmentation on the rate of stiffness increase up to about 37 days of age followed by a decrease on the rate until the end of the testing period.

The same behaviour on E-modulus evolution can also be observed on Figure 5.14, where the EMM-ARM results obtained at 20ºC, 30ºC and 40ºC are presented. These results show that the elevation of the curing temperature dramatically increases the rate of E-modulus evolution. As the case of the curing at 30ºC, is also possible to observe the existence of two distinct phases on the E-modulus evolution curves of 20º and 40ºC.

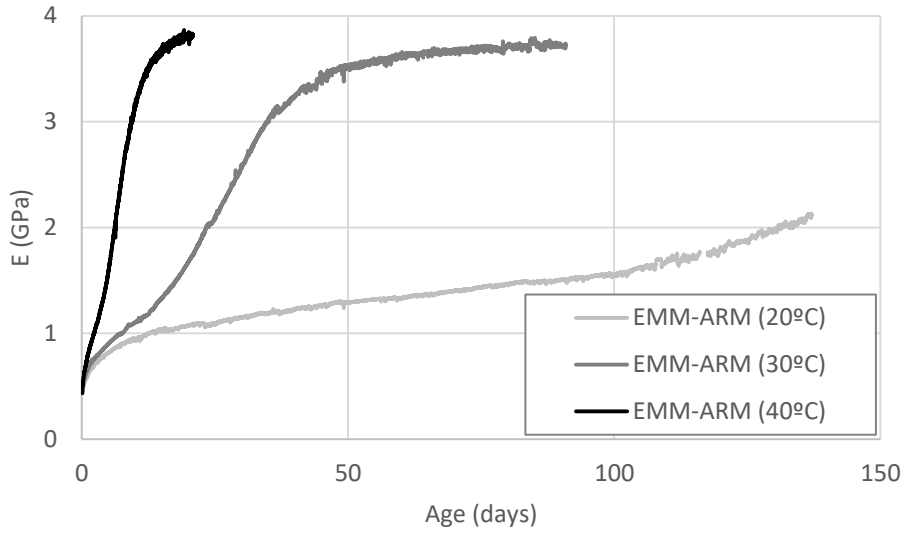

Figure 5.14. E-modulus evolution obtained by EMM-ARM at temperatures of 20ºC, 30ºC and 40ºC

This evolution in two stages was also observed, in terms of the strength evolution, in the works of De Bel *et. al.* (2013) for the same soil-lime mixture cured at 20ºC, as can be seen on Figure 5.15. By comparing these strength results with EMM-ARM results obtained at same temperature (20ºC) is possible to note the same trend on the evolution: In both results the first phase extends up to about 110 days of curing, age when the second phase starts.

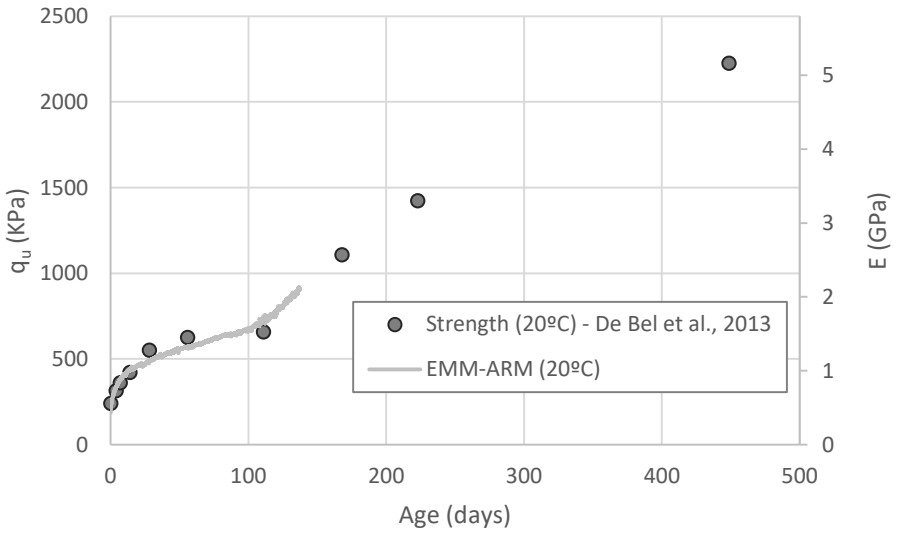

Figure 5.15. Strength evolution of MLD soil with 3% lime cured at 20ºC (Adapted from De Bel *et al.*, 2013)

X-ray diffraction (XRD) testing made by De Bel *et. al.* (2013) to the soil-lime mixture (cured at 20ºC) at different ages (Figure 5.16) revealed the appearance of calcium aluminate hydrates (CAH) in the first phase, that may partly explain the increase in mechanical properties during the this phase of curing, and the existence of portlandite ($Ca(OH)_2$) and calcite ($CaCO_3$), indicating the presence of lime. In the second phase of evolution the peaks related to calcite had lower intensity and the portlandite peaks were not visible anymore, meaning the lime had been almost completely consumed. So, the evolution of the mechanical properties during the second phase may result of different processes, including: first, the reduction observed on the CAH may result from some structural rearrangement along the curing time, resulting on an increase of the E-modulus; secondly, it was possible to observe an alteration (attack) of the clay fraction, which could generate poorly crystallized CSH, having no distinct diffraction peaks, that contributes to the increase of the mechanical properties.

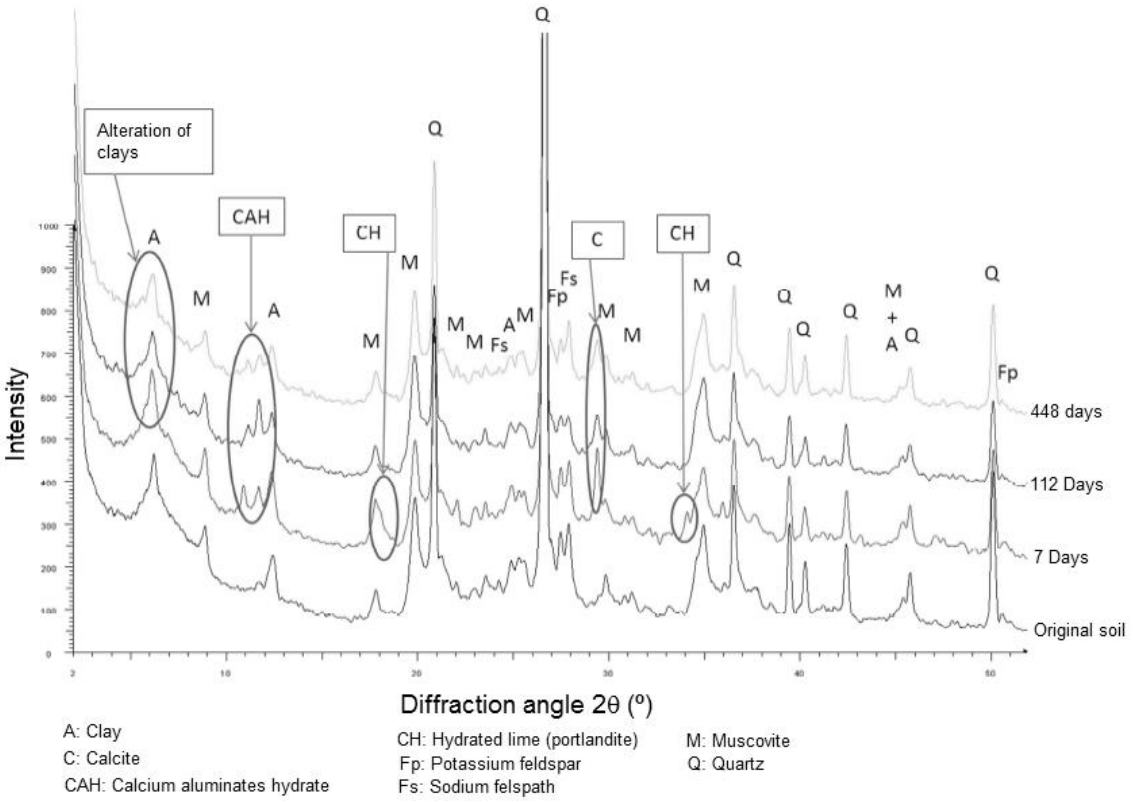

Figure 5.16. X-ray diffraction testing of MLD soil and MLD soil with 3% lime cured at 20ºC (Adapted from De Bel *et al.*, 2013)

Due to the different nature of the reactions involved in the two phases, it is here speculated that the curing temperature may be possibly influencing the kinetics of the reactions in phases 1 and 2 in distinct manners. This evaluation is presented on the following section 5.4.5

5.4.5 Evaluation of temperature effect

5.4.5.1 Fitting model

The method of equivalent age is widely used for estimation of the mechanical properties of cement based mixtures as concrete (Weiss & Berke, 2002) and soil-cement (Chitambira *et al.*, 2007). This method takes in account the combined effects of time and temperature on the development of the mechanical properties, as strength or stiffness and is based on the Arrhenius' Law presented on Equation (5.1), where K is the reaction rate constant, A a proportionality constant, E_a the apparent activation energy (J/mol), T the absolute temperature (K) and R the ideal gas constant (8.314 J/(mol.K)).

$$K = A \exp[-E_a/(RT)] \quad (5.1)$$

However, the application of Arrhenius' law to the binders hydration is an approximation because it allows to describe the influence of temperature on a simple chemical reaction kinetic but the binders hydration involves multiple chemical reactions. Therefore, the activation energy is designated as 'apparent'.

Equivalent age can be defined as the age of curing at reference temperature, usually 20ºC, at which it is possible to achieve the same mechanical properties of curing for a defined period with different known temperature history. One of the most popular models based on the activation energy concepts was proposed by Freiesleben Hansen & Pedersen (1977) which is presented on Equation (5.2), where t_e is the equivalent age (days), T the curing temperature (K), T_{ref} the reference temperature (K), t the time period (days), E_a and R as previously defined.

$$t_e = \sum_0^t e^{\left[(Ea/R)\left((1/T)-(1/T_{ref})\right)\right]} \Delta t \quad (5.2)$$

Equation (5.3) (Rostásy *et al.*, 2001) relates the E-modulus, $E(\alpha)$, of a cementitious mixture with the degree of hydration (α), the degree of hydration of the binder (α_0) at the instant when starts the increase on the mechanical properties (for stabilized soils $\alpha_0 = 0$ as it has initial stiffness) and E_1, the hypothetic value of E when $\alpha = 1$.

Equation (5.4) (Schindler & Folliard, 2005) describes the degree of hydration $\alpha(t)$ along the curing time, t, where α_u is the ultimate degree of hydration, β is a hydration shape parameter, τ is a hydration time parameter and a is a constant ($a = E_1 \times {\alpha_u}^{1/2}$). For a cementitious material was demonstrated that the parameters a and β are temperature independent (Schindler & Folliard, 2005) and only τ is temperature dependent.

$$E(\alpha) = E_1 \times [(\alpha - \alpha_0)/(1 - \alpha_0)]^{1/2} \quad (5.3)$$

$$\alpha(t) = \alpha_u \times e^{\left[-(\tau/t)^{\beta}\right]} \tag{5.4}$$

Combining Equation (5.3) with Equation (5.4) is possible to obtain Equation (5.5) proposed by Silva *et. al.* (2013) to be used as a best-fit mathematical model to describe the E-modulus (*E*) evolution of a curing mixture, as soil-cement, in function of the curing age (*t*).

$$E(t) = \ a \times e^{\left[-\frac{1}{2}\times(\tau/t)^{\beta}\right]} \tag{5.5}$$

Nevertheless, Equation (5.5) is appropriate to fit the typical "S" shape evolution found on cementitious mixtures and cannot accurately describe the E-modulus curves with multiple phases of evolution as the ones obtained for the soil-lime mixture studied in the present work. Assuming that the E-modulus ($E(t)$) of the soil-lime mixture results of the initial E-modulus of the mixture (E_0) and the combined stiffness contribution of reactions initiated on phase 1 and reactions initiated on phase 2 (E_{r1} and E_{r2} respectively), it is possible to express $E(t)$ by Equation (5.6). Thus, assuming E_{r1} and E_{r2} can be individually fitted by Equation (5.5), as presented on Equation (5.7), then Equation (5.6) takes the form presented on Equation (5.8), where the indexes $_1$ and $_2$ means that the parameter concerns the reactions initiated on phase 1 and reactions initiated on phase 2, respectively.

$$E(t) = E_0 + E_{r1}(t) + E_{r2}(t) \tag{5.6}$$

$$E_{r1}(t) = a_{r1}\ e^{\left[-\frac{1}{2}(\tau_{r1}/t)^{\beta r1}\right]}, E_{r2}(t) = \ a_{r2}\ e^{\left[-\frac{1}{2}(\tau_{r2}/t)^{\beta r2}\right]} \tag{5.7}$$

$$E(t) = E_0 + a_{r1}\ e^{\left[-\frac{1}{2}(\tau_{r1}/t)^{\beta r1}\right]} + a_{r2}\ e^{\left[-\frac{1}{2}(\tau_{r2}/t)^{\beta r2}\right]} \tag{5.8}$$

Table 5.10 presents the parameters of Equation (5.8) determined by fitting the experimental E-modulus results obtained at curing temperatures of 20ºC, 30ºC and 40ºC using the least squares method and assuming that the parameters a and β are independent of temperature. Figure 5.17 presents the fit of Equation (5.8) to the experimental data and Figure 5.18a-c shows the E-modulus decomposition, E_{r1} and E_{r2}, into the contribution of the reactions initiated on phase 1 and reactions initiated on phase 2,.

Table 5.10. Parameters of the model fit to experimental results

T (ºC)	20	30	40
a_{r1}	2.91	2.91	2.91
β_{r1}	0.25	0.25	0.25
a_{r2}	2.15	2.15	2.15
β_{r2}	3.13	3.13	3.13
τ_{r1}	1514.94	477.82	138.36
τ_{r2}	189.82	30.78	8.23
E_0 (GPa)		0.401	

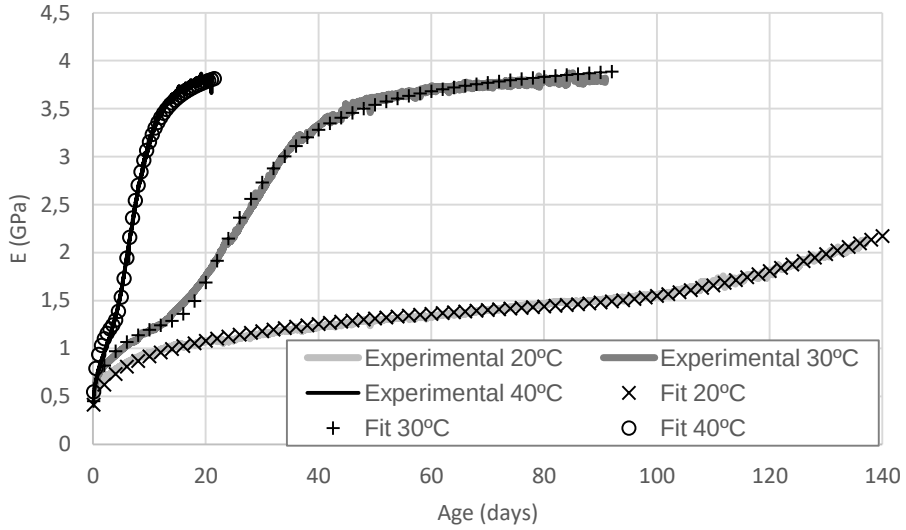

Figure 5.17. Fit to EMM-ARM experimental results at temperatures of 20ºC, 30ºC and 40ºC

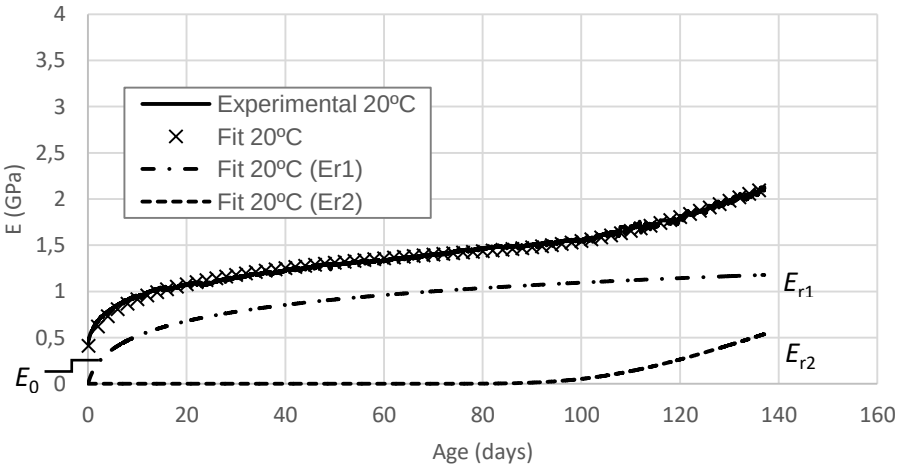

a)

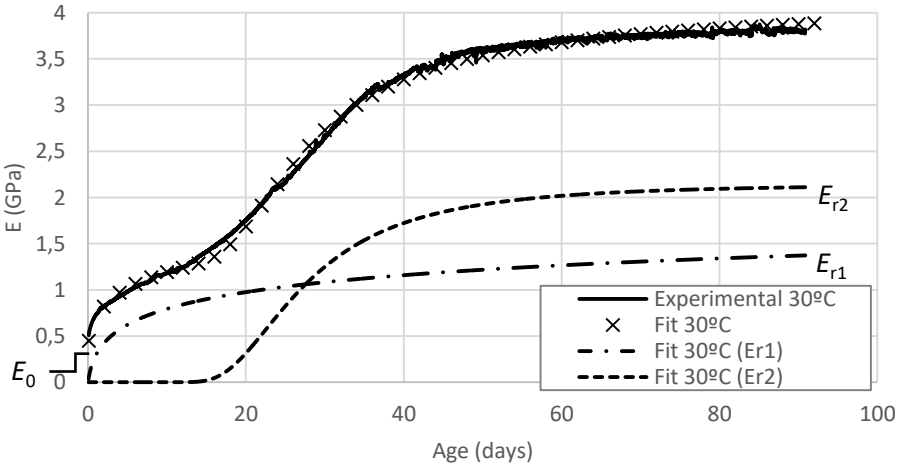

b)

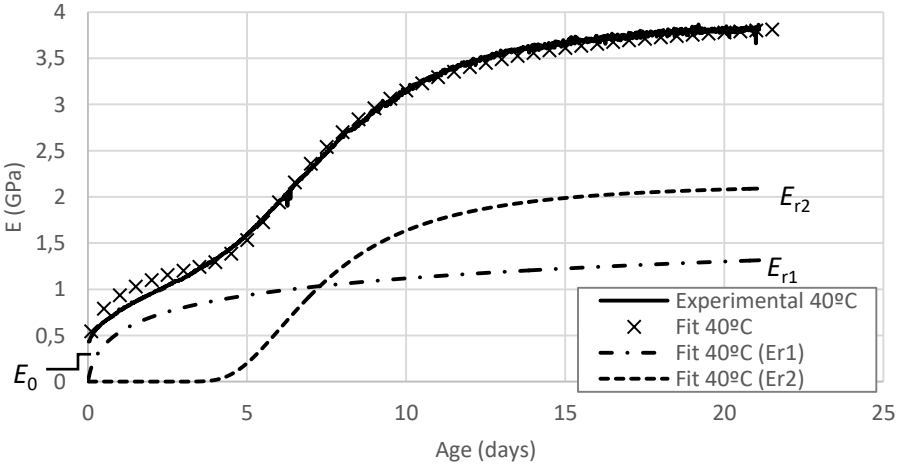

c)

Figure 5.18. Fit to EMM-ARM experimental results and decomposition of the E-modulus evolution in two contributions: a) 20ºC; b) 30ºC; 40ºC

5.4.5.2 Apparent activation energy estimation

The temperature history recorded during EMM-ARM tests is depicted on Figure 5.19 and the respective averages and variation intervals are presented on Table 5.9. From these results is possible to note that the temperature control was relatively effective as the intervals of variation were less than ±1ºC.

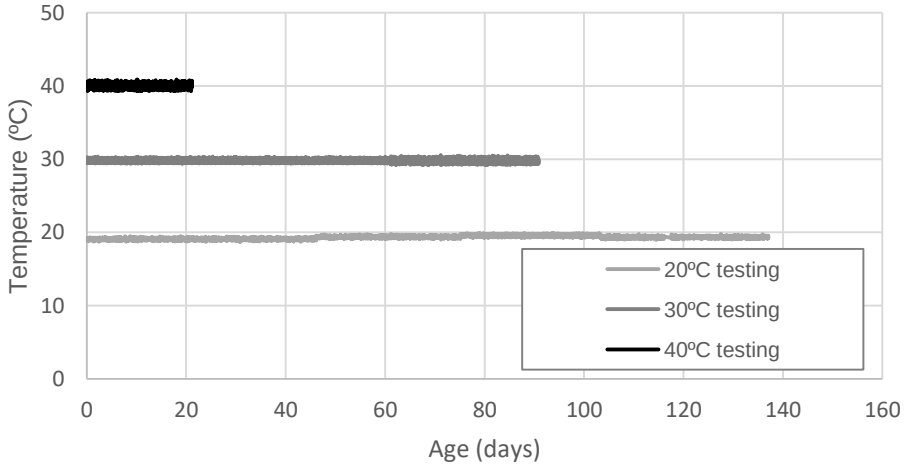

Figure 5.19. Temperature history of EMM-ARM testing

Table 5.11. Average temperatures recorded and respective variation intervals

Temperature set (ºC)	Temperature recorded	
	Average(ºC)	Variation (ºC)
20	19.3	±0.6
30	29.9	±0.7
40	40.1	± 0.8

Replacing t of Equation (5.7) by the equivalent age (Equation (5.2)) is possible to obtain Equation (5.9) that allows to relate E_{ri} (E-modulus contribution of phase *i*) with Ea_i (apparent activation energy of phase *i*), the temperature history, T, and the parameters a_{ri}, τ_{ri} and β_{ri}.

$$E_{ri}(t) = a_{ri}\, e^{\left[-\frac{1}{2}\left(\tau_{ri}/\left(\sum_0^t e^{\left[(Ea_i/R)\left((1/T)-\left(1/T_{ref}\right)\right)\right]\Delta t}\right)\right)^{\beta_{ri}}\right]}, i = \{1,2\} \quad (5.9)$$

To estimate the apparent energy, Equation (5.9) was fitted, by the least square method, to the data E_{r1} and E_{r2} obtained for 30ºC and 40ºC (presented on Figure 5.18b-c) using as parameters a_{ri}, τ_{ri} and β_{ri} the values obtained for the test at 20ºC (Table 5.10) and as T_{ref} the temperature history of the 20ºC test. By means of the least square method was possible to obtain the apparent activation energies of each phase, Ea_1 = 84265 J/mol and Ea_2 = 119469 J/mol. This procedure is similar to the widespread superposition method (Geoffroy, 2004). These values of Ea are considerably higher when comparing to the values observed in cementitious materials, which are typically about 40 kJ/mol (Azenha, 2009). This means the reactions involved are very sensitive to the curing temperatures.

In order to verify the Ea_i results obtained the E-modulus curves at 30ºC and 40ºC were estimated with the results of 20ºC test. Figure 5.20 presents the E_{r1} curves (E-modulus contribution of phase 1 reactions) and Figure 5.21 presents E_{r2} curves (E-modulus contribution of phase 2 reactions) at 30ºC and 40ºC obtained with Equation (5.9) (using a_{ri}, τ_{ri} β_{ri} and E_0 of 20ºC test from Table 5.10 and the respective activation energies determined). Figure 5.22 presents the experimental E-modulus results and the estimates ($E_0 + E_{r1} + E_{r1}$) for 30ºC and 40ºC. In these figures, it is possible to observe a good coherence between the experimental results and the values estimated, which is a good indicator of the validity of the methodology used to access the apparent activation energies of the two types of reactions involved in the curing of this soil-lime mixture.

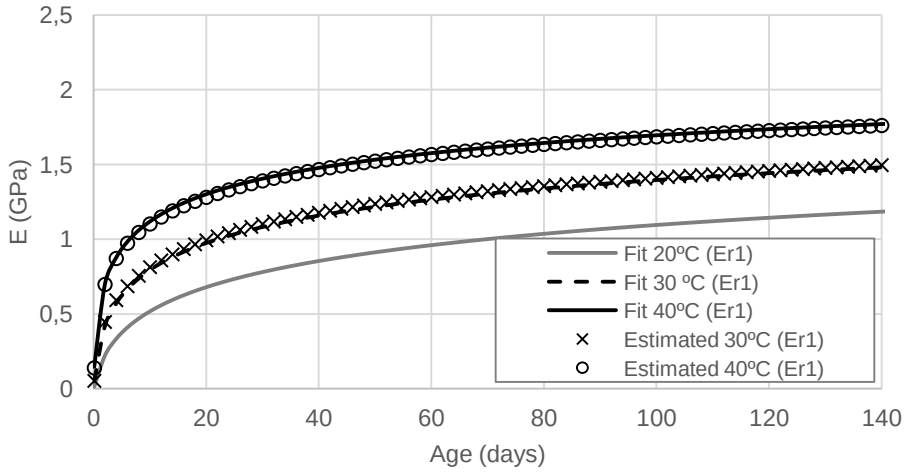

Figure 5.20. Estimation E_{r1} curves (E-modulus contribution of phase 1 reactions) for 30ºC and 40ºC from the 20ºC results

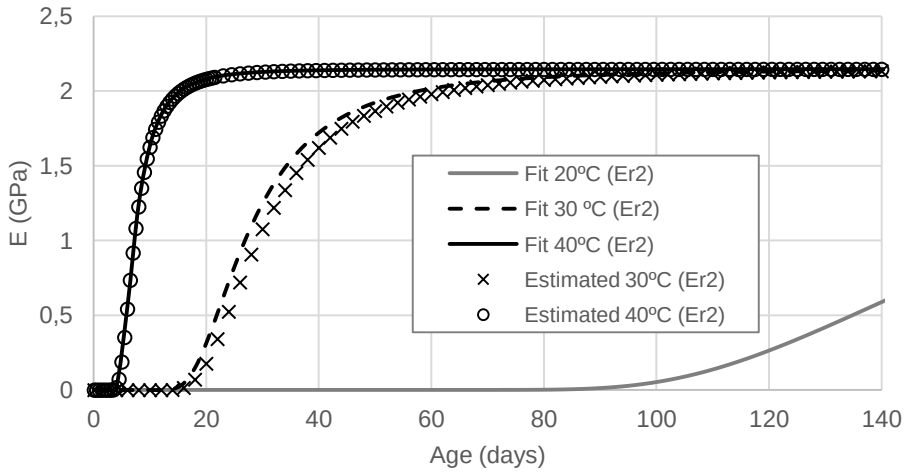

Figure 5.21. Estimation E_{r2} curves (E-modulus contribution of phase 2 reactions) for 30ºC and 40ºC from the 20ºC results

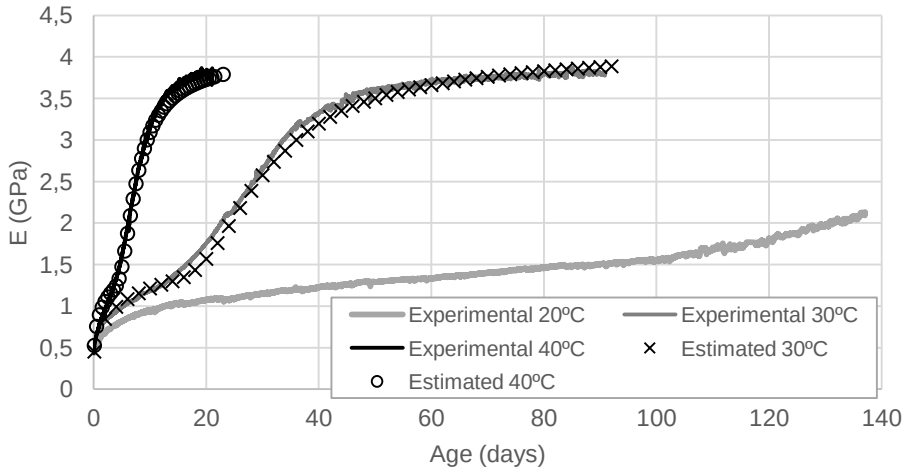

Figure 5.22. Estimation of E-modulus evolution at temperatures of 30ºC and 40ºC from the 20ºC data

5.4.6 Overall discussion

A very good coherence was found when comparing the EMM-ARM results with the E-modulus determined with classical UCC testing, at curing temperature of 30ºC, confirming the validity of EMM-ARM applied to soil-lime mixtures. A similar trend in

stiffness evolution was observed when comparing the relative evolution of M-modulus results obtained from US testing with E-modulus obtained from EMM-ARM.

The results obtained by the different methodologies revealed two different phases on the stiffness evolution, suggesting the existence of two different chemical phenomena. Based on the previous work of De Bel et al. (De Bel *et al.*, 2013), that tested same soil-lime mixture, it was possible to conclude that the E-modulus evolution in the first phase seems to be mostly related to the formation of calcium aluminate hydrates (CAH). However, the E evolution in the second phase can be more related to a structural rearrangement of CAH and the formation of calcium silicate hydrates (CSH).

Taking into account the occurrence of two distinct processes during the curing of the studied mixture, two apparent activation energies were estimated (one for each process). For this purpose, a procedure involving a decomposition of a mathematical model in to the contribution of two phases was proposed. The activation energies estimated where 84265 J/mol and 119469 J/mol for the reactions initiated on phase 1 and reactions initiated on phase 2, respectively. These are much higher than the values found for other type of materials, as concrete, and means that the reactions involved are very sensitive to the curing temperature.

Chapter 6

STIFFNESS PREDICTION BASED ON EMM-ARM RESULTS

6.1 INTRODUCTION

The possibility of using a technique such as EMM-ARM for quality control of *in-situ* collected soil-cement samples, providing continuous quantitative data on the stiffness of the tested material, opens new opportunities. Indeed, there is an interesting potential for reliable estimation of the stiffness at ages of reference (such as 28 days) based on data collected at early ages (such as up to 3 days). This chapter evaluates the possibility to estimate the E-modulus of soil-cement mixtures at 28 days using the results obtained with the EMM-ARM since two days of curing.

The determination of uncertainties related to many areas of geotechnical engineering is an aspect that has been performed by many authors (Cruden & Fell, 1997, Einstein *et al.*, 1999, Min *et al.*, 2005). However, only a few reliable updating processes have been developed in geotechnics, and these are mainly based on Bayes' theorem (Einstein, 1988, Karam, 2005). Concerning the update of strength or deformability, the number of works is even more limited (Miranda *et al.*, 2009).

The proposed methodology uses the data obtained with EMM-ARM and a model based on the cement hydration to predict the E-modulus evolution, together with a Bayesian inference approach to deal with the uncertainty levels of the prediction. This is an innovative approach as it uses an analytical model coupled to a mathematically valid methodology (Bayesian inference) and the results obtained continuously with EMM-ARM for the prediction of E-modulus in an unprecedented manner.

The example of Bayesian inference applied to EMM-ARM uses the results presented in subchapter 4.5 for EMM-ARM T1 and EMM-ARM T2 specimens, and in subchapter 4.6 for EMM-FRM S1 and EMM-ARM S2 specimens.

6.2 PRINCIPLES OF BAYESIAN METHODS

Bayesian statistics are a set of methodologies for data analysis that are based on principles of subjective probability and use the uncertainty probability as a key measure. The knowledge of a given parameter is translated by a probability distribution that is assumed to belong to some common distribution (e.g Normal or log-Normal). As

opposed to the classical perspective of probability, that takes probability as an objective concept, the Bayesian perspective determines that the probability is the degree of individual confidence that a given event can occur (Gelman *et al.*, 2004). Thus, under the Bayesian perspective a given unknown parameter (x) (as the E-modulus) can have a distribution of possible values contrasting the traditional approach that considers a parameter as a fixed quantity. Therefore, the probability density function $p(x)$ reflects the level of confidence where the actual parameter value may be.

Bayesian methods provide tools to incorporate data and information into the data analysis process. In a Bayesian approach, the data processing starts with a given probability distribution with parameters (e.g. the average and standard deviation for the case of a normal distribution) that can be estimated based on existing experimental results and empirical experience. This is the prior distribution (henceforward referred as 'prior') and represents the initial uncertainty about the parameters. The purpose of the prior is to establish an uncertainty rather than randomness to the studied parameter. The establishment of the prior distribution is one of the main issues of the Bayesian procedure. The prior distribution represents the possible values of the parameter and must include all plausible possibilities. The parameters of prior distributions can be calculated or chosen in such way that prior includes information of known initial observations of random variables or subjective knowledge on the distribution of the parameters.

As new information is available this can be used to update the initial distribution in a subsequent distribution, termed the posterior distribution, through the Bayes' theorem. The posterior distribution can be considered as a compromise of reduced uncertainty between the prior distribution and the information provided by the new experimental data (Box & Tiao, 2011, Miranda *et al.*, 2009).

This process can be divided into three steps (Ditlevsen & Madsen, 1996): 1) Establishment of probability distributions for the variables consistent with the available data; 2) Calculation of the posterior distribution of the variables of interest including the new information obtained; 3) Assess the fit of the data model by analysing the reasonableness of conclusions and the results sensitivity to the assumptions of step 1. Bayesian statistics are capable of quantifying the uncertainties associated to predictions and, consequently, providing a perception of the confidence level in it. Additionally, it

is a process that permits the dynamic update of predictions and of the associated uncertainty, making a quite interesting match with EMM-ARM which is also based on continuous data collection. This way, the data provided by EMM-ARM can also be continuously fed to the developed methodology updating the predictions in "real time". The estimation is then a continuous process that involves observations over a period of time and the update of prior estimates at each instant.

6.3 BAYES THEOREM

Considering a continuous initial distribution of a parameter θ with n possible values (θ_1,...,θ_k) and x new information available (sample), Bayes' theorem is given by Equation (6.1), where $p(\theta)$ is the initial (or prior) distribution of possible values of θ, $p(x|\theta)$ is the conditional probability of new information data given θ, $p(\theta|x)$ is the posterior distribution of θ given new information x.

$$p(\theta|x) = \frac{p(\theta).p(x|\theta)}{\int p(\theta).p(x|\theta)\,d\theta} \tag{6.1}$$

The prior and posterior distributions of θ can be represented by probability density functions. The joint probability distribution $p(x|\theta)$ of the initial information given new information x_i of parameter θ is denominated likelihood and is defined by Equation (6.2).

$$p(x|\theta) = L(\theta) = \prod_i p(x_i|\theta) \tag{6.2}$$

Bayes' theorem application consists in the multiplication of the prior distribution by the likelihood and subsequent normalization of the result, thus obtaining the posterior distribution, which is the conditional distribution of the unknown parameter with the new information that was included. The posterior distribution condenses the full

information after inclusion of the new information and it is the basis for new inferences of θ. The posterior distribution will have lower variance as it incorporates more information than the original prior distribution.

The property that posterior distribution is of the same parametric family (follows the same parametric form) of the prior distribution is called conjugacy and it presents computational advantages since they simplify calculations and can be frequently translated in analytical form (Miranda *et al.*, 2009). The consideration that the data under analysis follows a normal distribution has the computational advantage of allowing the use of conjugate priors, which results in proper posteriors (Ditlevsen & Madsen, 1996). However, the use of normal distributions to model geomechanical parameters is questionable as it allows negative values of the parameter to have positive probabilities which is, obviously, impossible. Usually, the use of a truncated normal distribution for the lower values of the parameter is sufficient to avoid this to happen. The central limit theorem helps to justify the use of the normal distributions and the results are frequently acceptable (Ditlevsen & Madsen, 1996, Miranda *et al.*, 2009). Therefore, the modelling assumptions should always be verified by analysing the results given by the posterior distribution.

6.4 BAYESIAN INFERENCE APPLIED TO EMM-ARM

The methodology here proposed to predict the E-modulus, based on EMM-ARM results, includes the following steps (represented in Figure 6.1): a) the selection of an E-modulus evolution model able to describe the E-modulus evolution of the studied material; b) the definition of the mean of prior distribution of the parameters of the model, by fitting the selected model to the experimental obtained during an initial period of curing time; c) including some empirical knowledge, namely to estimate the initial variance of the prior distribution of the parameters of the model; d) estimation of the prior distribution of the E-modulus by applying the simulation methodology using the model and the prior distribution of the parameters of the model; e) compute the posterior distribution of the E-modulus through an updating process of the prior distribution of the E-modulus using new EMM-ARM experimental results obtained during a period of time.

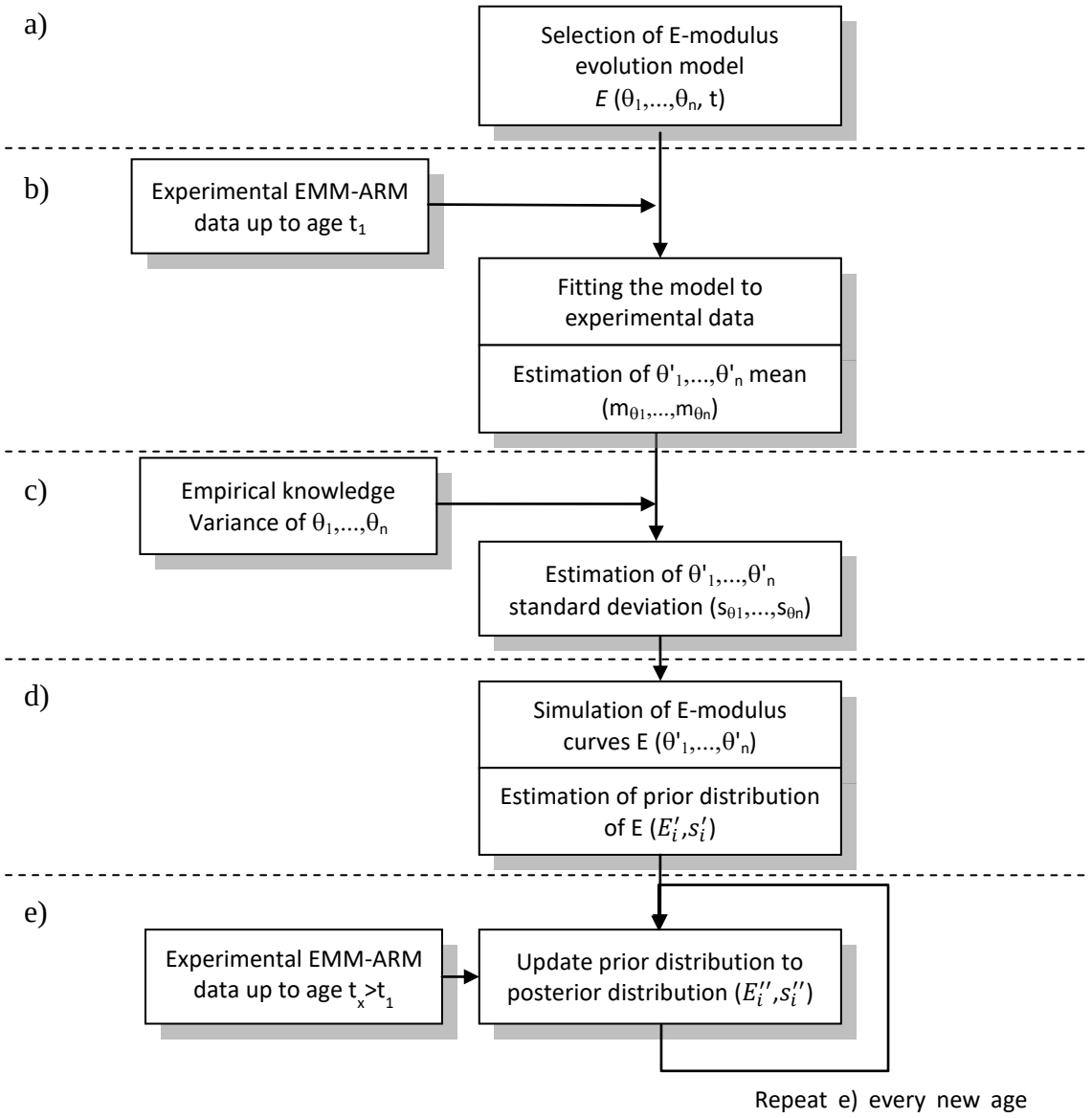

Figure 6.1. Flowchart of Bayesian inference applied to EMM-ARM

6.4.1 Prediction (Fitting) model

The fitting model selected is presented on Equation (6.3), which is an extension of Equation (5.5) presented in subsection 5.4.5.1, were was added E_0 to include the E-modulus value of the soil-cement mixture obtained at the beginning of EMM-ARM testing. This model has three θ parameters: $\theta_1 = a$; $\theta_2 = \tau$; $\theta_3 = \beta$.

$$E_i(t) = E_0 + a \times e^{\left[-\frac{1}{2}\times(\tau/t)^{\beta}\right]} \quad (6.3)$$

6.4.2 Prior distribution

Consider E_i as the E-modulus at age t_i that is function of certain random parameters θ. So, $E_i = e_i(\theta)$, where e_i is a function of θ (i.e. e_i is the E-modulus prediction model) and θ is the vector of the k random parameters that can be related with the E-modulus ($\theta = \theta_1, \theta_2, \dots, \theta_k$). For the predicting model presented on Equation (6.3) $k = 3$ and $\theta_1 = a$, $\theta_2 = \beta$, $\theta_3 = \tau$. With the knowledge of the prior probability density distribution of θ, termed as θ', is possible to obtain the initial statistical distribution, or prior distribution, of the E-modulus (E_i') by means of simulation methods (using the distribution θ').

In this work, the means of prior distributions, θ', were obtained by fitting Equation (6.3), using method of least squares, to the prior experimental data obtained with EMM-ARM during an initial period of time (was the data obtained during the first two days of curing). Due to the lack of information concerning the standard deviations of prior distributions, θ', it was simply assumed a value (standard deviations were assumed as 50% of the respective means). Then the Latin Hypercube Sampling (LHS) (McKay *et al.*, 1979) was used to simulate the values for the initial prior distribution, (E_i'). The concept of the LHS method is based on Monte Carlo (Brooks *et al.*, 2011) techniques. However, it uses a stratified sampling approach that allows efficient estimation of output statistics. For each θ, LHS subdivides the parameter range into N segments, each with a probability of occurrence equal to $1/N$. Each segment is sampled only once, thus generating N random values $\theta^{(n)}$, with $n = 1\ to\ N$, for each parameter θ. The components of the various θ are then matched randomly. So, from N simulation runs of the E-modulus prediction model, with input parameters $\theta^{(n)}$, is then possible to obtain a set of $E_i'^{(n)}$ values. The prior mean and standard deviation of the E-modulus can be obtained, respectively, with relations presented by Equations (6.4) and (6.5). This procedure, was only used to compute the first prior distribution of E-modulus ($\overline{E_i'}, s_i'$). The priors used in subsequent iterations consisted on the posterior distribution obtained in the preceding iteration (i.e. after updating the prior, the posterior distribution obtained was used as the prior distribution of the subsequent update).

$$\overline{E_i'} = \frac{1}{N}\sum_{n=1}^{N} E_i'^{(n)} \tag{6.4}$$

$$s_i' = \sqrt{\frac{1}{N}\sum_{n=1}^{N}\left(E_i'^{(n)} - E_i'\right)^2} \tag{6.5}$$

6.4.3 Posterior distribution

By including on the prior distribution the available EMM-ARM measurements (E_m), obtained up to the age t_m, the statistical information can be improved and an updated, or posterior, distribution (E_i'') is then obtained. The relationships used in the present work for posterior prediction, which are presented below, are based on the methodology proposed by Bažant (1985) and posteriorly used by Yang (2007) to predict time-dependent effects in concrete.

Assuming $E_i^{(n)}$ as the E-modulus obtained from each random sample $\theta^{(n)}$, i.e. $E_i^{(n)} = e_i\,(\theta^{(n)})$, from the Bayes theorem is possible to write the relation expressed by Equation (6.6), where: ‘’ and ‘’’ means before and after update with new measured values, respectively; E_m=$E_1, \dots, E_M$ is the vector of the M measured E-modulus values on which updating is based; $L\left(E|\theta^{(n)}\right) = L\left(E_1, \dots, E_M|\theta_1^{(n)}, \dots, \theta_M^{(n)}\right)$ is the likelihood function that represents the relative joint conditional probability of the measured values (E_m), under the condition that θ vector coincides with the n-th sample $\theta^{(n)}$; $p'\left(\theta^{(n)}\right) = p'\left(E_i^{(n)}\right) = 1/N$; and $c_{\,1}$ is a normalizing constant.

$$p''\left(E_i^{(n)}\right) = p''\left(\theta^{(n)}\right) = p\left(\theta^{(n)}|E_m\right) = c_{\,1}\,L\left(E_m|\theta^{(n)}\right)\,p'\left(\theta^{(n)}\right) \tag{6.6}$$

The likelihood can now be written as presented on Equation (6.7), where $f\left(E_m|\theta^{(n)}\right)$ is the density distribution of the conditional probability to obtain any E_m value under the condition that θ vector coincides with the n-th sample $\theta^{(n)}$.

$$L\left(E_m|\theta^{(n)}\right) = \prod_{m=1}^{M} f\left(E_m|\theta^{(n)}\right) \tag{6.7}$$

Considering all distributions as normal, the prior and likelihood distributions can be written as presented on Equation (6.8) and Equation (6.9), respectively, where $E_i'^{(n)}$ and $E_m'^{(n)}$represents the value obtained from the simulation with n-th sample of parameter $\theta^{(n)}$ and s_m is the standard deviation of the measured values E_m.

$$f'(E_i') = \frac{1}{s_i'\sqrt{2\pi}} \exp\left[-\frac{1}{2}\left(\frac{E_i'^{(n)} - \overline{E_i'}}{s_i'}\right)^2\right] \tag{6.8}$$

$$f'\left(E_m|\theta^{(n)}\right) = \frac{1}{s_m\sqrt{2\pi}} \exp\left[-\frac{1}{2}\left(\frac{E_m - E_m'^{(n)}}{s_m}\right)^2\right] \tag{6.9}$$

Substituting $p'\left(\theta^{(n)}\right)$ and Equation (6.7) into Equation (6.6) is possible to obtain the relations presented on Equations (6.10) and (6.11), where $c_0 = 1/N$ is a constant that can be obtained from the normalizing condition of Equation (6.7), for example $c_0 = 1/\sum p_n$.

$$p''\left(E_i^{(n)}\right) = p''\left(\theta^{(n)}\right) = c_0 p_{(n)} \tag{6.10}$$

$$p_{(n)} = \prod_{m=1}^{M} f\left(E_m|\theta^{(n)}\right) \tag{6.11}$$

Combining Equation (6.9) with equation (6.11) the relation presented on Equation (6.12) is obtained.

$$p_{(n)} = \exp\left[-\sum_{m=1}^{M}\frac{1}{2}\left(\frac{E_m - E_m^{\prime(n)}}{s_m}\right)^2\right] \tag{6.12}$$

The updated, or posterior, mean $\overline{E_i''}$ and standard deviation s_i'' of the posterior distribution, that permits to obtain the predictions E_i, are presented on Equations (6.13) and (6.14), respectively, and the posterior normal probability distribution is presented on Equation (6.15).

$$\overline{E_i''} = \frac{1}{\sum_n p_n}\sum_n p_{(n)} E_i^{\prime(n)} \tag{6.13}$$

$$s_i'' = \left[\frac{1}{\sum_n p_n}\sum_n p_{(n)}\left(E_i^{\prime(n)} - E_i''\right)\right] \tag{6.14}$$

$$f''(E_i'') = \frac{1}{s_i''\sqrt{2\pi}}\exp\left[-\frac{1}{2}\left(\frac{E_i'' - \overline{E_i''}}{s_i''}\right)^2\right] \tag{6.15}$$

6.5 EXAMPLE OF APPLICATION OF BAYESIAN INFERENCE TO EMM-ARM RESULTS

6.5.1 Determination of prior distributions

In this work, the means of prior distributions θ', were obtained by fitting Equation (6.3) to EMM-ARM experimental data obtained during the first two days of curing, using method of least squares, implemented in a MatLab algorithm (the MatLab nonlinear least-squares solver 'lsqcurvefit', using the default step size tolerance of 10^{-6}). Due to the limited knowledge about the parameters, and in order to cover a large number of possibilities, the prior standard deviations of θ were assumed as 50% of the prior means (a coefficient of variation of 50%). After determination of the prior distributions of the parameters θ, the prior distribution of the E-modulus (E_i',s_i') was calculated. For that, 20000 random numbers for each parameter θ (20000 × 3) were generated via the LHS simulation algorithm and the respective E-modulus curves were computed through Equation (6.3). The number of the random numbers was selected based on the results obtained in a convergence test. In fact, for simulations with random numbers above 20000 the increase in the number of points did not lead to significant changes in the results of the standard deviation. The prior mean, E_i', and standard deviation, s_i', of the E-modulus were then calculated by applying Equations (6.4) and (6.5) to the simulated data.

6.5.2 Updating procedure

After the computation of the prior E-modulus distribution the posterior distribution was determined by applying the updating procedure presented on section 6.4.3. The new information used to update the prior distribution consisted on the experimental EMM-ARM results obtained during the subsequent day after the latest day used to determinate the prior determination (assuming *j* as the number of days used to determine the prior distribution the posterior was computed by using the data of *j+1* days). This update process was successively performed since 2 days up to 7 days of age with increments of 1 day, using as prior distribution the posterior distribution of the previous iteration, as depicted on Figure 6.2.

The updating procedure was initially applied individually to the results of each specimen, T1, T2 (presented on subsection 4.5.3.5), S1 and S2 (presented on subsection 4.5.4.4). As each pair of EMM-ARM beams T1/T2 and S1/S2 are specimens of same mixtures (mixtures M1 and M2, respectively) an alternative approach was used. The EMM-ARM results obtained with each pair of specimens (as each pair is from same mixture) were grouped and then the same Bayesian procedure was applied to the grouped data.

In order to facilitate the interpretation of results obtained along the updating process, each distribution was plotted with the respective mean and an interval with a probability of 95% percent (lower limit of 2.5% and upper limit of 97.5%). The computation of the interval limits was made by using the principles of the inverse cumulative distribution function (also known as quantile function) (Steinbrecher & Shaw, 2008) of each distribution in a MatLab algorithm (MatLab 'norminv' function).

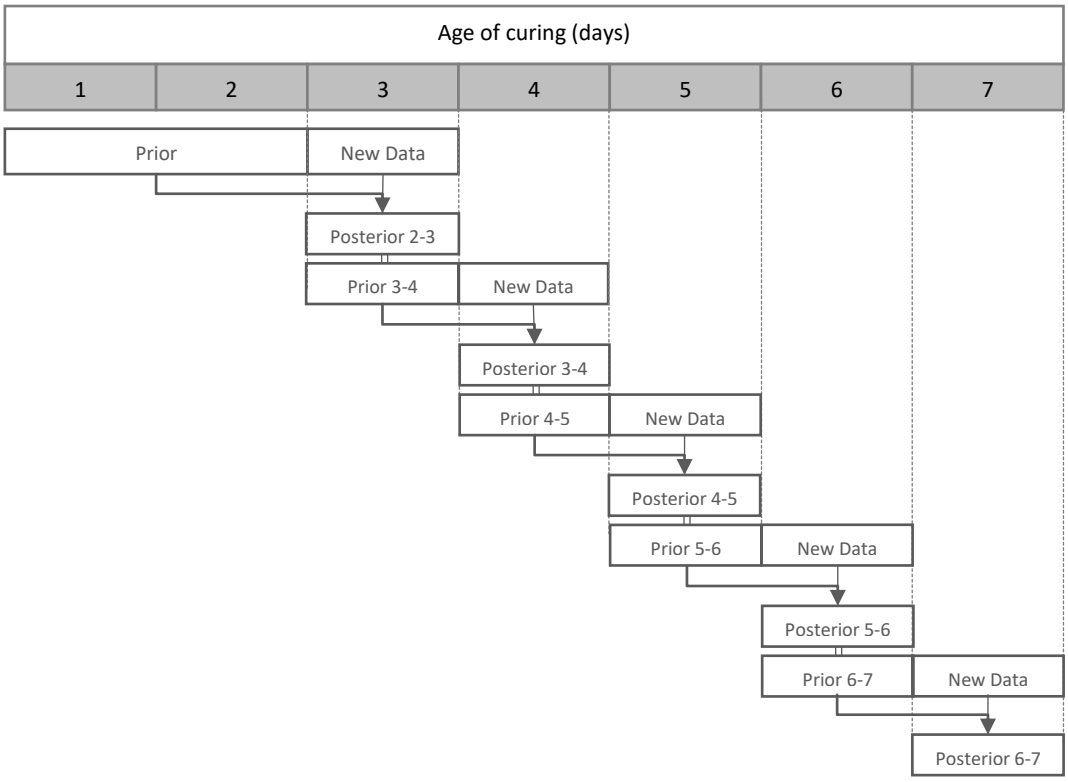

Figure 6.2. Strategy used for successive updating up to 7 days of age

6.5.3 Results and discussion

The process described above allowed the estimation of probability intervals for each update. This process was applied to individually to each specimen data, T1, T2, S1 and S2, and to combine data of pairs T1/T2 and S1/S2.

Figure 6.3 presents the 95% probability intervals obtained at each selected date for specimen T1. Table 6.1 presents the limits of the estimated intervals containing 95% of the values of each distribution estimated for 28 days of age, together with the amplitude of the interval, the computed mean ($\overline{E''_{28}}$), the standard deviation (s''_{28}) and the actual E-modulus values obtained with EMM-ARM at age of 28 days. The probability density functions at 28 days of age computed with data since 2 to 7 days of curing for specimen T1 is presented on Figure 6.4. As globally the results obtained were similar for the remaining specimens these are presented on the Appendix.

By observing Figure 6.3 (a-f), Table 6.1 and Figure 6.4 is possible to note that the adoption of a standard deviation of 50% of the initial θ for the model parameters resulted on E-modulus prior distributions with high variance. So, the predictions provided by these priors are vague or uninformative. However, after the first update at 3 days (Figure 6.3b, Figure 6.4) was possible to note a significant reduction of the 95% confidence interval and, consequently, a reduction of uncertainty.

Table 6.1. E-modulus at predicted (95% probability interval) at age of 28 days for specimen T1

	Prior	Post. 2-3	Post. 3-4	Post. 4-5	Post. 5-6	Post. 6-7
Prob. 2.5%	0.487	4.520	4.514	4.665	4.798	4.898
Conf. 97.5%	10.331	6.235	5.885	5.756	5.664	5.593
Dif. 97.5-2.5	9.844	1.714	1.371	1.091	0.866	0.695
Mean	5.409	5.378	5.200	5.210	5.231	5.246
Standard deviation	2.511	0.437	0.350	0.278	0.221	0.177
Experimental (E) - T1	5.407	[E-modulus at 28 days of age (GPa)]				

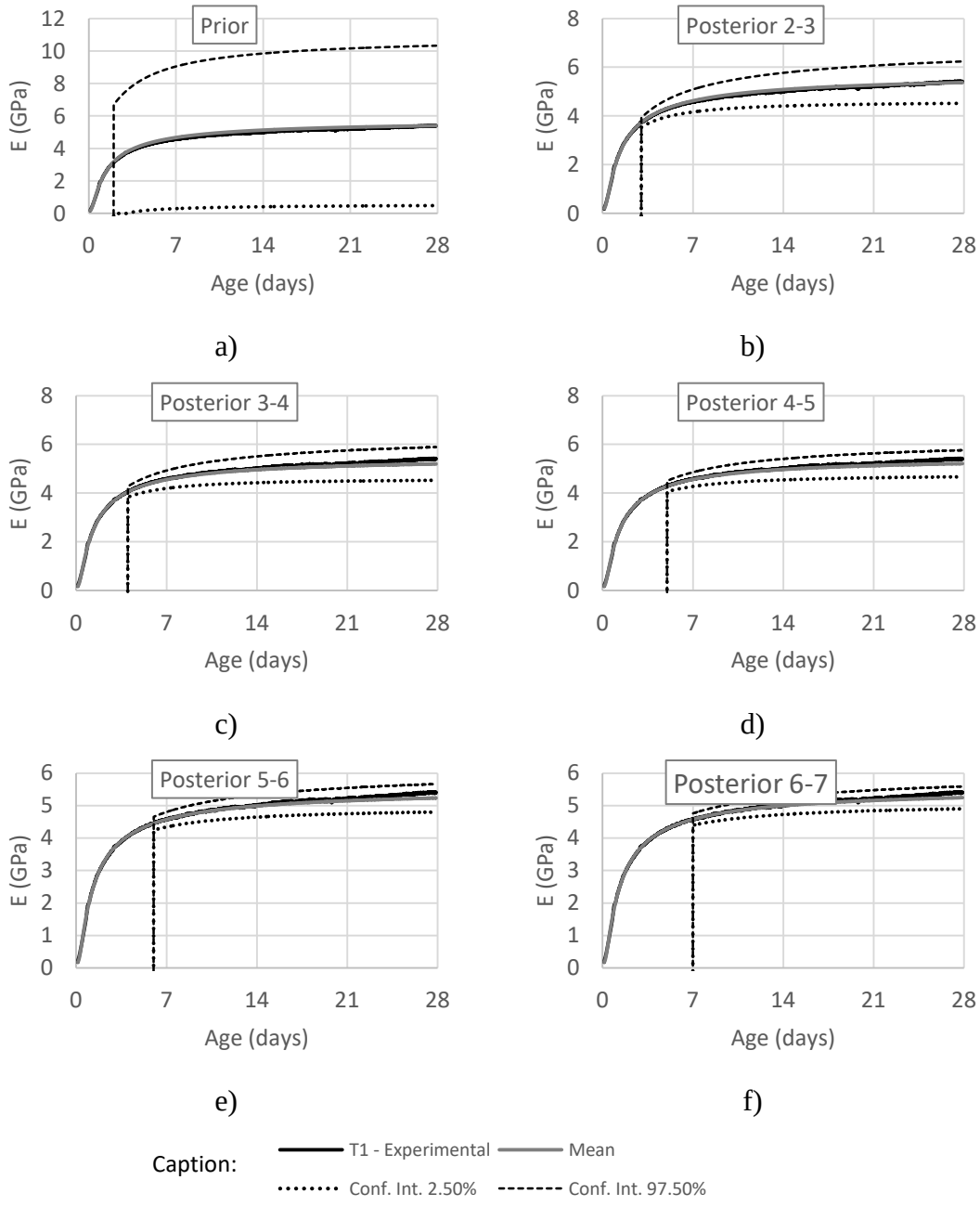

Figure 6.3. Prior distribution and updated posteriors (95% probability interval) for specimen T1

On Figure 6.4 it is possible to observe the approximation of the mean of the distributions to the experimental value after each update and the consequent reduction of uncertainty. This option of such large variance was used to test the Bayesian methodology in adverse conditions of great uncertainty and even under these conditions is possible to consider that the methodology had a good performance.

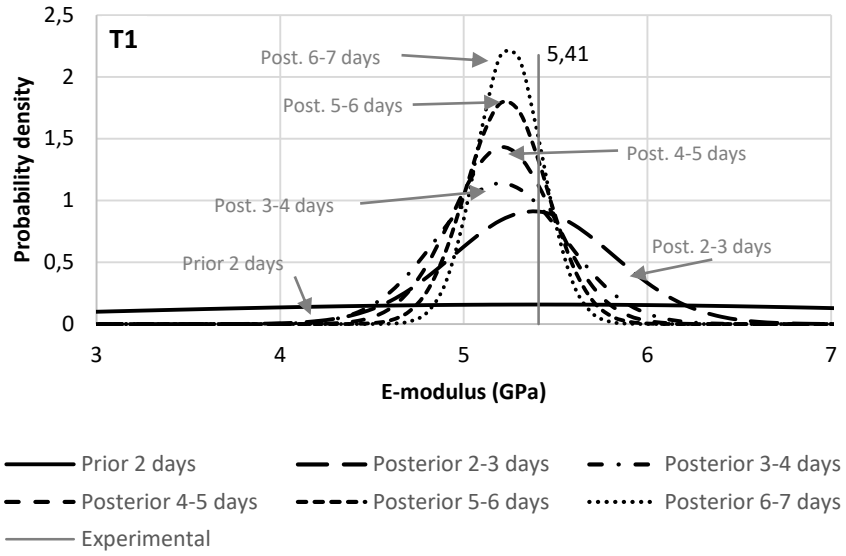

Figure 6.4. Probability density functions predicted at 28 days with EMM-ARM results obtained up to 2, 3, 4, 5, 6 and 7 days for specimen T1

Figure 6.5 and Table 6.2 presents the results obtained for when combining the data obtained of specimens T1 and T2 (pair T1/T2). Globally the results are similar to those obtained with the pair of specimens S1/S1 results, presented on the Appendix (Figure A.0.4 and Table 0.4).

Table 6.2. E-modulus at predicted (95% prob. int.) at age of 28 days for specimen pair T1/T2

	Prior	Post. 2-3	Post. 3-4	Post. 4-5	Post. 5-6	Post. 6-7
Prob. 2.5%	0.490	4.329	4.318	4.530	4.686	4.794
Prob. 97.5%	9.599	5.872	5.559	5.517	5.480	5.430
Dif. 97.5-2.5	9.109	1.543	1.241	0.987	0.794	0.635
Mean	5.045	5.100	4.938	5.024	5.083	5.112
Standard deviation	2.324	0.394	0.317	0.252	0.203	0.162
Experimental (E) - T1	5.407					
Experimental (E) - T2	5.274	[E-modulus at 28 days of age (GPa)]				

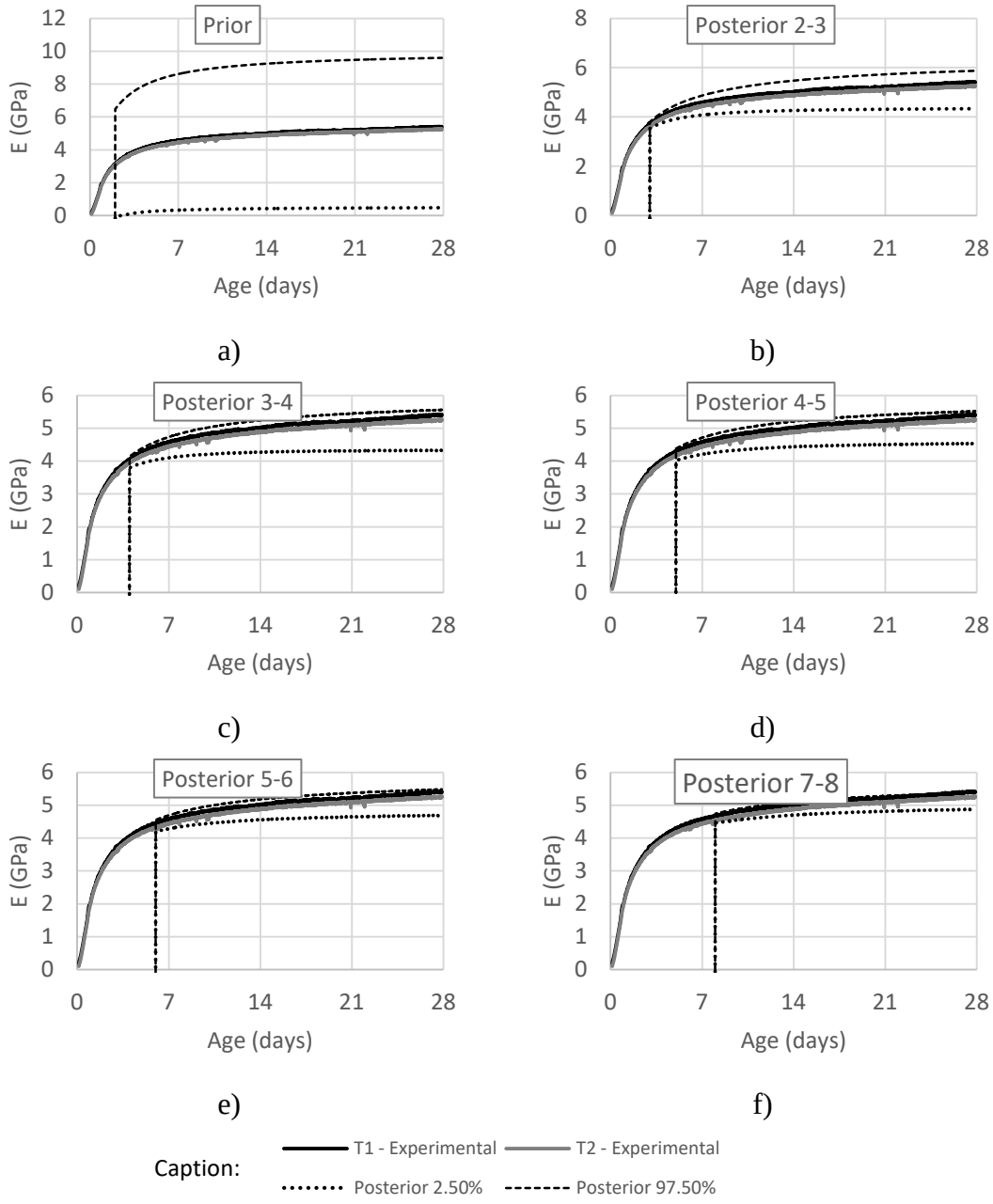

Figure 6.5. Prior distribution and updated posteriors (95% prob. int.) for specimen pair T1/T2

Regarding specimens T1 (Figure 6.3) and T2 (Figure A.0.1), it is possible to observe that the experimental EMM-ARM results are within the limits of all inferred 95% probability interval. This is observed both for the cases where T1 and T2 results were updated individually and when the experimental results were updated together (T1/T2) (Figure 6.5). In the case of specimens S1 (Figure A.0.2, Table 0.2) and S2 (Figure A.0.3, Table 0.3), some of the 95% confidence intervals inferred do not envelope the experimental results, namely in the posteriors 2-3, 3-4 and 4-5. However, the maximum

difference between the experimental results and the closest limit of the 95% probability interval is less than 5%, which can be considered as a minor difference. The same type of behaviour is observed in the results obtained when the experimental results were updated together (S1/S2) (Figure A.0.4, Table 0.4). Nevertheless, with the introduction of new data, namely since the posterior 5-6, the 95% confidence interval of posteriors starts including the experimental E-modulus results.

When comparing the two alternative approaches, of updating individually or the grouped results of specimens of same mixture, is possible to note that the 95% confidence intervals are slightly tighter for the cases when the data was used grouped together and used as a single sample (pairs S1/S2 and T1/T2). This means that by using individually the data obtained with each sample, predictions will be more conservative than the case when data obtained from several specimens of the same mixture is grouped and used together in the same updating.

For the studied data was possible to observe that the analytical model used predicted accurately the E-modulus evolution, the Bayesian model made a realistic management of the uncertainty associated to the model predictions and was possible to accurately predict the E-modulus at reference ages using the limited information obtained during the early days.

Chapter 7

CONCLUSIONS AND FINAL CONSIDERATIONS

7.1 INTRODUCTION

This thesis presents several modifications to Elastic Modulus Measurement-Ambient Response Method (EMM-ARM) that were proposed in order to increase the robustness of this method applied to stabilized soils, and to improve the representativeness of the tested samples. The main modifications comprised changes on mould geometry and material, the proposal of sampling procedures for in-situ application and the use of explicit excitation together with experimental (input-output) modal identification technique. The thesis also comprises a systematic application to several mix formulations, the study of the temperature effect on the curing kinetics of a soil-lime mixture and prediction of the E-modulus at reference ages based on EMM-ARM results obtained during the first days of curing.

7.2 MODIFICATIONS TO MOULDS AND SAMPLING

Two different types of moulds were developed with the objective to overcome the limitations raised in previous works of Silva (2010) and Azenha *et. al.* (2011), namely the difficulties with modal analysis, the robustness issues of the mould and the representativeness of the specimens. For that, parametric simulations were made in order to redefine the geometry of the moulds. The principles considered for the redesigned moulds included the easy excitation of testing beams by the ambient vibrations allowing the easy application of operational (ambient) modal analysis, a significant resonant frequency shift of the composite beam during the experiment, resulting in a good resolution in the E-modulus estimation, and ensuring negligible deflections for the testing beam, thus avoiding second-order geometric effects. As result, redesigned moulds were setup, with prismatic and tubular geometries and with higher slenderness than those used in previous works. The prismatic mould consisted on polycarbonate plates that were connected with screws forming a hollow beam. For tubular moulds polyvinyl chloride (PVC) was adopted as an alternative cheaper material.

The performance of the new moulds was evaluated in an experimental program that involved the collection of samples from a sand-cement pilot layer directly to the moulds

to be tested by EMM-ARM. The sampling with prismatic mould was performed from the top of the pilot layer with assistance of a wooden sampler. However, this sampling process was extremely slow and laborious and the representativeness was considered somewhat dubious. In fact, the sampler experienced some observable deformation during the insertion into the compacted layer as result of its low stiffness and the final sample exhibit higher density than the material on the compacted layer. The use of tubular mould to collect the sample was more straightforward. Tubular PVC moulds were inserted laterally on the layer with no need of special equipment.

Concerning EMM-ARM testing, the results obtained with operational (output-only) modal analysis were very clear and no difficulties were found to identify the resonant frequencies. Even so, the normalized power spectra density (NPSD) functions obtained from prismatic beams presented some secondary peaks which had no relevance in the identification process. When comparing the performance of the two types of moulds, the use of PVC tubular moulds revealed to be more practical for sampling operations, and the NPSDs obtained with these beams were clearer, presenting very distinct peaks at resonant frequencies. In terms of E-modulus results, the tubular PVC moulds presented good repeatability and agreement with results obtained from unconfined cyclic compression testing on specimens both collected from the layer and reconstituted with the same material.

7.3 IMPROVEMENTS ON SAMPLING

Despite the success obtained with the tubular moulds, the sampling procedure used may not be practical for in-situ application as the access to the layer needs to be made from the side, which, in many cases, may not be possible. Moreover, the use of PVC tubes as sampler may result in some damage to them, particularly with coarse materials or has is stiffer than the material studied. Thus, additional improvements were made in EMM-ARM to simplify the experimental procedure and minimise possible damages of PVC tubes during sampling operations, by using geotechnical sampling background. A metallic sampler was then developed with objective to protect the PVC tubes and allow the collection of samples from the top of the layers. During the sampling operations the PVC tubes were used as liners of the metallic sampler to receive the collected material. The length of PVC tubes were reduced in order decrease the size of the collected sample

and making sampling operations easier. Additionally, this reduction in specimen length resulted in an increase of the testing resolution.

The metallic sampler, with the PVC mould inside, was used to collect samples from the top of small pilot sand-cement layers. The first indication of the good performance of this sampling methodology was provided by the similarity between the density of the samples and density of the compacted layers. The feasibility of this sampling methodology was confirmed by the very good coherence of the E-modulus results obtained from classical EMM-ARM test performed in one of the collected samples with results obtained from UCC testing. Despite the lower slenderness, and consequently the lower excitability of the testing beams, the NPSDs obtained presented distinct peaks at resonant frequencies and no relevant perturbations were observed. These results confirm the good performance of operational modal analysis for these conditions of testing. However, ambient vibration modal identification can be affected by eventual contaminations of the ambient random noise in the vicinity of the testing site making difficult the identification of the resonant frequency.

Simultaneously to the improvements on sampling, a new type of support system for EMM-ARM system was developed in order to increase the support stiffness and to simplify the beam positioning for testing. The new supports were made of steel and each pair was composed by a fixed support and a support that allows some rotation around an axis parallel to the longitudinal axis of the beam. These supports provide a stiffer base for the testing beams and the correct positioning becomes easier and faster. They also ensure higher tolerance of the system towards slight inaccuracies and misalignments between the supporting rods at the extremity of the specimen.

7.4 EXPERIMENTAL MODAL ANALYSIS

The use of operational modal analysis techniques assumes the excitation is a stationary Gaussian white noise stochastic process in the frequency range of interest. However, this condition cannot always be ensured, namely *in-situ* where heavy machinery may be operating in the vicinity of the EMM-ARM testing site, compromising the easy identification of the resonant frequencies. Therefore, experimental (input-output) modal analysis (EMA) with explicit known excitation of very low magnitude was applied to EMM-ARM in order to overcome this potential limitation.

The implementation of EMA to EMM-ARM required the implementation of an excitation device, or exciter, to impose the intended vibration to the testing beams. A proposed exciter was specifically developed for this purpose, and it was composed by a cooper wire coil with a cylindrical shaped permanent magnet inside it, without any physical contact. During the test, the magnet was kept vertically attached to the testing beam at mid span, an excitation signal was sent to the coil and both imposed signal and beam acceleration response were recorded. The resonant frequencies were then determined by identifying the peaks on the Frequency Response Functions (FRFs) obtained from the imposed and response signals. The feasibility of this approach was verified by applying EMA to a testing beam collected with the tubular metallic sampler developed previously in this work. The testing beam was sequentially evaluated with either forced or ambient vibrations during the duration of the experiment. This test occurred simultaneously with the classical EMM-ARM test of a second testing beam collected using the same sampler and procedure from a similar compacted layer. The Frequency Response Functions (FRFs) obtained with EMA revealed to be effective identifying the resonant frequencies. In fact, with EMA was possible to minimise some contaminations of the ambient noise occurred during the curing time, which were visible in the NPSDs obtained with classical EMM-ARM during some periods of time. A very good coherence was found when comparing the E-modulus results obtained from the beam tested by EMA with the results obtained from the beam tested with classical EMM-ARM and the results from UCC testing on reconstituted specimens of same mixture.

This new possibility of using forced vibration techniques is considered to be an important development to EMM-ARM technique. This new feature provides more robustness and accuracy to the methodology, gives more confidence to the results and allows to perform tests in environments which would be adverse to the classical EMM-ARM testing.

7.5 SYSTEMATIC APPLICATION OF EMM-ARM

An experimental program was conducted with aim to evaluate EMM-ARM performance on soil-cement mixtures prepared with different types of soils, including a uniform sand (S3), a sand (S4) and a granitic soil (GS). For the preparation of the mixtures were used

two types of Portland cement (CEM II/B-L 32.5 N and CEM I 52.5 N) and three different cement proportions (3%, 5% and 7%) for each soil.

EMM-ARM testing was started immediately after the sample preparation and interrupted at 7 days of age, due to limited availability of equipment for testing (data logger channels and accelerometers). At that age the data acquisition was stopped and the accelerometers were removed from the testing beams and used in subsequent specimens. When the originally tested specimens reached 28 days of age, the accelerometers were re-attached as to resume the testing of the beams and acquisition was continued at such instant. With this strategy it was possible to test 16 distinct beams simultaneously with a single set of 4 accelerometers. Even so, from the results obtained, it was possible to infer the kinetics occurred within the period without data (7 to 28 days). The coherence between EMM-ARM and unconfined cyclic compression results obtained confirms the possibility to interrupt the acceleration monitoring and accelerometer removal without compromising the results of EMM-ARM testing after reinstalling the accelerometers. This strategy can be very useful to obtain important information of the E-modulus evolution during the first days of age when the rate of stiffness evolution is higher, making available the monitoring equipment to be used with different specimens when the rate of the stiffness evolution is lower and then make discrete EMM-ARM tests to confirm the obtained values at reference ages.

It was observed that higher quantities of cement resulted on higher E-modulus values at 7 and 28 days and mixtures with CEM I 52.5 N cement developed higher E-modulus at 28 days than mixtures with CEM II/B-L 32.5 N. The mixtures of S4 soil with lower proportions of cement exhibit a peculiar behaviour in terms of E-modulus evolution. After the E-modulus increase rate observed during the first hours, E-modulus evolution became somewhat stagnant. A new increase on E-modulus was then observed after a period of at least 2 days. A possible explanation for this phenomenon may rely in the fact that small amounts of cement can form independent cores in the soil mass whilst high cement proportions can form interconnected cores in the soil mass. Initially, as the cement hydrates it fills the voids and does not constitute a solid skeleton with the surrounding particles. A new increase on E-modulus is only observed when the connexion between particles is assured. This phenomena is more evident for S4 soil as it has larger particles than S3 soil and is more uniform than GS soil. This question could

be explored in future works with the study of different soil-cement mixtures of uniform soils with different particle sizes.

EMM-ARM was further used to test a mixture of a silt soil with lime cured at temperatures of 20ºC, 30ºC and 40ºC. EMM-ARM results at the three tested temperatures revealed that this material exhibits two distinct phases in terms of E-modulus evolution that can be related to the different reactions involved during the curing. The first phase that starts immediately after compaction takes less time than the second phase and can be related to the formation of calcium aluminate hydrates. During the second phase the E-modulus increase may result from a structural rearrangement of the calcium aluminate hydrates formed during the first phase and from other substances released by pozzolanic reactions as calcium silicate hydrates.

With results obtained from EMM-ARM testing performed at different curing temperatures, and by applying Arrhenius based laws (e.g. the equivalent age principle), it was possible to compute the apparent activation energies of the reactions involved in the two phases of curing. For this purpose, a multiphase mathematical model was proposed to fit the experimental E-modulus curves obtained. By using this model, performing the decomposition on each of the contributions of each phase and applying a superposition method was the possible to estimate the apparent activation energy of each phase. The values obtained are considerably higher than the values found for other type of materials, as concrete, meaning the reactions involved are very sensitive to the curing temperature.

The results obtained show the potential of using EMM-ARM allied to the proposed methodology for activation energy estimation helping to understand the process of curing and to study the stiffness kinetics of complex materials as soil-lime mixtures.

7.6 STIFFNESS PREDICTION BASED ON EMM-ARM RESULTS

A methodology based on Bayesian inference was proposed to estimate the E-modulus of soil-cement mixtures at 28 days using the results obtained with the EMM-ARM since two days of curing. The main innovation of the proposed methodology is related to the combination of the EMM-ARM results obtained continuously with an analytical model of the cement hydration and a validated process of Bayesian statistics to quantifying the

uncertainties associated to predictions and thus providing a perception of the respective confidence level in it.

The initial prior distribution of the predictions is obtained from the EMM-ARM results available in the first two days of curing and by including some empirical knowledge. As new information is available from EMM-ARM testing, the initial distribution is updated in a subsequent distribution, the posterior distribution, through a mathematical procedure based on the Bayes' theorem. The update is dynamically repeated along the subsequent curing days resulting on a reduction of the uncertainty of the predictions and, therefore, an increase of the confidence of the predictions.

The performance of the proposed methodology was evaluated by applying it to the data obtained from two pairs of EMM-ARM testing beams performed with two sand-cement mixtures. For the first prior distributions, a considerably high variance was adopted. After the estimation of the posterior distributions the 95% confidence intervals were computed and compared to the actual results obtained from EMM-ARM results at 28 days of age. Despite a few cases where the inferred intervals do not actually envelope the experimental data, it is possible to state that the presented methodology was able to satisfactorily predict the E-modulus at reference ages based on results obtained at first days of age. In fact, with the availability of new data along the curing time, the predictions became more accurate and after some updates the actual E-modulus values at reference age of 28 days were estimated within a 95% confidence. Based on this, is possible to state that the analytical model was able to accurately predict the E-modulus evolution and the Bayesian model made a realistic management of the uncertainty associated to the model predictions.

The possibility of having a continuous feed of quantitative information regarding the stiffness of an *in situ* collected cement-stabilised soil associated to a reliable methodology to predict the stiffness at reference ages based on the information of the early ages can have special interest for constructions in progress. This valuable information allows owners, contractors and quality control services to make fundamental decisions about the best construction strategies (e.g., rejection of a layer or continuing construction), which may have strong economic benefits.

7.7 FUTURE WORKS AND RECOMMENDATIONS

During the present thesis EMM-ARM was object of several modifications and improvements allowing its application in different conditions of testing. Based on this experience are here presented some recommendations and suggestions for possible future applications of the methodology.

EMM-ARM can be extremely useful for laboratory studies of the E-modulus evolution and hydration kinetics of curing materials. Its application could be extended to different types of mixtures that have not been studied yet with this methodology, including other different types of soils and different treatment agents. Those could also comprise the study of the effect of the curing conditions, as temperature and water content, and combinations of different treatment agents (binders and other additives). The effect of the soil properties, as the particle size, on the kinetics of curing could also be subject of study with EMM-ARM.

It could be very interesting and useful to use EMM-ARM as a quality-control tool in *in-situ* environment. In fact, EMM-ARM can provide important information in real-time concerning the development of the mechanical properties of stabilized materials. The possibility of having a continuous feed of quantitative information regarding the stiffness of an *in-situ* collected cement-stabilised soil opens up interesting opportunities for the anticipated prediction of the achievable stiffness over time. Thus, as a complement of the developments presented in this thesis regarding the collection of intact samples, it is here proposed that pilot experiments actually take place in the field as to assess feasibility and usability of results. Additionally, the application of the prediction methodology based Bayesian inference proposed in this thesis to EMM-ARM data obtained in real-time in a construction site can be a powerful tool to estimate the E-modulus at reference ages and so assist the decision-making since the early ages of the stabilized materials. This valuable information allows owners, contractors and quality control services to make and anticipate fundamental decisions about the best construction strategies (e.g., rejection of a layer or continuing construction), which may have strong economic, logistic, and environmental benefits.

Another important subject is the evaluation of the performance of EMM-ARM tests in a construction site where heavy equipment is running and generating contaminations of the ambient noise. In these conditions is recommended the application of EMM-ARM

variant that uses the experimental modal analysis (forced vibration) instead the operational modal analysis (ambient vibration).

As it is well known and has also been showed in this thesis the temperature strongly affects the kinetics of curing. Therefore, for the cases when EMM-ARM is used to monitor the E-modulus evolution of stabilized layers it is important to take in to account the *in-situ* temperature history. This can be done by perform EMM-ARM testing at one reference temperature, monitoring the actual i*n-situ* temperature and adjusting EMM-ARM results based on the apparent activation energy. Alternatively, EMM-ARM tests can be performed inside a climatic chamber were are imposed the same temperature history observed *in-situ*.

References

AASHTO (1993). *Guide for Design of Pavement Structures*, American Association of State Highway and Transportation Officials.

AASHTO (1994). TP 46 Standard test method for determining the resilient modulus of soils and aggregate materials.

Abu-Farsakh, M. Y., Alshibli, K., Nazzal, M. & Seyman, E. (2004). Assessment of in-situ test technology for construction control of base courses and embankments Baton Rouge, LA: Louisiana Transportation Research Center.

AFNOR (1992). NF P 94-057 Sols : Reconnaissance et essais - Analyse granulométrique des sols - Méthode par sédimentation.: Association Française de Normalisation.

AFNOR (1993). NF P 94-051 - Determination des Limites d'Atterberg. Association Française de Normalisation.

AFNOR (1996). NF P 94-056 Sols: Reconnaissance et essais - Analyse granulométrique - Méthode par tamisage à sec après lavage.: Association Française de Normalisation.

AFNOR (1999). NF P 94-093 - Sols: Reconnaissance et essais - Détermination des références de compactage d'un matériau - Essai Proctor Normal - Essai Proctor modifié. Association Française de Normalisation.

Ahmed, A. & Issa, U. H. (2014). Stability of soft clay soil stabilised with recycled gypsum in a wet environment. *Soils and Foundations* **54**, No. 3, 405-416.

Ajorloo, A., Mroueh, H. & Lancelot, L. (2012). Experimental Investigation of Cement Treated Sand Behavior Under Triaxial Test. *Geotechnical and Geological Engineering* **30**, No. 1, 129-143.

Al-Mukhtar, M., Khattab, S. & Alcover, J.-F. (2012). Microstructure and geotechnical properties of lime-treated expansive clayey soil. *Engineering Geology* **139–140**, No. 0, 17-27.

Al-Mukhtar, M., Lasledj, A. & Alcover, J.-F. (2010). Behaviour and mineralogy changes in lime-treated expansive soil at 20°C. *Applied Clay Science* **50**, No. 2, 191-198.

Alshibli, K. A., Abu-Farsakh, M. & Seyman, E. (2005). Laboratory Evaluation of the Geogauge and Light Falling Weight Deflectometer as Construction Control Tools. *Journal of Materials in Civil Engineering, ASCE* **17**, No. 5, 560-569.

Amaral, M. F. (2009). Dynamic shear modulus evaluation in soil-cement mixtures using time domain ultrasonic impulses and recording the resonant frequencies with Fourier spectral analysis. (in Portuguese) M.Sc. Thesis. Porto: University of Porto, Portugal.

Amaral, M. F., Viana da Fonseca, A., Arroyo, M., Cascante, G. & Carvalho, J. (2011). Compression and shear wave propagation in cemented-sand. *Géotechnique Letters* **1**, No. 3, 79-84.

Arroyo, M., Muir Wood, D., Greening, P., Medina, L. & Rio, J. (2006). Effects of sample size on bender-based axial G0 measurements. *Géotechnique* **56**, No. 1, 39-52.

Arroyo, M., Wood, D. M. & Greening, P. (2003). Source near-field effects and pulse tests in soil samples. *Géotechnique* **53**, No. 3, 337-345.

ASTM (1991). Standard Test Method for Pulse Velocity Through Concrete. C597. *Annual Book of ASTM Standards.* ASTM International.

ASTM (2002). C192/C 192M, Standard Practice for Making and Curing Concrete Test Specimens in the Laboratory.

ASTM (2008). D1587, Standard Practice for Thin-Walled Tube Sampling of Soils for Geotechnical Purposes. ASTM International.

ASTM (2009). ASTM D6913 - 04 - Standard Test Methods for Particle-Size Distribution (Gradation) of Soils Using Sieve Analysis. West Conshohocken, PA: ASTM International.

Atkinson, J. H. (2000). Non-linear soil stiffness in routine design. *Géotechnique* **50**, No. 5, 487-508.

Atkinson, J. H. & Sallfors, G. Experimental determination of soil properties. *10th European Conference on Soil Mechanics and Foundation Engineering, Firenze* 3, 915-956.

Azenha, M. (2009). Numerical simulation of the structural behaviour of concrete since its early ages, Ph.D. Thesis. Porto: Faculty of Engineering of the University of Porto.

Azenha, M., Faria, R., Magalhães, F., Ramos, L. & Cunha, Á. (2012a). Measurement of the E-modulus of cement pastes and mortars since casting, using a vibration based technique. *Materials and Structures* **45**, No. 1, 81-92.

Azenha, M., Ferreira, C., Silva, J., Correia, A. G., Aguilar, R. & Ramos, L. (2011). Continuous stiffness monitoring of cemented sand through resonant frequency. *American Society of Civil Engineeres - Geotechnical Special Publication: Emerging Technologies for Material, Design, Rehabilitation, and Inspection of Road-way Pavements* **GSP**, No. 218, 174-183.

Azenha, M., Magalhães, F., Faria, R., Ramos, L. & Cunha, Á. (2010). Mesurement of concrete E-modulus evolution since casting: A novel method based on ambient vibration. *Cement and Concret Research* **40**, No. 7, 1096-1105.

Azenha, M., Ramos, L. F., Aguilar, R. & Granja, J. L. (2012b). Continuous monitoring of concrete E-modulus since casting based on modal identification: A case study for in situ application. *Cement and Concrete Composites* **34**, No. 7, 881-890.

Baligh, M. M., Azzouz, A. S. & Chin, C. T. (1987). Disturbances due to "ideal" tube sampling. *Journal of geotechnical engineering* **113**, No. 7, 739-757.

Bartlett, S. & Farnsworth, C. (2002). Performance of Lime Cement-Stabilized Soils for the I-15 Reconstruction Project: Salt Lake City, Utah. *Transportation Research Record: Journal of the Transportation Research Board* **1808**, No. 1, 58-66.

Bažant, Z. Probabilistic analysis of creep effects in concrete structures. *4th International Conference on Structural Safety and Reliability, Kobe, Japan* 1, 331-344.

Beaty, K. S., Schmitt, D. R. & Sacchi, M. (2002). Simulated annealing inversion of multimode Rayleigh wave dispersion curves for geological structure. *Geophysical Journal International* **151**, No. 2, 622-631.

Bell, F. G. (1996). Lime stabilization of clay minerals and soils. *Engineering Geology* **42**, No. 4, 223-237.

Bell, F. G. (2004). *Engineering Geology and Construction*, London, UK, Spon Press.

Bendat, J. & Piersol, A. (1980). *Engineering Applications of Correlation and Spectral Analysis*, John Wiley & Sons, USA.

Benedetto, A., Tosti, F. & Di Domenico, L. (2012). Elliptic model for prediction of deflections induced by a Light Falling Weight Deflectometer. *Journal of Terramechanics* **49**, No. 1, 1-12.

Benz, T. (2007). *Small-Strain Stiffness of Soils and its Numerical Consequences.* PhD, Universitat Stuttgart.

Biarez, A., Gomes Correia, A. & Lopez-Caballero, F. From very small strains to failure. *Deformation Characteristics of Geomaterials, London*, 125-141.

Box, G. E. & Tiao, G. C. (2011). *Bayesian inference in statistical analysis*, John Wiley & Sons.

Briaud, J.-L. (2013). *Geotechnical Engineering: Unsaturated and Saturated Soils*, New Jersey, USA, y John Wiley & Sons, Inc.

Brincker, R., Ventura, C. & Andersen, P. (2001). Damping Estimation by Frequency Domain Decomposition. *IMAC XIX*. Kissimmee, USA.

Brooks, S., Gelman, A., Jones, G. & Meng, X.-L. (2011). *Handbook of Markov Chain Monte Carlo*, CRC press.

Burland, J. B. Contribution to discussion on session 4. *7th European Conference on Soil Mechanics, Brighton* 4, 137.

Burland, J. B. (1989). Small is Beautiful: The Stiffness of Soils at Small Strains. *Canadian Geotechnical Journal* **26**, No. 4, 499-516.

Butler, K. E. & Russell, R. D. (2003). Cancellation of multiple harmonic noise series in geophysical records. *Geophysics* **68**, No. 3, 1083-1090.

Caetano, E. (1992). Identificação experimental de parâmetros dinâmicos em sistemas estruturais, MSc. Porto: Faculdade de Engenharia da Universidade do Porto.

Caetano, E. (2000). *Dynamic of Cable-stayed Bridges: Experimental Assessment of Cable-Structure Interaction.* Tese de doutoramento, Faculdade de Engenharia da Universidade do Porto.

Camacho-Tauta, J. F. (2011). *Evaluation of the small-strain stiffness of soil by non-conventional dynamic testing methods.* PhD thesis, Universidade Técnica de Lisboa: Instituto Superior Técnico.

CEN (2005). EN 197-1:2000, Cement - Part 1: Composition, specifications and conformity criteria for common cements.

CEN (2010a). EN 459-1 - Building lime - Part 1: Definitions, specifications and conformity criteria.

CEN (2010b). EN 1992-1-1 Eurocode 2 - Design of Concrete. Structures - Part 1: General rules and rules for buildings.

Chitambira, B., Al-Tabbaa, A., Perera, A. S. R. & Yu, X. D. (2007). The activation energy of stabilised/solidified contaminated soils. *Journal of Hazardous Materials* **141**, No. 2, 422-429.

Chopra, A. K. (1995). *Dynamics of Structures: Theory and Application to Earthquake Engeneering*, New Jersey, Electronic Publishing Services, Inc.

Christ, M. & Park, J.-B. (2009). Ultrasonic technique as tool for determining physical and mechanical properties of frozen soils. *Cold Regions Science and Technology* **58**, No. 3, 136-142.

Clayton, C., Siddique, A. & Hopper, R. J. (1998). Effects of sampler design on tube sampling disturbance-numerical and analytical investigations. *Geotechnique* **48**, No. 6, 847-867.

Clayton, C. R. I. (2011). Stiffness at small strain: research and practice. *Geotechnique* **61**, No. 1, 5-37.

Clayton, C. R. I., Matthews, M. C. & Simons, N. E. (1995). *Site Investigation*, Oxford, England, Blackwell Science.

Clayton, C. R. I., Priest, J. A. & Rees, E. V. L. (2010). The effects of hydrate cement on the stiffness of some sands. *Géotechnique* **60**, No. 6, 435–445.

Clough, R. W. & Penzien, J. (2003). *Dynamics of Structures, 3rd Edition*, Berkley, USA, Computers & Structures, Inc.

Cooley, J. W. & Tukey, J. W. (1965). An Algorithm for the Machine Calculation of Complex Fourier Series. *Mathematics of Computation* **19**, No. 90, 297-301.

Correia, A. (2011). *Applicability of deep mixing technique to the soft soil of Baixo Mondego (in portuguese).* PhD, Faculdade de Ciências e Tecnologia da Universidade de Coimbra.

Correia, G. (1985). Contribuition à l'Étude Mécanique des Sols Soumis à des Chargements Cycliques. Thèse de Docteur-Ingénieur en Génie Civil. Paris: École National des Ponts et Chaussées.

Cristelo, N. M. & Jalali, S. (2007). *Estabilização de solos com cal,* Guimarães, Universidade do Minho.

Cruden, D. & Fell, R. (1997). *Land slide risk assessment,* Rotterdam, Balkema.

Cruz, M. d. L. & Jalali, S. (2006). Melhoramento do desempenho de misturas solo-cimento com recurso a activadores de baixo custo. SPG.

Cunha, A. (1990). *Dinâmica Estrutural Estocástica; Aplicações à Engenharia Sísmica, Tese de doutoramento.* Faculdade de Engenharia da Universidade do Porto.

Dano, C., Hicher, P. Y. & Tailliez, S. (2004). Engineering Properties of Grouted Sands. *Journal of Geotechnical and Geoenvironmental Engineering* **130**, No. 3, 328-338.

De Bel, R., Gomes Correia, A., Duvigneaud, P.-H., Francois, B., Herrier, G. & Verbrugge, J.-C. (2013). Long-term mechanical and physico-chemical evolution of silty soil treated with lime. *Colloque TerDOUEST 2013.* Marne-la-Vallée.

De Bel, R., Verbrugge, J.-C. & Gomes Correia, A. (2010). Geomechanical behavior of soils treated with lime. Main contributions of the project COGESTAC. *XII Congresso Nacional de Geotecnia.* Guimarães, Portugal.

DeJong, J. T., Mortensen, B. M., Martinez, B. C. & Nelson, D. C. (2010). Bio-mediated soil improvement. *Ecological Engineering* **36**, No. 2, 197-210.

Dimter, S., Rukavina, T. & Barišić, I. (2011). Application of the ultrasonic method in evaluation of properties of stabilized mixes. *Baltic Journal of Road and Bridge Engineering* **6**, No. 3, 177-184

Ditlevsen, O. & Madsen, H. (1996). *Structural reliability methods,* New York, John Wiley & Sons.

Dupas, J. & Pecker, A. (1979). Static and dynamic properties of sand-cement. *Journal of the Geotechnical Engineering Division* **105**, No. 3, 419-436.

Dyvik, R. & Madshus, C. (1985). Lab measurements of Gmax using bender element. *ASCE Convention on Advances in the Art of Testing Soils under Cyclic Conditions.*

Einstein, H. Land slide risk assessment procedure. *Proceedings of the fifth international symposium on land slides, Lausanne*.

Einstein, H., Indermitte, C., Sinfield, J., Descoeudres, F. & Dudt, J. (1999). The decision aids for tunnelling. *Transp Res Record* **1656**, No. 6–13.

F.G.Bell (2005). *Engineering Treatment of Soils,* E & FN Spon - Taylor & Francis Group.

Fam, M. & Santamarina, C. (1995). Study of geoprocesses with complementary mechanical and electromagnetic wave measurements in an oedometer. *Geotechnical Testing Journal, ASTM.* **18**, No. 3, 307-314.

Fernandes, J., Bittencourt, T. & Helene, P. (2011). Concrete subjected to vibrations in early-ages Ibracon structures and materials. *Ibracon structures and materials* **4**, No. 4, 592-609.

Ferreira, C. (2009). The use of seismic wave velocities in the measurement of stiffness of a residual soil. Ph.D. Thesis. Porto: Faculty of Engineering of the University of Porto.

Ferreira, C., Martins, J. P. & Correia, A. G. Determination of the small-strain stiffness of hard soils by means of bender elements and accelerometers. *15th European Conference on Soil Mechanics and Geotechnical Engineering, Athens*, 179-184.

Freiesleben Hansen, P. & Pedersen, J. (1977). Maturity Computer for Controlled Curing and Hardening of Concrete. *Nordisk Betong* **1**, No. 19-34.

GDSInstruments. (2009). *Bender elements datasheet* [Online]. Available: http://www.gdsinstruments.com/products/gdsbes.htm [Accessed August 2012].

Gelman, A., Carlin, J., Stern, H. & Rubin, D. (2004). *Bayesian data analysis*, Chapman & Hall/CRC.

Geoffroy, J.-M. (2004). *Résultats et recommandations du projet national Calibé - La maîtrise de la qualité du béton,* Paris, Presses des Ponts et Chaussées.

Gomes Correia, A. (2004). Soil stifness interesting the serviceability of structures (in Portuguese). *Geotecnia* **100**, No. 103-122.

Gomes Correia, A., Antão, A. & Gambin, M. (2004). Using non linear constitutive law to compare Menard PMT and PLT E-moduli. *In International Conference on Site Characterization (ISC'2), Porto*, 927-933.

Gomes Correia, A., Martins, J., Caldeira, L., Maranha das Neves, E. & Delgado, J. Comparison of in situ performance-based tests methods to evaluate moduli of railway embankments. Bearing Capacity of Roads, Railways and Airfields. *8th International Conference (BCR2A'09), Unversity of Illinois, Champaign, Illinois, USA* 1, 1331-1340.

Gomes Correia, A., Reis Ferreira, S. M. & Faria Araújo, N. (2006). Precision triaxial tests to determine deformability characteristics *In:* Geotechnics, N. C. o. (ed.) *Congresso Nacional de Geotecnia 10.* Lisbon, Portugal.

Gomes Correia, A., Valente, T., Tinoco, J., Falcão, J., Barata, J., Cebola, D. & Coelho, S. (2009). Evaluation of mechanical properties of jet-grouting columns using different test methods. *The academia and practice of Geotechnical Engineering : proceedings of the 17th International Conference on Soil Mechanics and Geotechnical Engineering, Alexandria, Egypt*, 2169-2171.

Goto, S., Tatsuoka, F., Shibuya, S., Kim, Y. & Sato, T. (1991). A simple gauge for local small strain measurements in the laboratory. *Soils and Foundations* **31**, No. 1, 169-180.

Granja, J., Azenha, M., Carvalho, J. & Carvalho, N. (2014). Monitorização contínua das propriedades mecânicas do betão nas primeiras idades para apoio ao faseamento construtivo. *5as Jornadas Portuguesas de Engenharia de Estruturas.* Lisboa.

Hallam, J. R. & Northmore, K. J. (1993). *Engineering Geology of Tropical Red Clay Soils: Geotechnical borehole sampling of Tropical Red Clay soil*, Keyworth, Nottingham, Keyworth, Nottingham.

Hight, D. W. & Burland, J. B. (1990). Review of soil sampling and laboratory testing for the Science and Engineering Research Council. *Summary Report.* Swindon, England: SERC.

Highways-England (2015). Design Manual for Roads and Bridges - Pavement Design and Maintenance. Highways England.

Hong, S. & Park, S.-K. (2015). Effect of vehicle-induced vibrations on early-age concrete during bridge widening. *Construction and Building Materials* **77**, No. 179-86.

Hopper, R. J. (1992). *The effects and implications of sampling clay soils.* PhD thesis, University of Surrey.

Hossain, K. M. A., Lachemi, M. & Easa, S. (2007). Stabilized soils for construction applications incorporating natural resources of Papua new Guinea. *Resources, Conservation and Recycling* **51**, No. 4, 711-731.

Hvorslev, M. J. (1949). Subsurface Exploration and Sapling of Soils for Civil Engineering Purposes. *Waterways Experimental Station, Vicksburg, USA.*

Ingles, O. G. & Metcalf, J. B. (1972). *Soil stabilization - principles and practice*, Sydney, Australia, Butterworths.

Jackson, N. M., Mark, R., Schlutz, S. & Malek, M. (2007). Pavement subgrade stabilization and construction using bed and fly ash. *World of coal ash.* Kovington, Kentucky, USA: University of Kentucky Center for Applied Energy Research and American Coal Ash Association.

Jardine, R. J., Symes, M. J. & Burland, J. B. (1984). The Measurement of soil stiffness in the triaxial apparatus. *Géotechnique* **34**, No. 3, 323 –340.

Jauberthie, R., Rendell, F., Rangeard, D. & Molez, L. (2010). Stabilisation of estuarine silt with lime and/or cement. *Applied Clay Science* **50**, No. 3, 395-400.

Kang, X., Kang, G. & Ge, L. (2013). Modified Time of Setting Test for Fly Ash Paste and Fly Ash–Soil Mixtures. *Journal of Materials in Civil Engineering* **25**, No. 2, 296–301.

Karam, J. (2005). *Decision aids for tunnel exploration.* MSthesis.

Khan, Z., Majid, A., Cascante, G., Hutchinson, D. J. & Pezeshkpour, P. (2006). Characterization of a cemented sand with the pulse-velocity method. *Canadian Geotechnical Journal* **43**, No. 3, 294-309.

Kolias, S., Kasselouri-Rigopoulou, V. & Karahalios, A. (2005). Stabilisation of clayey soils with high calcium fly ash and cement. *Cement & Concrete Composites* **27**, No. 2, 301-313.

Ladd, C. C. & DeGroot, D. J. Recommended practice for soft ground site characterization: Arthur Casagrande lecture. *12th Panamerican Conference on Soil Mechanics and Geotechnical Engineering, Boston*, 3-57.

LCPC-SETRA (2000). *Réalisation de remblais et des couches de forme*, Laboratoire Central des Ponts et Chaussées-Service d'Etudes Techniques des Routes et Autoroutes.

Lemaire, K., Deneele, D., Bonnet, S. & Legret, M. (2013). Effects of lime and cement treatment on the physicochemical, microstructural and mechanical characteristics of a plastic silt. *Engineering Geology* **166**, No. 0, 255-261.

Little, D. N. & Nair, S. (2009). Recommended Practice for Stabilization of Subgrade Soils and Base Materials. *NCHRP Project 20-07.* National Cooperative Highway Research Program.

Liu, J., Shi, B., Jiang, H., Bae, S. & Huang, H. (2009). Improvement of water-stability of clay aggregates admixed with aqueous polymer soil stabilizers. *CATENA* **77**, No. 3, 175-179.

LNEC (1966a). E 196-1966 Grain size testing (in Portuguese). Lisbon: Laboratório Nacional de Engenharia Civil.

LNEC (1966b). E 197 -1966 Soils. Compaction testing (in Portuguese). Lisbon: Laboratório Nacional de Engenharia Civil.

LNEC (1972a). E 262-1972. Soil-Cement, Compaction testing (in Portuguese). Lisbon: Laboratório Nacional de Engenharia Civil.

LNEC (1972b). E 264-1972. Soil-Cement, Compression testing (in Portuguese).

Love, A. E. H. (1892). *Mathematical Theory of Elasticity, Cambridge Univeristy*.

Love, A. E. H. (1927). *A treatise on the mathematical theory of elasticity,* Cambridge, Cambridge University Press.

Magalhães, F. (2004). *Stochastic modal identification for experimental validation of numerical models. MSc (in Portuguese).* MSc, Faculdade de Engenharia da Universidade do Porto.

Maia, N. & Silva, J. (1997). Theoretical and Experimental Modal Analysis. *Research Studies Press Ltd*, No.

Mair, R. J. Developments in geotechnical engineering research: applications to tunnels and deep excavations. *Institution of Civil Engineers, Civil Engineering, Unwin Memorial Lecture 1992.*, 27-41.

Marcunson III, W. F. & Franklin, A. G. (1979). State-of-the-art of undisturbed sampling of cohesionless sands. *International Symposium on Soil Sampling.* Singapore.

Marcuson III, W. F. & Franklin, A. G. (1979). State of the art of undisturbed sampling cohesionless soils. Vicksburg: Geotechinical Laboratory - U. S. Army Engineer Waterways Experiment Station.

Mayne, P. W., Christopher, B. R. & DeJong, J. (2002). Subsurface Investigations - Geotechnical Site Characterization. Washington, D.C.: National Highway Institute - Federal Highway Administration - U.S. Department of Transportation.

McKay, M. D., Beckman, R. J. & Conover, W. J. (1979). A comparison of three methods for selecting values of input variables in the analysis of output from a computer code. *Technometrics* **21**, No. 2, 239-245.

Meyers, M. A. & Chawla, K. K. (2008). Mechanical Behavior of Materials. *New York, Cambridge University Press*, No.

Miller, G. A. & Azad, S. (2000). Influence of soil type on stabilization with cement kiln dust. *Construction and Building Materials* **14**, No. 2, 89-97.

Millogo, Y., Hajjaji, M. & Ouedraogo, R. (2008). Microstructure and physical properties of lime-clayey adobe bricks. *Construction and Building Materials* **22**, No. 12, 2386-2392.

Min, S., Einstein, H. & Lee, J. (2005). Application of the decision aids for tunnelling (DAT) to update excavation cost/time information

335–46. *KSCEJ Civ Eng* **9**, No. 4.

Miranda, T., Gomes Correia, A. & Ribeiro e Sousa, L. (2009). Bayesian methodology for updating geomechanical parameters and uncertainty quantification. *International Journal of Rock Mechanics and Mining Sciences* **46**, No. 7, 1144-1153.

Murthy, V. N. S. (2002). *Geotechnical Engineering: Principles and Practices of Soil Mechanics and Foundation Engineering*, New York, USA, CRC Press.

Nagaraj, T. S. (1993). *Principles of Testing Soils, Rocks and Concrete*, Elsevier.

NLA (2004). Lime Treated Soil Construction Manual - Lime Stabilization and Lime Modification, Bulletin 326. National Lime Association.

Okyay, U. S. & Dias, D. (2010). Use of lime and cement treated soils as pile supported load transfer platform. *Engineering Geology* **114**, No. 1–2, 34-44.

Pallara, O., Mattone, M. & Lo Presti, D. (2008). Bender Elements: Bad Source – Good Receiver. *Atlanta 4th International Symposium on Deformation Characteristics of Geomaterials* **2**, No. 697-702.

Petry, T. M. & Little, D. N. (2002). Review of Stabilization of Clays and Expansive Soils in Pavements and Lightly Loaded Structures—History, Practice, and Future. *Journal of Materials in Civil Engineering* **14**, No. 6, 447.

Poceq. (2013). *Ultrasonic Pulse Velocity - Pundit Lab* [Online]. Available: http://www.proceq.com/en/non-destructive-test-equipment/concrete-testing/ultrasonic-pulse-velocity/pundit-lab.html?pqr=17 [Accessed May 2013].

Presti, D. C. F. L., Jamiolkowski, M., Pallara, O. & Cavallaro, A. (1996). Rate and creep effect on the stiffness of soils. *In:* Sheahan, T. C. & Kaliakin, V. N. (eds.) *Measuring and Modeling Time Dependent Soil Behavior.* ASCE.

Puppala, A. J. (2008). Estimating Stiffness of Subgrade and Unbound Materials for Pavement Design. *In:* Board, T. R. (ed.) *NCHRP Synthesis 382.* Washington, D.C.: National Cooperative Highway Research Program.

Rajasekaran, G. (2005). Sulphate attack and ettringite formation in the lime and cement stabilized marine clays. *Ocean Engineering* **32**, No. 8–9, 1133-1159.

Ramos, L. (2007). *Damage identification on masonry structures based on vibration signatures.* Tese de doutoramento, Universidade do Minho.

Rao, S. M. & Shivananda, P. (2005). Role of curing temperature in progress of lime-soil reactions. *Geotechnical and Geological Engineering* **23**, No. 1, 79-85.

Rayleigh, L. (1885). On waves propagated along the plane surface of an elastic solid. *Proceedings of the London Mathematical Society* **17**, No. 4-11.

Reinhardt, H. W. & Grosse, C. U. (2004). Continuous monitoring of setting and hardening of mortar and concrete. *Construction and Building Materials* **18**, No. 145-154.

Reis Ferreira, S. (2003). Influência da não saturação e da granulometria nas características de deformabilidade de um Agregado Granítico, Tese de Mestrado. Instituto Superior Técnico.

Ren, W.-X. & Zong, Z.-H. (2004). Output-only modal parameter identification of civil engineering structures. *Structural Engineering and Mechanics* **17**, No. 3-4, 1-16.

RILEM, T. C. (2011). Recommendation of RILEM TC 218-SFC: Sonic methods for quality control of fresh cementitious materials. *Materials and Structures* **44**, No. 1047–1062.

Rios Silva, S., Viana da Fonseca, A. & Consoli, N. Strenght and stiffness properties of mixtures of granitic soil-cement. *17th International Conference on Soil Mechanics and Geotechnical Engineering - The Academia & Practice of Geotechnical Engineering, Alexandria, Egypt* 1, 2, 3 and 4, 312-315.

Rodrigues, J. (2004). *Stochastic Modal Identification: Analysis Methods and Applications in Civil Engineering Structures (PhD Thesis, in Portuguese).* Tese de doutoramento, Faculdade de Engenharia da Universidade do Porto.

Rogers, J. D. (2006). Subsurface Exploration Using the Standard Penetration Test and the Cone Penetrometer Test. *Environmental & Engineering Geoscience* **XII**, No. 2, 161-179.

Rostásy, F., Gutsch, A. & Krauß, M. (2001). *Computation of stresses and cracking criteria for early age concrete - Methods of iBMB.*

Santos, J. (2008). *Geotechnical works: Compaction (in Portuguese)*, Lisbon, Instituto Superior Técnico - Departamento de Engenharia Civil e Arquitetura.

Sariosseiri, F. & Muhunthan, B. (2009). Effect of cement treatment on geotechnical properties of some Washington State soils. *Engineering Geology* **104**, No. 1–2, 119-125.

Schindler, A. K. & Folliard, K. J. (2005). Heat of hydration models for cementitious materials. *ACI Materials Journal* **101**, No. 1, 24-33.

SETRA-LCPC (2004). Traitement des sols à la chaux et/ou aux liants hydrauliques (GTS) - Application à la réalisation des remblais et des couches de forme - Guide technique. Service d'Etudes Techniques des Routes et Autoroutes - Laboratoire Central des Ponts et Chaussées.

Siddique, A., Ameen, S. F. & Islam, M. J. (2009). A comparative study on engineering properties of "Block" and "Tube" samples of a soft clay *Journal of Civil Engineering* **37**, No. 1, 11-30.

Silva, J. (2010). Contribution to the study of the treatment of soils: Evaluation of deformability (in Portuguese). M.Sc. Thesis. Guimarães: Universidade do Minho.

Silva, J., Azenha, M., Correia, A. G. & Ferreira, C. (2013). Continuous stiffness assessment of cement-stabilised soils from early age. *Géotechnique* **63**, No. 16, 1419-1432.

Silva, J., Azenha, M., Gomes Correia, A. & Granja, J. (2014). Continuous monitoring of sand–cement stiffness starting from layer compaction with a resonant frequency-based method: Issues on mould geometry and sampling. *Soils and Foundations* **54**, No. 1, 56-66.

Skempton, A. W. & Sowa, V. A. (1963). The behaviour of saturated clays during sampling and testing. *Géotechnique* **13**, No. 4, 269-290.

Steinbrecher, G. & Shaw, W. T. (2008). Quantile mechanics. *European Journal of Applied Mathematics* **19**, No. 2, 87-112.

Stephenson, R. W. (1978). Ultrasonic testing for determining dynamic soil moduli. *ASTM STP 654, American Society for Testing and Materials*, No. 179–195.

Stokoe, K. H. & Santamarina, J. C. (2000). Seismic-Wave-Based Testing in Geotechnical Engineering. *GeoEng 2000 Conference.* Melbourne, Australia.

Tingle, J. & Santoni, R. (2003). Stabilization of Clay Soils with Nontraditional Additives. *Transportation Research Record: Journal of the Transportation Research Board* **1819**, No. 72-84.

Toohey, N. M. & Mooney, M. A. (2012). Seismic modulus growth of lime-stabilized soil during curing. *Géotechnique* **62**, No. 2, 161-170.

Van Overschee, P. & De Moor, B. Subspace Algorithms for the Stochastic Identification Problem. *Proceedings of the 30th Conference on Decision and Control, Brighthon, England*.

Venkatarama-Reddy, B. V. & Latha, M. S. (2014). Retrieving clay minerals from stabilised soil compacts. *Applied Clay Science* **101**, No. 1, 362-368.

Verbrugge, J. C., De Bel, R., Correia, A. G., Duvigneaud, P. H. & Herrier, G. (2011). Strength and micro observations on a lime treated silty soil. *ASCE-Geotechnical Special Publication* **GSP**, No. 223, 89-96.

Viana da Fonseca, A., Cruz, R. & Consoli, N. (2009a). Strength Properties of Sandy Soil-Cement Admixtures. *Geotechnical and Geological Engineering* **27**, No. 6, 681-686.

Viana da Fonseca, A., Cruz, R. & Consoli, N. (2009b). Strength Properties of Sandy Soil–Cement Admixtures. *Geotechnical and Geological Engineering* **27**, No. 6, 681-686.

Viana da Fonseca, A., Ferreira, C. & Fahey, M. (2009c). A Framework interpreting bender element tests combining time-domain and frequency-domain methods. *Geotechnical Testing Journal, ASTM.* **32**, No. 2, 1-17.

Viggiani, G. & Atkinson, J. H. (1995). Interpretation of bender element tests. *Géotechnique* **45, No. 2**, No. 149-154.

Voigt, T., Sun, Z. & Shah, S. P. (2006). Comparison of ultrasonic wave reflection method and maturity method in evaluating early-age compressive strength of mortar. *Cement and Concrete Composites* **28**, No. 4, 307-316.

Wang, X. & Subramaniam, K. V. (2011). Ultrasonic monitoring of capillary porosity and elastic properties in hydrating cement paste. *Cement and Concrete Composites* **33**, No. 3, 389-401.

Weiss, J. & Berke, N. (2002). Shrinkage Reducing Admixtures. *Early Age Cracking in Cementitious Systems, Report of RILEM Technical Committee TC 181-EAS.*

Welch, P. (1967). The use of fast Fourier transform for the estimation of power spectra: A method based on time averaging over short modified periodograms. *IEEE Transaction on Audio and Electro-Acoustics* **15**, No. 2, 70-73.

Yang, I. H. (2007). Prediction of time-dependent effects in concrete structures using early measurement data. *Engineering Structures* **29**, No. 10, 2701-2710.

Yesiller, N., Hanson, J. L., Rener, A. T. & Usmen, M. A. (2001). Ultrasonic testing for evaluation of stabilized mixtures. *Transportation Research Record* **1757**, No. 1, 32-42.

Yuan, D. & Nazarian, S. (1993). Rapid determination of layer properties from surface wave method. *Transportation Research Record: Journal of the Transportation Research Board* **1377**, No. 1, 159-166.

Appendix

APPENDIX

Figure A.0.1, Figure A.0.2, Figure A.0.3 and Figure A.0.4: 95% probability intervals obtained at each selected date for specimens T2, S1, S2 and pair S1/S2, respectively.

Table 0.1, Table 0.2, Table 0.3, and Table 0.4: Limits of the estimated intervals containing 95% of the values of each distribution estimated for 28 days of age, together with the amplitude of the interval, the computed mean ($\overline{E''_{28}}$), the standard deviation (s''_{28}) and the actual E-modulus values obtained with EMM-ARM at age of 28 days, for specimens T2, S1, S2 and pair S1/S2, respectively.

Figure A.0.5: Probability density functions at 28 days of age, the respective mean and standard deviation, predicted with data since 2 to 7 days of curing.

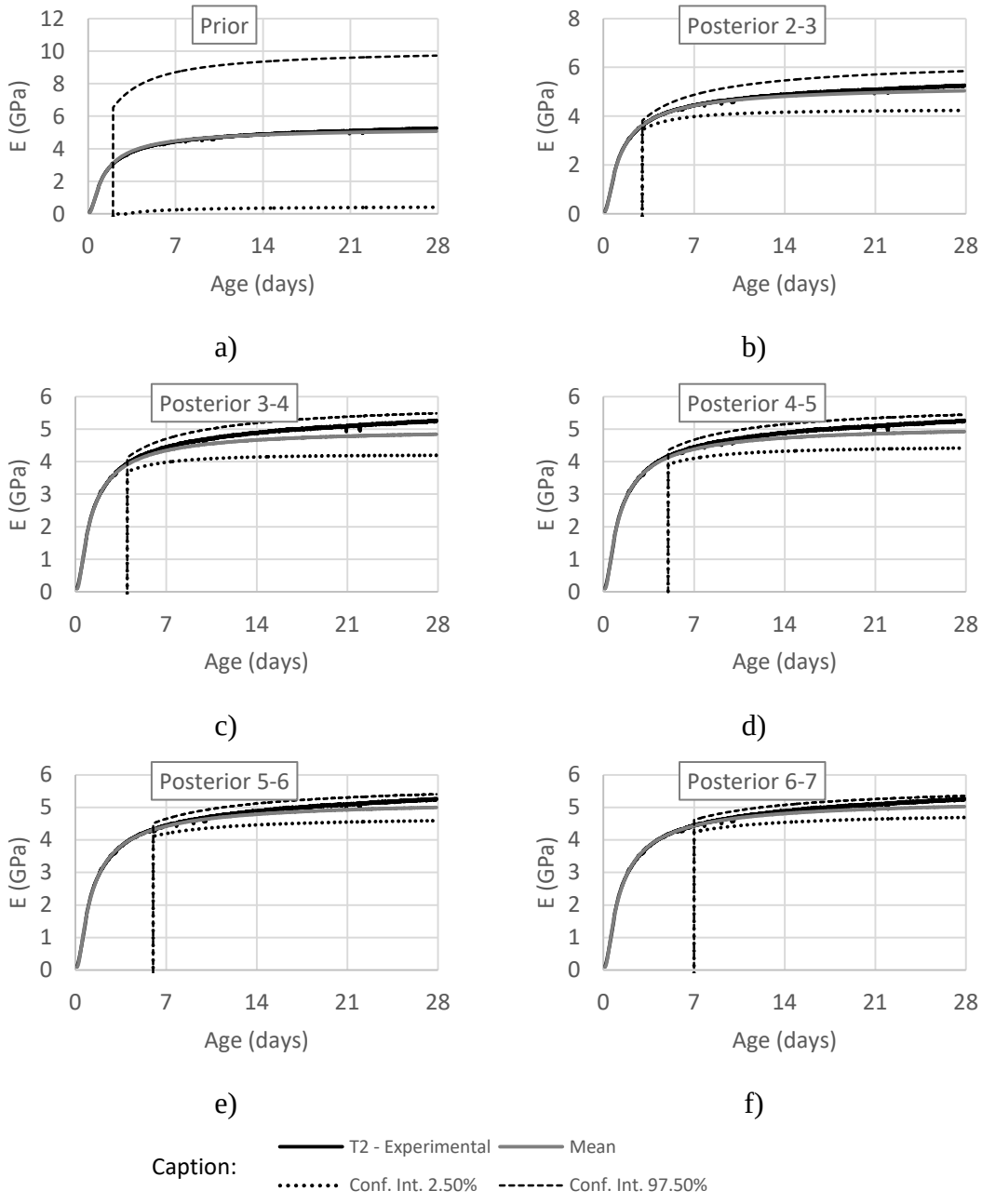

Figure A.0.1. Prior distribution and updated posteriors (95% probability interval) for specimen T2

Table 0.1. E-modulus at predicted (95% probability interval) at age of 28 days for specimen T2

	Prior	Post. 2-3	Post. 3-4	Post. 4-5	Post. 5-6	Post. 6-7
Prob. 2.5%	0.417	4.233	4.195	4.414	4.588	4.694
Prob. 97.5%	9.718	5.845	5.485	5.441	5.405	5.346
Dif. 97.5-2.5	9.301	1.611	1.290	1.027	0.816	0.652
Mean	5.067	5.039	4.840	4.927	4.997	5.020
Standard deviation	2.373	0.411	0.329	0.262	0.208	0.166
Experimental (E) - T2	5.274	[E-modulus at 28 days of age (GPa)]				

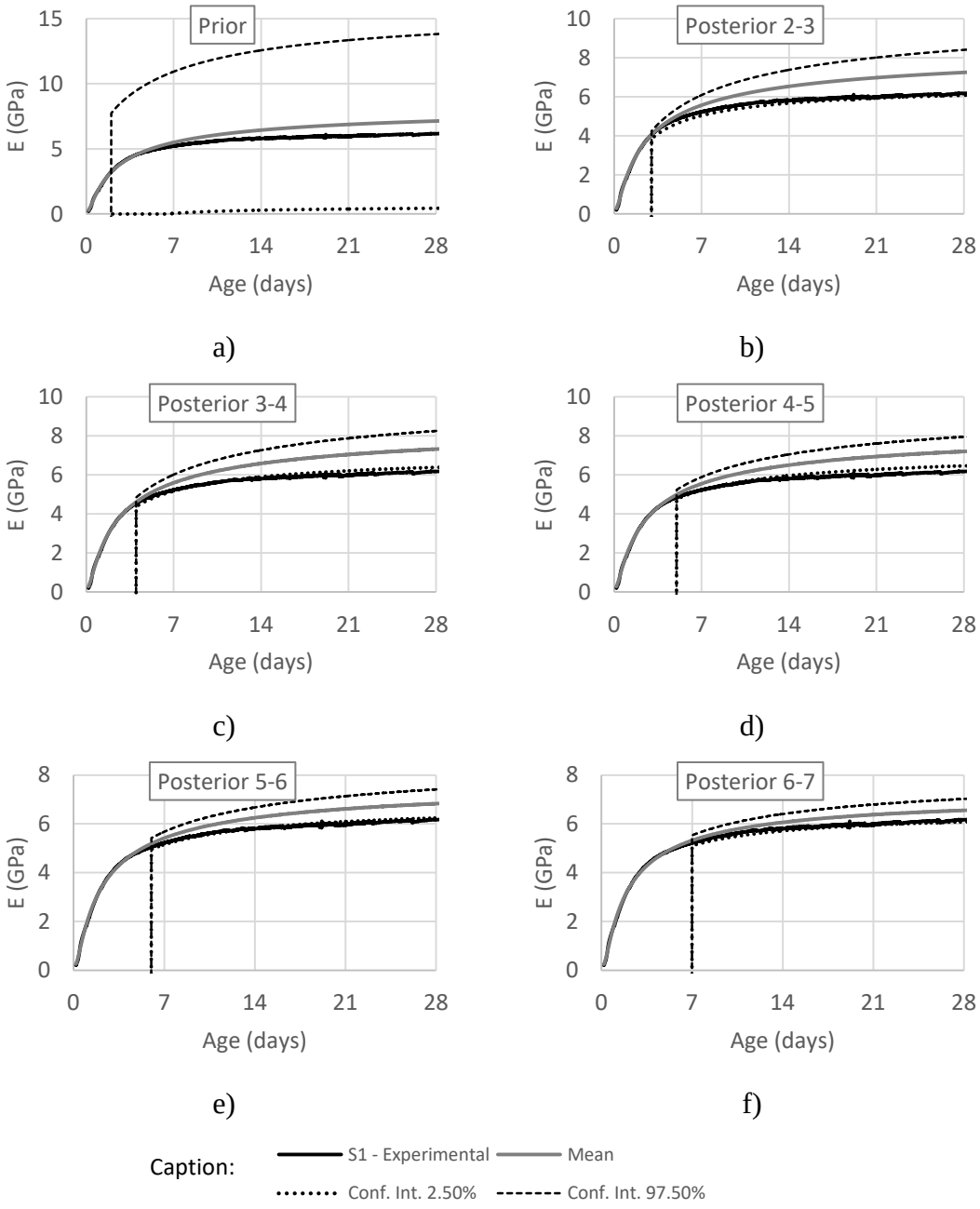

Figure A.0.2. Prior distribution and updated posteriors (95% probability interval) for specimen S1

Table 0.2. E-modulus at predicted (95% probability interval) at age of 28 days for specimen S1

	Prior	Post. 2-3	Post. 3-4	Post. 4-5	Post. 5-6	Post. 6-7
Prob. 2.5%	0.453	6.094	6.407	6.477	6.254	6.104
Prob. 97.5%	13.873	8.454	8.289	7.982	7.447	7.054
Dif. 97.5-2.5	13.420	2.360	1.883	1.504	1.193	0.950
Mean	7.163	7.274	7.348	7.230	6.851	6.579
Standard deviation	3.423	0.602	0.480	0.384	0.304	0.242
Experimental (E) - S1	6.226	[E-modulus at 28 days of age (GPa)]				

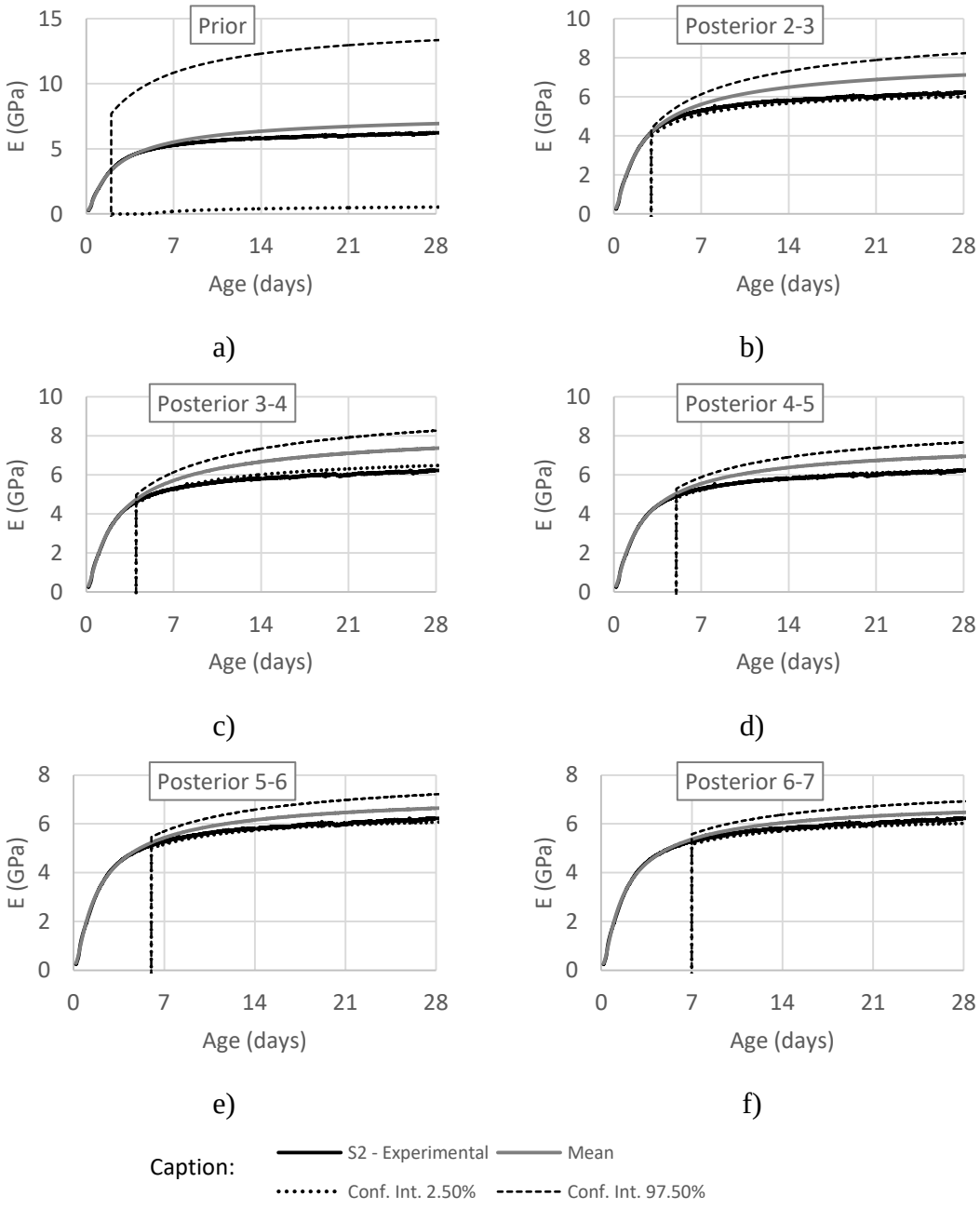

Figure A.0.3. Prior distribution and updated posteriors (95% prob. int.) for specimen S2

Table 0.3. E-modulus at predicted (95% prob. int.) at age of 28 days for specimen S2

	Prior	Post. 2-3	Post. 3-4	Post. 4-5	Post. 5-6	Post. 6-7
Conf. 2.5%	0.544	6.006	6.493	6.248	6.087	6.031
Conf. 97.5%	13.382	8.277	8.310	7.699	7.244	6.960
Dif. 97.5-2.5	12.838	2.271	1.817	1.451	1.156	0.930
Mean	6.963	7.142	7.401	6.974	6.665	6.496
Standard deviation	3.275	0.579	0.464	0.370	0.295	0.237
Experimental (E) - S2	6.205	[E-modulus at 28 days of age (GPa)]				

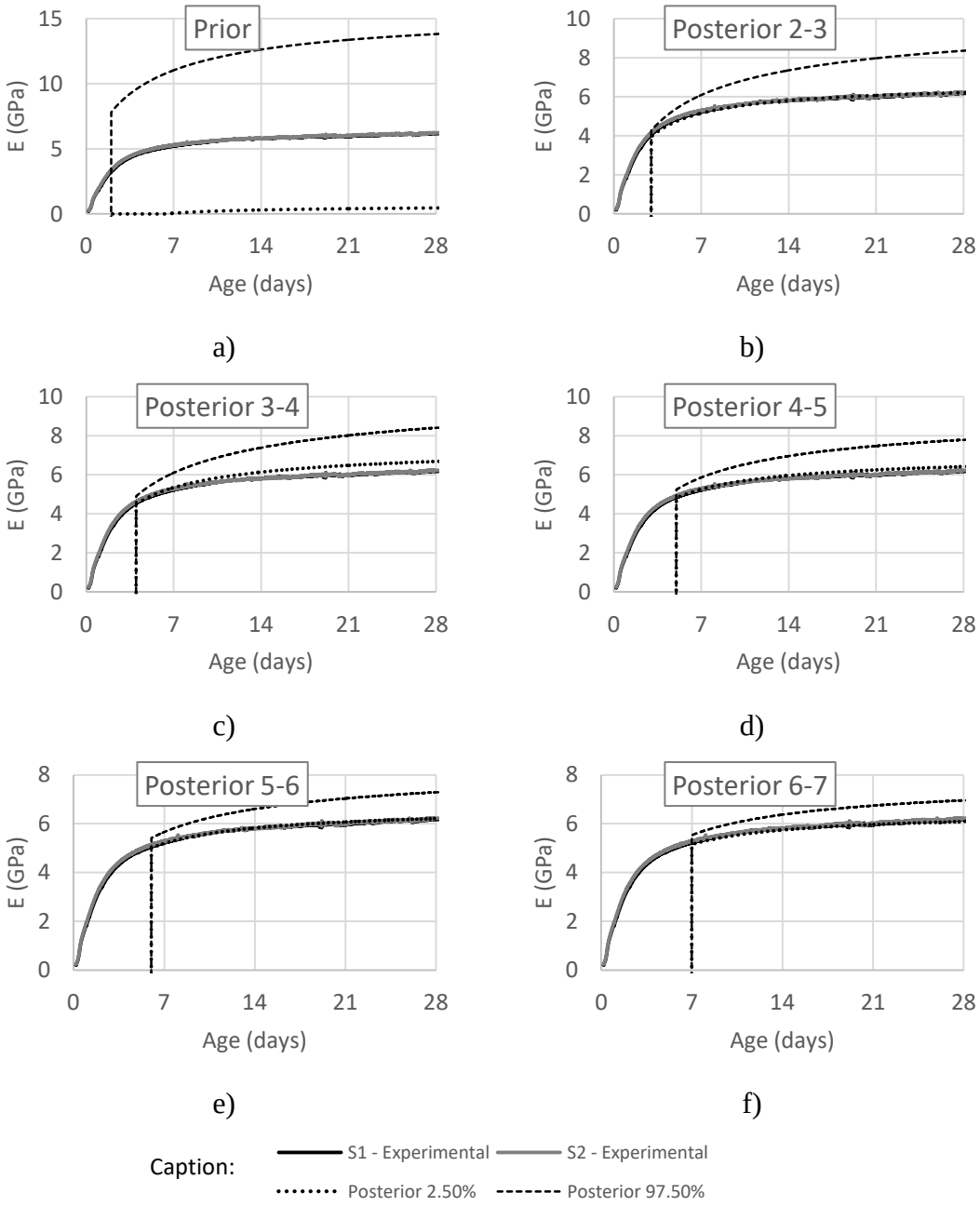

Figure A.0.4. Prior distribution and updated posteriors (95% prob. int.) for specimen pair S1/S2

Table 0.4. E-modulus at predicted (95% prob. int.) at age of 28 days for specimen pair S1/S2

	Prior	Post. 2-3	Post. 3-4	Post. 4-5	Post. 5-6	Post. 6-7
Conf. 2.5%	0.470	6.224	6.712	6.441	6.227	6.108
Conf. 97.5%	13.860	8.411	8.449	7.824	7.335	6.993
Dif. 97.5-2.5	13.390	2.188	1.738	1.384	1.108	0.885
Mean	7.165	7.317	7.581	7.133	6.781	6.551
Standard deviation	3.416	0.558	0.443	0.353	0.283	0.226
Experimental (E) - S1	6.226					
Experimental (E) - S2	6.205		[E-modulus at 28 days of age (GPa)]			

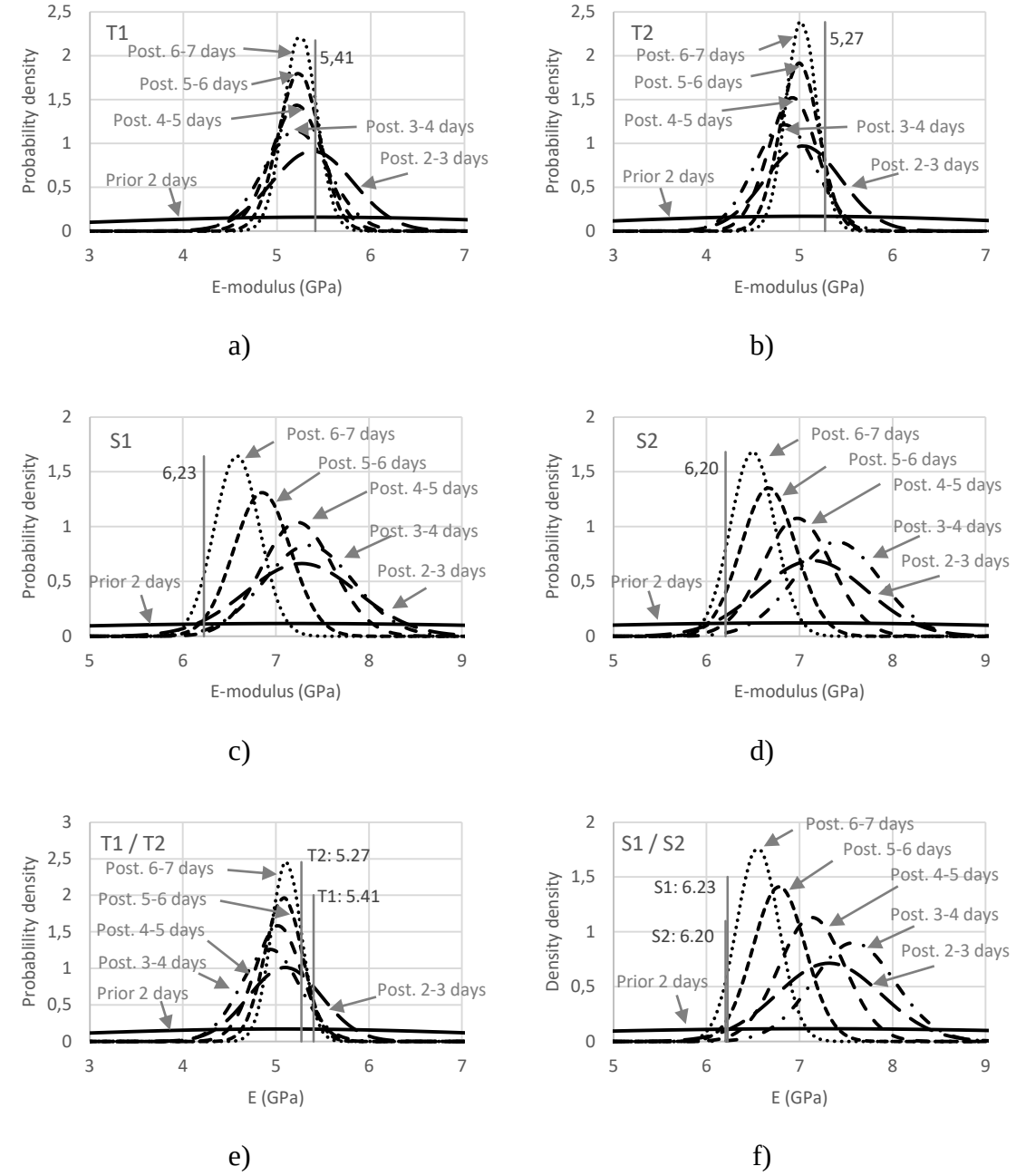

Figure A.0.5. Probability density functions predicted at 28 days with EMM-ARM results obtained up to 2, 3, 4, 5, 6 and 7 days: a) T1; b) T2; c) S1), d) S2, e) T1/T2, f) S1/S2